THÈSE DE DOCTORAT DE
L'UNIVERSITÉ PIERRE ET MARIE CURIE – PARIS 6

Spécialité

Physique théorique

École doctorale Physique de la Région Parisienne – ED 107

DISSERTATION,

der

Fakultät Mathematik und Naturwissenschaften
der Technischen Universität Dresden

Présentée par / vorgelegt von

Jonas M. Ranft

Pour obtenir le grade de / zur Erlangung des akademischen Grades

Docteur de l'Université Pierre et Marie Curie /
Doctor rerum naturalium (Dr. rer. nat.)

Sujet de la thèse / Titel der Arbeit

Mechanics of Growing Tissues: A Continuum Description Approach

Date de soutenance : le 21 juin 2012

Membres du jury : Mme Martine BEN AMAR (Présidente)
M. Ray GOLDSTEIN (Rapporteur)
M. Frank GROSSMANN
M. Lars HUFNAGEL (Rapporteur)
M. Jean-François JOANNY (Directeur de thèse)
M. Frank JÜLICHER (Directeur de thèse)

Membre invité du jury : M. Jacques Prost

This manuscript was set in LaTeX 2_ε.

Laboratoire Physico-Chimie Curie
UMR 168
11, rue Pierre et Marie Curie
75005 Paris
France

Max-Planck-Institut für Physik komplexer Systeme
Nöthnitzer Straße 38
01087 Dresden
Allemagne

“ ‘Talent borrows, genius steals.’ ”

Tocotronic, Gegen den Strich

“Die Wolke der Unwissenheit
wird für immer bei uns sein.”

Tocotronic, Wolke der Unwissenheit

Remerciements

A la fin de la rédaction, après que même les références bibliographiques ont été bichonnées (ce que je viens de faire), il ne reste que le plaisir d'écrire les remerciements – un plaisir d'autant plus grand que j'ai fait cette thèse dans le cadre d'une cotutelle, ce qui veut forcement dire que je ressens un besoin doublement fort de remercier tout le monde... Cela est ma première pensée en tout cas.

Pendant ces trois dernières années, j'ai eu l'énorme chance de connaître un nouveau « foyer scientifique », ici au Laboratoire Physico-Chimie Curie à Paris, tout en en gardant un autre, celui du Max-Planck-Institut für Physik komplexer Systeme à Dresde. Je suis infiniment reconnaissant à toutes et tous qui y ont contribué. Tout d'abord, ce sont évidemment mes deux directeurs de thèse, Jean-François Joanny et Frank Jülicher. Sans la volonté de Jean-François d'accepter encore un de ces étudiants allemands qui envahissent son labo, s'il ne m'avait pas accordé toute cette confiance le long de la thèse, je n'en serais pas là. Cela vaut également pour Frank, qui m'a tôt encouragé à entreprendre une thèse et dont le goût de cette collaboration m'a constamment accompagné. Sur le plan scientifique, j'inclue également Jacques Prost, mon troisième directeur non-officiel de thèse en quelque sorte. Travailler et discuter avec ces trois là a toujours été inspirant, voire rafraîchissant, et nos « sessions » étaient une source principale de motivation pour ce travail. S'il y a une chose que j'espère avoir apprise pendant ma thèse, c'est quelque chose qui ne s'apprend pas me dira-t-on : cette façon de faire la science avec un esprit vif et curieux.

The defense being not the least important part of the doctorate, it is my most delightful duty to thank the referees of my thesis and the committee members. I felt extremely honored when Ray Goldstein, Lars Hufnagel, and Jens-Uwe Sommer accepted to review my manuscript, and I am very grateful for their insightful comments and questions. The same holds true for the remaining committee members, Martine Ben Amar and Frank Großmann. Martine Ben Amar has seen my thesis evolve from the neighboring lab buildings of the École normale supérieure, and it was at a summer school organized by her that I discussed the ideas developed here for the first time with fellow students. Her presence is more than anecdotal, and I am grateful for her willingness to preside over the committee. I thank furthermore Frank Großmann for coming all the way from Dresden to represent my *alma mater*; his readiness to delve into a subject rather unrelated to his own research impressed me a lot.

My thankfulness doesn't stop here. A big "merci" to Sebastian, Matthias, and

Maryam from Dresden as well as to our colleagues from floor 1B1 (plus a few rare exceptions, isn't it Amitabha?): not only have our discussions often been extremely hilarious, they have by no means been inferior to those with "the big guys" regarding their appetite for science. When I returned from Paris after the first 13 month abroad, I immediately felt back home again at the PKS, and I spent nine fantastic months over there.

A Paris aussi, ce fût grâce à mes collègues que je me senti vite chez moi. D'abord, ce sont tous les membres de l'équipe évidemment, depuis les permanents Philippe, Thomas (qui m'a souvent sauvé de la mort de faim avec des pauses goûter à l'heure du dîner) et Andrew (oui, je triche ici, ce délicieux café que l'on prend à la « nouvelle mairie » le vaut bien) jusqu'à mes co-thésards de ces derniers mois de rédaction, Hervé, Edouard et Alexandre. J'ai pleinement profité de nos discussions au déjeuner, au bureau ou encore pendant des sorties communes. Parlant de mes collègues, un grand merci à part à Markus Basan et Jens Elgeti pour leur énorme contribution à ce travail que fût le développement des simulations pour tester les résultats analytiques. Merci aussi à Richard (notre quatrième compatriote) pour son regard particulier sur la science et la ville. Mais « Curie » ne serait rien sans ces innombrables expérimentateurs qui peuplent les couloirs et la cafète : au bout du compte, ce sont eux qui font vivre l'ambiance de ce lieu et rendent le quotidien si agréable, merci pour cela ! Enfin, c'est le personnel administratif qui nous permet de travailler dans de si bonnes conditions, donc ce merci embrasse tout également Brigitte, Nicole, Laurence et Agnès.

Merci à Paris, cette ville qui m'a également si bien accueilli. Merci à mes amis de Dresde et d'ici qui m'ont souvent remonté le moral quand la thèse s'est fait remarquer. De même pour ma famille, qui m'a toujours encouragé et soutenu : « ich danke euch allen herzlich! »

Je remercie enfin Hélène, qui en quelque sorte a été le plus grand succès de ma thèse. Sans elle, cette thèse aurait peut-être vu le jour tout de même, mais cela avec infiniment moins de joie et bonheur. Son soutien ces derniers mois a été inestimable (elle ne saurais pas dire pour qui parmi nous deux ce temps a été plus dur), et c'est à elle que je dédie cet ouvrage.

Abstract

During development, higher organisms grow from a single fertilized egg cell to the adult animal. The many processes that lead to the eventual shape of the developed organism are subsumed as morphogenesis, which notably involves the growth of tissues by repeated rounds of cell division. Whereas coordinated tissue growth is a prerequisite for animal development, excessive cell division in adult animals is the key ingredient to cancer.

In this thesis, we investigate the collective organization of cells by cell division and cell death. The multicellular dynamics of growing tissues is influenced by mechanical conditions and can give rise to cell rearrangements and movements. We develop a continuum description of tissue dynamics, which describes the stress distribution and the cell flow field on large scales. Cell division and apoptosis introduce stress sources that, in general, are anisotropic. By combining cell number balance with dynamic equations for the stress source, we show that the tissue effectively behaves as a viscoelastic fluid with a relaxation time set by the rates of division and apoptosis. If the tissue is confined in a fixed volume, it reaches a homeostatic state in which division and apoptosis balance. In this state, cells undergo a diffusive random motion driven by the stochasticity of division and apoptosis. We calculate the effective diffusion coefficient as a function of the tissue parameters and compare our results concerning both diffusion and viscosity to simulations of multicellular systems.

Introducing a second material component that accounts for the extracellular fluid, we show that a finite permeability of the tissue gives rise to additional mechanical effects. In the limit of long times, the mechanical response of the tissue to external perturbations is confined to a region of which the size depends on the ratio of tissue viscosity and cell-fluid friction. The two-component description furthermore allows to clearly distinguish the different contributions to the isotropic part of the mechanical stress, *i.e.*, the fluid pressure and the stress exerted by cells.

Last but not least, we study the propagation of an interface between two different cell populations within a tissue driven by differences in the mechanical control of the rates of cell division and apoptosis. Combining simple analytical limits and numerical simulations, we distinguish two different modes of propagation of the more proliferative population: a diffusive regime in which relative fluxes dominate the expansion, and a propulsive regime in which the proliferation gives rise to dominating convective flows.

Résumé

Les organismes supérieurs se développent à partir d'une seule cellule fécondée jusqu'à l'animal adulte. Les nombreux processus qui conduisent à la forme finale de l'organisme sont connus sous le nom de morphogenèse, qui comprend notamment la croissance des tissus par des cycles répétés de division cellulaire. Alors que la croissance coordonnée des tissus est une condition nécessaire au développement des animaux, la division cellulaire excessive chez les animaux adultes est l'ingrédient clé du cancer.

Dans cette thèse, nous étudions l'organisation collective des cellules par division et mort cellulaire. La dynamique multicellulaire des tissus en croissance est influencée par des conditions mécaniques et peut donner lieu à des réarrangements ainsi qu'à des mouvements cellulaires. Nous élaborons une description continue de la dynamique des tissus qui décrit la distribution des contraintes et le champ d'écoulement des cellules sur de grandes échelles. La division cellulaire et l'apoptose introduisent des sources de contraintes qui, en général, sont anisotropes. En combinant l'équation de conservation du nombre de cellules avec des équations dynamiques des sources de contraintes, nous montrons que le tissu se comporte de manière effective comme un fluide viscoélastique avec un temps de relaxation fixé par les taux de division et d'apoptose. Si le tissu est confiné dans un volume donné, il atteint un état homéostatique dans lequel division et apoptose s'équilibrent. Dans cet état, les cellules subissent un mouvement diffusif aléatoire dû à la stochasticité de la division et de l'apoptose. Nous calculons le coefficient de diffusion effectif en fonction des paramètres du tissu et comparons nos résultats concernant à la fois la diffusion et la viscosité à des simulations numériques de tels systèmes multicellulaires.

En introduisant un deuxième composant qui représente le liquide extracellulaire, nous montrons qu'une perméabilité finie du tissu donne lieu à des effets mécaniques supplémentaires. Dans la limite des temps longs, la réponse mécanique du tissu à des perturbations extérieures est confinée à une région dont la taille dépend du rapport entre la viscosité tissulaire et le coefficient de frottement entre les cellules et le liquide extracellulaire. La description à deux composants permet en outre de distinguer clairement les différentes contributions à la partie isotrope de la contrainte mécanique, c'est-à-dire la pression du fluide et la contrainte exercée par les cellules.

Finalement, nous étudions la propagation d'une interface entre deux populations de cellules différentes, due à des différences dans le contrôle mécanique des taux de division et de mort cellulaire. En combinant de simples limites analytiques et des simulations numériques, nous distinguons deux modes de propagation différents de la population cellulaire la plus proliférante : un régime diffusif dans lequel les flux relatifs dominent l'expansion, et un régime de propulsion dans lequel la prolifération domine et entraine des flux convectifs.

Kurzzusammenfassung

Die Entwicklung höherer Organismen beginnt mit einer einzelnen befruchteten Eizelle und endet beim erwachsenen Tier. Die vielen Prozesse, die zur endgültigen Form des entwickelten Organismus führen, werden als Morphogenese zusammengefasst; diese umfasst insbesondere das Wachstum von Geweben durch wiederholte Zellteilungszyklen. Während koordiniertes Gewebewachstum eine Voraussetzung normaler Entwicklung ist, führt übermäßige, unkontrollierte Zellteilung letztlich zu Krebs.

In dieser Arbeit untersuchen wir den Einfluss von Zellteilung und Zelltod auf die Organisation von Zellen in Geweben. Die Dynamik wachsender Gewebe wird durch mechanische Bedingungen beeinflusst, die u.a. Anlass zu Zellbewegungen sein können. Wir entwickeln eine Kontinuumsbeschreibung der Gewebedynamik, die die mechanischen Spannungen und das Zellströmungsfeld auf großen Skalen beschreibt. Zellteilung und Apoptose wirken als Spannungsquellen, die in der Regel anisotrop sind. Indem wir die Erhaltungsgleichung für die Zellanzahldichte mit dynamischen Gleichungen für die Spannungsquellen kombinieren, zeigen wir, dass sich das Gewebe effektiv wie eine viskoelastische Flüssigkeit verhält, deren Relaxationszeit von Zellteilungs- und Apoptose-Raten abhängt. Wenn das Gewebe in einem gegebenen Volumen eingeschlossen ist, erreicht es einen homöostatischen Zustand, in dem Zellteilung und der Apoptose im Gleichgewicht sind. In diesem Zustand unterliegen die Zellen einer diffusiven Bewegung aufgrund der Stochastizität von Zellteilung und Apoptose. Wir berechnen den effektiven Diffusionskoeffizienten als Funktion der Gewebeparameter und vergleichen unsere Ergebnisse sowohl hinsichtlich der Diffusion und als auch der Viskosität mit numerischen Simulationen solcher vielzelliger Systeme.

Die Berücksichtigung der extrazellulären Flüssigkeit als einer zweiten Materialkomponente erlaubt uns zu zeigen, dass eine endliche Permeabilität des Gewebes zusätzliche mechanische Effekte bedingt. Auf langer Zeitskalen bleibt die mechanische Reaktion des Gewebes auf externe Störungen auf einen Bereich der Größe λ beschränkt, wobei λ vom Verhältnis der Gewebeviskosität zum Permeabilitätskoeffizienten abhängt. Die Zweikomponenten-Beschreibung erlaubt darüber hinaus eine klare Unterscheidung der verschiedenen Beiträge zum isotropen Teil der mechanischen Spannung, d.h., des hydrodynamischen und des von Zellen ausgeübten Drucks.

Zuletzt untersuchen wir die Dynamik einer Grenzfläche zwischen zwei verschiedenen Zellpopulationen innerhalb eines Gewebes, die durch Unterschiede in der mechanischen Kontrolle der effektiven Zellteilungsraten angetrieben wird. Mithilfe der Kombination einfacher analytischer Grenzfälle und numerischer Simulationen zeigen wir, dass zwei unterschiedliche Ausbreitungsmodi unterschieden werden können: ein diffusives Regime, in dem relative Flüsse die Expansion der stärker wachsenden Zellpopulation dominieren, sowie ein Regime, in dem die Grenzfläche durch konvektive Strömungen angetrieben wird.

Contents

Chapter 1

General introduction

Developmental biology is concerned with the intricate, fascinating phenomena which mark the beginning of life. Physics is concerned with everything that obeys the laws of nature, themselves of surprising beauty often enough. It thus may seem promising to bring these two disciplines together, and researchers have indeed tried to bridge the gap between these two throughout the history of science. More recently, however, the field of "developmental biophysics"[1] has seen a rapid, accelerating growth driven by increasingly quantitative insight into the molecular mechanisms at work in biology. In the past decade, more and more research has aimed at a deeper physical understanding of the processes involved in development and eventually at physical descriptions of biological phenomena.[2]

A recurrent task for the scientist engaged in developmental biophysics is to rationalize experimental data. In general, this is achieved via modeling of the phenomenon under study: if a model that draws on simple, generic physical principles is able to reproduce the experimental findings, the task can be considered accomplished, at least until the model has been proven wrong. Here, "generic physical principles" refers to concepts such as conservation of mass or momentum, and to mechanisms that will inevitably take place in a given physical environment whether alive or not, for example the flattening of concentration gradients due to diffusion (as long as no additional fluxes counteract this tendency). They can be contrasted with genetic mechanisms that would rely on a precise encoding in space and time of the observed cell and tissue behavior [139]. Due to the inherent complexity of the biological system under study, however, it is not obvious which kind of model, or biophysical description, to choose. The development of higher organisms is coordinated over many time and length scales, and "generic physical mechanisms" and

[1] It is probably best to think of developmental biophysics not in terms of a discipline (or a couple of them) but as an area of research where scientists with different backgrounds work together on questions that arise in development. Needless to say, this includes all the work done in biomechanics, mathematical biology, applied mathematics, ...

[2] Anecdotal evidence that this has not always been a commonly shared goal is retold in a portrait of George Oster, an early pioneer in the field: Apparently, he once received a negative referee report because he and his co-authors "[attempted] to apply Newton's laws to embryos", for "as all biologists know, biological systems don't obey the laws of physics." [143].

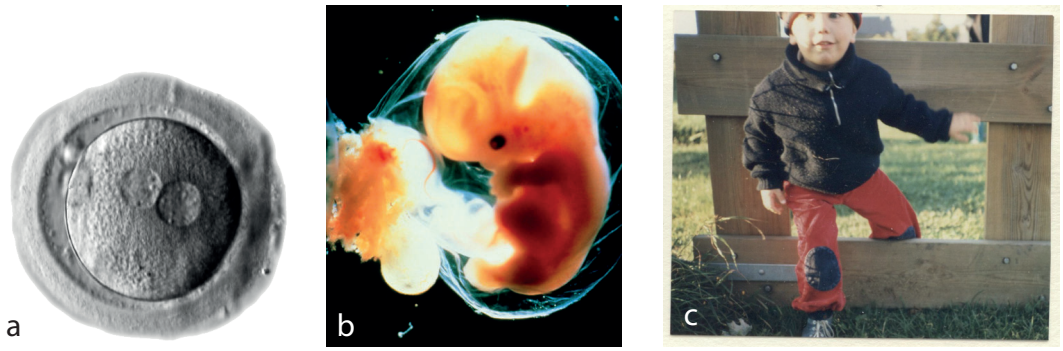

Figure 1.1. Human development. (a) A human fertilized egg zell (zygote) 18-20 h after fertilization [140], (b) a 5-6 weeks old embryo [1], and (c) the author as a young man.

gene regulation are more and more known to be intertwined [30, 58, 151, 191, 195].

Before we turn our attention to the aims of this thesis, we discuss some basic aspects of animal development as well as of its evil counterpart, cancer biology, where we review recent advances in the field along the way. We then discuss biophysical descriptions of tissue growth put forward in the literature, and we conclude the introduction with an overview of the remainder of this thesis.

1.1 Animal morphogenesis

One of the ultimate goals of developmental biology is to eventually understand human development, see Fig. 1.1. The underlying principles of development are mostly studied in a few model organisms, however, which typically exhibit a couple of advantageous characteristics like a fully sequenced genome; rapid, well-characterized embryonic development; and short generation times [192]. In general, these traits make the whole battery of molecular cell biology methods available and allow for a thorough characterization of the effects of mutations using advanced imaging methods [8, 192].

Zebrafish development

Two prominent examples are the fruit fly *Drosophila melanogaster* and the zebrafish *Danio rerio*. Although both develop as most multicellular organisms from a single fertilized egg cell (called the zygote), their actual developmental programs are rather quite different. An overview of the different stages of zebrafish embryogenesis is shown in Fig. 1.2. In early development, cells undergo repeated rounds of cell division without actually increasing the total cell mass, forming the so-called blastula. The blastula is an undifferentiated tissue that subsequently differentiates into the three germ layers ectoderm, mesoderm, and endoderm during gastrulation [108]. These germ layers eventually give rise to distinct adult tissues and organs such as neuronal tissues and skin (ectoderm); the skeleton, heart, and connective tissue (mesoderm); and intestinal organs (endoderm).

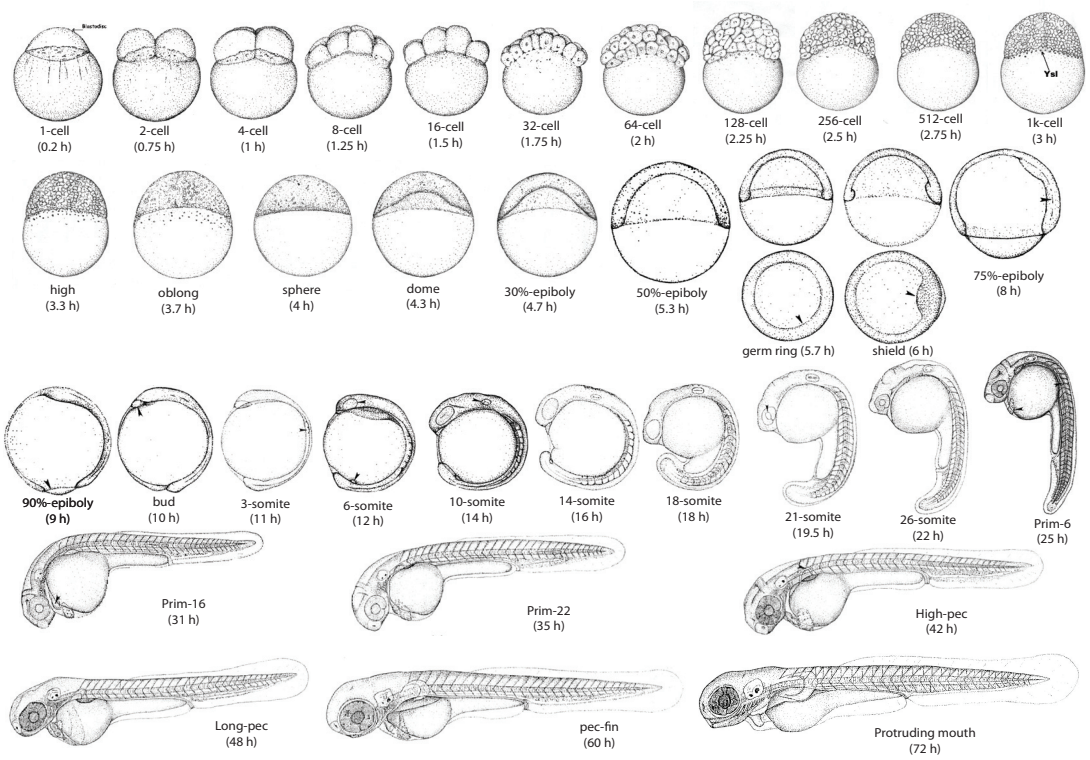

Figure 1.2. Zebrafish embryogenesis. Figure modified after [108].

All aspects of development that contribute to the actual shaping of the animal are referred to as morphogenesis, and gastrulation is the first instance of important morphogenetic movements of cells and tissues in developing animals. In the zebrafish, gastrulation comprehends epiboly, which denotes the spreading movement of the blastula (and later ectoderm) over the yolk cell, as well as an additional inward movement of lateral cells after the establishment of the anterio-posterior (head-to-tail) axis in the developing embryo. Additionally, cells at the advancing tissue margin differentiate into mesoderm and endoderm cells that move upwards inside the developing embryo [108, 115, 192]. After gastrulation, zebrafish development proceeds to the segmentation period, during which the precursors of the skeletal segments form (the so-called somites) as well as rudiments of the primary organs. The embryo elongates further during pharyngula and hatching period, before it finally starts to swim on its own [108, 192], see also Fig. 1.2.

Although much is known about the genes involved in zebrafish morphogenesis [89, 192][3], only few studies have addressed the physical basis of morphogenetic movements during zebrafish development on a tissue scale. A remarkable exception is the work of Schötz *et al.*, in which the authors explored the possibility that the relative positioning of the germ layers during gastrulation can be understood as wetting of two immiscible

[3]The scholarly journal *Development* devoted a special issue to the role of genes in zebrafish development in order to celebrate the landmark success of huge genetic forward screens, see [89, ff.].

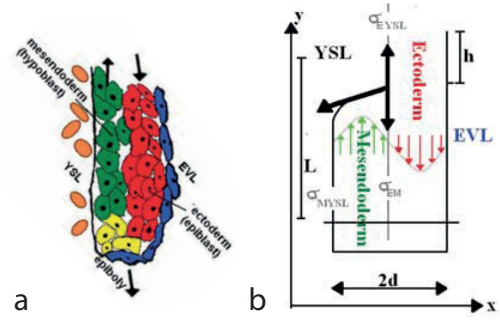

Figure 1.3. Germ layer positioning during zebrafish gastrulation. (a) A sketch of the leading edge of the advancing tissue at shield stage (∼60% epiboly). Mesendoderm cells are induced at the blastula margin (yellow) and move subsequently upward, while outer cells differentiate into ectoderm (red). The yolk cell is to the left. (b) Schötz *et al.* hypothesized that the relative positioning is caused by differences in cell surface tension and that the relative movement is analogous to wetting of immiscible liquids. Figure modified after [165].

liquids [165]. The authors show that ectoderm and mesendoderm cell aggregates sort out *in vitro* due to differences in tissue surface tension[4], and they calculate the maximal driving force for mesendoderm invagination that could possibly result from differential adhesiveness of ectoderm and mesendoderm with the yolk, see Fig. 1.3. Strong conclusions cannot be drawn, however, mainly because the adhesion between cells of the different germ layers and the yolk is difficult to access, and the authors themselves point out that other contributions such as active migration may be relevant.

D. melanogaster gastrulation

The life cycle of the fruit fly is shown in Fig. 1.4(a). Its development is quite distinct from zebrafish and human development, although the genetic overlap between *Drosophila melanogaster* and *homo sapiens sapiens* is still enormous.[5] During the first 13 rounds of nuclear divisions, the nuclei do not yet form independent cells and share all the same cytoplasm [192]. They assemble into a layer at the inner surface of the egg before cellularization starts. The surrounding plasma membrane then bulges in and the nuclei separate into independent cells, eventually forming the cellular blastoderm. At this stage, gastrulation sets in, see Fig. 1.4(b).

Drosophila gastrulation comprises a complex sequence of morphogenetic movements, which have been extensively studied in the literature. As early as 1981, Odell and colleagues proposed a mechanical model of the ventral furrow formation in the *Drosophila* embryo [144], see Fig. 1.5(a). At the beginning of gastrulation, the cellular blastoderm invaginates at the ventral side of the embryo (the dorso-ventral axis being defined as the back-to-front axis of the adult animal), giving rise to a hollow structure inside of the embryo. The authors of the cited study showed with computer simulations that this tissue movement can be understood as the sole consequence of a wave of the mechanically triggered constriction of cells at their apical (external) side. Recent studies established a rather precise picture of the nature of the mechanical forces at work [122, 123], see

[4] We discuss the concept of tissue surface tension below in more detail, see sec. 2.1.

[5] Approximately 75% of known human disease genes have recognizable counterparts in the fly genome, and about one third of these homologues is similar to a degree that functional equivalence can be expected [22].

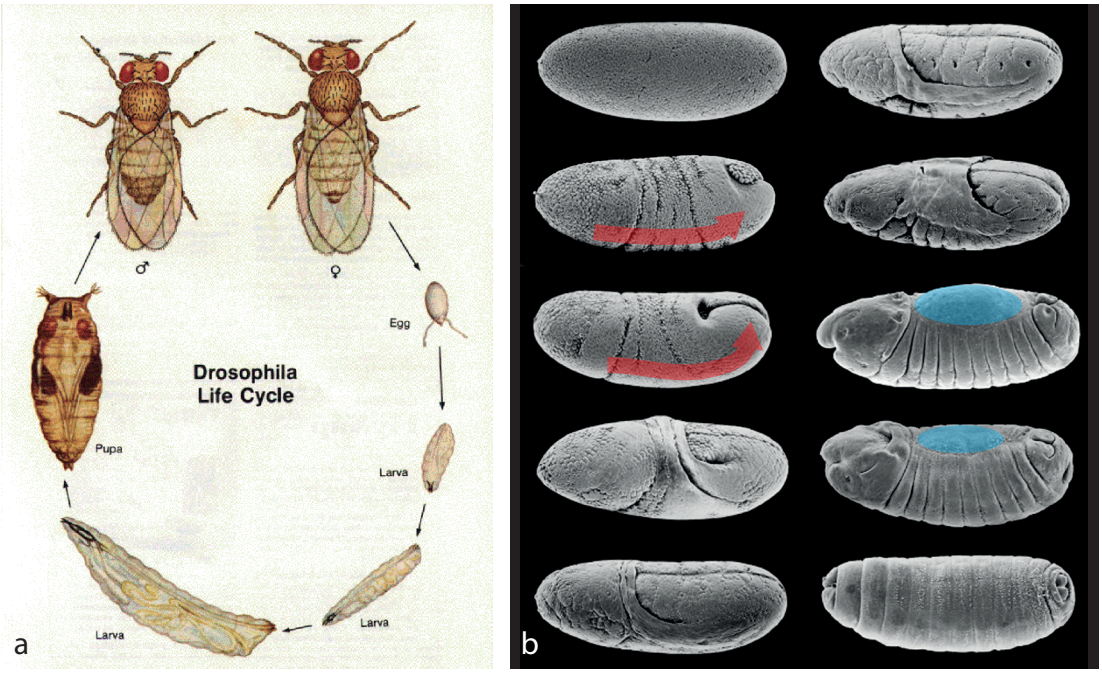

Figure 1.4. Life cycle and gastrulation of *Drosophila*. (a) After the female fly ays the fertilized eggs, the early embryo develops in the egg—notably undergoing gastrulation—before it eventually hatches $12 - 15$ h post fertilization. Development continues through three larval stages, during which the precursors of adult appendages grow and form. After approx. 5 days, the 3rd instar larva forms the pupa and undergoes metamorphosis. The adult fly is fully developed after about 9 days. Figure kindly provided by the Carolina Biological Supply Company. (b) The first important morphogenetic movements take place during gastrulation. The image sequence (top to bottom, left to right) shows the *Drosophila* embryo slightly rotated along the anterior-posterior axis (anterior being left in the image) so that the dorsal side can be seen at the upper side. Gastrulation starts with the cellularized blastoderm (upper left image), before ventral furrow formation (not shown) sets in. Subsequently, the germ band elongates along the anterior-posterior axis and moves dorsally as indicated by the red arrows. The last step of gastrulation is dorsal closure during which an epidermal opening at the back (blue shaded regions) of the embryo is eventually covered, see text for details. Images publicly available at `http://www.flybase.org`, see also [184, ff.].

Fig. 1.5(b,c). The medial acto-myosin networks that cover the apices of the invaginating cells constrict in a non-synchronized, pulsed fashion and pull adherens junction sites inward during constriction. During subsequent pauses, the cells' apices remain constricted as long as the actomyosin networks and their inter-cellular coupling via adherens junctions are not compromised, *e.g.*, due to genetic mutations. Ventral furrow formation is thus a classic example of a morphogenetic process that is caused by force generation on the cellular scale, where these forces eventually give rise to movements on a supra-cellular scale because of mechanical coupling between cells. Note that this process is nevertheless genetically regulated: the expression of the gene *snail* is indeed necessary for onset of

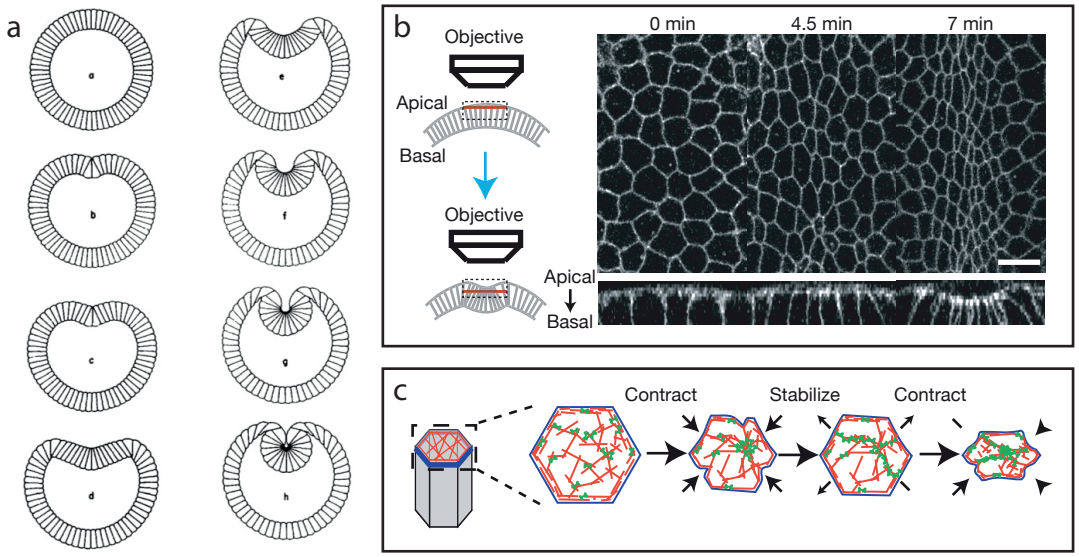

Figure 1.5. Ventral furrow formation. (a) Early computer simulations of epithelial invagination caused by mechanically triggered cell constriction at the apical side [144]. (b) Micrographs of the constriction of cells along the ventral midline. (c) A sketch of the underlying mechanics at the cellular scale: Cells exhibit an actin-myosin network on their apices that actively generate contractile forces and pulls adherens junctions inwards, thus reducing their apical area. This contraction happens in a pulsatile fashion with intermediate stabilization of the actin-myosin network. Figures (b,c) modified after [123].

constriction, and the expression of the gene *twist* is a prerequisite of the stabilization of the achieved reduction in apex area [123, 122]. As mentioned earlier, however, there exists crosstalk between mechanical forces and the observed gene expression patterns. Another study suggested that *twist* expression may be triggered by the mechanical deformation of cells due to a first constriction wave triggered by *snail* [151].

Ventral furrow formation is not the only tissue movement during gastrulation. After ventral furrow formation, the germ band elongates along the anterio-posterior axis of the embryo and shrinks along the perpendicular axis, showing a so-called convergence-extension movement [79, 114, 192]. The germ-band extension is indicated in Fig. 1.4(b). Recent studies addressed the contribution of actively generated force anisotropies due to polarized acto-myosin flows at the cellular scale [157] as well as the role of externally applied tension that acts on the germ band [35]. Here, it is interesting to note that this externally applied tension stems itself from the active constriction and invagination movement of other parts of the embryo [35, 79].

A third aspect of gastrulation—its grand finale, kind of—is dorsal closure, see also Fig. 1.4(b). After a sequence of tissue rearrangements and retraction, the embryo's back exhibits an epidermal opening that needs to be closed before the embryo enters the first larval stage [192]. The opening is initially covered by a sheet of cells (the amnioserosa), which contributes actively to closure. Dorsal closure is another example of the coordina-

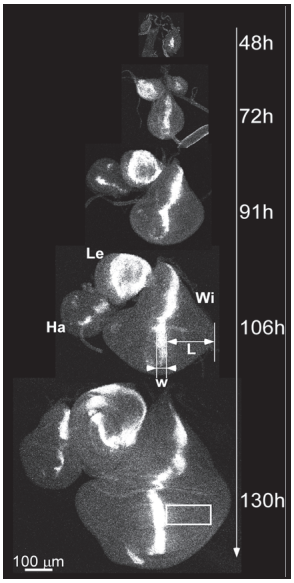

Figure 1.6. Growth of imaginal discs in *Drosophila*. During the three larval stages, haltere (Ha), leg (Le), and wing (Wi) precursors grow in size by repeated rounds of cell division. The Dpp signaling molecule is fluorescently labeled, and the Dpp producing cells along the A/P compartment boundary (separating an anterior and a posterior cell population) can clearly be distinguished, see text for details. Figure modified after [189].

tion of forces generated at cellular and supra-cellular scale [79]. Amnioserosa cells show pulsatile contractions similar to the cell contractions that lead to mesoderm invagination [28, 80, 170], thus pulling epidermal cells dorsally. This contraction is stabilized by a ratchet-like mechanism mediated by a supra-cellular actin-cable along the margin of the epidermis [79, 80, 180]. The shrinking amnioserosa cells eventually undergo programmed cell death (apoptosis), which in itself contributes to the constricting forces [180].

The *Drosophila* wing imaginal disc

While gastrulation is indeed an important step in early development[6] and serves as a fascinating model system to study forces at the tissue scale, the actual growth of the developing fly is far from ending there. During gastrulation, small groups of cells are put aside that constitute the precursors of the adult appendages such as the antennae, wings, and legs [192]. These so-called imaginal discs grow substantially during the three larval stages of *Drosophila* development, and especially the wing imaginal disc has been the subject of many studies that focused on mechanical aspects of growth and on growth control [6, 26, 59, 100, 113, 124, 189]. The wing imaginal disc grows from approx. 50 to $5 \cdot 10^4$ cells in about five days, see Fig. 1.6. Throughout this time, cells remain firmly attached to each other, forming a monolayer of cells [192]. Growth critically depends on intact signaling of the morphogen (signaling molecule involved in morphogenesis) Dpp [6, 192]. Dpp, which is produced in a small stripe of cells along the dorso-ventral axis in the wing disc (see also Fig. 1.6), diffuses from the source and sets up a concentration gradient in both the anterior and the posterior compartment of the wing disc [6]. Different models have been put forward to account for the observed uniform growth pattern, invoking

[6] As Lewis Wolpert famously said, "it is not birth, marriage, or death, but gastrulation, which is truly the most important time in your life."

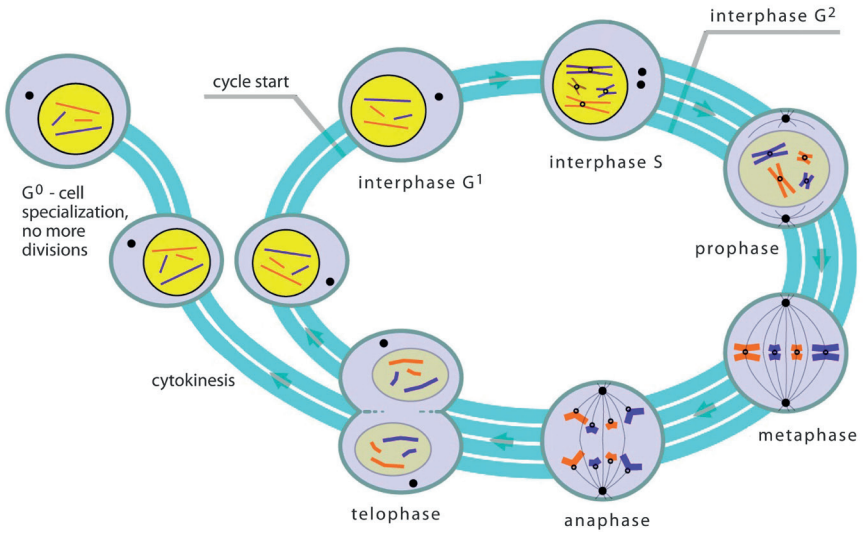

Figure 1.7. The mitotic cell cycle. Cells that undergo mitosis go through a sequence of well-defined steps before eventually undergoing cytokinesis. Many genetic pathways exist that closely regulate the progression from one stage to the next [8]. Figure adapted from Open High School of Utah OCW (Open Course Ware), see `http://ocw.openhighschool.org/`.

mechanical [4, 5, 100, 168] or genetic regulation [166, 189]. In a recent paper, Wartlick and colleagues showed evidence suggesting that cells divide after experiencing a relative increase in Dpp concentration of 50%, which leads to homogenous cell division because of the reported scaling of the Dpp concentration gradient with tissue size [189]. This view has already been contested, however, other authors preferring a model that relies on absolute concentration thresholds and takes additional morphogens into account [91, 166].

1.2 Cancerous tissue growth

After this quick tour through animal development, where we could only touch upon a few interesting concepts and notions related to morphogenesis, we now present some key aspects of the biology of cancer. Cancer is rather a class of diseases than a specific illness, which all involve uncontrolled cell proliferation and growth [190]. Cancer is caused by genetic mutations that interfere with natural control mechanisms of the cell cycle, see Fig. 1.7, and with genetic pathways that lead to programmed cell death when cell growth becomes abnormal [190]. Because cells usually have to acquire more than one mutation to become cancerous, the risk of becoming cancer increases with age, as mutations can add up over time. But age is not the only factor favoring tumor development. By now, many chemical carcinogens are known to considerably increase the chances of developing a cancer, of which more than 50 are found in tobacco alone [111].

The progression of cancer is illustrated in Fig. 1.8. In most cancer cells, DNA repair mechanisms are substantially impaired, which implies that cancer cells have a high rate of mutations [190]. This allows them to adopt an increasingly malignant phenotype,

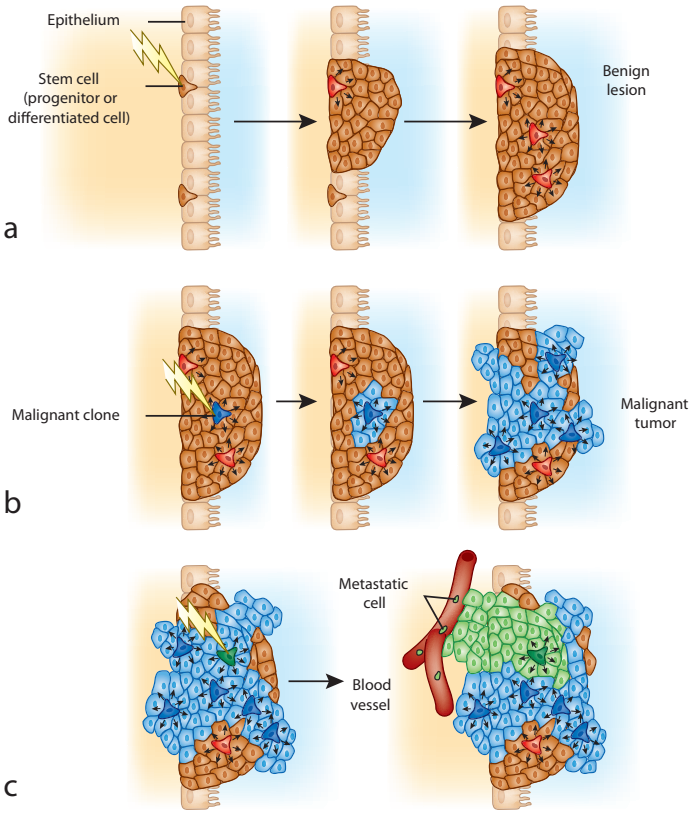

Figure 1.8. The progression of cancer. (a) First, a cell adopts a mutation that compromises its growth control, and the cell begins to proliferate abnormally. A benign tumor forms that is still contained within the original tissue environment. (b) At a later stage, a benign tumor cell acquires an additional mutation that renders it more malignant. Its offspring divides more aggressively, eventually compromising tissue structure. The tumor becomes malignant. (c) Additional mutations allow malignant cancer cells to become metastatic and invade other tissues via the lymphatic system or the blood stream. Figure modified after [43].

eventually giving rise to metastatic cells that invade the surrounding tissue. Via the lymphatic system or the blood stream, metastatic cells can reach sites in the body far from the primary tumor. Although only a small fraction manages to leave the vessel and form a secondary tumor, metastatic tumors are the most probable cause of deaths related to cancer [190].

During the last decades (after Richard Nixon declared the "war on cancer" in 1971), much has been learned about the genes involved in cancer progression [8, 190]. With advances in cellular biophysics regarding the understanding of cell motility and cell-cortex mechanics [98, 160], the mechanical properties of cancer cells became another area of interest [69, 173]. As there is such a huge variety of different cancers, and cancer cell types, no unique conclusion can be drawn from this research. Not surprisingly, however, in highly malignant cells mechanical properties are often altered in a way that facilitates

migration through microchannels [173], and cells seem to be mechanically softer than their healthy counterparts [87]. In the last couple of years, research has additionally been focussing on the tumor microenvironment [25, 93, 107, 116, 135]. Here, microenvironment refers to the healthy tissue sourrounding the nascent tumor, which mostly consists of extracellular matrix and fibroblast cells embedded therein [8, 68], see also the introduction to chapter 3. Although normal mechano-response of cancer cells seems to be compromised [54, 173], the mechanical properties of the tumor microenvironment seem to play an important role in whether cancer cells adopt a malignant phenotype [34, 116, 145].

1.3 Biophysical descriptions of growing tissues

The study of tissue mechanical properties led to the development of a whole range of biophysical descriptions of tissue mechanics and tissue growth. The notorious D'Arcy Thompson advocated as early as 1917 that one should employ the principles of mathematical mechanics to understand the growth and form of living organisms [179], and this agenda has found a rich echo in the meantime. Here, we try to focus on rather recent work with an emphasis on those descriptions and models of tissue mechanics that explicitly account for growth. Among those, an obvious distinction can be made between (i) discrete models that at least to some degree account for single-cell behavior and (ii) continuum-mechanics descriptions that do not explicitly consider details on the cellular scale.

Discrete descriptions of tissue mechanics

One can further roughly distinguish two types of discrete models present in the literature, independent of their implementation. In a first class of models, one finds single-cell based models that represent cells as discrete, point-like particles [27, 29, 36, 55, 57, 56, 142]. The interactions between particles are described by potential functions that—roughly speaking—emulate those of sticky elastic spheres in order to model finite cell stiffness, cortex elasticity, and cell-cell adhesion in a comprehensive way [56]. The implementation of the dynamics of these models varies across the literature, ranging from Metropolis [57], Langevin-type [73], and dissipative-particle dynamics-like time evolution [27]. Similarly, the implementation of cell division varies across models, but amounts to replacing one of the basic interacting particles by two. The variability of such models is enormous as the number of possible parameters to model tissue mechanical characteristics is *a priori* unlimited; and various extensions of growth rules, coupling to nutriment concentrations, or cell-substrate interactions can be conceived [73, 96].

Whereas this flexibility and the straightforward computational approach are certainly advantages to simulate large systems of almost arbitrary complexity, it does come at a cost. The discrete, point-like representation of cells makes it difficult to relate model parameters to actual cell mechanical properties, and the energy dissipation in these models, which is linked to the dynamics, is not always well-defined.[7] A second class of biophysical

[7] In many models, the instantaneous cell velocities follow from the balance of viscous and potential

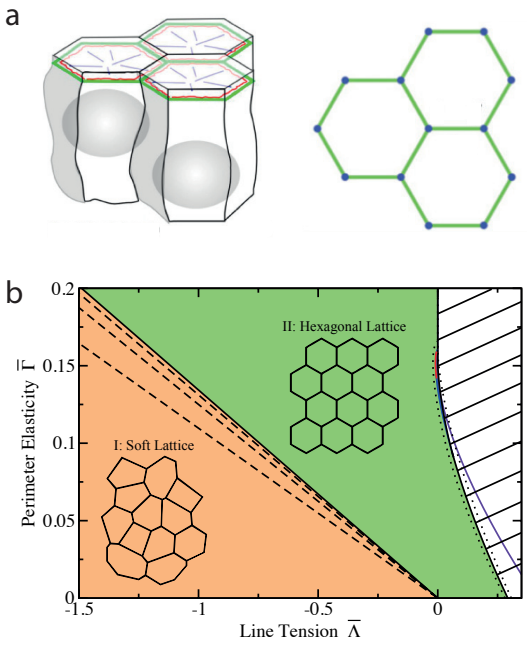

Figure 1.9. The vertex model. (a) The packing of epithelial cells is described by a two-dimensional polygonal tiling that represents cell-cell junctions at the apical (upper) side of the epithelium. The forces that act on a vertex are balanced. These forces stem from the compression of cells, adhesion between cells, and contractile forces along the cell edges and are described by an energy function. A stable cell configuration corresponds to a local minimum of the energy. (b) Ground state diagram of the vertex model proposed by Farhadifar *et al.* [59]. For a certain parameter range, the global energy minimum of the cell network corresponds to a soft lattice with vanishing shear modulus. In the *Drosophila* wing imaginal disc, laser ablation experiments suggest that the global energy minimum corresponds to a stable, hexagonal cell packing, and random cell division leads to the irregular packings observed *in vivo* [59]. Figures modified after [59, 171].

models approaches tissue mechanics at the mesoscale: instead of representing individual cells by a single coordinate, they rather describe the junctional network defined by cell-cell contacts [59, 100, 171]. In these models, epithelial cell packings are represented as polygonal tilings, see Fig. 1.9(a). Under the assumption that the observed cell configurations can be described by the balance of conservative forces, the authors write down an energy function that depends on the positions of the vertices where cell edges meet. Note that, to date, this approach remains limited to sheet-like tissues that can be represented as two-dimensional networks. The effective energy contains terms that account for cell elasticity, cell-cortex contractility, and cell-cell adhesion [59, 100]. Farhadifar and coworkers have shown that their "vertex model" exhibits different ground state properties depending on the ratio between a perimeter elasticity of cells and the tension at cell-cell bonds, see Fig. 1.9, and concluded from experiments that the developing wing disc can be considered as an elastic tissue on short times [59].

Similar approaches that make use of an effective energy to describe the mechanics of tissues have been introduced earlier in the context of cell-cell sorting experiments [78, 85] or to describe cell configurations in the retina of *Drosophila* [106]. These models are derived from the so-called large-Q Potts model of domain growth and represent a cell as a compact domain of identical spins. Manning and colleagues considered the interfacial energies associated with cell-cell contacts and used a standard surface-evolver routine to find equilibrium cell configurations [120]. Far from being complete, we mention just one more formulation, where tissues have been modeled as a polygonal tiling of cells that

forces; however, the contribution to the viscous forces is not unequivocally defined. In order to be more precise, we would need to discuss individual models in greater detail.

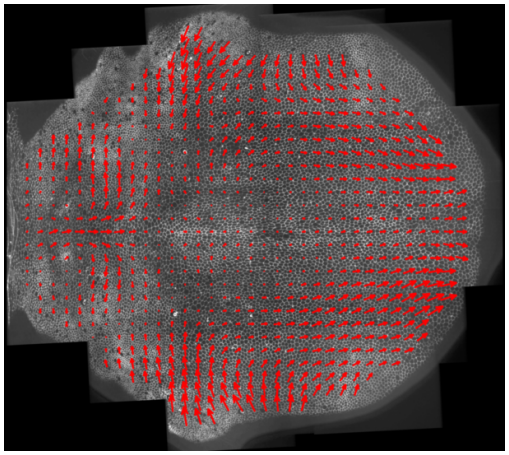

Figure 1.10. Large scale flows in the developing *Drosophila* dorsal thorax. Red arrows correspond to cell flows obtained by particle image velocimetry, averaged over the time course of two hours. The dorsal thorax shows large scale cell rearrangements during *Drosophila* metamorphosis due to active cell contractility and cell proliferation. Image courtesy of Y. Bellaïche (Inst. Curie), see also [30].

in turn are represented as an ensemble of viscoelastic rods [102]. Note also that as for single-cell based models, the dynamics in the aforementioned mesoscale models is not unequivocally defined.[8]

An advantage of the vertex model and related formulations is that the obtained epithelial packings can be compared to experimental data in a straightforward way. For considerably large systems, however, discrete models of growing tissues are increasingly hard to computationally solve. Although such technical limitations might soon be overcome by increasing computational power, it is questionable whether cellular detail needs to be considered when investigating large scale pattern formation and dynamics. Another disadvantage of discrete models and corresponding simulations of tissue growth is intrinsic to numerical simulations in general: the obtained results can only be interpreted *a posteriori*, and in the absence of analytical expressions for the dynamics and mechanical stresses no strong predictions of the model behavior upon parameter variations can be made.

Continuum descriptions of tissue mechanics

The advantage of continuum descriptions of (growing) tissues is two-fold. First, continuum mechanics provides a well-established framework to discuss material behavior on macroscopic scales, at least for passive materials.[9] Second, the formulation of the tissue-mechanics problem in terms of partial differential equations allows in principle to derive analytical expressions for the stress distribution and the cell flow field. For large systems, these flow patterns can vary over length scales large compared to a single cell, see Fig. 1.10, and continuum descriptions may turn out to be appropriate.

It is less obvious, however, how to describe the tissue mechanical properties within the

[8] In quasi-static models that aim to describe stable stationary configurations, different energy minimization routines could lead to different local minima; in finite-element models, the exact placement of viscous elements is somehow arbitrary.

[9] The theory of elasticity has been formalized in the 19$^{\text{th}}$ century by Euler, Cauchy, Barré de Saint-Venant, Lamé and many others.

framework of continuum mechanics. In the context of tissue growth, different constitutive equations have been proposed [105, 153, 181]. The descriptions range from elastic [11, 84], visco-plastic [12, 154], to liquid-like [17, 27] behavior in the absence growth, reflecting the diversity of mechanical properties among different tissues. In addition, the way how growth of the tissue is considered varies across the literature [105, 181]. Finally, some of these models describe the dynamics of more than one material component, taking the extracellular matrix and/or the interstitial fluid additionally into account, or couple the growth dynamics to nutriment abundance [38, 37, 153, 154].

Elastic growth models have proven well suited to describe the residual stresses that result from incompatible growth [51, 84, 164]. The assumption that the tissue behaves as an elastic solid at all times seems to be appropriate for plants in particular, mostly because plant cells have a solid cell wall which is not continually remodeled [8, 84]. However, other soft animal tissues such as arterial walls have been successfully described as hyperelastic materials, based upon the collagen-fiber reinforced microstructure of the tissue [76]. A class of models known as morphoelasticity uses finite elasticity theory in conjunction with volumetric growth to address the stability of resulting tissue configurations, and different instabilities due to growth have been found [11, 81, 83]. A central assumption of morphoelasticity is that the total, finite deformation can be decomposed into a contribution due to growth and an elastic deformation that ensures material compatibility [161]. Therefore, these models implicitly assume the existence of an unstressed reference state, which is not necessarily compatible with material or tissue integrity. An incremental morphoelasticity theory has been proposed that may circumvent conceptual problems in the limit of large deformations [82, 185].

At the other end of possible choices of constitutive relations, we find growing tissues described as viscous liquids [17, 27]. Basan and colleagues discussed a hydrodynamic instability related to tissue growth that stems from viscous shear stresses due to differential proliferation [15]. In between these extremes—fully viscous and solid-like tissues—mixture theory allows to separately account for an elastic extracellular matrix component and an "elastic fluid"-like cell component [105, 154]. Recently, Ciarletta and coworkers used this approach to analyze shape instabilities of early-stage melanoma [10, 42].

1.4 Overview of this thesis

Although the rich variety of biophysical descriptions of tissue growth present in the literature might to some degree reflect the skill and taste of the dedicated scientist, it is foremost due to the richness of organic life itself. For the physics of tissues may well obey the laws of Newton, the variety of biological functions performed by different tissues suggests that these may also behave differently from a mechanical point of view.

In this thesis, we address the physics of tissue growth from a slightly different angle. Starting from an elastic tissue behavior in the absence of cell division and apoptosis, we aim at understanding the effect of cell division and cell death on the material properties at long times. In chapter 2, we introduce the continuum mechanics framework that we employ and derive effective constitutive equations in the presence of cell division

and cell death. We then discuss two examples of tissue growth where we make use of the obtained equations. We introduce noise related to cell division and apoptosis and calculate the effective diffusion coefficient of cells at the homeostatic state at which cell division and apoptosis balance. A calculation of the height-fluctuations of a thin tissue layer is furthermore presented.

In chapter 3, we extend our continuum description to a two-component model of tissues, taking the interstitial fluid explicitly into account. This allows us to discuss the effect of a finite permeability of the tissue on its dynamics when subjected to an external pressure. If the material densities of fluid and cell phase differ, gravity leads to additional forces, and we discuss a hypothetical "gravitational treadmilling" non-stationary steady state of a tissue. The calculation of the diffusion constant of cells at the homeostatic state reveals a damping of cell diffusion due to cell-fluid friction.

Finally, we address in chapter 4 the dynamics of two distinct cell populations within one tissue. Here, as throughout this thesis, we focus on the role of a coupling between the rate of cell division and the mechanical stress. We combine analytical limits and numerical calculations to study the dynamics of an interface between two cell populations that differ in their mechanical control of growth.

Each of these chapters is framed by a short introduction and a discussion of the results. We conclude this thesis with some general remarks and point out future directions of research.

Chapter 2

Fluidization of tissues due to cell division and apoptosis

In this chapter, we develop a continuum description of tissue mechanics that takes into account the effects of cell division and apoptosis. Whereas various models of tissue growth have been proposed before, including models that are formulated in terms of continuum mechanics, these models mostly postulate constitutive equations for the tissue stress that seem appropriate to describe their relevant mechanical properties. Although the respective choice of constitutive equation may often be well corroborated by experiments or by resemblance with well-studied materials, our approach here is different. Based on a few assumptions about the tissue material properties in the absence of cell division and apoptosis—for simplicity, we consider tissues then to be elastic—, we try to derive the constitutive equation for the tissue stress in the presence of cell division and cell death.

2.1 Introduction: Tissue rheology revisited

Biological tissues exhibit a wide variability of mechanical properties. On the cellular level, this is illustrated by the completely different architecture of plant cells compared to animal cells. Whereas plant cells have a solid cell wall to resist a high internal turgor pressure, such a cell wall is totally absent in animal cells. On the tissue level, we find that tissue mechanical properties are often closely linked to tissue function; a non-comprehensive list of mechanically distinct tissues includes bone, skin, arteries, and grey matter. In the following, and throughout this work, we focus our analysis on soft animal tissues which are composed of large assemblies of (living) cells. What does soft mean in this context? We consider tissues as soft if their elastic response at the time scale of several seconds is characterized by an elastic modulus in the range of several to several thousand Pa. In general, this definition coincides with less physical and more physiological inspired definitions put forward elsewhere[1]; note however that we do not exclude

[1]Wikipedia cites the online Dictionary of Cancer Terms of the National Cancer Institute, which states that soft tissue refers to "muscle, fat, fibrous tissue, blood vessels, or other supporting tissue of the

epithelia or cell monolayers by our definition as might be the case for other authors.

The mechanical properties of tissues have mostly been characterized by their response to applied forces or deformations. Step-stress or step-strain experiments allow for measurements of the elastic modulus and viscoelastic stress relaxation times. For soft tissues, it makes sense to refer to this characteristic behavior as tissue rheology. Various continuum mechanics models have been put forward to account for the stress-strain curves obtained for skin [117], adipose [77] and brain tissue [99], for example. The theoretical approaches range from finite elasticity models described by non-linear strain energy functions to modeling by constitutive equations that describe generalized viscoelastic solids (see [71, especially chap. 2 & 7] for an exhaustive discussion and references therein). Rheological measurements are mostly carried out for adult non-proliferating tissues and on macroscopic length scales of several mm, however, and the models that aim at reproducing the experimental data do not apply in a straightforward way to embryonic tissues or early-stage tumors.

Morphogenetic processes during animal development already suggest that the mechanical properties of embryonic and adult tissues ought to be different, given that the former repeatedly need to change their form and position in the developing body. It has been argued that embryonic tissues can effectively be considered as viscous fluids—as opposed to elastic solids—on the time scales of several minutes up to hours; most notably, the late Malcolm Steinberg proposed as early as 1963 an explanation for cell sorting experiments that drew on an analogy between aggregates of embryonic cells and liquids [172]. His Differential Adhesion Hypothesis (DAH) suggests that differences in cell-cell adhesion drive the sorting out of cells of different type and can explain the observed engulfment patterns of cell aggregates. In the meantime, his ideas have been tested experimentally for aggregates of various embryonic cell types and in different experimental settings [21, 63, 64, 65, 66]. Although the DAH may be over-simplifying in neglecting certain relevant cell mechanical contributions to cell sorting such as cell contractility [109], his key idea—differences in interfacial tensions lead to cell sorting—has not been proven wrong.[2] Later, this idea has been refined by Brodland and colleagues, who introduced their formulation under the name of the Differential Interfacial Tension Hypothesis [31, 32]. In a recent paper Manning and colleagues disentangled the respective contributions from cell-cell adhesion and cortical tension to tissue surface tension [120].

The analogy between tissues and viscous fluids itself does not yet explain how elastic stresses relax, however. First of all, whether a tissue effectively behaves as a viscous fluid depends on the time scale of the phenomenon under study. Moreover, different relaxation processes may take place in tissues which would give rise to a hierarchy of different relaxation times. As tissue growth implies repeated rounds of cell division and takes place on time scales going from several hours to days, it is natural to ask how

body" [2]; another source cited defines soft tissues as "nonepithelial, extraskeletal mesenchyme exclusive of the reticuloendothelial system and glia" [169] (after [3]). Sometimes this term is extensively used without being defined at all as for example does Fung in his book on biomechanics of living tissues [71].

[2]The debate whether visco-elastoplastic constitutive equations are more appropriate to describe experimental data of tissue surface tension measurements is not yet completely settled, however, see [119, 152] for a view contesting Steinberg and followers.

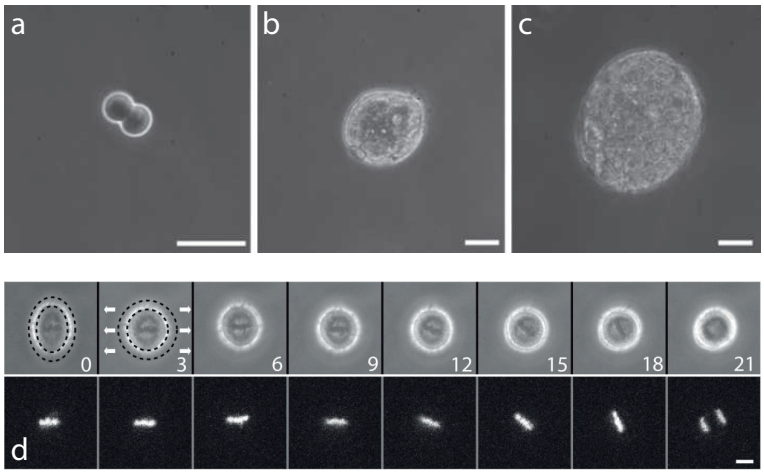

Figure 2.1. Coupling between mechanical conditions and proliferation. (a-c) Multicellular tissue spheroids can grow against an elastic matrix, where the final size depends on the opposing matrix rigidity. Here, we show a tumor spheroid made up of cells of the human breast cancer cell line MCF-7 growing in an agarose hydrogel of a stiffness 1-2 kPa after 1, 11, and 27 days, respectively. The scale bars are 50 μm; figure modified after [69]. (d) Here, the stretch-induced reorientation of the mitotic spindle is shown. Fink and colleagues plate a cell (retinal pigment epithelial cell line, hTERT-RPE1) on a silicon substrate, where the cell attaches to an oval fibronectin pattern (leftmost image). The lower panel shows the mitotic spindle of the cell before cell division via DNA staining, which is indicative of the cell division orientation. In the absence of additional clues, the cell divides along its long axis. By stretching the substrate along the perpendicular axis (see arrows), the oval pattern is deformed into a circle and the geometric anisotropy no longer persists. The cell responds to the induced anisotropy of the mechanical stress by reorientation of the mitotic spindle (from left to right, relative times are given in minutes). Scale bar 10 μm; figure taken from [60].

cell proliferation might influence the tissue mechanical properties over long times. Many experiments suggest that the interplay between tissue mechanics and growth is two-fold: not only may cell proliferation alter tissue mechanical properties, but mechanical conditions interfere with cell division and apoptosis. A classic experiment is the growth of multicellular aggregates embedded in an elastic hydrogel [95], see Fig. 2.1(a-c) for an example of such growth. The final size of the tissue aggregates depends on the matrix stiffness, indicating that accumulated elastic stress due to the deformation of the matrix eventually prevents further cell proliferation. Another example of a possible coupling between mechanical conditions and growth concerns the orientation of the cell division axis by external mechanical stresses [61, 126]. Recently, Fink *et al.* reported that in the absence of geometrical cues, the anisotropy of externally applied stresses suffices to reorient the mitotic spindle of dividing cells [61], see also Fig. 2.1(d). In our study, we thus try to unravel the implications of such mutual interplay between tissue mechanics and growth.

This chapter is organized as follows. In the next section, we introduce the basic

balance equations and establish the mechanical stress contributions of cell division and cell death. This allows us to develop effective constitutive equations for the stress that take cell division and apoptosis into account. For tissues growing in a fixed volume, cell division and apoptosis eventually balance, which leads us to a discussion of the homeostatic state (sec. 2.3). In section 2.4, we discuss two examples of tissue growth in which the mechanical coupling between cell division/apoptosis and stress plays a decisive role. We then discuss the role of noise, which allows us to calculate an effective diffusion coefficient of cells at the homeostatic state (sec. 2.5), before we close this chapter with a discussion of the results.

2.2 Growing tissues as elastic media

We aim at describing the stress distribution and cell flows on large length scales. We thus consider the tissue as a continuous material without accounting for its structure at the cellular scale. In particular, we do not distinguish individual cells but formulate balance equations in terms of averaged (cell number and momentum flux) densities, see Fig. 2.2 for an illustration. Furthermore, we assume that the tissue is highly permeable to interstitial fluid flow at the relevant time and length scales, which allows us to describe the tissue by a single material component only. In the next chapter, we will relax this assumption and extend the one-component theory presented here to a multi-component description.

We first discuss the balance equations for cell number and momentum flux densities. We then introduce the constitutive relations that describe the tissue elasticity at short times, *i.e.*, in the absence of cell turn-over, before establishing the concept of stress sources introduced by cell division and apoptosis.

2.2.1 Cell number and momentum balance

Cell number balance

Cell number balance is described by a conservation equation for the cell number density n,

$$\partial_t n + \partial_\alpha (n v_\alpha) = (k_\mathrm{d} - k_\mathrm{a})\, n. \tag{2.1}$$

Here, we introduced the cell flow velocity v_α, which appears in the convective term on the left-hand side. Greek indices denote the Cartesian coordinates x, y, z; and ∂_α is short-hand for $\partial/\partial x_\alpha$. Einstein's summation convention over repeated indices is implied. In addition to convective transport, however, cell division and cell death can change the local density of cells, which gives rise to the source term on the right-hand side. Here, k_d and k_a denote the rates of cell division and apoptosis, respectively. Note that the above equation can be rewritten as

$$\frac{\mathrm{d}}{\mathrm{d}t} n = n\,(k_\mathrm{d} - k_\mathrm{a} - \partial_\alpha v_\alpha)\,,$$

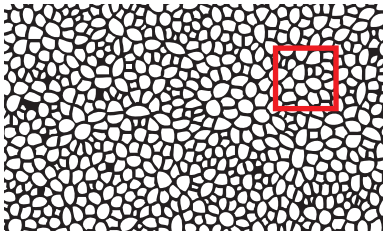

Figure 2.2. Continuous quantities such as the cell number density n and the cell flow velocity v_α are obtained via an averaging procedure. A typical averaging volume (here shown in red) is large compared to the size of a single cell and small compared to typical length scales over which the averaged quantities vary.

where we introduced the convected time derivative $(\mathrm{d}/\mathrm{d}t) = \partial_t + v_\alpha \partial_\alpha$; in a convected volume element, the cell number density remains constant if the number growth rate $k_\mathrm{a} - k_\mathrm{d}$ is equal to the volume growth rate $\partial_\alpha v_\alpha$.

Another remark is due here. Let ρ be the actual mass density of the tissue. The average cell volume Ω_c is simply given by n^{-1}, and subsequently $M_\mathrm{c} = \rho\Omega_\mathrm{c} = \rho/n$ is the average mass of a single cell. The cell number balance (2.1) then leads to

$$\partial_t \rho + \partial_\alpha(\rho v_\alpha) = (k_\mathrm{d} - k_\mathrm{a})\,\rho + \frac{\rho}{M_\mathrm{c}} \frac{\mathrm{d}}{\mathrm{d}t} M_\mathrm{c}, \tag{2.2}$$

i.e., we obtain a mass conservation equation with source terms. In other words, the total mass of the tissue is not conserved, which is not surprising in the case of growing tissues. Obviously, a one-component description simply cannot account for actual mass conservation at the cellular level, which points to the necessity to introduce a second component if mass conservation should be obeyed. This program is carried out in chapter 3 of this work. In the following, we simply assume that the actual mass density $\rho = M_\mathrm{c}/\Omega_\mathrm{c}$ of cells and thus of the tissue is constant in space and time.

Momentum balance

For systems with finite mass density ρ, the conservation of linear momentum is expressed by

$$\partial_t(\rho v_\alpha) + \partial_\beta(\rho v_\alpha v_\beta) = \partial_\beta \sigma_{\alpha\beta} + f_\alpha^\mathrm{ext}. \tag{2.3}$$

In the absence of internal and external forces, the rate of change of the linear momentum density ρv_α is only due to a convective momentum density flux described by $\rho v_\alpha v_\beta$. Internal and external forces act as momentum sources, however, and are taken into account on the right-hand side of the above equation. Here, internal forces can be described as the divergence of a momentum density flux tensor $\sigma_{\alpha\beta}$, which is called the stress tensor. External forces are described by the force density f_α^ext.

We can estimate the respective orders of magnitude of the different terms by a simple argument. The mass density of the tissue is approximately the mass density of water, $\rho \approx \rho_{\mathrm{H_2O}} \approx 10^3\,\mathrm{kg\,m^{-3}}$. Typical velocities of cells are in the range of several μm/s to μm/d, *i.e.*, $v_\alpha \lesssim 10^{-7}\,\mathrm{m\,s^{-1}}$, and we can safely assume that typical time and length scales are also in the range of several seconds and μm, respectively. We thus obtain upper estimates $\partial_t(\rho v_\alpha) \approx 10^{-6}\,\mathrm{N\,m^{-3}}$ and $\partial_\beta(\rho v_\alpha v_\beta) \approx 10^{-5}\,\mathrm{N\,m^{-3}}$ for the convected rate of change of momentum per unit volume. What are the corresponding orders of

magnitude for the source terms on the right-hand side? Without specifying the actual form of $\sigma_{\alpha\beta}$, we know that typical forces exerted by cells lie in the range of several nN, which corresponds to a force density of $\approx \mathrm{nN}/\mu\mathrm{m}^3 = 10^9\,\mathrm{N\,m^{-3}}$! Even if our estimates were wrong by some orders of magnitude, we still could safely neglect the inertial terms on the left-hand side of equation (2.3). We thus consider that internal and external forces are always balanced and write force balance as

$$\partial_\beta \sigma_{\alpha\beta} = -f_\alpha^{\mathrm{ext}}. \tag{2.4}$$

In hydrodynamics, this equation corresponds to the so-called Stokes limit of the Navier-Stokes equation for small Reynolds number. Biological microswimmers like sperm or bacteria such as *Escherichia coli*, for example, move at low Reynolds number; see also the classic account of Purcell [156].

We finally note that if the total angular momentum is conserved, the stress tensor $\sigma_{\alpha\beta}$ can always be taken symmetric, see Ref. [125, appendix A] for a detailed discussion.[3]

2.2.2 Elastic stress and source stress due to cell division and apoptosis

In order to describe the actual tissue dynamics, we need to specify the constitutive relations that govern the tissue mechanical behavior. Here, we elaborate on what we mean by "growing tissues as elastic media." Whereas we try to present the theory as self-contained as possible, we will occasionally refer to appendix A for some further technical details.

Cell division and apoptosis as force dipoles

We consider a tissue in which cells are linked to their neighbors by adhesion molecules. We assume that at time scales short compared to cell division and apoptosis, this tissue behaves as an elastic solid. For small deformations, the tissue elasticity is described by a linear relation between stress and strain,

$$\sigma_{\alpha\beta}^{\mathrm{el}} = C_{\alpha\beta\gamma\nu} u_{\gamma\nu}\,, \tag{2.5}$$

where $\sigma_{\alpha\beta}^{\mathrm{el}}$ denotes the elastic stress in the tissue and $u_{\gamma\nu} = \frac{1}{2}(\partial_\gamma u_\nu + \partial_\nu u_\gamma)$ is the strain tensor, the deformation field being denoted by u_γ. For simplicity, we consider that the tissue is isotropic; the tensor of elastic constants is then given by $C_{\alpha\beta\gamma\nu} = \chi\,\delta_{\alpha\beta}\delta_{\gamma\nu} + 2\mu\,(\delta_{\alpha\gamma}\delta_{\beta\nu} - \delta_{\alpha\beta}\delta_{\gamma\nu}/3)$, where χ and μ are the bulk and shear elastic moduli, respectively.

At longer time scales, the tissue is remodeled by the appearance of new cells by division and the disappearance of cells by cell death. Division and apoptosis imply a

[3] The total angular momentum density can be split into an orbital contribution due to the center-of-mass motion of individual volume elements and a spin contribution that describes the angular momentum in the rest frame of local volume elements. The antisymmetric part of the stress tensor then describes the transfer of angular momentum between these contributions. Recent work on active chiral fluids by Fürthauer and colleagues considers cases of active torque generation at the microscopic level in which it is advantageous to keep the antisymmetric part of the stress tensor, see ref. [177] for a detailed discussion.

change of local stress generated actively. Thermodynamically speaking, tissues are far-from-equilibrium systems, and cells can consume free energy in order to drive all kinds of active processes [137]. Here, we consider the sum of the forces generated by cells during the process of duplication or cell death, *i.e.*, we include the phases of cell growth and the subsequent division when referring to a cell division event. Because these forces are of internal origin and have to be balanced locally, cells cannot exert any net force, and the local force distribution associated with division and apoptosis events can be characterized by its dipole moment, see appendix A. In a continuum description, the local stress associated with each event can thus be described by a point force dipole $d_{\alpha\beta}$. Because division and apoptosis do not generate any net torque in general, we take $d_{\alpha\beta} = d_{\beta\alpha}$. The associated force dipole density in the tissue is $D_{\alpha\beta} = \sum_n d^{(n)}_{\alpha\beta}\delta(\mathbf{r} - \mathbf{r}_n)$, where we sum over all force dipoles. The strain induced by a static ensemble of force dipoles is given by

$$u^{\mathrm{d}}_{\alpha\beta} = \sum_n H_{\alpha\beta\gamma\nu}(\mathbf{r} - \mathbf{r}_n) d^{(n)}_{\gamma\nu}\,, \tag{2.6}$$

where $H_{\alpha\beta\gamma\nu}$ is the Green's function corresponding to a point dipole (appendix A). The elastic stress $\sigma^{\mathrm{el}}_{\alpha\beta}$ now contains contributions $C_{\alpha\beta\gamma\nu}u^{\mathrm{ext}}_{\gamma\nu}$ due to external forces $f^{\mathrm{ext}}_{\alpha}$ and contributions from the strain induced by the force dipole density $D_{\alpha\beta}$. In the presence of both internal force dipoles and external forces, the elastic stress satisfies the force balance equation

$$\begin{aligned} \partial_\beta \sigma^{\mathrm{el}}_{\alpha\beta} &= -f^{\mathrm{int}}_{\alpha} - f^{\mathrm{ext}}_{\alpha} \\ &= \partial_\beta D_{\alpha\beta} - f^{\mathrm{ext}}_{\alpha}\,, \end{aligned} \tag{2.7}$$

where we used that $f^{\mathrm{int}}_{\alpha} = -\partial_\beta D_{\alpha\beta}$ is the density of internal forces associated with a force dipole density $D_{\alpha\beta}$. The total stress $\sigma_{\alpha\beta}$ satisfies the force balance $\partial_\beta \sigma_{\alpha\beta} = -f^{\mathrm{ext}}_{\alpha}$, and from Eq. (2.7), it follows that the total stress in the tissue is given by

$$\sigma_{\alpha\beta} = \sigma^{\mathrm{el}}_{\alpha\beta} - D_{\alpha\beta}\,. \tag{2.8}$$

We can identify the stresses that are introduced by cell division and apoptosis as $\sigma^{\mathrm{s}}_{\alpha\beta} = -D_{\alpha\beta}$, which act as a source of stress in the tissue.

Dynamic force dipole densities: From deformation to flow

For a simple elastic material in the absence of remodeling, the elastic stress can be expressed in terms of the deformation gradient $u_{\alpha\beta}$ as expressed in Eq. (2.5). Here, u_α is the deformation with respect to a stress-free reference configuration. In the presence of permanent cell division and apoptosis, such a unique reference state of the strain can no longer be defined. However, differences of strain between subsequent states still have a meaning. In general, a local flow field $\mathbf{v}(\mathbf{r}, t)$ exists such that

$$u_{\alpha\beta}(t) - u_{\alpha\beta}(t_0) = \int_{t_0}^{t} \mathrm{d}t'\, v_{\alpha\beta}(t') \tag{2.9}$$

to linear order. Here, $v_{\alpha\beta} = \frac{1}{2}(\partial_\alpha v_\beta + \partial_\beta v_\alpha)$ denotes the velocity gradient of the flow. The changes in stress at time t, starting from an initial state at t_0, are given to linear order by

$$\sigma_{\alpha\beta}(t) - \sigma_{\alpha\beta}(t_0) = C_{\alpha\beta\gamma\nu}\left[u_{\gamma\nu}(t) - u_{\gamma\nu}(t_0)\right] + \sigma^{\mathrm{s}}_{\alpha\beta}(t) - \sigma^{\mathrm{s}}_{\alpha\beta}(t_0)\,, \tag{2.10}$$

where we assumed that eventual external forces are constant in time. Alternatively, we can express the dynamic change of the stress as a differential equation,

$$\frac{\mathrm{D}}{\mathrm{D}t}\sigma_{\alpha\beta} = C_{\alpha\beta\gamma\nu}v_{\gamma\nu} + \frac{\mathrm{D}}{\mathrm{D}t}\sigma^{\mathrm{s}}_{\alpha\beta}\,, \tag{2.11}$$

where $(\mathrm{D}/\mathrm{D}t)\sigma_{\alpha\beta} = \partial_t\sigma_{\alpha\beta} + v_\gamma\partial_\gamma\sigma_{\alpha\beta} + \omega_{\alpha\gamma}\sigma_{\gamma\beta} + \omega_{\beta\gamma}\sigma_{\alpha\gamma}$ is the co-rotational time derivative which captures geometric nonlinearities and $\omega_{\alpha\beta} = (1/2)(\partial_\alpha v_\beta - \partial_\beta v_\alpha)$ is the vorticity of the flow. Equations (2.10) and (2.11) are independent of any reference state, in contrast to equation (2.8). Note that the elastic behavior at short times is still captured by the first term on the right-hand side. The second term on the right-hand side describes the stress increments in time due to dynamic force dipole densities. In the following, we establish the form of the rate of change of the source stress caused by cell division and apoptosis. In order to discuss the respective contributions separately, we introduce the isotropic and the traceless parts of the total stress, σ and $\tilde{\sigma}_{\alpha\beta}$, respectively, with $\sigma_{\alpha\beta} = \sigma\delta_{\alpha\beta} + \tilde{\sigma}_{\alpha\beta}$.

2.2.3 Isotropic contribution to the source stress, equation of state

The force dipoles associated with cell division and apoptosis can similarly be split into isotropic and traceless parts. We discuss the isotropic contributions first. In addition to the traceless part discussed later, each cell division creates a positive isotropic force dipole $d_{\mathrm{d}}\delta_{\alpha\beta}$, with $d_{\mathrm{d}} > 0$, that contributes to the source stress $\sigma^{\mathrm{s}}_{\alpha\beta}$; each apoptosis event contributes a negative force dipole $d_{\mathrm{a}}\delta_{\alpha\beta}$, with $d_{\mathrm{a}} < 0$. The rate of change of the isotropic component of the source stress is related to the rates of cell division and of apoptosis. In a tissue with permanent cell division and apoptosis, the isotropic part of the source stress therefore changes as

$$\frac{\mathrm{d}}{\mathrm{d}t}\sigma^{\mathrm{s}} = -n\left(d_{\mathrm{d}}k_{\mathrm{d}} + d_{\mathrm{a}}k_{\mathrm{a}}\right)\,, \tag{2.12}$$

where we used that $\sigma^{\mathrm{s}}_{\alpha\beta} = -D_{\alpha\beta}$ and that there are nk_{d} cell divisions and nk_{a} apoptosis events per unit volume per unit time. From Eq. (2.11) we then find the dynamic equation for the isotropic part of the stress in the presence of cell division and apoptosis,

$$\frac{\mathrm{d}}{\mathrm{d}t}\sigma = \chi v_{\gamma\gamma} - n\left(d_{\mathrm{d}}k_{\mathrm{d}} + d_{\mathrm{a}}k_{\mathrm{a}}\right)\,, \tag{2.13}$$

where $v_{\gamma\gamma} = \partial_\gamma v_\gamma$ is the divergence of the cell flow. Note that the rates of division and apoptosis k_{d} and k_{a} generally depend on local stress as well as on cell density.

The stress increments d_{d} and d_{a} are phenomenological, macroscopic parameters describing forces generated at the cellular scale. In principle, these forces can vary with the

state of a cell, *i.e.*, cell size, cell stress, or abundance of certain proteins. Let us consider the two limit cases $d_\mathrm{d} = 0$ and $d_\mathrm{a} = 0$. If we had $d_\mathrm{d} = 0$, dividing cells would not exert any force on the surrounding cells. This case describes cell divisions without subsequent growth where cells divide by simply introducing a new cell-cell contact. In developing embryos, this form of cell division without increasing total tissue mass is called cleavage. In many species, the fertilized egg cell undergoes rapid rounds of cleavage to form a large cluster of undifferentiated cells before morphogenesis starts [192]. Divisions of this type are certainly limited by the finite size of the nucleus which cannot be reduced further. In the case $d_\mathrm{a} = 0$, cell death does not introduce any force dipole in the tissue; this limit corresponds to cell death being described by discounting the dead cell from the number density n of (living) cells without removing the debris from the tissue. Note that mechanical equilibrium for vanishing net number growth rate $k_\mathrm{d} - k_\mathrm{a} = 0$ implies $d_\mathrm{a} = -d_\mathrm{d}$, however, although strictly speaking this needs to be true on average only.[4]

Equation of state for the cell volume

Can we be more precise? We assume that the cell volume $\Omega_\mathrm{c} = n^{-1}$ is under cellular control and depends on the isotropic part of the stress. In the simplest form this implies an equation of state

$$\sigma = \sigma(n)\,, \tag{2.14}$$

relating isotropic stress and cell density. As a consequence of this simple choice, the stress σ depends only on the current cell configuration but not on history. Note that in general the relation between cell density and stress is more complex and can involve memory. Developmental, genetic programs could give rise to changes in cell volume that are not accompanied by or due to changes in stress; we mentioned the repeated rounds of cleavage of the fertilized egg above.

The existence of an equation of state thus implies that we can express changes in stress in terms of changes in cell number density, or more precisely

$$\frac{\mathrm{d}\sigma}{\mathrm{d}t} = \frac{\mathrm{d}\sigma}{\mathrm{d}n}\frac{\mathrm{d}n}{\mathrm{d}t}\,.$$

Using the cell number balance (2.1), we find that this is compatible with Eq. (2.13) only if $n(d_\mathrm{d}k_\mathrm{d} + d_\mathrm{a}k_\mathrm{a}) = \chi(k_\mathrm{d} - k_\mathrm{a})$, so that $d = d_\mathrm{d} = -d_\mathrm{a}$ and $d = \chi/n$. In order to squeeze new cells into the tissue, dividing cells have to expend on average an elastic energy d which scales with the bulk modulus χ and the cell volume n^{-1}. The same elastic energy is liberated on average when cells die and are disposed of after cell death. The total stress thus obeys

$$\frac{\mathrm{d}}{\mathrm{d}t}\sigma = -\frac{\chi}{n}\frac{\mathrm{d}n}{\mathrm{d}t}\,,$$

which using once more cell number balance (2.1) can finally be rewritten as

$$\frac{\mathrm{d}}{\mathrm{d}t}\sigma = \chi\left[v_{\gamma\gamma} - (k_\mathrm{d} - k_\mathrm{a})\right]\,. \tag{2.15}$$

[4] This average is two-fold, averaging forces over the cell cycle and in a local volume element as implied by a continuum theory.

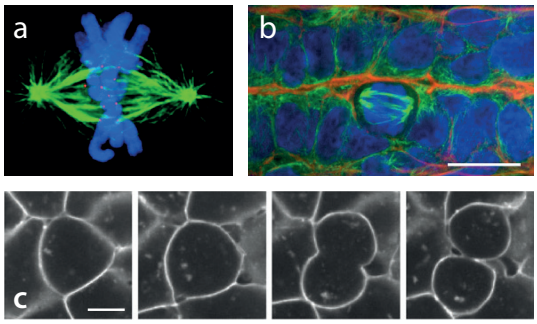

Figure 2.3. Orientation of the mitotic spindle and subsequent cell division. (a) A mitotic spindle in metaphase, *i.e.*, before the separation of the duplicated chromosomes. The spindle is formed by microtubules (green) that emanate from the two opposed spindle poles. During anaphase, the DNA (blue) is pulled towards the two ends of the spindle via pulling forces exerted on the kinetochores (red); figure taken from [53]. (b) An epithelial cell (mouse mammary duct) in metaphase-to-anaphase transition. Note that the mitotic spindle defines an axis along which the cell eventually divides. Instead of the kinetochores, polymerized actin is additionally shown in red. Scale bar 10 μm; figure modified from [146]. (c) Fluorescence micrograph of a dividing cell in the zebrafish neuro-ectoderm during late epiboly. Embryos were labeled with membrane-GFP. Scale bar 10 μm; figure modified from [167].

We remark here that for $d \neq \chi/n$, Eq. (2.13) corresponds to more complicated equations of state for the cell stress that involve memory.

Incompressible tissue

Let us quickly discuss the limit of an incompressible tissue. Here, we consider a tissue to be incompressible if the cell number density is constant, $n = n_0$, and the bulk elastic modulus $\chi = -n\frac{\mathrm{d}\sigma}{\mathrm{d}n} \to \infty$. In this case, the isotropic part of the stress σ is no longer defined by an equation of state but becomes a Lagrange multiplier in order to ensure the constraint $v_{\gamma\gamma} = k_\mathrm{d} - k_\mathrm{a}$.

2.2.4 Anisotropic contribution to the source stress

We now discuss the anisotropic contribution to the source stress generated by cell division and apoptosis. Cell division is an intrinsically oriented process. The orientation of cell division first manifests itself in the orientation of the mitotic spindle, see Fig. 2.3. In the absence of external cues and for cells that do not exhibit a pronounced shape anisotropy, the orientation of the mitotic spindle is necessarily uniformly distributed. The orientation of the mitotic spindle can be aligned on average, however, such that there exists a preferred axis of cell division. This anisotropy can be induced by external stresses [61], by internal factors such as the planar cell polarity pathway [167], or signaling cues such as morphogen gradients [26]. Here, it is not important whether this anisotropy of cell division is mediated via a finite shape anisotropy of cells or not. Note however that for isotropic tissues, shape anisotropy and cell division orientation align on average for small perturbations. Averaging the cell division anisotropy in a small volume defines

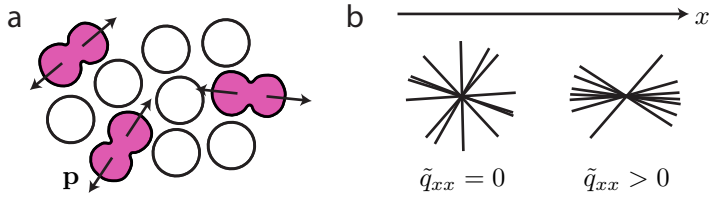

Figure 2.4. Average anisotropy of the cell division axis. (a) The axis of cell division is characterized by a vector $\mathbf{p}$ of unit length. The average over these orientations defines the nematic tensor $\tilde{q}_{\alpha\beta}$, see text for details. (b) If cell divisions are random, the order parameter vanishes (left panel). If cell divisions are aligned on average along the x-axis, one finds $\tilde{q}_{xx} > 0$.

the nematic tensor $\tilde{q}_{\alpha\beta} = \langle p_\alpha p_\beta - \frac{1}{3}\delta_{\alpha\beta} \rangle$, where the unit vector $\mathbf{p}$ defines the axis of cell division, see Fig. 2.4.

For simplicity, we consider first the case of an isotropic tissue in the absence of external cues such as morphogen gradients or planar cell polarity. The effect of additional guidance cues will be discussed further below. In a perfectly isotropic tissue, the nematic order tensor vanishes, as is the case for the traceless part of the stress due to symmetry. For small perturbations, the relaxation of the nematic tensor is driven mainly by the local anisotropic stress, and the rate of change of the nematic tensor to linear order is then given by

$$\partial_t \tilde{q}_{\alpha\beta} = -\frac{1}{\tau_\mathrm{q}} \left(\tilde{q}_{\alpha\beta} - \frac{\tilde{\sigma}_{\alpha\beta}}{\sigma_0} \right) . \tag{2.16}$$

Here, we have introduced the characteristic time scale $\tau_\mathrm{q} > 0$, which describes the dynamics of the alignment after a mechanical perturbation. The response of the cell anisotropy to stress is described by the coefficient $\sigma_0 > 0$. Note that the isotropic component of the stress does not contribute to the relaxation of the nematic tensor, which is traceless. In the following, we consider the case where the anisotropy relaxation is faster than cell division and apoptosis, such that

$$\tilde{q}_{\alpha\beta} \simeq \tilde{\sigma}_{\alpha\beta}/\sigma_0 \tag{2.17}$$

on the relevant time scales in the absence of additional fields that influence orientation.

Shear stress relaxation by oriented cell division

Cell division is anisotropic. In addition to the isotropic part discussed before, each division event contributes a change $-\tilde{d}^\mathrm{d}_{\alpha\beta}$ to the anisotropic component of the source stress $\tilde{\sigma}^\mathrm{s}_{\alpha\beta}$. Because the cell division axis is on average aligned with the local tissue anisotropy, the force dipole $\tilde{d}^\mathrm{d}_{\alpha\beta}$ is proportional to the nematic tensor, $\tilde{d}^\mathrm{d}_{\alpha\beta} = \tilde{d}_\mathrm{d}\tilde{q}_{\alpha\beta}$. Analogously, the contribution of force dipoles associated with apoptosis events $\tilde{d}_\mathrm{a}$ can be written as $\tilde{d}^\mathrm{a}_{\alpha\beta} = \tilde{d}_\mathrm{a}\tilde{q}_{\alpha\beta}$. Typically, one finds $\tilde{d}_\mathrm{d} > 0$ and $\tilde{d}_\mathrm{a} < 0$, see appendix A. Note

that for an isotropic tissue, mechanical balance does not require $\tilde{d}_\mathrm{a} = -\tilde{d}_\mathrm{d}$. For isotropic cells, $\tilde{d}_\mathrm{a} \approx 0$ even for small but finite cell division anisotropy.

The rate of change of the traceless part of the source stress is then given by

$$\frac{\mathrm{D}}{\mathrm{D}t}\tilde{\sigma}^\mathrm{s}_{\alpha\beta} = -n\left(\tilde{d}_\mathrm{d}k_\mathrm{d} + \tilde{d}_\mathrm{a}k_\mathrm{a}\right)\tilde{q}_{\alpha\beta}\,, \tag{2.18}$$

and we find for the rate of change of the anisotropic stress, Eq. (2.11),

$$\frac{\mathrm{D}}{\mathrm{D}t}\tilde{\sigma}_{\alpha\beta} = 2\mu v_{\alpha\beta} - n\left(\tilde{d}_\mathrm{d}k_\mathrm{d} + \tilde{d}_\mathrm{a}k_\mathrm{a}\right)\tilde{q}_{\alpha\beta}\,. \tag{2.19}$$

Using $\tilde{q}_{\alpha\beta} \simeq \tilde{\sigma}_{\alpha\beta}/\sigma_0$, we finally obtain a constitutive relation for the traceless part of the stress for times which takes into account cell division and apoptosis,

$$\left(1 + \tau_\mathrm{a}\frac{\mathrm{D}}{\mathrm{D}t}\right)\tilde{\sigma}_{\alpha\beta} = 2\eta\tilde{v}_{\alpha\beta}\,. \tag{2.20}$$

Here, we introduced the relaxation time $\tau_\mathrm{a} = \left[n(\tilde{d}_\mathrm{d}k_\mathrm{d} + \tilde{d}_\mathrm{a}k_\mathrm{d})/\sigma_0\right]^{-1}$ and the effective shear viscosity $\eta = \tau_\mathrm{a}\mu$. The above equation is the constitutive equation of a Maxwell viscoelastic fluid. At short times $t < \tau_\mathrm{a}$, the tissue response is essentially elastic, whereas for long times $t \gg \tau_\mathrm{a}$ the traceless stress relaxes to zero and the tissue exhibits a fluid behavior. The cross-over time scale between the elastic and the viscous regime is set by the relaxation time τ_a. Note that for a growing tissue, this time scale is expected to be of the order of hours to days: If we assume that $\sigma_0 \sim \tilde{d}_\mathrm{d}/n \sim \mu$ as suggested by dimensional analysis, we find $\tau_\mathrm{a} \sim k_\mathrm{d}^{-1} \sim 10^5 - 10^6\,\mathrm{s}$ which is the average time it takes a cell to divide. The effective viscosity is then of order $\eta \sim k_\mathrm{d}^{-1}\mu \sim 10^6 - 10^{10}\,\mathrm{Pa\,s}$, depending on the cell division rate and the shear modulus μ. Whereas at first glance such orders of magnitude appear to be extremely slow or highly viscous, respectively, this stress relaxation mechanism may still play a role in developmental processes that take place on the time scale of days to weeks.

2.2.5 Polarized tissues

In the previous paragraphs, we considered that the tissue anisotropy described by the nematic tensor $\tilde{q}_{\alpha\beta}$ is small and set by the the anisotropic part of the stress only. In that case, tissue growth is essentially isotropic if no anisotropic external stresses are applied. However, in many situations tissues exhibit finite polarity even in the absence of externally applied stresses. In this case, cell polarity in the tissue is aligned on large scales. Such large scale patterns of cell polarity are known to exist in epithelia and other tissues [33, 186, 187, 194]. They could arise due to the existence of signaling gradients in the tissue, *e.g.*, morphogen gradients, or could be due to cells aligning their polarity with their neighbors. As argued above, cell division is on average oriented along the axis of cell polarity. Therefore, because cell division generates anisotropic stresses, tissue growth is anisotropic.

If the anisotropy is set by an external field such as a morphogen gradient, the anisotropy of the tissue in the absence of stress is given by a traceless nematic tensor $\tilde{q}^0_{\alpha\beta}$, see also [7]. In the presence of stress, the nematic tensor in the tissue relaxes toward this value according to

$$\partial_t \tilde{q}_{\alpha\beta} = -\frac{1}{\tau_\mathrm{q}} \left[\left(\tilde{q}_{\alpha\beta} - \tilde{q}^0_{\alpha\beta} \right) - \frac{\tilde{\sigma}_{\alpha\beta}}{\sigma_0} \right] . \tag{2.21}$$

As for isotropic tissues, we assume that the orientation dynamics of the nematic tensor is fast compared to cell division, and we can therefore write

$$\tilde{q}_{\alpha\beta} = \tilde{q}^0_{\alpha\beta} + \tilde{\sigma}_{\alpha\beta}/\sigma_0 \tag{2.22}$$

on the relevant time scales.

In polarized tissues, symmetry arguments suggest that the finite order parameter $\tilde{q}^0_{\alpha\beta}$ can couple to the elastic deformation and give rise to a spontaneous deformation $u^0_{\alpha\beta}$ in the stress-free state. We assume that the isotropic part of the stress is still defined by an equation of state (2.14). The traceless part of the elastic stress is then given by

$$\tilde{\sigma}^\mathrm{el}_{\alpha\beta} = C^\mathrm{uni}_{\alpha\beta\gamma\nu} \tilde{u}_{\gamma\nu} + w \tilde{q}^0_{\alpha\beta} \,, \tag{2.23}$$

where $C^\mathrm{uni}_{\alpha\beta\gamma\nu}$ is the tensor of elastic constants for a uniaxial material[5] and w is an elasto-nematic coupling coefficient [188]. In the theory of nematic elastomers, such a coupling arises naturally when writing down all the allowed terms in the free energy [118]. In a continuum description of tissues, which are systems that are intrinsically out-of-equilibrium, the stress $w\tilde{q}^0_{\alpha\beta}$ can be interpreted as an active stress due to anisotropic cell contractility; such active anisotropic stresses have been observed in the developing *Drosophila* germband, for example [157, 158].

We now discuss the traceless component of the stress tensor. The source stress due to cell division and cell apoptosis is still given by Eqs. (2.12) and (2.18), as for an isotropic tissue. For simplicity, we ignore the elastic anisotropy and choose elastic constants such

[5]For materials with uniaxial symmetry, the general form of the tensor of elastic constants is given by

$$C^\mathrm{uni}_{\alpha\beta\gamma\nu} = C_1 n_\alpha n_\beta n_\gamma n_\nu + C_2 \left(n_\alpha n_\beta \delta^\perp_{\gamma\nu} + \delta^\perp_{\alpha\beta} n_\gamma n_\nu \right) + C_3 \delta^\perp_{\alpha\beta} \delta^\perp_{\gamma\nu} + C_4 \left(\delta^\perp_{\alpha\gamma} \delta^\perp_{\beta\nu} + \delta^\perp_{\alpha\nu} \delta^\perp_{\beta\gamma} \right) + \tfrac{1}{2} C_5 \left(\delta^\perp_{\alpha\gamma} n_\beta n_\nu + \delta^\perp_{\alpha\nu} n_\beta n_\gamma + \delta^\perp_{\beta\gamma} n_\alpha n_\nu + \delta^\perp_{\beta\nu} n_\alpha n_\gamma \right) ,$$

where $\mathbf{n}$ is a unit vector pointing along the axis of anisotropy and $\delta^\perp_{\alpha\beta} = \delta_{\alpha\beta} - n_\alpha n_\beta$. The existence of an equation of state (2.14) requires that isotropic and anisotropic deformations decouple, which implies

$$C_1 + 2C_2 = 3C_3 + 2C_4 \,.$$

For nematic elastomers, symmetry furthermore requires that when describing deformations with respect to the new reference state $u^0_{\alpha\beta}$, the elastic constant C_5 vanishes as long as the isotropy of the unstressed reference state is *spontaneously* broken, *i.e.*, in the course of an isotropic-to-nematic phase transition, without any external fields or boundary conditions enforcing a precise axis of anisotropy. This so-called soft elasticity is neglected here because we assume that the "spontaneous" finite order parameter $\tilde{q}^0_{\alpha\beta}$ is set by external fields such as morphogen gradients or set by boundary conditions.

that $C^{\rm uni}_{\alpha\beta\gamma\nu}\tilde{u}_{\gamma\nu} = 2\mu\tilde{u}_{\alpha\beta}$.[6] Using the above expression, we then find that the traceless part of the stress tensor satisfies

$$\left(1 + \tau_{\rm a}\frac{\rm D}{{\rm D}t}\right)\tilde{\sigma}_{\alpha\beta} = 2\eta\tilde{v}_{\alpha\beta} - \sigma_0\tilde{q}^0_{\alpha\beta}\,. \tag{2.24}$$

Analogous to isotropic tissues, polarized tissues behave as a Maxwell viscoelastic fluid: The shear stress relaxes over a time $\tau_{\rm a} = \left[n(\tilde{d}_{\rm d}k_{\rm d} + \tilde{d}_{\rm a}k_{\rm d})/\sigma_0\right]^{-1}$ and the tissue is described by an effective shear viscosity $\eta = \tau_{\rm a}\mu$ at long times. Note that the effective shear viscosity becomes a tensor if elastic anisotropy is taken into account. However, there is an additional component of the stress on the right hand side of Eq. (2.24), which is proportional to the spontaneous nematic tensor $\tilde{q}^0_{\alpha\beta}$. This active stress is due to large scale patterns of cell polarity which locally orient cell division, and it has contributions proportional to the cell division rate and to the apoptosis rate, respectively. The magnitude $-\sigma_0$ of the active stress is negative if the cells orient along the principal axis of the stress as the tissue grows. This corresponds to a dilative active stress driving tissue elongation along the direction of cell division. Active stresses due to cell division have been first introduced by Bittig *et al.* [27]. Note furthermore that the above constitutive equation is similar to the constitutive equation obtained for active polar gels as a description of the cell cytoskeleton developed in Ref. [110], and the active stress has the same form as the active stress proposed therein.

2.3 The homeostatic state

In many situations, tissues do not actually grow in size or in cell number: Although cells might divide, they do so rather to compensate eventual cell death and guarantee tissue maintenance. Following other authors, we call such a state of balanced cell division and apoptosis a homeostatic state [17, 70]. In this section, we develop the concept of the homeostatic pressure as introduced by Basan and colleagues [17] and explore its consequences for the tissue dynamics close to the homeostatic state.

The isotropic homeostatic state

The isotropic homeostatic state is a homogeneous stationary state in which the cell density is constant, $n = n_{\rm h}$, there is no cell flow, $v_\alpha = 0$, the nematic tensor vanishes, $\tilde{q}_{\alpha\beta} = 0$, and the source stress $\sigma^{\rm s}_{\alpha\beta}$ is isotropic and time independent. Constant cell density and vanishing cell flow requires that $k_{\rm d} = k_{\rm a}$, *i.e.*, that cell division and apoptosis balance as discussed above. Constant source stress requires $d_{\rm d}k_{\rm d} + d_{\rm a}k_{\rm a} = 0$, and because $d_{\rm d} = -d_{\rm a} = d$, both conditions are identical.

[6] This corresponds to the choice

$$C_1 = C_3 + 2C_4\,, \quad C_2 = C_3\,, \quad C_5 = 2C_4\,,$$

where $C_4 = \mu$ and $C_3 = \chi - \frac{2}{3}\mu$; see also note 5 above.

We assume that for constant biochemical conditions, the rates of cell division and apoptosis, k_d and k_a, respectively, are functions of the cell number density n only. The condition $k_\mathrm{d}(n_\mathrm{h}) = k_\mathrm{a}(n_\mathrm{h})$ then determines the homeostatic density n_h, and via the equation of state this condition defines the isotropic stress at the homeostatic state, *i.e.*, the homeostatic pressure $P_\mathrm{h} = -\sigma(n_\mathrm{h})$. In principle, the rates of cell division and apoptosis depend also on the local concentration of nutrients, growth factors, and possibly other cell signaling molecules, which translates to a homeostatic pressure that will depend on the biochemical conditions. Note that the rates may depend also on the cell stress σ, which is here already taken into account since $\sigma = \sigma(n)$.

Close to the homeostatic state, the properties of the tissue are obtained by expanding the effective cell number growth rate $k_\mathrm{d} - k_\mathrm{a}$ to linear order in the density deviations $\delta n = n - n_\mathrm{h}$, assuming that nutriment conditions remain constant. We therefore write

$$k_\mathrm{d} - k_\mathrm{a} = -\frac{1}{\tau}\frac{\delta n}{n_\mathrm{h}}\,, \tag{2.25}$$

where $\tau^{-1} = -n_\mathrm{h}\frac{\partial(k_\mathrm{d}-k_\mathrm{a})}{\partial n}$. Density deviations and stress deviations $\delta\sigma = \sigma + P_\mathrm{h}$ are related via the equation of state (2.14), and we thus obtain

$$\left(1 + \tau\frac{\mathrm{d}}{\mathrm{d}t}\right)(n - n_\mathrm{h}) = -n_\mathrm{h}\tau v_{\gamma\gamma}\,, \tag{2.26a}$$

$$\left(1 + \tau\frac{\mathrm{d}}{\mathrm{d}t}\right)(\sigma + P_\mathrm{h}) = \zeta v_{\gamma\gamma}\,, \tag{2.26b}$$

where we introduced the effective bulk viscosity $\zeta = \tau\chi$. Note that the viscous term is not due to internal friction but describes the coupling of the net cell division rate to variations in the isotropic stress. The dynamics of the traceless part of the stress is still described by Eq. (2.20). The two equations are equivalent and show that the density and the isotropic part of the stress tend to relax to a fixed homeostatic density and pressure within the relaxation time τ. The Maxwell dynamics of the isotropic part of the stress is a unique feature of the homeostatic state, which is absent in fluids with a conserved number of particles even at a liquid vapor critical point [23]. This property is associated with the fact that in the homeostatic state, the tissue is infinitely compressible. The pressure does not depend on the volume of the tissue as the number of cells is regulated by cell division and apoptosis. As a consequence, one can expect giant fluctuations of the volume of the tissue at constant (homeostatic) pressure.

What does the dynamics look like for an incompressible tissue? In this case, both χ and τ would be ill-defined since the cell number density is constant, $n = n_{0,\mathrm{h}}$. Before taking the limit $\chi \to \infty$, however, one can express the dependence of the rates of cell division and apoptosis on the cell number density as a dependence of the isotropic part of the stress σ via the equation of state (2.14). The obtained functions $k_\mathrm{d}(\sigma)$ and $k_\mathrm{a}(\sigma)$ remain well-defined in the limit $\chi \to \infty$, *i.e.*, for an incompressible tissue. We can now expand the cell number growth rate $k_\mathrm{d} - k_\mathrm{a}$ close to the homeostatic pressure and introduce an effective bulk viscosity ζ via

$$k_\mathrm{d} - k_\mathrm{a} = \frac{\sigma + P_\mathrm{h}}{\zeta}\,. \tag{2.27}$$

Here, ζ is no longer the product of an elastic modulus and a characteristic time scale defined by Eq. (2.25), but appears naturally in the expansion as $\zeta^{-1} = \frac{\partial(k_\mathrm{d}-k_\mathrm{a})}{\partial\sigma}$. The isotropic part of the stress is now determined by

$$\sigma = -P_\mathrm{h} + \zeta v_{\gamma\gamma}\,, \tag{2.28}$$

where the constraint $v_{\gamma\gamma} = k_\mathrm{d} - k_\mathrm{a}$ is already taken into account. Not surprisingly, the above equation can be considered as the limit $\tau \to 0$, $\chi \to \infty$ of Eq. (2.26b) such that $\tau\chi \to \zeta$ remains finite. Because cells are incompressible, one can neglect the elastic term at all times, and variations in the isotropic stress immediately translate to tissue volume growth or shrinkage via an increase or decrease of the net cell division rate. The time scale τ defined via $\tau = \zeta/\chi$ tends to zero for $\chi \to \infty$ while ζ remains finite.

The anisotropic homeostatic state

Similarly, a polarized tissue can reach a steady homeostatic state. The steady state behavior implies again that the cell number density remains constant, $n = n_\mathrm{h}$, and that the cell flow vanishes, $v_\alpha = 0$. The latter condition together with stationarity requires the existence of a finite anisotropic homeostatic stress $\tilde{\sigma}^\mathrm{h}_{\alpha\beta} = -\sigma_0\tilde{q}^0_{\alpha\beta}$, as can be seen from Eq. (2.24). This is the value of the anisotropic stress for which cell division is randomly oriented on average, see Eq. (2.22), which guarantees stationarity of the source stress. Though the nematic order parameter $\tilde{q}_{\alpha\beta}$ vanishes at the homeostatic state, note that the rates of cell division and apoptosis may still depend on the nematic order parameter $\tilde{q}^0_{\alpha\beta}$ which we consider to be set by external conditions.[7] Assuming again constant biochemical conditions and constant $\tilde{q}^0_{\alpha\beta}$, the balance of cell division and apoptosis then defines the homeostatic density via the condition $k_\mathrm{d}(n_\mathrm{h}) = k_\mathrm{a}(n_\mathrm{h})$.

As a consequence of the finite polarity of the tissue, if one measures the stress developed by a uniaxial tissue at steady state, the homeostatic stress in the symmetry axis direction is different from the homeostatic stress in the directions perpendicular to it. Conversely, in an ensemble where one imposes stresses, in order to obtain a homeostatic state one has to set both stresses to their homeostatic values. The case of biaxial order follows the same logic: In this case, the tissue develops three different homeostatic stress values in three orthogonal directions of space. In turn, in order to obtain a steady state in a stress imposed ensemble one has to impose three different values in the three directions.

2.4 Examples of tissue growth

Having laid out the theoretical foundations of a continuum description of tissue mechanics, we discuss two examples of tissue growth in which our framework can be applied. First, we consider the growth of a spherical cell aggregate, or multicellular tissue spheroid, embedded in an elastic matrix. Due to the elastic deformation of the matrix, growth will finally come to a halt. Second, we discuss the growth of an epithelial layer spreading on

[7] Rotational invariance implies that the rates of cell division and apoptosis depend on scalar invariants of $\tilde{q}^0_{\alpha\beta}$, which for a traceless tensor is to lowest order the contraction $\tilde{q}^0_{\alpha\beta}\tilde{q}^0_{\beta\alpha}$.

a spherical cap. Here, the nontrivial geometry—which is inspired by the epiboly of the developing zebrafish embryo [192]—allows predictions about the cell division orientation due to the stress distribution in a proliferating tissue.

2.4.1 Spheroid growth in an elastic matrix

We consider a tissue spheroid with an initial radius $R(0) = R_0$ at time $t = 0$, embedded in an infinite elastic matrix that is initially unstressed, see Fig. 2.5(a) for a sketch. We assume that the tissue dynamics is described by the constitutive equations (2.20) and (2.26b), although strictly speaking we do not consider a perturbation close to the homeostatic state. We want to discuss the dynamics of growth in the limit of long times, *i.e.*, for $t \gg \tau, \tau_\mathrm{a}$, and neglect therefore the elastic contributions to the tissue stress. Spherical symmetry implies that $\mathbf{v} = v_r(r)\mathbf{e}_r$, and the constitutive equations become

$$\sigma = -P_\mathrm{h} + \zeta \left(\partial_r v_r + 2\frac{v_r}{r}\right) , \tag{2.29a}$$

$$\tilde{\sigma}_{rr} = \tfrac{4}{3}\eta \left(\partial_r v_r - \frac{v_r}{r}\right) , \tag{2.29b}$$

in the limit of long times. Furthermore, $\tilde{\sigma}_{\theta\theta} = \tilde{\sigma}_{\phi\phi} = -\tilde{\sigma}_{rr}/2$ and $\tilde{\sigma}_{r\theta} = \tilde{\sigma}_{r\phi} = \tilde{\sigma}_{\theta\phi} = 0$ due to symmetry. For simplicity, we consider that the matrix can be described as a simple linear elastic material with shear modulus G. The stress exerted by the matrix on the tissue is then given by

$$\sigma_{rr}^\mathrm{E}\big|_R = -4G\frac{R - R_0}{R_0} , \tag{2.30}$$

which is a classic textbook exercise (see *e.g.* [112] for a derivation). Force balance implies that $\sigma_{rr}(R) = \sigma_{rr}^\mathrm{E}\big|_R$, and by using $v_r = 0$ we can already find the equilibrium radius at which growth stops,

$$R_\infty = R_0 \left(1 + \frac{P_\mathrm{h}}{4G}\right) . \tag{2.31}$$

Note that we neglected tissue surface tension for simplicity, which would add another term to the force balance at R. Instead, we would have $\sigma_{rr}(R) = \sigma_{rr}^\mathrm{E}\big|_R - \gamma/R$, where γ is a surface tension. Our simplification is justified as long as $\gamma \ll G(1 + \frac{P_\mathrm{h}}{4G})^2 R_0$, given that $\gamma/R_0 < P_\mathrm{h}$ such that the tissue starts to grow at $t = 0$.

Let us now solve for the dynamics of $R(t)$. Force balance in the tissue is expressed by

$$\partial_r \sigma + \partial_r \tilde{\sigma}_{rr} + 2\frac{\tilde{\sigma}_{rr} - \tilde{\sigma}_{\theta\theta}}{r} = 0 , \tag{2.32}$$

which leads to an ordinary differential equation for $v_r(r)$,

$$\partial_r \left[\frac{1}{r^2}\partial_r \left(v_r r^2\right)\right] = 0 . \tag{2.33}$$

This equation together with the boundary condition $v_r|_{r=0} = 0$ is fulfilled for $v_r = cr$, where $c(t)$ is a (time-dependent, *i.e.* quasi-static) constant to be determined from the

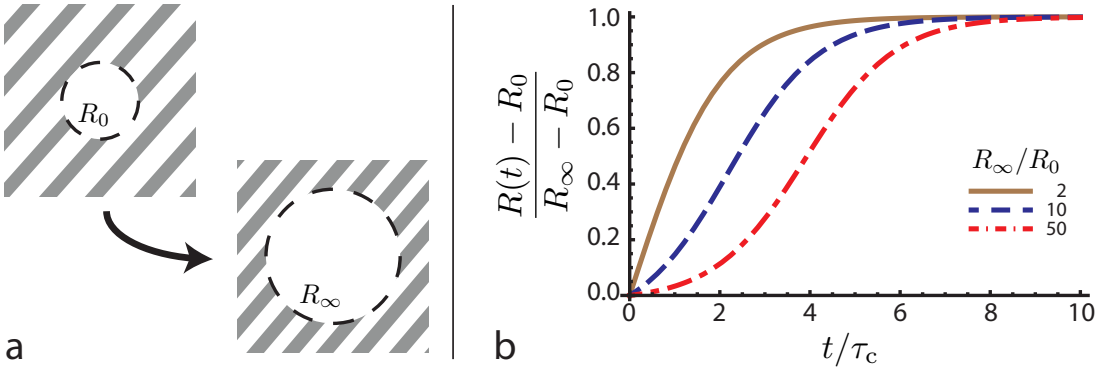

Figure 2.5. Spheroid growth in an elastic matrix. (a) Cartoon of the initial state and growth arrest: At time $t = 0$, the cell aggregate has a radius R_0 and the elastic matrix is uncompressed. Growth stops when the tissue has reached a size R_∞ due to the elastic stress of the compressed matrix. (b) Exemplary growth curves for different values of $R_\infty/R_0 = 1 + \frac{P_h}{4G}$ with time rescaled by τ_c, see text for details.

stress boundary condition at $r = R$. Using Eqs. (2.29) and with $\dot{R} = v_r(R, t)$, we finally find a dynamic equation for $R(t)$,

$$\dot{R} = \frac{R}{3\zeta}\left(P_h - 4G\frac{R - R_0}{R}\right) . \tag{2.34}$$

The growth dynamics is thus given by

$$R(t) = \frac{R_0 R_\infty e^{t/\tau_c}}{R_\infty + R_0\left(e^{t/\tau_c} - 1\right)} , \tag{2.35}$$

where we introduced the characteristic time scale $\tau_c = 3\zeta/(4G+P_h)$. Examples of growth curves described by the above equation are shown in Fig. 2.5(b). Note that since the tissue grows homogeneously, shear stresses do not exist, and the effective shear viscosity does not appear in the dynamic equation for $R(t)$.

Although the proposed model is quite simple, it qualitatively captures the observed growth curves for tumor spheroids grown in agarose gels of different stiffness [95]: After a fast initial growth phase, growth slows down until an equilibrium size is reached, which diminishes with increasing gel stiffness. For quantitative inferences, however, it is not obvious whether the ensemble of our assumptions are correct. Most probably, the assumed linear dependence of the cell number growth rate on the isotropic part of the stress does not hold over a long pressure range. Also, the same authors of the study cited above observed the free growth of tumor spheroids in culture medium and found a characteristic time scale of growth arrest comparable to the confined spheroids [95], which cannot be understood within our model. In general, it is understood that tumor spheroid growth is eventually limited by nutrient conditions [133], whereas we assumed nutrient abundance and constant biochemical conditions. Furthermore, recent experiments on tumor

spheroid growth suggest that cells differentiate and adopt different stress dependence of division and apoptosis close to the edge of the spheroid and in the bulk, respectively [130], an effect that we neglected here.

2.4.2 Epithelial growth on a sphere

During early zebrafish development, a thin layer of proliferating cells spreads over the central yolk cell, a process called epiboly [115, 192]. Epiboly is a concerted movement of cells in which different groups of cells are involved. At the onset of epiboly, blastoderm cells are located at the animal pole of the yolk cell, see also Fig. 1.2. The blastoderm is covered by an epithelial monolayer of cells, the so-called enveloping cell layer (EVL). During epiboly ($\sim 3-10.5\,\mathrm{h}$ after fertilization), blastoderm and EVL cells spread over the yolk towards the vegetal pole. Notably, cells do not switch between the blastoderm and the EVL, so that we can discuss the dynamics of these tissues independently. Inspired by this geometry, we discuss the growth of an epithelial sheet of cells on a sphere. For simplicity, we assume that the sphere is rigid and its radius R constant. First, we introduce an effective two-dimensional description of growing tissues, which can be obtained as a limit of the bulk equations developed in the previous section. We then consider the case of an incompressible tissue with constant proliferation rate, which allows to capture the main effects of the imposed geometry on cell division orientation. We finally take a possible coupling between stress and proliferation rate into account, which gives rise to spatial inhomogeneities in the proliferation rate.

Effective two-dimensional description

In this section, we derive the effective equations describing tissue dynamics in two dimensions for thin, sheet-like tissues like epithelia. We follow the classic thin plate or shell approximation which is commonly used in the context of elasticity theory [112]. First, we develop the equations for a planar thin sheet, before using these expressions later with the corresponding modifications in a curved geometry.

Neglecting external body forces, the total force balance in three dimensions is given by Eq. (2.4),

$$\partial_\beta \sigma_{\alpha\beta} = 0\,,$$

where Greek indices stand for the Cartesian coordinates (x, y, z). Let us assume that the tissue is a thin layer of height h along the z-direction. We now express force balance independently along z and in the (x, y)-plane,

$$\partial_\beta \sigma_{z\beta} = 0\,, \tag{2.36a}$$
$$\partial_\beta \sigma_{i\beta} = 0\,, \tag{2.36b}$$

where latin indices stand for Cartesian coordinates in the (x, y)-plane. Integrating the

latter equation over z, we obtain

$$0 = \int_0^h \mathrm{d}z\, \partial_\beta \sigma_{i\beta} \tag{2.37a}$$

$$= \partial_k \left(\int_0^h \mathrm{d}z\, \sigma_{ik} \right) + \int_0^h \mathrm{d}z\, \partial_z \sigma_{iz} \tag{2.37b}$$

$$\equiv \partial_k \varsigma_{ik} + \sigma_{iz}\big|_0^h \,. \tag{2.37c}$$

Here, ς_{ik} denotes the tensor of tensions in the two-dimensional plane; note that the dimension of ς_{ik} is [Force]/[Length], *i.e.*, a length times the a (three-dimensional) stress. The first term in the last line is the divergence of the tension tensor in two dimensions. The second term contains the forces that are transmitted at the upper and lower boundaries, which are given by the boundary conditions. Due to the reduction of one dimension, they appear as external body forces in the two-dimensional force balance. The force balance in the plane can thus be written as

$$\partial_k \varsigma_{ik} = -f_i^{\mathrm{ext}}, \tag{2.38}$$

where f_i^{ext} is now a surfacial force density. In general, one considers momentum transfer at the boundary due to passive friction, which gives rise to a friction force $f_i^{\mathrm{ext}} = -\gamma v_i$.

Analogously, integrating the force balance along z gives

$$0 = \partial_k \left(\int_0^h \mathrm{d}z\, \sigma_{zk} \right) + \sigma_{zz}\big|_0^h \,, \tag{2.39}$$

where the first term corresponds to forces in z-direction exerted by the tissue on the (x,z)- and (y,z)-planes and $\sigma_{zz}\big|_0^h = \sigma_{zz}(h) - \sigma_{zz}(0)$ is the sum of the normal forces exerted at the upper and lower surface. The shear stresses σ_{zk} vanish for sufficiently small h since they are caused by gradients along z of the elastic deformation or flow velocity in the plane or, respectively, by gradients along (x,y) of the z-components of the elastic deformation or flow velocity. Force balance normal to the plane thus simply implies that the forces exerted on the top and bottom surface cancel.

Having discussed force balance, we need to specify how the constitutive equations for $\sigma_{\alpha\beta}$ in the bulk translate to constitutive equations for ς_{ik} in the plane. The latter being defined by

$$\varsigma_{ik} = \int_0^h \mathrm{d}z\, \sigma_{ik} \,, \tag{2.40}$$

we can in principle calculate them straight away. Since all the arguments developed in the previous section carry over to two-dimensional, *i.e.* sheet-like, tissues, however, we can proceed along the same lines in order to obtain the corresponding constitutive equations. Therefore, we can write for the traceless part

$$(1 + \tau_a \partial_t)\, \varsigma_{ik} = 2\eta' \tilde{v}_{ik} \,, \tag{2.41}$$

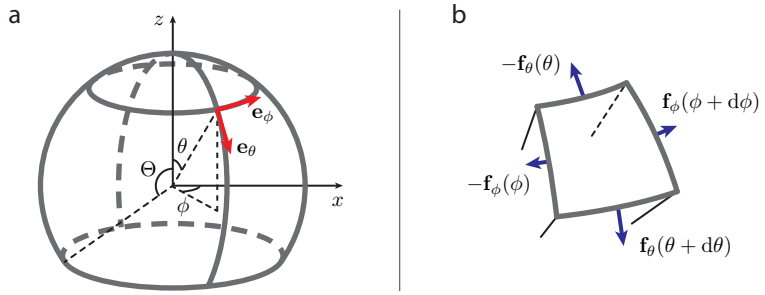

Figure 2.6. Geometry of a tissue growing on a sphere. (a) The surface of the sphere is parametrized by the polar coordinates θ and ϕ which induce a local, orthonormal basis $(\mathbf{e}_\theta, \mathbf{e}_\phi)$. At time t, the tissue covers the sphere up to an opening angle $\Theta(t)$. (b) On a sphere, force balance in the tangential plane involves the forces $\mathbf{f}_\theta(\theta) = \varsigma_{\theta\theta}(\theta)\, R\, \sin(\theta)\, \mathrm{d}\phi\, \mathbf{e}_\theta(\theta)$ and $\mathbf{f}_\theta(\theta) = \varsigma_{\phi\phi}(\phi)\, R\, \mathrm{d}\theta\, \mathbf{e}_\phi(\phi)$. The change of $(\mathbf{e}_\theta, \mathbf{e}_\phi)$ with θ and ϕ gives rise to additional terms in the force balance, see text for details.

where $\tilde{v}_{ik} = v_{ik} - \frac{1}{2} v_{ll} \delta_{ik}$ such that $\tilde{v}_{ii} = 0$ and we neglect geometric nonlinearities for simplicity. Note that $\eta' \sim h\eta$ is a two-dimensional viscosity with the physical dimension [Force]/[Length]×[Time]. We assume that the isotropic part of the tension tensor is given by an equation of state

$$\varsigma = \varsigma(n)\,, \tag{2.42}$$

where n is now a surface number density of cells, for which still holds

$$\partial_t n + \partial_k \left(n v_k\right) = n \left(k_\mathrm{d} - k_\mathrm{a}\right)\,. \tag{2.43}$$

For an incompressible tissue, the cell number density is constant, $n = n_0$, and the area growth rate equals the number growth rate, $v_{kk} = k_\mathrm{d} - k_\mathrm{a}$. In this case, the isotropic part of the tension ς becomes a Lagrange multiplier in order to satisfy the force balance (2.38).

Force balance in spherical geometry

We now discuss the two-dimensional force balance for a thin sheet in a spherical geometry. The geometry of the growing epithelium is illustrated in Fig. 2.6(a): The tissue partially covers the surface of a sphere of radius R up to the opening angle Θ. Each point $\mathbf{r}$ on the surface is parametrized by two angles θ and ϕ, which induce a local orthonormal basis tangential to the surface via $\mathbf{e}_\theta = \partial_\theta \mathbf{r}/||\partial_\theta \mathbf{r}||$ and $\mathbf{e}_\phi = \partial_\phi \mathbf{r}/||\partial_\phi \mathbf{r}||$.[8] The tension tensor and the cell flow field are defined on the surface and become functions of the spherical polar coordinates θ and ϕ. Due to the rotational symmetry around the z-axis, the fields do not explicitly depend on ϕ, however. Rotational symmetry implies furthermore that the cell flow field can be expressed as $\mathbf{v} = v_\theta(\theta)\mathbf{e}_\theta$. Note that although $\partial_\phi v_\theta = 0$,

[8] The surface of a sphere is given by all points $\mathbf{r} = R\sin\theta\cos\phi\,\mathbf{e}_x + R\sin\theta\sin\phi\,\mathbf{e}_y + R\cos\theta\,\mathbf{e}_z$. The orthonormal basis $(\mathbf{e}_\theta, \mathbf{e}_\phi)$ is then defined by $\mathbf{e}_\theta = \cos\theta\cos\phi\,\mathbf{e}_x + \cos\theta\sin\phi\,\mathbf{e}_y - \sin\theta\,\mathbf{e}_z$ and $\mathbf{e}_\phi = -\sin\phi\,\mathbf{e}_x + \cos\phi\,\mathbf{e}_y$.

the unit vector $\mathbf{e}_\theta$ remains a function of ϕ. This dependence of the local orthonormal basis on (θ, ϕ) induces additional terms in the planar force balance, see Fig. 2.6(b). In the preceding paragraphs, we assumed a planar geometry in order to derive the two-dimensional force balance in Cartesian coordinates. In coordinate-free notation, force balance can be expressed as $\nabla \cdot \boldsymbol{\varsigma} = \gamma \mathbf{v}$, where $\nabla \cdot \boldsymbol{\varsigma}$ is the two-dimensional divergence of the tensor $\boldsymbol{\varsigma}$. Taking the variation of the basis into account, we obtain[9]

$$\partial_\theta \varsigma_{\theta\theta} + \cot\theta \, (\varsigma_{\theta\theta} - \varsigma_{\phi\phi}) = R\gamma v_\theta \tag{2.44}$$

for the force balance in spherical polar coordinates, where $\varsigma_{\theta\theta}$ and $\varsigma_{\phi\phi}$ are given by the constitutive equations (2.41) and (2.42). A more complete account of the force balance of thin sheets for arbitrary curved surfaces using a differential geometry approach can be found in [75]. Because we assume that the sphere is rigid, and the radius of the sphere constant, we do not need to consider the force balance along the radial direction. Note however that the isotropic part of the tension gives rise to a Laplace pressure acting on the underlying sphere.

Growing epithelium with fixed proliferation rate

In the following, we consider an incompressible tissue that proliferates with a fixed proliferation rate $k_\mathrm{d} - k_\mathrm{a} \equiv k_0$. We consider the growth dynamics in the limit of long times and assume that the tensions are purely viscous. Incompressibility implies that the divergence of the cell flow field is set by the proliferation rate. We can write the divergence of the cell flow field in spherical polar coordinates, and we obtain[10]

$$\partial_\theta v_\theta + \cot\theta \, v_\theta = R k_0 \, . \tag{2.45}$$

For an incompressible, proliferating epithelium the cell flow velocity is thus given by

$$v_\theta = R k_0 \, \tan\theta/2 \, , \tag{2.46}$$

which is plotted in Fig. 2.7(a). For $k_0 > 0$, cells flow from the pole at $\theta = 0$ towards the equator and further with increasing velocity, as all cells behind proliferate and thus contribute to the flow. With the analytical expression for the cell flow given above, we can solve the dynamics for the opening angle $\Theta(t)$ as a function of time. Since $\mathrm{d}\Theta/\mathrm{d}t = v_\theta(\Theta)/R$,

$$\frac{\mathrm{d}\Theta}{\mathrm{d}t} = k_0 \tan\Theta/2 \, , \tag{2.47}$$

[9] In Cartesian coordinates, $\nabla = \mathbf{e}_x \partial_x + \mathbf{e}_y \partial_y$ and $\boldsymbol{\varsigma} = \varsigma_{ik} \mathbf{e}_i \otimes \mathbf{e}_k$, where $\otimes$ denotes the dyadic (or tensorial) product and $i, k = x, y$. Force balance $\nabla \cdot \boldsymbol{\varsigma} = \gamma \mathbf{v}$ can then simply be expressed as $\partial_k \varsigma_{ik} = \gamma v_i$ since the basis $(\mathbf{e}_x, \mathbf{e}_y)$ does not vary in space. In spherical polar coordinates, we have $\nabla = \mathbf{e}_\theta \frac{1}{R} \partial_\theta + \mathbf{e}_\phi \frac{1}{R \sin\theta} \partial_\phi$, and the stress tensor can be written as $\boldsymbol{\varsigma} = \varsigma_{\theta\theta} \mathbf{e}_\theta \otimes \mathbf{e}_\theta + \varsigma_{\phi\phi} \mathbf{e}_\phi \otimes \mathbf{e}_\phi$. Note that we used $\varsigma_{\theta\phi} = 0$ due to symmetry. The divergence $\nabla \cdot \boldsymbol{\varsigma}$ now includes additional terms due to $\partial_m \mathbf{e}_n \neq 0$ for $m, n = \theta, \phi$ (*cf.* note 8), and we obtain the result presented above.

[10] In coordinate-free notation, the divergence of the cell flow is given by $\nabla \cdot \mathbf{v}$. Taking the variation of $\mathbf{e}_\theta$ into account, one obtains the above expression, see also notes 8 and 9.

which for the initial condition $\Theta(0) = \Theta_0$ is solved by

$$\Theta(t) = 2\sin^{-1}\left(e^{tk_0/2}\sin\Theta_0/2\right). \tag{2.48}$$

Note that we neglected here any explicit time dependence of the proliferation rate k_0. The time T it takes the tissue to cover the sphere completely is a function of Θ_0 and given by $T(\Theta_0) = -2k_0^{-1}\ln\sin\Theta_0$. An example of $\Theta(t)$ is shown in Fig. 2.7(e).

In the viscous limit, the traceless part of the tensions depends on the velocity gradient of the cell flow only, which in spherical geometry is given by[11]

$$\tilde{\varsigma}_{\theta\theta} = \eta' \tfrac{1}{R}\left(\partial_\theta v_\theta - \cot\theta\, v_\theta\right) \tag{2.49}$$

and $\tilde{\varsigma}_{\phi\phi} = -\tilde{\varsigma}_{\theta\theta}$. Here, we used that $\mathbf{v} = v_\theta(\theta)\mathbf{e}_\theta$. The isotropic tension ς serves as a Lagrange multiplier and has to be determined from the force balance. Although all cells divide homogeneously, *i.e.*, with a constant cell division rate, the resulting cell flow gives rise to shear tensions due to the nontrivial geometry. Without having to solve force balance, the traceless part of the tension immediately follows from the above equation, and we obtain

$$\tilde{\varsigma}_{\theta\theta} = \eta' k_0 \tan^2\theta/2\,. \tag{2.50}$$

In analogy to the theory developed in the previous section, the average cell division orientation can be described by a two-dimensional nematic tensor $\tilde{q}_{mn}$, where $m, n = \theta, \phi$, and we assume that $\tilde{q}_{mn} \propto \varsigma_{mn}$. Therefore, our results imply that cell divisions are increasingly oriented along $\mathbf{e}_\theta$ for increasing θ, see Fig. 2.7(b). This mechanism of cell division orientation is purely mechanical and does not depend on external morphogen gradients or planar cell polarity. Note that this effect is independent of the cell-substrate friction because of the imposed proliferation rate.

We now discuss the isotropic part of the tension. Force balance (2.44) leads to an equation for ς,

$$\partial_\theta\varsigma = -\eta' k_0\left(2 - \frac{R^2}{\lambda^2}\right)\tan\theta/2\,, \tag{2.51}$$

where we introduced the characteristic length scale $\lambda = \sqrt{\eta'/\gamma}$. Together with the boundary condition $\varsigma_{\theta\theta}(\Theta) = \varsigma_0$, where ς_0 is the tension applied at the outer rim of the tissue, we thus obtain

$$\varsigma - \varsigma_0 = \eta' k_0\left[2\left(2 - \frac{R^2}{\lambda^2}\right)\ln\frac{\cos\theta/2}{\cos\Theta/2} - \tan^2\Theta/2\right]. \tag{2.52}$$

Note that in general, the isotropic tension is not homogeneous. This inhomogeneity of the (surface) tension translates to spatially varying forces exerted by the tissue on

[11] In coordinate-free notation, the traceless part of tensions is given by

$$\tilde{\boldsymbol{\varsigma}} = \eta' \mathrm{Tg}\left[\nabla\otimes\mathbf{v} + (\nabla\otimes\mathbf{v})^{\mathrm{T}} - (\nabla\cdot\mathbf{v})\,\mathbf{1}\right],$$

where $\mathbf{1}$ denotes the unit tensor in the tangential plane and Tg takes the tangential part (all contributions proportional to $\mathbf{e}_m \otimes \mathbf{e}_n$ where $m, n = \theta, \phi$) of its argument. See also notes 8 and 9.

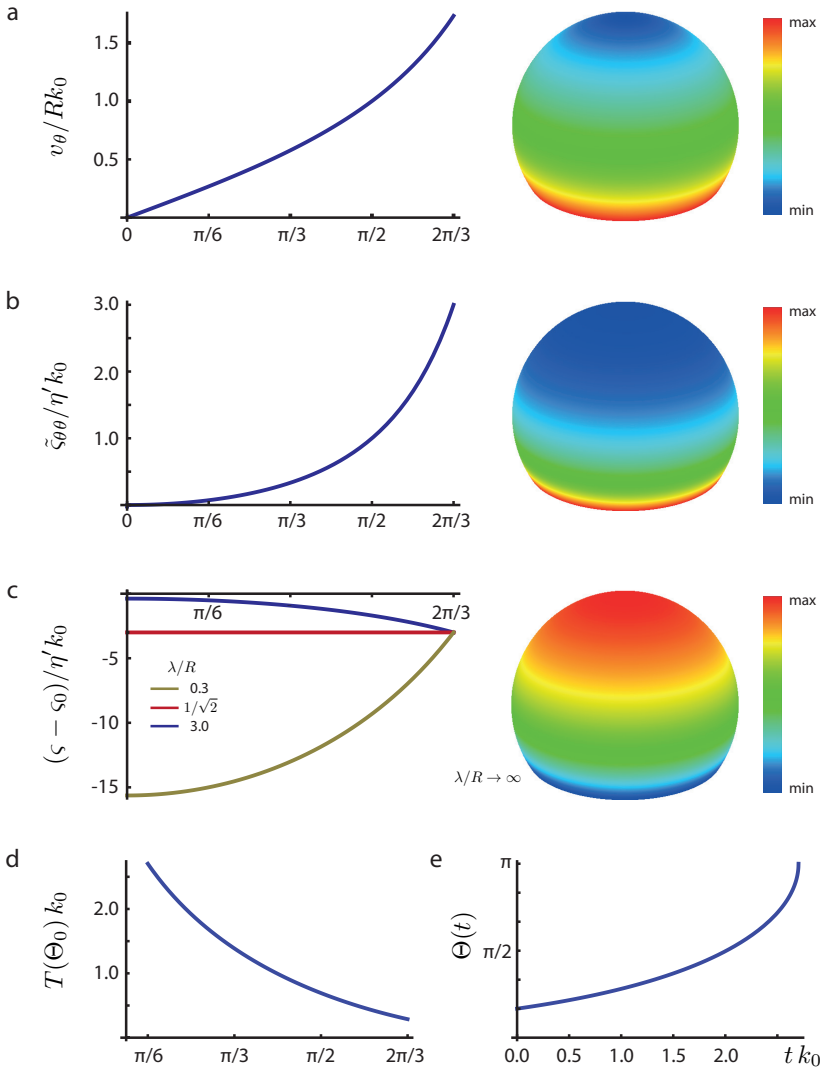

Figure 2.7. Tissue growth with fixed proliferation rate. The velocity profile (a) and—subsequently—the anisotropic part of the tension (b) within the expanding cell sheet are fixed by the incompressibility constraint. (c) The isotropic part of the tension depends on the ration λ/R where λ is a characteristic length scale of friction, see text for details. We plot all fields for an opening angle $\Theta = 2\pi/3$, which in general evolves in time. (d) The total time of closure depends on the initial opening angle Θ_0, and (e) we show an example of $\Theta(t)$ for $\Theta_0 = \pi/6$.

the underlying sphere. Since we assumed the sphere to be rigid, however, these radial forces do not have to be considered. The tension profile depends on the ratio λ/R, see Fig. 2.7(c). For low friction, *i.e.*, $\lambda > R/\sqrt{2} \equiv \lambda_c$, the isotropic tension ς decreases towards the tissue border, whereas this behavior is inverted for $\lambda < \lambda_c$.

Coupling of proliferation rate and isotropic stress

The above results suggest that, depending on the shear viscosity η' and the friction coefficient γ, the isotropic tension varies considerably along the surface. Therefore, one might ask how a coupling between the cell division rate and the isotropic part of the tension would influence the dynamics. In the previous example, we investigated the role of such a coupling for a growing tissue spheroid in three dimensions. Here, we consider that the cell proliferation rate varies with the isotropic tension and we expand the former around the tension applied at the outer rim. To first order, the proliferation rate varies linearly with the tension variations $\varsigma - \varsigma_0$, and we write

$$k_\mathrm{d} - k_\mathrm{a} = k_0 + \frac{\varsigma - \varsigma_0}{\zeta'} \,. \tag{2.53}$$

Here, $\zeta' \sim h\zeta$ (note that $\zeta \neq \varsigma$) is an effective two-dimensional bulk viscosity with the same dimension as η'. Strictly speaking, it is not important around which reference tension we expand the net cell division rate as long as we consider the dependence on the tension to be linear. A different reference tension simply translates to a change of the baseline cell division rate k_0.

The constitutive equation for the isotropic tension now reads

$$\varsigma = \varsigma_0 - \zeta' k_0 + \zeta' v_{ii} \,, \tag{2.54}$$

where we used the incompressibility condition $v_{ii} = k_\mathrm{d} - k_\mathrm{a}$. The divergence of the cell flow is no longer constant, and we need to determine v_θ via the force balance equation (2.44). With the above equation for ς, force balance becomes

$$\sin^2\theta\, \partial_\theta^2 v_\theta + \sin\theta\, \cos\theta\, \partial_\theta v_\theta + \left(\alpha \sin^2\theta - 1\right) v_\theta = 0 \,, \tag{2.55}$$

where

$$\alpha = \frac{2 - (R/\lambda)^2}{1 + \zeta'/\eta'}$$

is a dimensionless number. For $\alpha \to 0$, we recover the limit of constant and homogenous cell division. The above equation can be solved analytically [150][12], and we finally obtain

$$v_\theta = C \sin\theta\, f(\cos\theta) \,. \tag{2.57}$$

Here, we used the boundary condition $v_\theta(0) = 0$; the remaining constant C can finally be determined from the tension boundary condition at $\theta = \Theta$. The function $f(x)$ is given by

$$\begin{aligned} f(x) = (\nu + \nu^2 - 2)\Gamma(1 - \tfrac{\nu}{2})\Gamma(\tfrac{3+\nu}{2})\, \partial_x F(-\tfrac{\nu}{2}, \tfrac{1+\nu}{2}, \tfrac{1}{2}; x^2) \\ - 2\nu(1+\nu)\Gamma(\tfrac{3-\nu}{2})\Gamma(\tfrac{4+\nu}{2})\partial_x \left[x\, F(\tfrac{1-\nu}{2}, 1 + \tfrac{\nu}{2}, \tfrac{3}{2}; x^2)\right] \,, \end{aligned} \tag{2.58}$$

[12] The solution can be found by step-wise variable transformations, as shown in the cited reference [150], see Eq. 2.1.6.115 ibidem. We would like to point out a misprint in Eq. 2.1.2.154, however, where it has to be

$$y = C_1\, F(-\tfrac{\nu}{2}, \tfrac{1+\nu}{2}, \tfrac{1}{2}; x^2) + C_2\, x\, F(\tfrac{1-\nu}{2}, 1 + \tfrac{\nu}{2}, \tfrac{3}{2}; x^2) \,. \tag{2.56}$$

where $F(\alpha, \beta, \gamma; z)$ is the hypergeometric series[13] and ν is related to the dimensionless number α introduced above via $\nu^2 + \nu = \alpha$. Examples of the velocity profile v_θ for different ratios η'/ζ' and λ/R are shown in Fig. 2.8(a-c). The traceless part of the tension follows from the cell flow as given by Eq. (2.49). The isotropic part can now be determined via Eq. (2.54); note that incompressibility is automatically taken into account. Examples of flow and tension profiles for different values of λ/R and η'/ζ' are plotted in Fig. 2.8(d-i). Due to the coupling between isotropic stress and proliferation, we observe a variation of the cell division rate with increasing θ, an effect that becomes more pronounced as η'/ζ' is increased. Note that this effect crucially depends on the ratio λ/R: In the case of negligible friction, isotropic tension is increased at the animal pole ($\theta = 0$). Thus, cells divide more at the pole and division is reduced towards the tissue margin. This effect is again purely mechanical and caused by the geometrical constraints. For $\lambda < \lambda_c$, the opposite behavior can be observed. Due to the high cell-substrate friction, the tension applied at the tissue margin is reduced towards the animal pole. Therefore, cell division dominates at the margin. These results are in line with the results in the case of constant proliferation, given that in the limit of fixed proliferation rate, we obtained that the isotropic stress ς varies along θ qualitatively in the same way. In principle, the net proliferation rate can even become negative either close to the tissue border or at the pole. However, the assumed linear relation postulated in Eq. (2.54) does certainly not hold for cases in which the tension variations $\varsigma - \varsigma_0$ exceed the reference tension $k_0\zeta'$.

The above description of two-dimensional tissue growth on a sphere can hardly be considered to be anything more than an oversimplified toy model of zebrafish epiboly. Nonetheless, it is not unconceivable that the predicted pattern of cell division can be observed experimentally, which would be a significant confirmation of the theory of tissue growth developed in the previous sections. The nontrivial geometry gives rise to oriented cell divisions for an otherwise isotropic tissue, a new and purely mechanical effect. Furthermore, the reduction of our theory to two dimensions naturally leads to a cell-substrate friction term in the force balance that qualitatively changes the tension distribution in the tissue that might be observed experimentally. In order to get to a more complete description of the morphogenetic processes during epiboly, possible other contributions would probably have to be taken into account. First, we assumed substrate friction to be purely passive for simplicity. In principle, cells can generate forces and actively migrate on the underlying substrate, an effect that we neglected here. Second, we assumed the yolk cell to be rigid; a more detailed description might take the elastic deformation of the yolk into consideration. Last but not least, rotational symmetry around the z-axis is eventually broken, which definitely deserves careful study.

[13] The hypergeometric function is defined as

$$F(\alpha, \beta, \gamma; z) = 1 + \sum_{k=1}^{\infty} \frac{(\alpha)_k (\beta)_k}{(\gamma)_k} \frac{z^k}{k!},$$

where $(\alpha)_k = \alpha(\alpha + 1) \cdots (\alpha + n - 1)$.

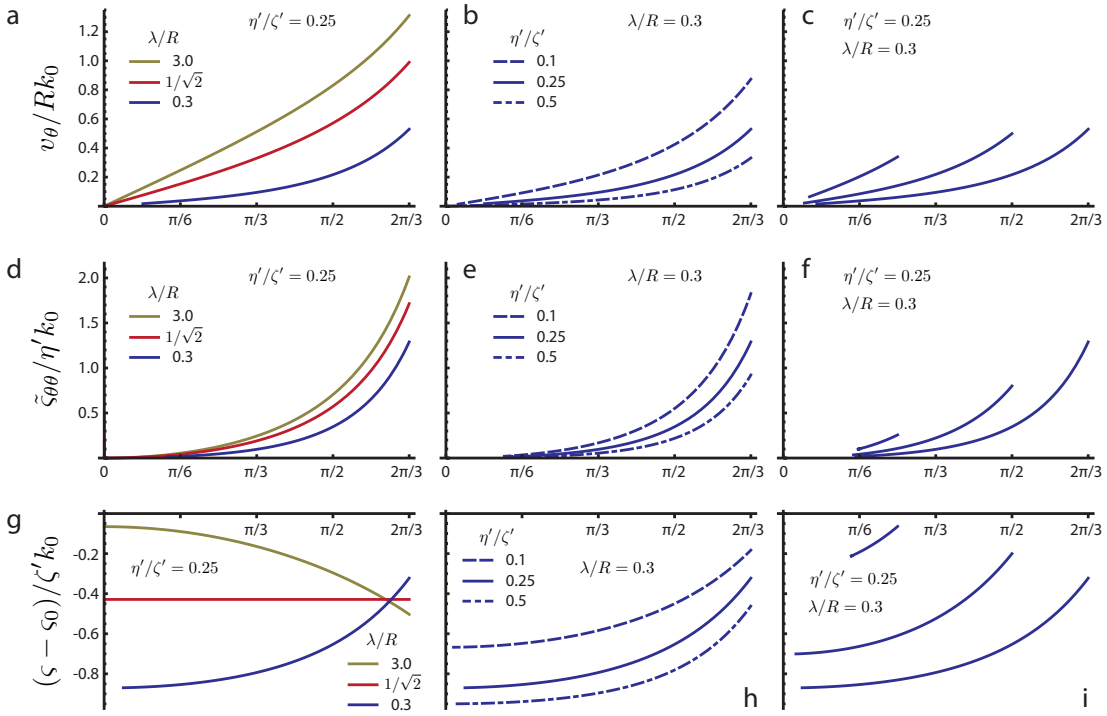

Figure 2.8. Coupling of isotropic tension and proliferation rate. (a-b) Velocity profile for different ratios λ/R and η'/ζ' and an opening angle $\Theta = 2\pi/3$. The dependence of v_θ on Θ is shown in (c). The corresponding plots for the traceless part of the tension and the isotropic tension are shown in (d-f) and (g-i), respectively. Note that the deviation of the proliferation rate $k_\mathrm{d} - k_\mathrm{a}$ from the "equilibrium" value k_0 is given by $(k_\mathrm{d} - k_\mathrm{a}) - k_0 = (\varsigma - \varsigma_0)/\zeta'$, see text for details.

2.5 Fluctuations

In the previous sections, we considered cell division and apoptosis as purely deterministic processes. In statistical-mechanical terms, we studied the mean-field behavior of tissue growth. However, cell division and cell death are stochastic processes, at least in the sense that the cell division times as well as the average life time of a cell follow a distribution of times.[14] To first order, this stochasticity can be described by additional noise terms in the dynamic equations. In this section, we study the effect of such noise on the mechanical properties of a tissue. For the sake of simplicity, here we only consider the vicinity of the homeostatic state of an isotropic non-polarized tissue.

[14] Biologists may feel offended by the notion of cell division and apoptosis being stochastic, given all the precise regulation machinery inside cells. Determinism at the cellular scale does not change our argument, however.

2.5.1 Stress and velocity fluctuations

The stochasticity of cell division and cell death introduces noise in the cell number balance equation (2.1), which we now write as

$$\partial_t \delta n + n_\mathrm{h} \partial_\alpha v_\alpha = -\frac{\delta n}{\tau} + \xi_\mathrm{c} \,. \tag{2.59}$$

Here, we introduced the number density variations $\delta n = n - n_\mathrm{h}$ and used the expansion of the net cell number growth rate around the homeostatic density, Eq. (2.25). The cell division and apoptosis noise has a vanishing average $\langle \xi_\mathrm{c} \rangle = 0$. In order to obtain an expression for the correlation function of this noise, we approximate the stochastic dynamics of the cell number density by a simple birth-and-death process with equal and constant rates. In the absence of convective flows, the noise correlator is then given by $\langle \xi_\mathrm{c}(\mathbf{r},t)\xi_\mathrm{c}(\mathbf{r}_0,t_0)\rangle = n_\mathrm{h}\,(k_\mathrm{d}+k_\mathrm{a})\,\delta(\mathbf{r}-\mathbf{r}_0)\,\delta(t-t_0)$ [74].

The random cell division and apoptosis events give rise to fluctuations in the stress. The isotropic stress fluctuation is related to the density fluctuation by the equation of state. Close to the homeostatic state, we therefore write

$$(1+\tau\partial_t)\,(\sigma + P_\mathrm{h}) = \zeta v_{\gamma\gamma} - \xi \,, \tag{2.60}$$

where $\zeta = \tau\chi$ is the effective bulk viscosity introduced above and $\xi = \xi_\mathrm{c}\zeta/n_\mathrm{h}$ the rescaled noise due to cell division and apoptosis. Noise must also be introduced in the equation for the traceless part of the stress tensor, associated with fluctuations of cell shape and of the orientation of cell division. The constitutive equation for the shear stress then becomes

$$(1+\tau_\mathrm{a}\partial_t)\,\tilde{\sigma}_{\alpha\beta} = 2\eta\tilde{v}_{\alpha\beta} + \tilde{\xi}_{\alpha\beta} \,. \tag{2.61}$$

We do not give here a microscopic description of this noise. We only assume that the fluctuations are correlated over time scales much shorter than the cell division time so that this noise can be considered as local in time. It has zero mean, $\langle \tilde{\xi}_{\alpha\beta}\rangle = 0$, and because of the symmetry of the traceless component of the stress tensor its correlations are characterized by a noise strength θ with $\langle \tilde{\xi}_{\alpha\beta}(\mathbf{r},t)\tilde{\xi}_{\gamma\delta}(\mathbf{r}_0,t_0)\rangle = \theta(\delta_{\alpha\gamma}\delta_{\beta\delta}+\delta_{\alpha\delta}\delta_{\beta\gamma} - \frac{2}{3}\delta_{\alpha\beta}\delta_{\gamma\delta})\delta(\mathbf{r}-\mathbf{r}_0)\delta(t-t_0)$.

We decompose all quantities in Fourier modes in space and time with the convention $f(\mathbf{q},\omega) = \int \mathrm{d}t \int \mathrm{d}\mathbf{r}\, e^{-i(\mathbf{q}\mathbf{r}-\omega t)} f(\mathbf{r},t)$. Using the force balance equation $\partial_\alpha \sigma_{\alpha\beta} = 0$ and Eqs. (2.60) and (2.61), one can calculate the density fluctuation and the velocity fluctuation as a function of noise. The density fluctuation in the homeostatic state reads

$$\delta n = \frac{\tau n_\mathrm{h}}{\bar{\eta}\,(1-i\omega\bar{\tau})}\left[\tfrac{4}{3}(\eta/\zeta)\xi + q_\alpha q_\beta \tilde{\xi}_{\alpha\beta}/q^2\right] , \tag{2.62}$$

where we introduced the longitudinal viscosity $\bar{\eta} = \zeta + \frac{4}{3}\eta$ and an effective relaxation time $\bar{\tau} = (\tau_\mathrm{a}\zeta + \tau\frac{4}{3}\eta)/\bar{\eta}$. In order to calculate the velocity fluctuations, we decompose the velocity into a longitudinal and a transverse component, $v_\alpha = v_{||} q_\alpha/q + v_{\perp\alpha}$. We

finally obtain

$$v_{||} = \frac{1}{iq}\frac{1}{\bar{\eta}\,(1-i\omega\bar{\tau})}\left[(1-i\omega\tau_{\rm a})\,\xi - (1-i\omega\tau)\,q_\alpha q_\beta \tilde{\xi}_{\alpha\beta}/q^2\right], \tag{2.63a}$$

$$v_{\perp\alpha} = \frac{i}{\eta q^2}\left(q_\beta \tilde{\xi}_{\alpha\beta} - q_\alpha q_\beta q_\gamma \tilde{\xi}_{\beta\gamma}/q^2\right). \tag{2.63b}$$

2.5.2 Diffusion of cells at the homeostatic state

In order to illustrate the role of the fluctuations in the tissue, we consider a tracer particle of radius a immersed in the tissue and moving by Brownian-type motion with the cell flow [20]. Due to random cell division and apoptosis, the particle diffuses in the tissue. In three dimensions, the diffusion constant is defined as

$$D = \lim_{t\to\infty}\frac{\langle \mathbf{r}_p^2(t)\rangle}{6t},$$

where $\mathbf{r}_p$ stands for the position of a tracer particle. The position can be expressed in terms of the flow field $v_\alpha(\mathbf{r},t)$ in which the particle moves, and we find

$$\begin{aligned} D &= \frac{1}{3}\int_0^\infty \mathrm{d}t\,\langle v_\alpha(\mathbf{r}_p(t),t)v_\alpha(\mathbf{r}_p(0),0)\rangle \\ &= \frac{1}{3}\int_0^\infty \mathrm{d}t \int \frac{\mathrm{d}^3q}{(2\pi)^3}\int\frac{\mathrm{d}^3q'}{(2\pi)^3}\left\langle e^{i[\mathbf{q}\mathbf{r}_p(t)+\mathbf{q}'\mathbf{r}_p(0)]}v_\alpha(\mathbf{q},t)v_\alpha(\mathbf{q}',0)\right\rangle. \end{aligned} \tag{2.64}$$

We make here the approximation that fluctuations in particle positions and velocity fluctuations in the tissue are decoupled and that the particle position fluctuations follow a Gaussian distribution,

$$\begin{aligned} \left\langle e^{i\mathbf{q}[\mathbf{r}_p(t)-\mathbf{r}_p(0)]}\right\rangle &= \int \mathrm{d}^3r \frac{1}{(4\pi Dt)^{3/2}} e^{-\frac{r^2}{4Dt}} e^{i\mathbf{q}\mathbf{r}} \\ &= e^{-q^2Dt}. \end{aligned} \tag{2.65}$$

The diffusion coefficient is thus given by

$$D = \frac{1}{3}\int_0^\infty \mathrm{d}t \int \frac{\mathrm{d}^3q}{(2\pi)^3}\, e^{-q^2Dt} C_{vv}(q,t), \tag{2.66}$$

where we introduced the velocity-velocity correlation function $C_{vv}(q,t)$ defined by

$$\langle v_\alpha(\mathbf{q},t)v_\alpha(\mathbf{q}',0)\rangle = (2\pi)^3\delta(\mathbf{q}+\mathbf{q}')\,C_{vv}(q,t). \tag{2.67}$$

Furthermore, we assume that the velocity-velocity correlations decay fast compared to the characteristic time scale defined by diffusion, *i.e.*, $\bar{\tau} \ll a^2/D$. A detailed discussion and a calculation where this latter assumption is relaxed can be found in appendix B. The finite size of the tracer particle implies the existence of a cut-off wave-length $q_{\rm max} = \pi/a$

related to the tracer particle's radius a. The expression of the diffusion constant then simplifies to

$$D = \frac{1}{6}\int_0^{q_{\max}} \frac{\mathrm{d}^3 q}{(2\pi)^3}\, \hat{C}^{\mathrm{c}}_{vv}(q,\omega)\big|_{\omega=0}\,, \tag{2.68}$$

where the Fourier transform $\hat{C}^{\mathrm{c}}_{vv}(q,\omega)$ of the cell velocity correlation function is defined according to

$$\langle v^{\mathrm{c}}_\alpha(\mathbf{q},\omega) v^{\mathrm{c}}_\alpha(\mathbf{q}',\omega')\rangle = \hat{C}^{\mathrm{c}}_{vv}(q,\omega)(2\pi)^4\delta(\mathbf{q}+\mathbf{q}')\delta(\omega+\omega')\,. \tag{2.69}$$

The velocity correlation function can be directly calculated from Eqs. (2.63). The diffusion constant in the homeostatic state then reads

$$D = \frac{1}{6\pi a}\left\{\frac{1}{(\zeta+\frac{4}{3}\eta)^2}\left[\frac{\zeta^2 k_{\mathrm{d}}}{n_{\mathrm{h}}}+\frac{2}{3}\theta\right]+\frac{\theta}{\eta^2}\right\}. \tag{2.70}$$

The diffusion constant therefore varies with the cell division rate k_{d}. In order to make the result more transparent, we assume in the following that the tissue is hardly compressible so that $\zeta \gg \eta$. In this limit, the expression for the diffusion constant reduces to $D = \frac{1}{6\pi a}\left[\frac{k_{\mathrm{d}}}{n_{\mathrm{h}}}+\left(\frac{n_{\mathrm{h}}\tilde{d}k_{\mathrm{d}}}{\sigma_0\mu}\right)^2\theta\right]$. Here, we have expressed $\eta = \tau_{\mathrm{a}}\mu$ and $\tilde{d} = \tilde{d}_{\mathrm{d}} + \tilde{d}_{\mathrm{a}}$. The diffusion coefficient increases with the cell division rate and varies linearly with the cell division rate at small values of k_{d}. Note however that the noise intensity θ could itself be a function of k_{d}.

2.5.3 Height fluctuations of a tissue layer

Another illustration of the role of cell division noise are the height fluctuations of a tissue at the homeostatic state. We consider a layer of tissue plated on a solid substrate; the height of the tissue layer along z is given by $h(x,y)$, see Fig. 2.9 for a sketch. On its upper surface, the tissue is covered by a membrane with surface tension γ and bending modulus κ. The membrane is subject to a constant external pressure P_{h} such that the tissue is at the homeostatic state to zeroth order. For simplicity, we consider the dynamics on long times only and keep only the viscous part of the stresses in the constitutive equations (2.20) and (2.26b).

The boundary conditions are specified as follows. The normal velocity v_z vanishes at $z = 0$, and the tangential stresses σ_{iz}, where $i = x, y$, vanish at $z = 0, h$ which corresponds to full-slip boundary conditions. The normal stresses at the upper boundary are continuous and given by

$$\sigma_{zz}(h) = -P_h + \gamma\Delta_\perp h - \kappa\Delta_\perp^2 h\,, \tag{2.71}$$

where $\Delta_\perp = \partial_k\partial_k$. Here, latin indices denote Cartesian coordinates in the (x,y)-plane, and the Einstein summation convention is implied.

In the following, we want to determine the mean square amplitude of the height fluctuations of the tissue due to cell division noise. Therefore, we calculate the spectrum

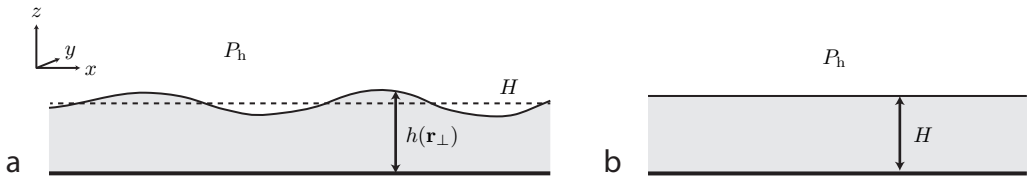

Figure 2.9. Cartoon of a tissue layer on a solid substrate. (a) Here, the tissue is covered by a membrane with surface tension γ and bending modulus κ. Spatial variations of tissue height $h(x,z)$ thus give rise to additional normal stresses at the upper surface on top of the homeostatic pressure, see text for details. Because of the stochasticity of cell division and apoptosis, the height h exhibits fluctuations around the mean height H. (b) The same tissue covered by a stiff piston. Due to cell division noise, the piston position, *i.e.*, the tissue height H, fluctuates as long as the system size is finite, see text for details.

of the height fluctuations by solving the force balance equation for the cell flow in Fourier space. We switch to the Fourier domain for the spatial dimensions in the (x,y)-plane according to $f(z,\mathbf{q},t) = \int \mathrm{d}x \int \mathrm{d}y\, e^{-i(q_x x+q_y y)} f(\mathbf{r},t)$. Furthermore, we introduce the deviatoric isotropic stress $\delta\sigma = \sigma + P_\mathrm{h}$ relative to the homeostatic pressure. Force balance then reads

$$\partial_z \delta\sigma + \partial_z \tilde{\sigma}_{zz} + iq_k \tilde{\sigma}_{zk} = 0\,, \tag{2.72a}$$

$$iq_k \delta\sigma + \partial_z \tilde{\sigma}_{zk} + iq_l \tilde{\sigma}_{kl} = 0\,, \tag{2.72b}$$

where the components of the stress tensor are given by

$$\delta\sigma = \zeta(\partial_z v_z + iq_k v_k) - \xi \tag{2.73a}$$

$$\tilde{\sigma}_{zz} = \eta(\tfrac{4}{3}\partial_z v_z - \tfrac{2}{3} iq_k v_k) + \tilde{\xi}_{zz} \tag{2.73b}$$

$$\tilde{\sigma}_{zk} = \eta(\partial_z v_k + iq_k v_z) + \tilde{\xi}_{zk} \tag{2.73c}$$

$$\tilde{\sigma}_{kl} = \eta(iq_k v_l + iq_l v_k - \tfrac{2}{3}(\partial_z v_z + iq_m v_m)\delta_{kl}) + \tilde{\xi}_{kl}\,. \tag{2.73d}$$

These are the constitutive equations (2.60) and (2.61) in the presence of noise in the limit of long times. In principle, one could keep the finite viscoelastic relaxation times. Then, one would have to switch to the Fourier domain in time in order to express the stresses as functions of the cell flow, which would give rise to prefactors $\sim (1 - i\omega\tau)^{-1}$. The limit of long times then corresponds to the limit $\omega \to 0$.

Inserting the above relations into the force balance, one can eliminate the v_i and we obtain an equation for v_z only. In the following, we restrict ourselves to the limit $q \ll 1/h$. In this case, variations along x and y are small and their contributions to the viscous stresses can be neglected. Equation (2.72a) then becomes $\partial_z(\delta\sigma + \tilde{\sigma}_{zz}) = 0$, and with the boundary condition (2.71) we obtain

$$\bar{\eta}\partial_z v_z - \xi + \tilde{\xi}_{zz} = -\left(q^2\gamma + q^4\kappa\right)\delta h\,, \tag{2.74}$$

where we introduced the height variations $\delta h = h - H$ around the mean height H of the tissue layer. Furthermore, $\bar{\eta} = \zeta + \frac{4}{3}\eta$ denotes the longitudinal viscosity.

In real space, the dynamics of the membrane is determined by the normal velocity at $z = h(\mathbf{r}_\perp, t)$ via

$$\partial_t \delta h(\mathbf{r}_\perp, t) = v_z(H + \delta h(\mathbf{r}_\perp, t), \mathbf{r}_\perp, t)\,. \tag{2.75}$$

This relation cannot be transformed into Fourier space because of the additional, implicit dependence of v_z on $\mathbf{r}_\perp$ via $h(\mathbf{r}_\perp, t)$ on the right-hand side. Doing linear fluctuation theory, however, the noise terms can be considered to be a small perturbation. Therefore, we can write

$$\partial_t \delta h(\mathbf{r}_\perp, t) \simeq v_z(H, \mathbf{r}_\perp, t) \tag{2.76}$$

to linear order, neglecting the dependence of v_z on δh. Because both $v_z(H, \mathbf{r}_\perp)$ and $\delta h(\mathbf{r}_\perp)$ scale with the noise (*i.e.*, vanish in the absence of noise), taking this dependence into account would give rise to terms of higher order. The relation can now be transposed to the Fourier domain in a straightforward way, such that one finds $\partial_t \delta h(\mathbf{q}_\perp, t) \simeq v_z(H, \mathbf{q}_\perp, t)$. Integrating equation (2.74) over z thus allows to determine the dynamics of the tissue height, and we obtain

$$\partial_t \delta h + \frac{q^2\gamma + q^4\kappa}{\bar{\eta}} H\, \delta h = \frac{1}{\bar{\eta}} \int_0^H \mathrm{d}z\, (\xi - \tilde{\xi}_{zz})\,. \tag{2.77}$$

Using the Fourier transform $\delta h(\mathbf{q}, \omega) = \int \mathrm{d}t\, e^{i\omega t} \delta h(\mathbf{r}, t)$, we can express the above equation as

$$\delta h(\mathbf{q}, \omega) = \frac{\int_0^H \mathrm{d}z\, (\xi - \tilde{\xi}_{zz})}{-\bar{\eta} i\omega + (q^2\gamma + q^4\kappa) H} \tag{2.78}$$

in the Fourier domain in time. From this expression we can now calculate the equal time mean square amplitude fluctuations $\langle |\delta h(\mathbf{r}, t)|^2 \rangle$. For the height-height correlation in Fourier space, we find

$$\langle \delta h(\mathbf{q}, \omega) \delta h(\mathbf{q}', \omega') \rangle = \frac{\int_0^H \mathrm{d}z \int_0^H \mathrm{d}z' \, \langle (\xi - \tilde{\xi}_{zz})(\xi - \tilde{\xi}_{zz}) \rangle}{[-i\bar{\eta}\omega + (q^2\gamma + q^4\kappa)H][-i\bar{\eta}\omega' + (q'^2\gamma + q'^4\kappa)H]} \tag{2.79a}$$

$$= \frac{2\left(\zeta^2 k_\mathrm{d}/n_\mathrm{h} + \frac{2}{3}\theta\right) H}{\bar{\eta}^2\omega^2 + (q^2\gamma + q^4\kappa)^2 H^2} (2\pi)^3 \delta(\mathbf{q} + \mathbf{q}') \delta(\omega + \omega')\,, \tag{2.79b}$$

where we used that the noise correlator in Fourier space is given by

$$\langle (\xi - \tilde{\xi}_{zz})(\xi - \tilde{\xi}_{zz}) \rangle = \langle \xi\xi \rangle + \langle \tilde{\xi}_{zz} \tilde{\xi}_{zz} \rangle \tag{2.80a}$$

$$= \left(\frac{2\zeta^2 k_\mathrm{d}}{n_\mathrm{h}} + \frac{4}{3}\theta \right) (2\pi)^3 \delta(z - z') \delta(\mathbf{q} + \mathbf{q}') \delta(\omega + \omega')\,. \tag{2.80b}$$

Note that the spectrum of height fluctuations given in Eq. (2.79) does not depend on the mean height H of the tissue. At first sight, this might seem surprising, given that the whole tissue below the membrane contributes to the fluctuations. The height fluctuations around the mean height H are governed by the excess pressure due to membrane deformation, however, and the mean height H drops out.

With

$$\langle \delta h(\mathbf{r},t)\delta h(\mathbf{r},t)\rangle = \int \frac{\mathrm{d}^2 q}{(2\pi)^2}\int \frac{\mathrm{d}^2 q'}{(2\pi)^2}\int \frac{\mathrm{d}\omega}{2\pi}\int \frac{\mathrm{d}\omega'}{2\pi}\, e^{i[(\mathbf{q}+\mathbf{q}')\mathbf{r}-(\omega+\omega')t]}\langle \delta h(\mathbf{q},\omega)\delta h(\mathbf{q}',\omega')\rangle \tag{2.81}$$

one finally finds

$$\langle |\delta h(\mathbf{r},t)|^2\rangle = \frac{1}{2\pi}\int_{\frac{\pi}{L}}^{\frac{\pi}{l_\mathrm{c}}} \mathrm{d}q\, \frac{\zeta^2 k_\mathrm{d}/n_\mathrm{h} + \frac{2}{3}\theta}{\bar{\eta}(q\gamma + q^3\kappa)} \tag{2.82}$$

for the mean square amplitude fluctuations of the tissue height. Here, we introduced two cut-off wavelengths. The large wavelength cut-off $L \simeq \sqrt{A}$ is related to the surface area A of the fluctuating tissue layer. For an infinitely extended tissue, the height fluctuations eventually diverge. The microscopic cut-off l_c is *a priori* related to the length scale of the tissue at which the continuum description fails and thus of the order of the size of a cell. Note however that we neglected viscous stresses in the plane under the assumption $q \ll 1/h$. We therefore choose a short wavelength cut-off which is a cross-over length scale $H \ll l_\mathrm{c} \ll L$. If large wave-length fluctuations dominate, the dependence on the microscopic cut-off can be neglected and the result is consistent with the assumption $q \ll 1/h$. In any case, we only have to convince ourselves that the short wave-length contributions for $q > \pi/l_\mathrm{c}$ do not contribute significantly to the amplitude of the height fluctuations.

Another remark is due here. The above expression that we obtained for the mode spectrum of the height-height correlations is analogous to the case of a fluid membrane subject to thermal fluctuations [41]. Whereas for a fluid membrane the mode spectrum follows in a straightforward way from the equipartition theorem, we used here force balance in order to calculate the fluctuations caused by non-thermal cell division noise. To linear order, the structure is equivalent, however, and we can discuss the tissue height fluctuations using the same concepts as for a thermally fluctuating membrane.

Let us consider two limiting cases. First, consider $q^2\kappa \ll \gamma$ for $q_\mathrm{min} \leq q \leq q_\mathrm{max}$. The integral in Eq. (2.82) then evaluates to

$$\langle |\delta h(\mathbf{r},t)|^2\rangle \simeq \frac{\zeta^2 k_\mathrm{d}/n_\mathrm{h} + \frac{2}{3}\theta}{2\pi\bar{\eta}\gamma}\ln\frac{L}{l_\mathrm{c}}\,. \tag{2.83}$$

In this case, we cannot neglect the dependence on the short wave-length cut-off l_c. Note however that we obtain the scaling of the mean square amplitude of the fluctuations with L, which shows a logarithmic divergence. Therefore, the tissue height does not display long-range positional order; however, orientational order is conserved, see also [41].

We now turn to the case $\gamma = 0$. In this limit, the mean square amplitude fluctuations are more violent and we get

$$\langle |\delta h(\mathbf{r},t)|^2\rangle \simeq \frac{\zeta^2 k_\mathrm{d}/n_\mathrm{h} + \frac{2}{3}\theta}{4\pi^3\bar{\eta}\kappa}\left(L^2 - l_\mathrm{c}^2\right)\,, \tag{2.84}$$

or

$$\langle |\delta h(\mathbf{r},t)|^2\rangle \simeq \frac{\zeta^2 k_\mathrm{d}/n_\mathrm{h} + \frac{2}{3}\theta}{4\pi^3\bar{\eta}\kappa}L^2 \tag{2.85}$$

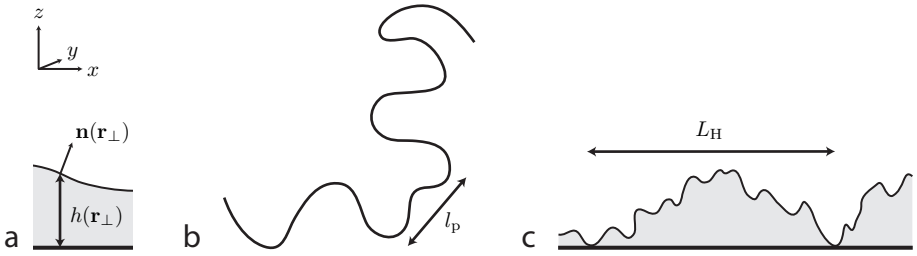

Figure 2.10. Fluctuating tissue surface. (a) The surface normal $\mathbf{n}$ varies along $\mathbf{r}_\perp$ due to cell division noise. (b) If a surface does not exhibit long-range orientational order, it crumbles on length scales larger than the persistence length l_p, and the assumption of no overhangs is no longer justified. (c) One can discuss the Helfrich collision length L_h for which the root mean square height fluctuations $\langle|\delta h|^2\rangle^{1/2}$ are of the order of the mean height H, see text for details.

provided $L \gg l_\mathrm{c}$. The root mean square of the height fluctuations scales with the lateral dimension of the tissue. In this case, the surface is said to be rough, and one can define a wandering exponent ν via $\langle|\delta h|^2\rangle^{1/2} \sim L^\nu$ [41]. Here, $\nu = 1$. A rough interface does not display long-range orientational order, and the surface becomes eventually crumpled on large length scales.

In principle, one can calculate the characteristic length scale on which the orientation of the surface decorrelates [41, 50]. We can calculate this persistence length in the following way. The variation of the surface normal $\mathbf{n}$ is given by $\delta\mathbf{n}(\mathbf{r}_\perp) = \mathbf{n}(\mathbf{r}_\perp) - \mathbf{e}_z \simeq -\nabla_\perp h(\mathbf{r}_\perp)$, see also Fig. 2.10(a). Therefore, one obtains

$$\begin{aligned}\langle|\delta n(\mathbf{r},t)|^2\rangle &\simeq \langle|\nabla_\perp \delta h(\mathbf{r},t)|^2\rangle \\ &= \frac{\zeta^2 k_\mathrm{d}/n_\mathrm{h} + \frac{2}{3}\theta}{2\pi\bar{\eta}\kappa} \ln\frac{l}{l_\mathrm{c}}\,,\end{aligned} \tag{2.86}$$

where l is an upper cut-off length. The persistence length l_p is defined as the length for which $\langle|\delta n(\mathbf{r},t)|^2\rangle$ is of the order of unity, and one finds

$$l_\mathrm{p} \propto e^{\frac{2\pi\bar{\eta}\kappa}{\zeta^2 k_\mathrm{d}/n_\mathrm{h} + \frac{2}{3}\theta}}\,. \tag{2.87}$$

For the dynamics of a tissue layer discussed here, the description breaks down on length scales larger than this persistence length. Most importantly, the tissue height h with respect to the solid substrate becomes ill-defined and the assumption of no overhangs does no longer hold, see Fig. 2.10(b).

There is another, shorter length scale at which the description breaks down, however. Because the tissue has a finite mean height H and the tissue surface is not fluctuating in free space as it could be the case for a fluid membrane, fluctuations eventually reach the solid substrate at $z = 0$. We can therefore define the Helfrich collision length L_H [94], being the system size at which the root mean square amplitude fluctuations are of the

order of the tissue height H. From Eq. (2.85) we find

$$L_{\mathrm{H}} = H\sqrt{\frac{2\pi\bar{\eta}\kappa}{\zeta^2 k_{\mathrm{d}}/n_{\mathrm{h}} + \frac{2}{3}\theta}}\,. \tag{2.88}$$

On length scales larger than L_{H}, the tissue layer eventually breaks up into islands of smaller aggregates, see Fig. 2.10(c). Strictly speaking, the linear approximation $\partial_t h(\mathbf{r}_\perp, t) = v(H, \mathbf{r}_\perp, t)$ does break down for height fluctuations of the order of the mean height. The existence of a characteristic length scale of tissue fracture can nevertheless be expected, and we expect its scaling to follow Eq. (2.88).

Diffusing piston

Let us now discuss the fluctuations of a tissue covered by a stiff piston. The tissue height, or piston position, is simply given by H and does not vary in space, see Fig. 2.9(b). Force balance at $z = H$ now simply reads $\sigma_{zz}(H) + P_{\mathrm{h}} = 0$, since no additional terms due to local height variations appear. Due to translational symmetry in the (x, y)-plane, *i.e.*, for large enough tissues, we can again neglect spatial variations along $\mathbf{r}_\perp$. The force balance along z then becomes

$$\bar{\eta}\partial_z v_z = \frac{1}{A}\int_A \mathrm{d}^2 r_\perp \left(\xi - \tilde{\xi}_{zz}\right), \tag{2.89}$$

where we averaged the cell division noise over the surface area of the piston. Integration over z is straightforward, and we obtain

$$\partial_t H = \frac{1}{\bar{\eta}A}\int_0^H \mathrm{d}z \int_A \mathrm{d}^2 r_\perp \left(\xi - \tilde{\xi}_{zz}\right). \tag{2.90}$$

This equation is not a linear approximation as the corresponding equation (2.77) in the previous case because H does not depend on $\mathbf{r}_\perp$. Note however that the height H is now a random variable and fluctuates in time.

If the tissue surface area A is large compared to the tissue height H such that $\sqrt{A} \gg H$, we can assume that fluctuations are small and $\delta H \equiv H - H_0 \ll H_0$ on intermediate times, where H_0 is a reference tissue height at $t = 0$. This allows us to calculate the fluctuations of δH at short times, *i.e.*, as long as the fluctuations are small compared to H_0. One can then define an effective diffusion constant for the piston via

$$D_{\mathrm{eff}} = \int_0^T \mathrm{d}t\, \langle \dot{H}(t)\dot{H}(0)\rangle \tag{2.91a}$$

$$\simeq \frac{1}{(\bar{\eta}A)^2}\int_0^{H_0}\mathrm{d}z\int_0^{H_0}\mathrm{d}z'\int_A \mathrm{d}^2 r_\perp \int_A \mathrm{d}^2 r'_\perp \left\langle (\xi - \tilde{\xi}_{zz})(\xi - \tilde{\xi}_{zz})\right\rangle, \tag{2.91b}$$

and one eventually obtains

$$D_{\mathrm{eff}} = \frac{2H_0}{\bar{\eta}^2 A}\left(\frac{\zeta^2 k_{\mathrm{d}}}{n_{\mathrm{h}}} + \frac{2}{3}\theta\right). \tag{2.92}$$

Due to the vanishing compressibility of the tissue at the homeostatic state, one can expect giant fluctuations of the tissue height. This is indeed reflected by the fact that $D_{\text{eff}} \propto H_0$. In principle, this diffusive mode of the mean height H adds up to the local height fluctuations discussed in the preceding paragraphs. Note however that this mode vanishes for $A \to \infty$.

What is the characteristic time scale t_D at which this approximation breaks down? If one naively assumes that $t_D D_{\text{eff}} = H_0^2$, one immediately finds

$$\begin{aligned} t_D &= H_0/\sqrt{D_{\text{eff}}} \\ &= \frac{\bar{\eta}\sqrt{AH_0}}{\sqrt{2\left(\zeta^2 k_{\text{d}}/n_{\text{h}} + \frac{2}{3}\theta\right)}}\,. \end{aligned} \tag{2.93}$$

For times $t \ll t_D$, the effective diffusion coefficient does capture the fluctuations of the piston. At times close to or longer than t_D, the tissue height fluctuations are of the order of the order of H_0, and the change of the diffusion constant needs to be taken into account. Moreover, the state $H = 0$ acts as an absorbing boundary, such that the tissue will eventually suppressed at long times. Note however that in analogy to a linear birth and death process with equal probability of birth and death, the mean first passage time to suppression diverges for all heights H_0 [74].

2.6 Comparison of analytical results to numerical simulations

In order to test the ideas presented in the previous sections, we performed numerical simulations of dynamic tissues. From these simulations we determined both the tissue viscosity and the diffusion constant of individual cells (which can be considered as tracer particles) as a function of the cell division rate in the homeostatic state.

A single-cell based model of tissue growth

The simulations have essentially been developed by Markus Basan and Jens Elgeti. Here, we give only a short summary of the model used to simulate tissues; a more detailed description can be found in appendix C.1. In short, we use a few intuitive rules for cell behavior to simulate the growth of a three dimensional tissue. Each cell is represented by two point particles which interact via a repulsive potential. The separation of the particles due to repulsion corresponds to cell growth. When the particles reach a critical distance, the cell divides. This is described by inserting two new particles close to the initial ones, thereby adding one new cell. As this process repeats, the tissue grows, see Fig. 2.11.

Neighboring cells interact with each other via a short range repulsive and a long range attractive potential. Furthermore, dissipative particle dynamics (DPD, [86, 97]) is used to describe effects of internal friction and fluctuations. The DPD method is a stochastic simulation technique that can locally conserve momentum as required for hydrodynamic

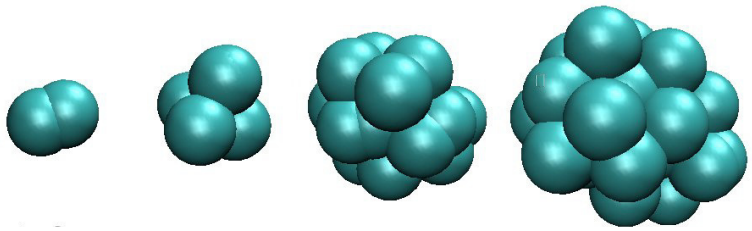

Figure 2.11. Single-cell based model of growing tissues. Individual cells are represented by two particles (left). Growth is mimicked by a repulsive potential that drives these particles apart, and the cell divides after a threshold distance between the two initial particles is reached. This process repeats in time (images from left to right), see text for details.

behavior. Finally, to mimic apoptosis cells are randomly removed at a rate independent of time and pressure.

Tissues that are grown in a box with fixed walls or with periodic boundary conditions reach a homeostatic state at which cell division and apoptosis balance on average. As we argued above, the tissue exhibits a finite characteristic pressure at the homeostatic state. The dependence of this homeostatic pressure on the model parameters has been studied in detail by Basan and colleagues, see reference [16]. Here, we focus on the results obtained for the effective viscosity at the homeostatic state and the diffusion constant of cells.

Viscosity

In our simulations, we measure the shear viscosity of a tissue grown between two walls until reaching the homeostatic state (using periodic boundary conditions in the plane). We shear the tissue by moving the top wall with a prescribed velocity relative to the bottom wall while keeping their distance fixed. The boundary conditions at the wall are described in appendix C.1. We determine the shear rate from the measured velocity profile in the tissue, and we measure the stress exerted on the walls. For most values of the imposed velocity gradient, the stress is a non-linear function of shear rate and the tissue shows shear thinning. At small shear rates however, the viscosity is given by the ratio of stress to shear rate in linear response. We also refer to a later work where the non-linear rheology has been probed in more depth [16].

We first perform these simulations for a reference system with parameters given in the appendix. Parameters used in the other simulations are specified relative to this reference system. Figure 2.12 shows the variation of the viscosity η as a function of the division rate k_d for different parameter choices. For large values of k_d, the viscosity decreases as a function of the division rate with a power law $\eta \propto k_\mathrm{d}^{-1.2}$ close to our prediction $\eta \propto k_\mathrm{d}^{-1}$.

On short time scales, the tissue behaves as a solid. On times long compared to the inverse cell division rate k_d, the tissue starts to flow and is well characterized by a shear viscosity η. Note however, that the tissue starts to flow even for vanishing cell division rate if the imposed stress is larger than a critical yield stress.

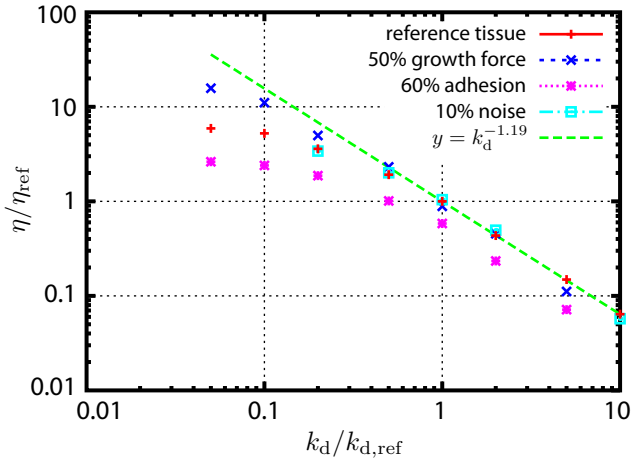

Figure 2.12. Viscosity in a shear simulation. The viscosity is determined for different tissue parameters: standard/reference tissue (red), reduced growth force ($B^* = 0.5$, blue), reduced adhesion ($f_1^* = 0.6$, pink), and reduced noise intensity ($T^*_{\mathrm{noise}} = 0.1$, light blue). The viscosity is rescaled to the value obtained for the reference tissue with reference cell division/apoptosis rate. We use simulation units p_0, t_0 and l_0, see appendix C.1. In these units, the viscosity of the standard tissue is $\eta_{\mathrm{ref}} = 0.15\, p_0 t_0$. The asterisks indicate dimensionless parameters which take the value 1 for the standard tissue.

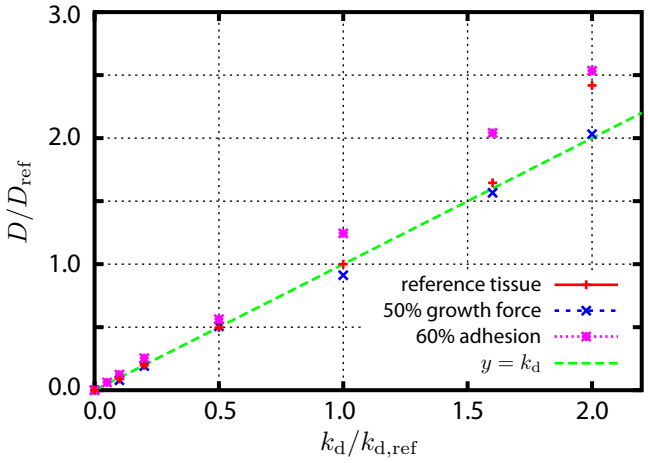

Figure 2.13. Diffusion coefficient of cells D in a tissue simulation. Here, the dependence of D on the division rate k_{d} in the homeostatic state is shown for a reference system (red), simulations with reduced growth force ($B^* = 0.5$, blue), and decreased adhesion strength ($f_1^* = 0.6$, purple). The green line shows a linear fit to the data. The diffusion coefficient is rescaled to the value obtained for the reference tissue with reference cell division/apoptosis rate. In simulation units (see appendix C.1), $D_{\mathrm{ref}} = 0.85\, l_0^2 t_0^{-1}$.

Diffusion

In order to determine the diffusion coefficient of cells in the simulations, we let a tissue grow in a cubic compartment with periodic boundary conditions until it reaches the homeostatic state. Subsequently, we track cells individually and calculate their mean squared displacement (MSD). In the absence of cell turnover (no division or apoptosis), the displacement increases initially with time, but saturates at a finite value. This indicates caging and solid-like behavior. In the presence of cell division and apoptosis, the displacement shows diffusive behavior. We determine the diffusion coefficient by a linear fit to the MSD. The resulting diffusion coefficients displayed in Fig. 2.13 are proportional to k_d as expected from our theory. Note that the MSD of a cell over its lifetime remains the same for different values of the cell division rate.

2.7 Discussion

In this chapter, we developed a continuum description of growing tissues incorporating the effects of cell division and apoptosis. The first important result of this work is that cell division and apoptosis introduce a dynamic reorganization of elastic tissues that leads to liquid-like behavior with well-defined shear and bulk viscosities on long time scales and in the vicinity of the homeostatic state. Whereas it has been argued before that tissues behave effectively as viscous fluids on long times, we show explicitly how the dynamic orientation of stress sources due to cell division and apoptosis events leads to a relaxation of the shear stress. Our analytical calculation of the shear viscosity can well describe simulations capturing the essence of cell duplication and apoptosis. The relaxation of the traceless part of the stress in the tissue is due to a bias of cell division anisotropy by local stress. From a theory point of view, the coupling of average cell division anisotropy to shear stresses arises naturally in isotropic tissues as a first order term in a linear expansion in the (mechanical) perturbation. The stipulated bias on the axis of cell division has been demonstrated in spectacular experiments for single cells in elastic environments [61, 178], and it is hypothesized that similar mechanisms are at work when orienting cell divisions in tissues [126]. Close to the homeostatic state at which cell division and cell death balance, an effective bulk viscosity arises from the coupling of the net cell division rate to excess isotropic stress relative to the homeostatic pressure [17]. A unique consequence of these cellular reorganizations in the vicinity of the homeostatic state is the absence of a compression modulus. As a result, imposing cell pressures either slightly larger or slightly smaller than the homeostatic pressure leads either to the complete disappearance of the tissue or on the contrary to a complete invasion of space by the growing tissue. However, these stress relaxation mechanisms due to cell division and apoptosis do not exist for all cell types. Whether or not these effects can be observed in practical situations depends on the actual values of τ and τ_a compared to the observation time.

To illustrate the described tissue dynamics, we considered the growth of a multicellular spheroid embedded in an elastic matrix. Growth eventually comes to a halt when the

elastic stress exerted by the gel equals the homeostatic pressure of the cell aggregate, and cell division and apoptosis balance. The growth dynamics corresponds qualitatively to experimentally observed growth curves [95]. In principle, one could calculate an effective homeostatic pressure from the observed radius at growth arrest if the initial radius and the matrix shear modulus are known. However, the strong dependence of the homeostatic pressure on the initial radius of the aggregate makes quantitative inferences rather difficult since the initial radius is experimentally hard to control, and it is not sure what is the equilibrium radius of the cavity in the unstressed matrix. Furthermore, other effects are supposed to play a role, such as nutrient limitation [133] and surface effects [130], which we neglected here.

Another example of tissue growth under mechanical constraints is the epiboly of the developing zebrafish embryo, see also Fig. 1.2 in the introduction. During epiboly, cell division is fast, as cells in the enveloping cell layer (EVL) divide approximately three times while spreading on the yolk cell [115]. As a simple toy model of zebrafish epiboly, we studied the example of a tissue layer that spreads on a rigid sphere due to continuous cell proliferation. Our results suggests that stresses due to cell division and apoptosis may contribute to the observed cell flow. Due to the spherical geometry, even isotropic growth gives rise to anisotropic shear stresses, which eventually may orient cell divisions in the EVL. An experimental confirmation of the predicted cell division pattern—if no other planar cell polarity pathways establish global tissue order—would be beautiful evidence in favor of the theory developed in this chapter. Oriented cell divisions of epiblast cells (below the EVL) along the animal-vegetal axis have been documented in the literature [44, 115]; however, the planar cell polarity pathway seems to be involved in spindle orientation [167]. More careful experimental analysis which probes tissue tension might be necessary to distinguish different contributions. Our model furthermore suggests that coupling between isotropic stresses and the rate of cell division may account for spatially varying cell division rates along the EVL. Here, the friction with the underlying substrate plays a decisive role: If the characteristic length $\lambda = \sqrt{\eta'/\gamma} < R/\sqrt{2}$, cell divisions are suppressed at the animal pole, whereas this pattern is inverted for $\lambda > R/\sqrt{2}$.

The second important result of our work concerns the study of noise in the tissue. Here, we mostly considered the noise due to cell division and cell death. Other sources of noise such as the noise due to cell shape fluctuations (formation of protrusions for example) could also play an important role [101, 127, 128]. Density correlation functions can be measured in the simulations and could be directly compared to experiments. In the future, such a fluctuation analysis could become an important way to characterize tissues. A spectacular illustration of the role of noise could be obtained in experiments in which a tissue is confined by a piston with a constant pressure equal to the homeostatic pressure acting on the tissue. Starting from the conservation equations with noise, we showed that the position of the piston is diffusing with a diffusion constant $D \approx \frac{H(k_\mathrm{d}+k_\mathrm{a})}{nA}$, where A is the area of the piston and H is the tissue thickness. These giant fluctuations are associated with the vanishing compressibility of the tissue that we obtain in the hydrodynamic theory.

In the description developed above, we assumed that the only stress relaxation mech-

anisms are cell division and cell death. In the case where the adhesion is not too strong, other stress relaxation mechanisms can exist, for example those related to fluctuations of cell shape and the remodeling of cell-cell junctions [128, 121]. The theory developed in this chapter can be easily modified to take additional relaxation modes into account. Instead of starting from the constitutive equation for an elastic material in the absence of cell division and apoptosis, one could consider a viscoelastic constitutive equation as describing the tissue on times short compared to cell division and apoptosis. The rate of change of the traceless part of the stress would then be given by $(\mathrm{D}/\mathrm{D}t)\tilde{\sigma}_{\alpha\beta} = C_{\alpha\beta\gamma\nu}\tilde{v}_{\gamma\nu} + (\mathrm{D}/\mathrm{D}t)\tilde{\sigma}^{\mathrm{s}}_{\alpha\beta} - \tilde{\sigma}_{\alpha\beta}/\tau_0$, where τ_0 is the rate of stress relaxation in the absence of cell turn-over. In this case, our predictions remain very similar but the stress relaxation rate becomes the sum of the relaxation rates of the various relaxation modes. The viscous relaxation time can become much smaller than the cell division time and accordingly the shear viscosity is strongly reduced. This is consistent with recent experiments on young tissues during development or on cancerous tissues where viscosities of the order or 10^5 Pa s and viscoelastic relaxation times of the order of a few minutes have been measured [63, 88]. However, these relaxation modes do not couple to the isotropic part of the stress, and the time scales for the compression/dilation deformations are still controlled by cell division and death.

Moreover, we presented here only a linear description of the rheology of tissues. Our simulations suggest that tissues show shear thinning, *i.e.*, that their viscosity decreases with the shear rate, when the shear rate is large compared to the division and apoptosis rates. Another non-linear effect observed in the simulation is the existence of a yield stress which corresponds to a plastic behavior of the tissue. The yield stress again exists only at very low values of the cell division rate. A more detailed analysis of the rheology of the tissues simulated by the model presented here can be found in reference [16]. The single-cell model of tissue growth has also been applied successfully in order to simulate the growth of tissue spheroids subject to an external pressure, see reference [130].

Last, we considered here that the tissue is a one-component fluid. We therefore implicitly neglect the roles of both the interstitial fluid and of the extracellular matrix and we do not keep track of total mass conservation. In the next chapter, we develop a two component hydrodynamic theory of tissues that takes the friction due to permeation as well as mass conservation into account.

Chapter 3

Tissue dynamics with permeation

In the previous chapter, we discussed the effects of cell division and apoptosis on the material properties of soft tissues. We described growing tissues as continuous media, which allowed us to understand the coupling between mechanical stresses and the orientation of cell division and the rates of cell division and apoptosis. In order to keep our argument simple, we considered the tissue as a one-component system not explicitly accounting for the material turnover that is necessarily implied by cell division and apoptosis. We therefore did not discuss the associated fluxes of non-cellular material that may give rise to additional mechanical conditions. In this chapter, we extend the theory developed above to a two-component description of tissue dynamics in order to investigate these effects.

3.1 Introduction: Extracellular matrix and interstitial flow

Animal tissues do not only consist of cells; they are complex assemblies of cells, the so-called extracellular matrix (ECM) which fills the interstitial space between cells as illustrated in Fig. 3.1, and the interstitial fluid. The ECM consists of macromolecules produced and assembled into an organized mesh by the surrounding cells. The actual composition of the ECM can vary a lot between different tissues and during development, as its function strongly depends on its structure. In general, the ECM can be described as a cross-linked network of fibrous proteins filled by a porous hydrated gel of amino polysaccharides (the glycosaminoglycans). Whereas the glycoaminoglycans usually do not contribute much to the overall ECM weight, as in the case of connective tissue, they fill most of the extracellular space [8]. Thus, by forming a hydrogel, the glycoaminoglycans can provide mechanical support to the tissue without impeding the fast diffusive transport of molecules solved in the interstitial fluid.

The glycosaminoglycan Hyaluronan (also called hyaluronic acid) is especially abundant in embryonic tissues, for example. It is a unusually large glycosaminoglycan with a molecular weight of $8 \cdot 10^6$ that forms hydrophilic gels that swell enormously with water. Spun out at a cell's surface, it often serves as means to create a cell-free space into which cells can migrate, as a small amount of Hyaluronan is enough to form a gel that

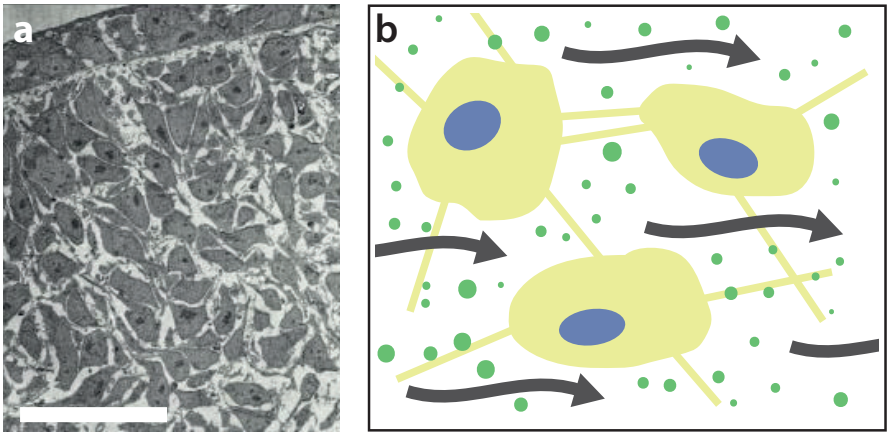

Figure 3.1. Extracellular matrix and interstitial flow. The interstitial space between cells is filled by a dense matrix of various proteins and polysaccharides. The latter form a swelled hydrogel which is permeated by the interstitial fluid. (a) A micrograph of cells and extracellular matrix in the developing limb bud of a chicken embryo. The scale bar indicates 100 μm, image taken from [8]. (b) Close-up sketch of the interstitial space, arrows indicating interstitial fluid flow. The green dots represent the abundance of different versatile proteins present in the extracellular space.

occupies a large volume. The volume ratio of ECM to cells is probably highest in connective tissues, where collagen proteins hierarchically organize into fibers and sheets that provide tensile strength. ECM elasticity is provided by another protein, Elastin, that assembles into an extensive cross-linked network of fibers which adopt a "random-coil" configuration if not stretched. The basal lamina, or basement membrane, that among other functions separates epithelial tissues from the underlying connective tissue, is a special form of extracellular matrix. It has a dense, intricate structure consisting of interconnected collagens, laminins (another fibrous protein), and specific proteoglycans (glycosaminoglycans attached to a core protein).

Cells can attach to the extracellular matrix via cellular adhesion proteins that attach to their respective ECM homologues. In many cases, this attachment is mediated via cellular adhesion proteins called integrins that bind to fibronectin, an ECM protein that has additional binding domains for collagen as well as for other ECM building blocks. Because integrins can assemble a cytoplasmic binding complex that links them firmly to the cell cortex, the latter is finally strongly connected to the collagen network of the extracellular matrix. A prominent example of such a mechanical link are focal adhesions, where many integrin-fibronectin binding complexes act together in a cluster. Note that focal adhesions are mostly formed by cells that are spread on a layer of extracellular matrix. For cells that are embedded in the ECM, the cell-ECM adhesion contacts are usually less focalized and more homogeneously distributed [67].

The important role of the ECM in development and in healthy tissue homeostasis only begins to emerge [103, 163]. The abundance of various ECM proteins and proteoglycans

suggest all kinds of different roles in cell-cell signaling, some of which already having been studied. Notably, the ECM is constantly remodeled by the embedded cells in response to different cues ranging from mechanical stress to specific molecular signals, for example those induced in the case of injury [68].

As mentioned above, the extracellular space is also penetrated by interstitial fluid which swells the ECM hydrogel. In normal tissues, the interstitial fluid consists mostly of blood plasma filtrate that leaks out of capillaries and is subsequently drained by the lymphatics [174]. In *in vitro* cell aggregates such as multicellular spheroids, the interstitial fluid is mostly made up of the culture medium provided. This interstitial fluid flow provides the cells with nutrients and removes metabolic waste.

Here, we develop a multi-component description of tissues in order to capture the effects of material turnover and interstitial fluid flow in the extracellular space in the framework of a continuum theory. Despite the apparent complexity and diversity of the extracellular matrix in tissues, however, we distinguish here only two different components constituting a tissue for simplicity. In the following, we address the dynamics of homogenous three-dimensional confluent tissues with low ECM to cell mass ratio. On the relevant time scales of cell division and apoptosis, the ECM surrounding a cell can be considered as part of that cell, being newly assembled after a cell division or degraded in the case of apoptosis. Thus, we consider the ECM as part of one single cell/ECM tissue component. In addition, we consider the permeating interstitial fluid as the second component independently taken into account.

This chapter is organized as follows. In section 3.2, we detail our two-component description of tissue dynamics. In line with the results obtained in the previous chapter, we consider the cell/ECM phase to behave as a viscoelastic fluid in the presence of cell division and apoptosis. We consider the interstitial fluid to behave as a purely viscous fluid. We show that friction between the fluid and the cell/ECM phase leads to a Darcy-like relation for the interstitial fluid velocity. We furthermore discuss the dynamics around the homeostatic state introduced above, where cell division and apoptosis balance at a given pressure [17]. The two-component description allows to clarify the nature of the homeostatic tissue pressure as opposed to the hydrostatic pressure. In section 3.3, we consider the example of a tissue confined in a chamber which is closed at one end with a movable piston. We solve for the dynamics in the case of both permeable and impermeable pistons for a tissue close to its homeostatic state. For tissues with low permeability, *i.e.*, high friction between fluid and cell/ECM phase, we find that the pressure induced cell division or apoptosis is limited to a region close to the permeable piston with a characteristic length scale given by the permeability and the effective tissue viscosity. Section 3.4 presents a discussion of gravitational forces in the context of a two-component description. As an application, we discuss a treadmilling steady state of a tissue under its own gravitational load, which can be found if the cell/ECM phase and the interstitial fluid have different mass densities. In section 3.5, we review the effective diffusion of cells due to stress fluctuations and find that the effective diffusion constant is modified by the tissue permeability. The last section of this chapter is devoted to a discussion of the results.

3.2 Two-component description of tissue mechanics

The idea to describe tissues as a multi-component system is not new and various mathematical models have been proposed in the literature [38, 154, 162], see also section 1.3. As argued above, we distinguish only two components in order to keep our description simple: (i) a cell/ECM phase that accounts for both the cells in the tissue and the surrounding ECM, which for simplicity we refer to subsequently as cell phase only, and (ii) the interstitial fluid that permeates the cell phase. Although the interstitial fluid is a complex fluid that contains many different proteins and other solvable molecules, we use here a simplified description and consider it as a simple fluid comprising a single effective "molecular" species.

The cell and fluid phases are characterized by the cell number density n_c and the fluid particle number density n_f, respectively, coarse grained over the size of several cells. We introduce the effective cell volume Ω_c (including a portion of the ECM) and the fluid particle volume Ω_f such that

$$n_\mathrm{c}\Omega_\mathrm{c} + n_\mathrm{f}\Omega_\mathrm{f} = 1\,, \tag{3.1}$$

which implies that cells and fluid fill space completely. We further define the cell volume fraction $\varphi = n_\mathrm{c}\Omega_\mathrm{c}$, and the fluid volume fraction is consequently given by $n_\mathrm{f}\Omega_\mathrm{f} = 1 - \varphi$.

3.2.1 Cell-number balance and material turnover

The cell number density n_c obeys a balance equation which includes advection due to cell flow as well as an additional source term due to cell division and apoptosis,

$$\partial_t n_\mathrm{c} + \partial_\alpha(n_\mathrm{c} v^\mathrm{c}_\alpha) = n_\mathrm{c}(k_\mathrm{d} - k_\mathrm{a})\,. \tag{3.2}$$

Here, v^c_α is the velocity field of the cells, and k_d and k_a denote the cell division and apoptosis rates, respectively. Note that this equation is identical to the cell number density balance equation in the one-component theory; no extra terms need to be considered because of the presence of the second component.

The cell balance equation alone does not imply the conservation of mass, however. In the two-component description, we can express total mass conservation as

$$\partial_t\left(n_\mathrm{c}M_\mathrm{c} + n_\mathrm{f}m_\mathrm{f}\right) + \partial_\alpha\left(n_\mathrm{c}M_\mathrm{c}v^\mathrm{c}_\alpha + n_\mathrm{f}m_\mathrm{f}v^\mathrm{f}_\alpha\right) = 0\,, \tag{3.3}$$

where M_c and m_f denote the average cell and fluid particle mass, respectively, and v^f_α is the fluid flow velocity. From (3.2) and (3.3) we thus find a balance equation for the fluid particle density,

$$\partial_t n_\mathrm{f} + \partial_\alpha\left(n_\mathrm{f}v^\mathrm{f}_\alpha\right) = -\frac{M_\mathrm{c}}{m_\mathrm{f}}n_\mathrm{c}(k_\mathrm{d} - k_\mathrm{a}) - \frac{n_\mathrm{c}}{m_\mathrm{f}}\frac{\mathrm{d}}{\mathrm{d}t}M_\mathrm{c}\,, \tag{3.4}$$

where $(\mathrm{d}/\mathrm{d}t) = \partial_t + v^\mathrm{c}_\gamma\partial_\gamma$ is the convected time derivative with respect to the cell flow. The above equation implies that a cell of mass M_c can be converted into $M_\mathrm{c}/m_\mathrm{f}$ fluid particles and vice versa when cells die or divide.

Let us define the compressibility Ξ of the two-component system. The compressibility is given by the response of the total volume to a variation in pressure with no exchange of matter,

$$\Xi = -\frac{1}{V}\frac{\partial V}{\partial P}\Big|_{N_\mathrm{c},N_\mathrm{f}} \tag{3.5a}$$

$$= -n_\mathrm{c}\frac{\partial \Omega_\mathrm{c}}{\partial P}\Big|_{N_\mathrm{c},N_\mathrm{f}} - n_\mathrm{f}\frac{\partial \Omega_\mathrm{f}}{\partial P}\Big|_{N_\mathrm{c},N_\mathrm{f}}\,, \tag{3.5b}$$

where we used $V = N_\mathrm{c}\Omega_\mathrm{c} + N_\mathrm{f}\Omega_\mathrm{f}$. In the following, we consider the system as incompressible. The incompressible limit corresponds to $\Xi \to 0$, and we find

$$0 = -n_\mathrm{c}\frac{\partial \Omega_\mathrm{c}}{\partial P}\Big|_{N_\mathrm{c},N_\mathrm{f}} - n_\mathrm{f}\frac{\partial \Omega_\mathrm{f}}{\partial P}\Big|_{N_\mathrm{c},N_\mathrm{f}}\,. \tag{3.6}$$

Mechanical stability implies that both cell volume Ω_c and fluid particle volume Ω_f must decrease with pressure P in general. Equation (3.6) then imposes that they do not depend on pressure when the tissue is incompressible. For simplicity, we assume that the fluid volume Ω_f is constant; the cell volume Ω_c does not depend on pressure, but can depend on the cell volume fraction φ. The pressure P is then determined by the constraint on the total volume flux $v_\alpha = n_\mathrm{c}\Omega_\mathrm{c}v_\alpha^\mathrm{c} + n_\mathrm{f}\Omega_\mathrm{f}v_\alpha^\mathrm{f}$. Using equations (3.1) to (3.3), we find that for an incompressible system

$$\partial_\alpha v_\alpha = \left(1 - \frac{M_\mathrm{c}/\Omega_\mathrm{c}}{m_\mathrm{f}/\Omega_\mathrm{f}}\right) n_\mathrm{c}\Omega_\mathrm{c}\,(k_\mathrm{d} - k_\mathrm{a}) + n_\mathrm{c}\left(\frac{\mathrm{d}}{\mathrm{d}t}\Omega_\mathrm{c} - \frac{\Omega_\mathrm{f}}{m_\mathrm{f}}\frac{\mathrm{d}}{\mathrm{d}t}M_\mathrm{c}\right)\,. \tag{3.7}$$

In the case of constant cell and fluid mass densities $M_\mathrm{c}/\Omega_\mathrm{c} = m_\mathrm{f}/\Omega_\mathrm{f} \equiv \rho_0$, this expression reduces to $\partial_\alpha v_\alpha = 0$. If not explicitly stated otherwise, we consider the tissue to be incompressible and assume that cell and fluid mass densities are equal and constant. For a thorough discussion of the incompressible limit for a two-component fluid, see appendix D.

3.2.2 Force balance

Tissues are subject to mechanical forces of various origins. Those can either be forces applied at tissue boundaries, external body forces such as gravity, or internal forces due to active processes such as cell division and apoptosis. Forces give rise to mechanical stresses in the tissue, which are described by the total stress tensor $\sigma_{\alpha\beta}$. In a two-component system, the total stress includes contributions from both phases. Thus, we write $\sigma_{\alpha\beta} = \sigma_{\alpha\beta}^\mathrm{c} + \sigma_{\alpha\beta}^\mathrm{f}$, where $\sigma_{\alpha\beta}^\mathrm{c}$ and $\sigma_{\alpha\beta}^\mathrm{f}$ are the stress tensors in the cell phase and in the fluid, respectively.

Neglecting inertia, we can write the total force balance for a volume element of unit volume as $\partial_\beta\sigma_{\alpha\beta} = -f_\alpha^\mathrm{ext}$, where f_α^ext are the external (body) forces acting on the tissue. In the following, we neglect gravity unless otherwise stated. In the absence of external forces, force balance then requires

$$\partial_\beta(\sigma_{\alpha\beta}^c + \sigma_{\alpha\beta}^f) = 0\,. \tag{3.8}$$

If we write separate force balance equations for each of the two different phases, the above equation implies that

$$\partial_\beta \sigma^c_{\alpha\beta} + f_\alpha = 0\,,$$
$$\partial_\beta \sigma^f_{\alpha\beta} - f_\alpha = 0\,.$$

Here, f_α denotes the momentum transfer between the two phases. In the absence of gravitational forces, we assume that momentum is transferred between the cell and the fluid phase solely due to friction in the presence of a relative flow between the two phases. Thus, we write

$$f_\alpha = -\kappa(v^{\mathrm{c}}_\alpha - v^{\mathrm{f}}_\alpha)\,, \tag{3.9}$$

where the inverse friction coefficient κ^{-1} is the effective permeability or hydraulic conductivity of the tissue.[1] The physical dimension of κ is [Viscosity]/[Length]^2, which allows a rough estimate of the tissue permeability. If we assume that $\kappa \sim \eta_{\mathrm{f}}/d_{\mathrm{p}}^2$, where $\eta_{\mathrm{f}} \sim 1 - 100\,\mathrm{mPa\,s}$ is the viscosity of the interstitial fluid (the viscosity of pure water is approx. $1\,\mathrm{mPa\,s}$ at room temperature) and $d_{\mathrm{p}} \sim 0.1 - 1\,\mu\mathrm{m}$ is an average pore size between the cells in the tissue, one finds $\kappa \sim 10^9 - 10^{13}\,\mathrm{Pa\,s\,m^{-2}}$. This estimate is consistent with experimental results [138], see also the discussion at the end of this chapter.

We describe the fluid flow coarse-grained over several cells. The deviatoric stress in the fluid is thus negligible compared to the isotropic stress in the fluid, because the effective pore size of the cell/ECM phase permeated by the interstitial fluid is of the order of a cell size or smaller. Therefore, we can express the total stress in the fluid as $\sigma^{\mathrm{f}}_{\alpha\beta} = -P_{\mathrm{f}}\delta_{\alpha\beta}$, where P_{f} is the fluid pressure in the tissue. Note that in the case of an incompressible tissue, the total pressure $P = -\sigma_{\alpha\alpha}/3$ due to cells and interstitial fluid plays the role of a Lagrange multiplier to ensure the constraint on $\partial_\alpha v_\alpha$. Equivalently, we can consider P_{f} to play the role of the Lagrange multiplier: For an incompressible tissue, the fluid pressure is equally determined by $\partial_\alpha v_\alpha$, as $P_{\mathrm{f}} = P + \sigma_{\mathrm{c}}$. Here, we used $\sigma_{\mathrm{c}} = \sigma^{\mathrm{c}}_{\alpha\alpha}/3$ as an abbreviation for the isotropic part of the cell stress, which one could refer to as (negative) cell pressure also. This contribution to the stress is discussed in more detail below.

Taking the above form of f_α and $\sigma^{\mathrm{f}}_{\alpha\beta}$ into account, the force balance equations finally read

$$\partial_\beta \sigma^{\mathrm{c}}_{\alpha\beta} - \partial_\alpha P_{\mathrm{f}} = 0\,, \tag{3.10a}$$
$$\kappa(v^{\mathrm{c}}_\alpha - v^{\mathrm{f}}_\alpha) = \partial_\alpha P_{\mathrm{f}}\,. \tag{3.10b}$$

For $v^{\mathrm{c}} \equiv 0$, the second equation is the famous Darcy equation describing fluid flow through porous media [47]. It reflects the fact that gradients in fluid pressure drive relative interstitial fluid flow through the extracellular matrix.

[1] Note that Galilean invariance imposes that f_α is proportional to the relative flow of cell and fluid phase if no other gradients or distinguished axes are present in the tissue. In the mechanics literature, symmetry arguments like Galilean invariance are also known as objectivity requirements, see for example [183].

3.2.3 Constitutive equations

In order to describe the tissue dynamics, we need to specify a constitutive equation for the cell phase that relates the stress tensor $\sigma^{\rm c}_{\alpha\beta}$ to other variables or kinematic quantities of the system. In doing so, the constitutive equation accounts for the cell/ECM component material properties. In the previous chapter, we studied the role of cell division and apoptosis on the mechanical properties of growing tissues; we found that tissues which are elastic in the absence of cell division and apoptosis behave in effect as viscoelastic fluids if cells divide or die. Here, we want to use these findings for the description of the cell phase. Note that the same arguments as developed in the previous chapter, section 2.2, hold true for the cell phase in a two-component description. An additional argument has to be made, however, for the dependence of the isotropic cell stress on cell density $n_{\rm c}$ and cell volume $\Omega_{\rm c}$, as in general $n_{\rm c} \neq \Omega_{\rm c}^{-1}$ for a two-component system.

We consider the cell network to behave as an elastic material in the absence of cell division and apoptosis, and we write

$$\frac{\rm D}{{\rm D}t}\sigma^{\rm c}_{\alpha\beta} = C_{\alpha\beta\gamma\nu} v^{\rm c}_{\gamma\nu} + \frac{\rm D}{{\rm D}t}\sigma^{\rm s}_{\alpha\beta} \tag{3.11}$$

for the rate of change of the cell stress. Here, $v^{\rm c}_{\alpha\beta} = (1/2)(\partial_\alpha v^{\rm c}_\beta + \partial_\beta v^{\rm c}_\alpha)$ is the strain rate tensor of the cell velocity field, $({\rm D}/{\rm D}t)\sigma_{\alpha\beta} = \partial_t\sigma_{\alpha\beta} + v^{\rm c}_\gamma\partial_\gamma\sigma_{\alpha\beta} + \omega_{\alpha\gamma}\sigma_{\gamma\beta} + \omega_{\beta\gamma}\sigma_{\alpha\gamma}$ denotes the co-rotational time derivative with respect to the cell flow, and $\omega_{\alpha\beta} = (1/2)(\partial_\alpha v^{\rm c}_\beta - \partial_\beta v^{\rm c}_\alpha)$ is the corresponding cell flow vorticity. The elastic properties of the cell phase are described by the tensor $C_{\alpha\beta\gamma\nu}$, which links the stress in the cell phase to the deformation gradient in the absence of cell division and apoptosis. In the following, we assume that the tissue material properties as characterized by $C_{\alpha\beta\gamma\nu}$ do not depend on orientation, *i.e.*, that $C_{\alpha\beta\gamma\nu} = \chi\,\delta_{\alpha\beta}\delta_{\gamma\nu} + 2\mu(\delta_{\alpha\gamma}\delta_{\beta\nu} - \delta_{\alpha\beta}\delta_{\gamma\nu}/3)$ as for an isotropic material. Here, χ and μ are the compressional and the shear elastic modulus, respectively. The last term in the above equation, $({\rm D}/{\rm D}t)\sigma^{\rm s}_{\alpha\beta}$, accounts for source stresses due to cell division and apoptosis.

The cell stress tensor $\sigma^{\rm c}_{\alpha\beta}$ can be separated into an isotropic contribution $\sigma_{\rm c}$ and a traceless part $\tilde\sigma^{\rm c}_{\alpha\beta}$, such that $\sigma^{\rm c}_{\alpha\beta} = \sigma_{\rm c}\delta_{\alpha\beta} + \tilde\sigma^{\rm c}_{\alpha\beta}$. We discuss the anisotropic part first. In line with the argument put forward in the case of the one-component theory, the corresponding rate of change of the source stress is given by Eq. (2.18),

$$\frac{\rm D}{{\rm D}t}\tilde\sigma^{\rm s}_{\alpha\beta} = -\frac{n_{\rm c}(\tilde d_{\rm d}k_{\rm d} + \tilde d_{\rm a}k_{\rm a})}{\sigma_0}\tilde\sigma^{\rm c}_{\alpha\beta}\,, \tag{3.12}$$

where we already used that the anisotropy of cell division $\tilde q_{\alpha\beta} = \tilde\sigma^{\rm c}_{\alpha\beta}/\sigma_0$ is biased by the shear stress on the relevant time scales. For a more detailed discussion please see section 2.2 in the previous chapter. In the above equation, $\tilde d_{\rm d}$ and $\tilde d_{\rm a}$ are the respective magnitudes of the stress increments related to cell division and apoptosis, and σ_0 is a susceptibility. Together with Eq. (3.11), this form of the source stress leads to Maxwell viscoelastic dynamics for the anisotropic part of the cell stress,

$$\left(1 + \tau_{\rm a}\frac{\rm D}{{\rm D}t}\right)\tilde\sigma^{c}_{\alpha\beta} = 2\eta\tilde v^{c}_{\alpha\beta}\,, \tag{3.13}$$

where $\tau_\mathrm{a}^{-1} = n_\mathrm{c}(\tilde{d}_\mathrm{d} k_\mathrm{d} + \tilde{d}_\mathrm{a} k_\mathrm{a})/\sigma_0$ is an (inverse) relaxation time and $\eta = \tau_\mathrm{a}\mu$ an effective shear viscosity. In the two-component description, the cell phase exhibits the same shear stress relaxation as found in the one-component theory developed in the previous chapter.

In order to discuss the isotropic part of the cell stress, we first consider the tissue in the absence of cell division and apoptosis. We assume that the cell stress depends on the cell volume Ω_c as well as on the cell number density n_c. Note that this distinction need not be made in a one-component description, where $\Omega_\mathrm{c} = n_\mathrm{c}^{-1}$ by definition. In its simplest form, such a dependence on n_c and Ω_c implies an equation of state $\sigma_\mathrm{c} = f(n_\mathrm{c}, \Omega_\mathrm{c})$. For simplicity, we consider such an equation of state in the following. In order to close the system of equations, however, we need one more constitutive equation. A simple choice is to assume that cells adjust their volume according to the cell number density, which implies an additional equation of state $\Omega_\mathrm{c} = g(n_\mathrm{c})$. This choice contains the case in which the cell volume fraction $\varphi = n_\mathrm{c}\Omega_\mathrm{c}$ is fixed to a constant value $\varphi = \varphi_0$: In this limit, the cell volume is given by $\Omega_\mathrm{c}(n_\mathrm{c}) = \varphi_0/n_\mathrm{c}$. Equivalently, we can write the equations of state of the tissue as

$$n_\mathrm{c} = h_1(\sigma_\mathrm{c}) \,, \qquad \Omega_\mathrm{c} = h_2(\sigma_\mathrm{c}) \,, \tag{3.14}$$

where h_1 and h_2 are positive functions. Note that both cell number density and cell volume may additionally depend on the fluid pressure, which we neglect here.

Using these equations of state, we can then define a tissue elastic bulk modulus $\bar{\chi}$ via

$$\frac{\mathrm{d}}{\mathrm{d}t}\sigma_\mathrm{c} = -\frac{\bar{\chi}}{n_\mathrm{c}}\frac{\mathrm{d}n_\mathrm{c}}{\mathrm{d}t} \,, \tag{3.15}$$

or $\bar{\chi} = -n_\mathrm{c}(\mathrm{d}/\mathrm{d}n_\mathrm{c})h_1^{-1}$, respectively. In the absence of cell division and apoptosis, cell number balance implies $(\mathrm{d}/\mathrm{d}t)n_\mathrm{c} = -n_\mathrm{c} v^\mathrm{c}_{\gamma\gamma}$, such that the above equation can be written as $(\mathrm{d}/\mathrm{d}t)\sigma_\mathrm{c} = \bar{\chi} v^\mathrm{c}_{\gamma\gamma}$. The isotropic part of the constitutive equation (3.11) on the other hand becomes $(\mathrm{d}/\mathrm{d}t)\sigma_\mathrm{c} = \chi v^\mathrm{c}_{\gamma\gamma}$ in the case of vanishing source stress, *i.e.*, in the absence of cell division and apoptosis. A comparison of the two latter expressions thus shows that $\bar{\chi} = \chi$; the elastic bulk modulus of the tissue is well-defined.

Cell division and apoptosis give rise to an isotropic source stress as discussed in the previous chapter, and we write

$$\frac{\mathrm{d}}{\mathrm{d}t}\sigma^\mathrm{s} = -n_\mathrm{c} d\,(k_\mathrm{d} - k_\mathrm{a}) \,. \tag{3.16}$$

Here, we already assume that the stress increments d due to single cell division and apoptosis events are of equal magnitude and opposite in sign, see chapter 2, sec. 2.2.2 for a more detailed account. This expression for the source term in Eq. (3.11) leads to

$$\frac{\mathrm{d}}{\mathrm{d}t}\sigma_\mathrm{c} = \chi v^\mathrm{c}_{\gamma\gamma} - n_\mathrm{c} d\,(k_\mathrm{d} - k_\mathrm{a})$$

for the rate of change of the isotropic cell stress. Using cell number balance, equation (3.15) on the other hand implies

$$\frac{\mathrm{d}}{\mathrm{d}t}\sigma_\mathrm{c} = -\chi\left[(k_\mathrm{d} - k_\mathrm{a}) - v^\mathrm{c}_{\gamma\gamma}\right] \,, \tag{3.17}$$

and it follows that $d = \chi/n_\mathrm{c}$. This result is again analogous to the one obtained in the one-component theory put forward in the previous chapter, such that the constitutive equation for the cell stress corresponds both for the isotropic and the traceless part to the constitutive equation for the total stress in the one-component description.

3.2.4 Homeostatic state

In the previous chapter, we discussed the case in which cell division and apoptosis balance on average in the framework of a one-component description. Basan and colleagues argued that this so-called homeostatic state is reached for a characteristic pressure exerted on the cells, as long as biochemical conditions such as nutrient concentrations are kept constant [17]. Even though the biochemical environment might be constant, the rates of cell division and cell death still vary with the mechanical stress in the tissue, which gives rise to a homeostatic pressure P_h at which $k_\mathrm{d}(P_\mathrm{h}) = k_\mathrm{a}(P_\mathrm{h})$, see chapter 2, sec. 2.3, for a more detailed account. Note also that any explicit dependence of the rates on the volume fraction φ could in principle be expressed as a dependence on σ_c for known equations of state (3.14).

Here, we argue that the cell division rate k_d and the apoptosis rate k_a mainly depend on the cell pressure $-\sigma_\mathrm{c}$ in the case that the biochemical environment does not change. Although they might explicitly depend on the fluid pressure P_f, we neglect such a dependence here. In the two-component description, the homeostatic pressure thus translates to a homeostatic cell stress $-\sigma_\mathrm{c} = P_\mathrm{h}$ at which cell division and apoptosis balance on average.

Close to the homeostatic state, we expand the effective cell number growth rate $k_\mathrm{d} - k_\mathrm{a}$ to linear order in the deviatory isotropic cell stress $\delta\sigma_\mathrm{c} \equiv \sigma_\mathrm{c} + P_\mathrm{h}$ around the homeostatic cell pressure P_h,

$$k_\mathrm{d} - k_\mathrm{a} \simeq \frac{1}{\tau}\frac{\delta\sigma_\mathrm{c}}{\chi}\,. \tag{3.18}$$

Together with Eq. (3.17), this expansion leads to Maxwell dynamics for the isotropic part of the stress close to the homeostatic state,

$$\left(1 + \tau\frac{\mathrm{d}}{\mathrm{d}t}\right)(\sigma_\mathrm{c} + P_\mathrm{h}) = \zeta v^\mathrm{c}_{\gamma\gamma}\,, \tag{3.19}$$

where $\zeta = \tau\chi$ is an effective bulk viscosity.

Not surprisingly, this result—relaxation of the isotropic stress at long times—is essentially the same as the one obtained for the one-component description. The distinction between isotropic cell stress and fluid pressure in the two-component description allows a more precise characterization of the homeostatic pressure, however: Assuming that the cell division and apoptosis rates depend on the isotropic cell stress, it turns out that the homeostatic pressure is not to be confounded with the actual fluid pressure. The example presented in the next section illustrates this point in more detail.

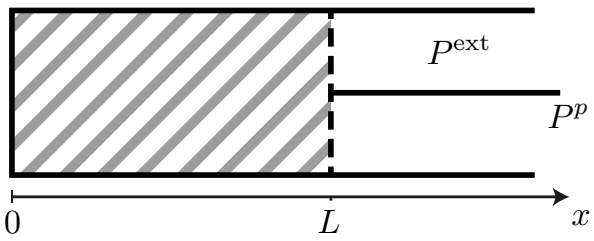

Figure 3.2. Sketch of tissue chamber with piston. The tissue is on the left, separated from a fluid reservoir on the other side of the piston. The piston can be considered as being either impermeable or permeable to the extracellular fluid, see text for details.

3.3 Example: Tissue chamber closed by a piston

With the basic equations being laid out, we now highlight specific features of tissue dynamics with permeation taken into account. As a toy model, we consider a tissue confined to a chamber with fixed lateral walls closed by a movable piston, as sketched in Fig. 3.2.

3.3.1 Steady state of the tissue and piston

We first identify the possible steady states of the system. Consider that both the walls and the piston are impermeable and exert an external pressure P_{ext}. In this case, the total pressure in the tissue chamber has to balance the external pressure, $-\sigma_{\text{c}} + P_{\text{f}} = P_{\text{ext}}$. Furthermore, since there is no cell flow at steady state, the cell pressure equals the homeostatic pressure, $\sigma_{\text{c}} = -P_{\text{h}}$, and the fluid pressure thus follows as $P_{\text{f}} = P_{\text{ext}} - P_{\text{h}}$. In principle, this steady state in the case of an impermeable piston exists irrespective of the applied external pressure.

The situation is different if one of the walls or the piston is semi-permeable and allows for fluid exchange: The flow through the wall or piston is related to the hydrostatic pressure drop over the wall, and a steady state thus requires $P_{\text{f}} = P_{\text{ext}}$, where P^{ext} is the external hydrostatic pressure. Furthermore, the existence of a steady state implies that the tissue is at its homeostatic state, and $\sigma_{\text{c}} = -P_{\text{h}}$. Thus, a steady state exists only if an additional force (per unit area) P_{p} is exerted by the piston; the total pressure in the chamber balances the sum of the external hydrostatic pressure and the additional force applied on the piston, and we find $P_{\text{p}} = P_{\text{h}}$. The force exerted by a semi-permeable piston at steady state therefore provides a measure of the homeostatic pressure. If $P_{\text{p}} \neq P_{\text{h}}$, either the piston moves and squeezes the tissue or the tissue pushes the piston and invades the chamber; there is no other possible steady state.

Note that at steady state, the cell volume and the volume fraction of the interstitial fluid can in principle be calculated from the equations of state of the tissue.

3.3.2 Tissue and piston dynamics close to steady state

In order to discuss the role of permeation on the possible growth dynamics of the tissue, we consider a tissue close to its homeostatic state confined by a semi-permeable piston at one end of the chamber. We choose free slip boundary conditions on the walls of the chamber for both the fluid and the cell phase, which allows for a one-dimensional treatment of the dynamics. Only the piston is permeable. As before, the pressure exerted on the tissue is given by $P_{\mathrm{ext}} + P_{\mathrm{p}}$. However, we now consider that the force exerted on the piston can be written as $P_{\mathrm{p}} = P_{\mathrm{h}} + \delta P$ with $\delta P \neq 0$. The position of the piston is given by the length L of the compartment filled by the tissue. Depending on the sign of δP, the piston moves in either direction.

Before we can solve for the dynamics, we need to specify the boundary conditions at $x = 0$ and $x = L$. At the origin, both the cell phase and the fluid are at rest, $v_x^{\mathrm{c}}(0) = v_x^{\mathrm{f}}(0) = 0$. In the following, we suppress the spatial index for better readability; note that all components orthogonal to the x-direction vanish for symmetry reasons. Using the incompressibility constraint $\partial_x(\varphi v^{\mathrm{c}} + (1-\varphi)v^{\mathrm{f}}) = 0$, we thus find

$$\varphi v^{\mathrm{c}} + (1-\varphi)v^{\mathrm{f}} = 0\,. \tag{3.20}$$

The velocity of the cell flow at $x = L$ corresponds to the velocity of the piston (the moving boundary) because the piston is impermeable to cells, $v^{\mathrm{c}}(L) = \dot{L}$. Assuming that the piston has a finite permeability ν for fluid flow, the boundary condition for the fluid velocity at $x = L$ can be written as

$$v^{\mathrm{f}}(L) - \dot{L} = \nu\left(P_{\mathrm{f}}(L) - P_{\mathrm{ext}}\right)\,. \tag{3.21}$$

Finally, force balance along x implies

$$-\sigma_{\mathrm{c}} - \tilde{\sigma}_{xx}^{\mathrm{c}} + P_{\mathrm{f}} = P_{\mathrm{ext}} + P_{\mathrm{h}} + \delta P\,. \tag{3.22}$$

The constitutive equations for the isotropic and the traceless part of the cell stress are given by Eqs. (3.19) and (3.13), respectively:

$$(1 + \tau\partial_t)\left(\sigma_{\mathrm{c}} + P_{\mathrm{h}}\right) = \zeta\partial_x v^{\mathrm{c}}\,, \tag{3.23a}$$

$$(1 + \tau_{\mathrm{a}}\partial_t)\,\tilde{\sigma}_{xx}^{\mathrm{c}} = \tfrac{4}{3}\eta\partial_x v^{\mathrm{c}}\,. \tag{3.23b}$$

Both the isotropic and the anisotropic stresses show a viscoelastic behavior with relaxation times τ and τ_{a}, respectively. Note that we already neglected the geometric nonlinearities in the convected time derivative. Because of the moving boundary condition at $L = L(t)$, however, we do not know how to solve analytically the full viscoelastic problem defined by the equations above. In the following, we therefore discuss approximations of the problem at short and long times.

Elastic limit at short times

In principle, we are interested in the dynamics at long times, *i.e.*, for times $t \gg \tau, \tau_{\mathrm{a}}$; in this limit, we can neglect the elastic stresses and consider the tissue to behave as a

purely viscous liquid. It is nonetheless instructive to discuss first the dynamics at short times. For times $t \ll \tau, \tau_\mathrm{a}$, the response to an additional force δP exerted by the piston is essentially elastic, and we can write

$$\sigma_\mathrm{c} + P_\mathrm{h} \simeq \chi \partial_x u^\mathrm{c} \,, \tag{3.24a}$$

$$\tilde{\sigma}^\mathrm{c}_{xx} \simeq \tfrac{4}{3}\mu \partial_x u^\mathrm{c} \,, \tag{3.24b}$$

where u^c is the deformation field of the cell phase along x. The cell velocity is given by the time derivative of the deformation, $v^\mathrm{c} = \dot{u}^\mathrm{c}$. Force balance and the permeation equation $\kappa(v^\mathrm{f} - \dot{u}^\mathrm{c}) = -\partial_x P_\mathrm{f}$ lead to a diffusion equation for the elastic deformation u^c,

$$\partial_t u^\mathrm{c} = D_\mathrm{el} \partial_x^2 u^\mathrm{c} \,, \tag{3.25}$$

with the effective diffusion coefficient $D_\mathrm{el} = (1-\varphi)(\chi + \frac{4}{3}\mu)/\kappa$. The strain propagates by diffusive motion only due to the friction with the interstitial fluid; the effective diffusion of the strain is not caused by thermal fluctuations. Note that such an effective diffusion equation for an elastic strain has also been discussed in the context of the swelling of chemical gels, as put forward by Tanaka and colleagues [176]; more recent work can be found in [193]. The swelling of chemical gels also found its application in studies of morphogenesis: In an intriguing study, Derveaux and colleagues discussed the growth dynamics and shape instabilities of tumors in skin using swelling hydrogels as an experimental analogon [52].

The time-dependent boundary condition at $L(t)$ can be rewritten as

$$\dot{u}^\mathrm{c}\big|_L = -v_\mathrm{el} \left(\frac{\delta P}{\bar{\chi}} + \partial_x u^\mathrm{c}\big|_L \right) , \tag{3.26}$$

where we introduced the longitudinal elastic modulus $\bar{\chi} = \chi + \frac{4}{3}\mu$ and the characteristic velocity $v_\mathrm{el} = (1-\varphi)\bar{\chi}\nu$. The constants D_el and v_el can be combined to obtain the characteristic length $l_\mathrm{el} = D_\mathrm{el}/v_\mathrm{el} = (\kappa\nu)^{-1}$ and the characteristic time $t_\mathrm{el} = D_\mathrm{el}/v_\mathrm{el}^2 = [(1-\varphi)\bar{\chi}\kappa\nu^2]^{-1}$ of the problem. Note that both depend on piston permeability ν and do not solely depend on tissue bulk properties. Without explicitly solving the dynamics of the deformation field u^c, we can already infer the steady state deformation after complete relaxation: The diffusion equation imposes that the strain field $\partial_x u^\mathrm{c}$ is constant, and from the boundary condition follows $\partial_x u^\mathrm{c}(x) = -\delta P/\bar{\chi}$. The equilibrium position of the piston L_∞ is then given by $L_\infty = L_0 + u(L_\infty) = L_0/(1 + \delta P/\bar{\chi})$.

The characteristic time and length allow for simple scaling arguments with respect to the dynamics. In the absence of viscous relaxation, the first (immediate) elastic response to a step stress δP for times up to $t \sim t_\mathrm{el}$ remains confined to a layer of thickness l_el until $(\sigma^\mathrm{c}_{xx} + P_\mathrm{h}) \sim -\delta P$ in this layer. The elastic deformation subsequently diffuses along the tissue during a time $T_\mathrm{el} \sim L^2/D_\mathrm{el} = (L/l_\mathrm{el})^2 t_\mathrm{el}$. Note that this time scale is independent of the piston permability ν and depends only on tissue elasticity and tissue permeability. Consequently, the friction between cell phase and interstitial fluid is essentially irrelevant for the initial elastic response if $L \ll l_\mathrm{el}$, *i.e.*, the tissue then behaves effectively like a

one-component system. In this case, the tissue strain is homogeneous and its dynamics depends only on the flux boundary condition at $L(t)$.

Let us discuss the limits $L/l_{\mathrm{el}} \to 0, \infty$ in more detail. In the first case, for $L \ll l_{\mathrm{el}}$, the strain can be considered as homogeneous throughout the tissue, $\partial_x u^{\mathrm{c}} = \text{const.}$, and the moving boundary condition (3.26) becomes an ordinary differential equation for the piston position L,

$$\dot{L} = -v_{\mathrm{el}} \left(\frac{\delta P}{\bar{\chi}} + \frac{L_0 - L}{L} \right) . \tag{3.27}$$

For small $\delta P/\bar{\chi}$, relative deformations are small, and we can approximate the above equation by $\dot{L} \simeq -v_{\mathrm{el}} \left(1 + \delta P/\bar{\chi} - L/L_0\right)$; the respective solution is then given by

$$L(t) \simeq L_0 \left[1 - \tfrac{\delta P}{\bar{\chi}} \left(1 - e^{-t\, v_{\mathrm{el}}/L_0} \right) \right] . \tag{3.28}$$

In the limit of $L/l_{\mathrm{el}} \to \infty$, the relaxation of the piston is entirely limited by the diffusion of the elastic strain. This limit corresponds to an infinite permeability of the semipermeable piston, *i.e.*, $\nu \to \infty$. In this case, the boundary condition at L becomes a condition on the strain at $x = L$ which imposes $\partial_x u^{\mathrm{c}}\big|_L = -\delta P/\bar{\chi}$. The dynamics can be mapped to the diffusion of a solute characterized by the concentration $c(x,t) \equiv \partial_x u^{\mathrm{c}}$ into a sheet of thickness $2L$ with a prescribed concentration $c_0 = -\delta P/\bar{\chi}$ at the boundaries $x = \pm L$; the symmetry around $x = 0$ ensures that the gradient of the concentration $\partial_x c \equiv \partial_x^2 u^{\mathrm{c}}$ vanishes at the origin as required by $u^{\mathrm{c}}(0,t) = 0$. The length L of the sheet would then be given by

$$L(t) = L_0 + u(L,t) = L_0 + \int_0^L \mathrm{d}x\, \partial_x u^{\mathrm{c}} \equiv L_0 + \int_0^L \mathrm{d}x\, c\,. \tag{3.29}$$

For small $\delta P/\bar{\chi}$, the relative deformation is small, and the solution is approximately given by the known result for solute diffusion with constant boundaries at $x = \pm L_0$ [45]:

$$L(t) \simeq L_0 \left[1 - \delta P \left(1 - \frac{8}{\pi^2} \sum_{n=1}^{\infty} \frac{1}{(2n+1)^2} e^{-D_{\mathrm{el}}(2n+1)^2 \pi^2 t/(4L_0^2)} \right) \right] \tag{3.30}$$

In order to check the validity of the above approximations, we compared the analytical results to the numerical solution of the full problem defined by Eqs. (3.25) and (3.26), see Fig. 3.3. For details on the numerical solution we refer to appendix C.2.

Viscoelastic cross-over

On times long compared to the viscous relaxation times $t \gg \tau, \tau_{\mathrm{a}}$, the elastic contribution to the total stress relaxes and the tissue behaves as a viscous fluid. Whether an "elastic steady state" of constant deformation is reached before the viscous regime takes over depends on the ratio of the viscous relaxation time over the time of elastic relaxation discussed above. For $L \gtrsim l_{\mathrm{el}}$, the time after which elastic equilibrium is reached scales as $T_{\mathrm{el}} \sim L^2/D_{\mathrm{el}} = (L/l_{\mathrm{el}})^2\, t_{\mathrm{el}}$; for $L \lesssim l_{\mathrm{el}}$ we found that $T_{\mathrm{el}} \sim L/v_{\mathrm{el}} = (L/l_{\mathrm{el}}) t_{\mathrm{el}}$.

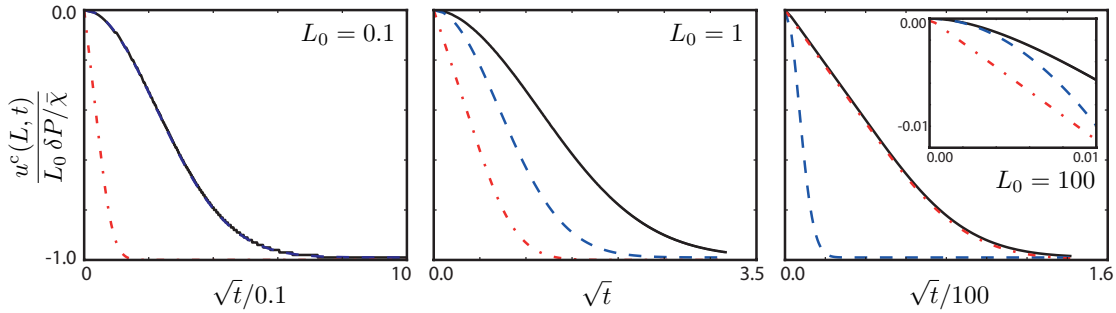

Figure 3.3. Elastic relaxation dynamics of a tissue under compressional load. On short time scales, the tissue response to an additional force δP exerted on the piston is essentially elastic. Here, we plot the piston position as a function of time for different initial tissue sizes L_0. All times and lengths are in units of $t_{\rm el}$ and $l_{\rm el}$, respectively, see text for details; furthermore, we chose $\delta P/\bar{\chi} = 0.01$. Note that for $L_0 = 0.1$, the dynamics is perfectly described by the solution to Eq. (3.27) which is plotted in blue (dashed line). For $L_0 = 100$, the dynamics is well accounted for by Eq. (3.30) which is plotted in red (dashed-dotted line). The inset shows that for times $t < t_{\rm el}$ the initial response is still limited by the relaxation dynamics at the boundary. As $L/l_{\rm el} \to \infty$, $t_{\rm el} \to 0$ and this effect becomes negligible.

Let us assume that $\tau = \tau_{\rm a}$ for simplicity. If $\tau \gg T_{\rm el}$, a homogeneous elastic stress will build up throughout the tissue before the stress starts to relax at times $t > \tau$. In this case, we expect the tissue to behave effectively as described by a one-component theory, *i.e.*, without effects of finite tissue permeability. If $\tau < T_{\rm el}$, however, the viscous response starts to dominate before the elastic deformation has propagated along the entire tissue, and we may expect to see the effects of a finite friction between cells and interstitial fluid. If $\tau \ll t_{\rm el}$, the elastic short time limit does not make much sense at all; the viscous relaxation dominates before any significant elastic stresses are built up.

For the special case $\tau = \tau_{\rm a}$, we can obtain an equation for the velocity field $v^{\rm c}$ that makes the above discussed cross-over more explicit. We differentiate the force balance equation $\partial_x(\sigma^{\rm c}_{xx} - P_{\rm f}) = 0$ with respect to time and make use of the operator identity $(1 - \tau\partial_t)\partial_x = \partial_x(1 - \tau\partial_t)$. With the constitutive equations (3.23) we then get

$$\partial_t v^{\rm c} = -\frac{1}{\tau}\left(v^{\rm c} - \lambda^2\partial_x^2 v^{\rm c}\right) , \tag{3.31}$$

where we introduced the characteristic length scale $\lambda = \sqrt{(1-\phi)\bar{\chi}\tau/\kappa}$ due to tissue viscosity and permeation. On short times (and for zero cell velocity at $t = 0$), the velocity field obeys a diffusion equation with $D = \lambda^2/\tau = D_{\rm el}$. Subsequently, however, the velocity field relaxes to a value that obeys a quasi-static differential equation which we discuss below in more detail. The corresponding boundary condition can be obtained analogously, and we find

$$(1 + \tau\partial_t)\, v^{\rm c}\big|_L = -\frac{\lambda}{\alpha}\left(\frac{\delta P}{\bar{\chi}} + \tau\partial_x v^{\rm c}\big|_L\right) , \tag{3.32}$$

where $\alpha = l_{\mathrm{el}}/\lambda$ is a dimensionless number related to piston permeability. For numerical solutions of the above equations please refer to C.2.

Viscous limit at long times

After this brief discussion of the elastic response at short times and the viscoelastic crossover for times $t \sim \tau, \tau_{\mathrm{a}}$, we turn to the dynamics at long times, *i.e.*, for times longer than the viscous relaxation times, or $t \gg \tau, \tau_{\mathrm{a}}$. In this limit, the viscous stresses are the dominating contribution in the constitutive equations, and we can write

$$\sigma_{\mathrm{c}} + P_{\mathrm{h}} \simeq \zeta \partial_x v^{\mathrm{c}} \,, \tag{3.33a}$$

$$\tilde{\sigma}^{\mathrm{c}}_{xx} \simeq \tfrac{4}{3}\eta \partial_x v^{\mathrm{c}} \,. \tag{3.33b}$$

We can check later for consistency by comparing explicitly the two terms on the left-hand side of Eqs. (3.23). Using the permeation equation $\kappa(v^{\mathrm{f}} - v^{\mathrm{c}}) = -\partial_x P_{\mathrm{f}}$ and incompressibility, the force balance $\partial_x(\sigma^{\mathrm{c}}_{xx} - P_{\mathrm{f}}) = 0$ becomes

$$\lambda^2 \partial_x^2 v^{\mathrm{c}} - v^{\mathrm{c}} = 0 \,. \tag{3.34}$$

Here, we (re)introduced the characteristic permeation length $\lambda = \sqrt{(1-\varphi)\bar{\eta}/\kappa}$, where $\bar{\eta} = \zeta + \frac{4}{3}\eta$ is the longitudinal viscosity. If $\tau = \tau_{\mathrm{a}}$, we have $\bar{\eta} = \tau\bar{\chi}$. Note however that the viscous limit is well-defined also for $\tau \neq \tau_{\mathrm{a}}$. Instead of a partial differential equation for the deformation field u^{c}, as was the case in the elastic limit, one obtains an ordinary differential equation for the cell flow velocity v^{c}. The viscous dynamics at long times is quasi-static not only in the sense that inertial terms are neglected, but also in the sense that the velocity field depends on the boundary conditions only: Any initial conditions necessarily have been "forgotten", *i.e.*, any possible elastic stresses built up at early times have been relaxed.

In the following, we assume that the cell volume fraction φ varies only weakly across the tissue such that $\delta\varphi \ll \varphi$, this is made more precise below. Thus, we may consider λ as constant when solving (3.34) for the cell velocity v^{c}; the general solution is given by

$$v^{\mathrm{c}}(x) = A \sinh \tfrac{x}{\lambda} + B \cosh \tfrac{x}{\lambda} \,.$$

Taking the boundary conditions $v^{\mathrm{c}}(0) = 0$ and $v^{\mathrm{c}}(L) = -(1-\varphi)\nu(\delta P + \bar{\eta}\partial_x v^{\mathrm{c}}(L))$ into account, we finally obtain

$$v^{\mathrm{c}}(x) = -\frac{v_0}{\cosh \frac{L}{\lambda} + \alpha \sinh \frac{L}{\lambda}} \sinh \tfrac{x}{\lambda} \,, \tag{3.35}$$

where $v_0 = \delta P \lambda/\bar{\eta}$ is a characteristic velocity and $\alpha = \lambda/[(1-\phi)\bar{\eta}\nu] = [(1-\phi)\bar{\eta}\kappa\nu^2]^{-1/2}$ is a dimensionless parameter related to the permeability of the piston.[2] Because the cell

[2]Note that with $l_{\mathrm{el}}, t_{\mathrm{el}}$ as defined above, $\alpha = l_{\mathrm{el}}/\lambda \approx (t_{\mathrm{el}}/\tau)^{1/2}$ for $\tau \approx \tau_{\mathrm{a}}$. Vanishing $\alpha \ll 1$ thus implies that elastic and viscous time scales are locally well separated; however, strain propagation may take just as much time as viscous relaxation. For large $\alpha \gg 1$, or sufficiently small piston permeability $\nu \ll (\bar{\eta}(1-\varphi)\kappa)^{-1/2}$, the overall dynamics is so slow that the elastic limit does not make any sense at all; on the relevant time scales, all stresses relax immediately.

velocity v^{c} does not explicitly depend on time, only geometric nonlinearities contribute to the rate of change of stress (which scales with $\partial_x v^{\mathrm{c}}$). These are of second order in δP, however, and can thus safely be neglegted.

Depending on the ratio L/λ, we can distinguish two different regimes of the tissue response:

a) $L \gg \lambda$:

If the permeation length is much smaller than the size of the tissue, we find

$$v^{\mathrm{c}}(x) = -\frac{v_0}{1+\alpha} e^{(x-L)/\lambda}\,, \tag{3.36a}$$

$$-\sigma_{\mathrm{c}}(x) = P_{\mathrm{h}} + \delta P \frac{\zeta}{\bar{\eta}} \frac{e^{(x-L)/\lambda}}{1+\alpha}\,, \tag{3.36b}$$

$$P_{\mathrm{f}}(x) = P_{\mathrm{ext}} + \delta P \left(1 - \frac{e^{(x-L)/\lambda}}{1+\alpha}\right)\,. \tag{3.36c}$$

Due to the finite permeability of the tissue, fluid pressure builds up over the length scale λ beyond which it compensates the additional force exerted by the piston. Thus, only a small region of thickness λ is perturbed, where apoptosis dominates if $\delta P > 0$ and division dominates if $\delta P < 0$. Most of the tissue is in its stationary state. The piston moves at constant velocity $\dot{L} = -v_0/(1+\alpha)$: For small $\alpha \ll 1$, the velocity scales with the size of the perturbed region λ; for $\alpha \gg 1$, *i.e.*, for low piston permeability ν, the velocity does not depend on tissue permeability κ and scales with ν. For $\alpha \to \infty$, the piston does not move and no cell turnover takes place. This limit corresponds to zero piston permeability and one recovers the stationary state as discussed for an impermeable piston. Examples of flow and pressure profiles are sketched in Fig. 3.4. A one-component description of tissues must fail to capture the dynamics of the regime $L \gg \lambda$ correctly.

b) $L \ll \lambda$:

If the permeation length is much larger than the size of the tissue, to lowest order in x/λ we find

$$v_x^{\mathrm{c}}(x) = -\frac{v_0}{1+\alpha L/\lambda} \frac{x}{\lambda}\,, \tag{3.37a}$$

$$-\sigma^{\mathrm{c}}(x) = P_{\mathrm{h}} + \delta P \frac{\zeta}{\bar{\eta}} \frac{1}{1+\alpha L/\lambda}\,, \tag{3.37b}$$

$$P_{\mathrm{f}}(x) = P_{\mathrm{ext}} + \delta P \frac{\alpha L/\lambda}{1+\alpha L/\lambda}\,. \tag{3.37c}$$

In this regime, one recovers the result that one would obtain in the one-component theory: Without permeation, any excess pressure δP acts on the whole tissue instantaneously in a homogeneous way because no momentum can be transferred to the fluid, and $\partial_x v_x^{\mathrm{c}} = \text{const}$. Note however that for the actual two-component

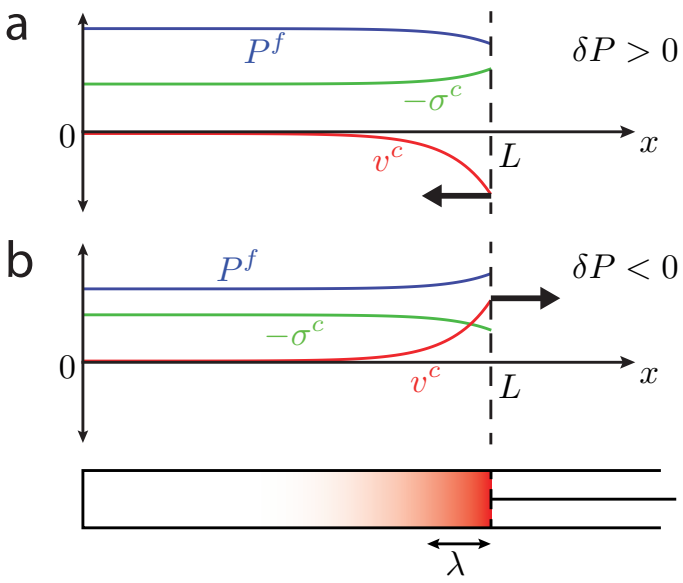

Figure 3.4. Tissue dynamics in response to an external force in the viscous limit. The force is exerted by a semipermeable piston, with its position being indicated by the dashed vertical line. Here, we illustrate the case in which the characteristic length λ is small compared to the size of the tissue chamber L. We find that the tissue response is confined to a zone of length λ close to the piston, see text for details. (a) For $\delta P > 0$, the cells undergo apoptosis which results in a negative net cell flow as indicated. (b) For $\delta P < 0$, the cells are dividing and thus give rise to a net expansion of the tissue.

system in the limit $L \ll \lambda$, the excess pressure δP exerted by the piston is rescaled due to the fluid pressure drop at $x = L$ caused by the finite piston permeability.

The position of the piston as a function of time is implicitly given by

$$\lambda \ln L/L_0 + \alpha(L - L_0) = -v_0 t\,. \tag{3.38}$$

For large α, *i.e.*, $\alpha \gg \lambda/L$, the piston moves with constant speed $\dot{L} \approx -v_0/\alpha$, as the finite permeability of the piston limits the velocity with which the tissue turns over. For reasonably small $L \ll \lambda/\alpha$, or for large enough piston permeability, *i.e.*, $\nu \gg L/(\bar{\eta}(1-\phi))$, this effect becomes negligible and the position of the piston varies according to $\dot{L} \approx -v_0 L/\lambda$. In this case, one recovers an exponential regime either for growth or for shrinkage.

The cell number density n_c and the cell volume Ω_c can in principle be determined via the equations of state (3.14). Eventually, one can check that for small δP their variations are small (but always time dependent). The assumption that the variation $\delta\varphi$ of the volume fraction is small can now be discussed more precisely: The above calculations are consistent if $\delta\varphi = (\mathrm{d}\varphi/\mathrm{d}\sigma_c)\delta\sigma_c \ll \varphi \approx 1$, where $\delta\sigma_c = \delta P\zeta/[\bar{\eta}(1+\alpha)]$

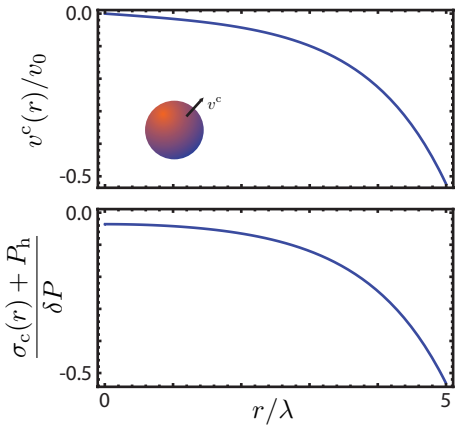

Figure 3.5. Cell flow and stress profiles for a spherical tissue aggregate in response to an excess piston pressure $\delta P > 0$. Here, we chose $\zeta = \eta$ and $R = 5\lambda$, see text for details.

in the case of $L \gg \lambda$ and $\delta\sigma_c = \delta P\zeta/[\bar{\eta}(1+\alpha L/\lambda)]$ in the case of $L \ll \lambda$, and $\mathrm{d}\phi/\mathrm{d}\sigma_c = (\mathrm{d}h_1/\mathrm{d}\sigma_c)\Omega_c + n_c(\mathrm{d}h_2/\mathrm{d}\sigma_c)$ for known h_1 and h_2 (*cf.* Eqs. (3.14)).

Finally, we show in appendix C.2 that the numerical solution to the viscoelastic problem with $\tau = \tau_a$ for both $L \gg \lambda$ and $L \ll \lambda$ confirms the long-time limits obtained in this section.

Viscous limit in spherical geometry

In principle, the same behavior can be found for spherical tissue aggregates under an external excess pressure δP acting on a semi-permeable membrane enclosing the tissue. Spherical symmetry imposes $\mathbf{v}^c = v^c(r)\mathbf{e}_r$. Radial force balance in spherical geometry reads

$$\partial_r\sigma_c + \partial_r\tilde{\sigma}^c_{rr} + 2\frac{\tilde{\sigma}^c_{rr} - \tilde{\sigma}^c_{\theta\theta}}{r} - \partial_r P_f = 0\,. \tag{3.39}$$

Using again incompressibility and the permeation equation, we obtain an equation for v^c in the limit of long times,

$$\lambda^2\left[\partial_r^2 v^c + 2\left(\frac{\partial_r v^c}{r} - \frac{v^c}{r^2}\right)\right] - v^c = 0\,, \tag{3.40}$$

where $\lambda^2 = (1-\varphi)\bar{\eta}/\kappa$ is defined as above. Taking the boundary condition $v^c(0) = 0$ into account, the solution to this equation is given by

$$v^c(r) = c\left[\tfrac{\lambda}{r}\cosh\tfrac{\lambda}{r} - \left(\tfrac{\lambda}{r}\right)^2\sinh\tfrac{\lambda}{r}\right]\,. \tag{3.41}$$

The integration constant c can be found from the boundary conditions at the outer radius $R(t)$. Using $\sigma_c + \tilde{\sigma}^c_{rr} - P_f = -P_{ext} - P_h - \delta P$, the flux boundary condition can be written as

$$v^c\big|_R = -\frac{\lambda}{\alpha}\left(\frac{\delta P}{\bar{\eta}} + \partial_r v^c\big|_R + \epsilon\frac{v^c}{r}\Big|_R\right)\,, \tag{3.42}$$

where $\epsilon = 2(\zeta - \frac{2}{3}\eta)/\bar{\eta}$ and all other constants defined as above. We finally find

$$v^{\mathrm{c}}(r) = -\frac{v_0\left(\cosh\frac{\lambda}{r} - \frac{\lambda}{r}\sinh\frac{\lambda}{r}\right)\frac{R}{r}}{\left[\alpha + (\epsilon-2)\frac{\lambda}{R}\right]\cosh\frac{\lambda}{R} + \left[1 - \alpha\frac{\lambda}{R} - (\epsilon-2)\left(\frac{\lambda}{R}\right)^2\right]\sinh\frac{\lambda}{R}} \tag{3.43}$$

for the radial velocity of the cell flow, with $v_0 = \delta P\lambda/\bar{\eta}$. Examples of flow and stress profiles are shown in Fig. 3.5. In principle, we could now discuss in more detail the same limits as before, *i.e.*, $R \gg \lambda$ and $R \ll \lambda$. The qualitative behavior remains the same as in the linear geometry, however.

3.4 Example: Tissue under its own gravitational load

In the previous section, we neglected gravitational forces, which are supposed to be small compared to other forces. Although they do not necessarily play a role in many biological contexts of tissue dynamics, taking the effects of gravitation into account allows to illustrate key aspects of a multi-component description of tissues.

3.4.1 Force balance in the presence of gravity as external body force

In the presence of external body forces, total force balance reads $\partial_\beta\sigma_{\alpha\beta} = -f_\alpha^{\mathrm{ext}}$. For gravitational forces, we have $f_\alpha^{\mathrm{ext}} = \rho g_\alpha$, where $\rho = \varphi\rho_{\mathrm{c}} + (1-\varphi)\rho_{\mathrm{f}}$ is the total mass density of the tissue (ρ_{c} and ρ_{f} being the mass densities of the cell phase and the interstitial fluid, respectively) and g_α is the gravitational acceleration. For each of the two components, we can write force balance separately as

$$\partial_\beta\sigma^{\mathrm{c}}_{\alpha\beta} + f_\alpha = -\varphi\rho_{\mathrm{c}}g_\alpha\,, \tag{3.44a}$$

$$-\partial_\alpha P_{\mathrm{f}} - f_\alpha = -(1-\varphi)\rho_{\mathrm{f}}g_\alpha\,, \tag{3.44b}$$

where the gravitational force on each of the components corresponds to its mass fraction. The momentum transfer between the two phases is again denoted by f_α. Whereas in the absence of gravity the momentum transfer was due only to a finite permeability of the cell phase for interstitial fluid flow, f_α now comprises not only friction forces $\propto (v^{\mathrm{c}}_\alpha - v^{\mathrm{f}}_\alpha)$ but contains an additional contribution due to buoyancy forces,

$$f_\alpha = -\kappa(v^{\mathrm{c}}_\alpha - v^{\mathrm{f}}_\alpha) - \varphi\rho_{\mathrm{f}}g_\alpha\,, \tag{3.45}$$

and we can rewrite the above equations as

$$\partial_\beta\sigma^{\mathrm{c}}_{\alpha\beta} - \kappa(v^{\mathrm{c}}_\alpha - v^{\mathrm{f}}_\alpha) = -\varphi(\rho_{\mathrm{c}} - \rho_{\mathrm{f}})g_\alpha\,, \tag{3.46a}$$

$$-\partial_\alpha P_{\mathrm{f}} + \kappa(v^{\mathrm{c}}_\alpha - v^{\mathrm{f}}_\alpha) = -\rho_{\mathrm{f}}g_\alpha\,. \tag{3.46b}$$

Two main conclusions can be drawn immediately: First, gravitation enters the force balance equation for the cell phase only for finite density differences $\rho_{\mathrm{c}} - \rho_{\mathrm{f}}$, *i.e.*, if the mass density of the cell/ECM phase is different from the mass density of the interstitial

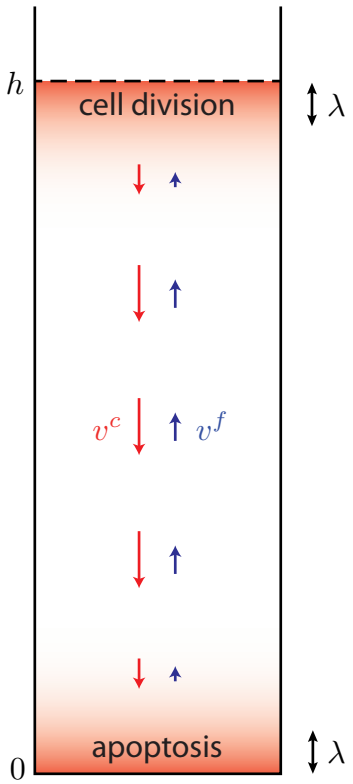

Figure 3.6. Sketch of a treadmilling tissue column of height h. Due to a difference in the mass densities of cells and fluid, cells are subject to gravitational forces. We find a solution where cells tend to divide at the top layer of a tissue column and undergo apoptosis at the bottom layer. In between, a constant cell flow maintains the stationary state, together with the opposed interstitial fluid flow.

fluid. In general, the mass density difference is small, $\rho_\mathrm{c} - \rho_\mathrm{f} \ll \rho_\mathrm{f}$. Second, in the absence of flow, *i.e.*, in a stationary state, gravitation gives rise to a barometric profile of the hydrostatic pressure P_f due to the finite mass density of the fluid.

Consider a tissue column of arbitrary height with $\rho_\mathrm{h} = \rho_\mathrm{f}$. Does the homeostatic stationary state still exist? Only excess weight with respect to the interstitial fluid would actually exert an additional stress on the cell phase, which is not the case. Therefore, force balance is readily satisfied for zero flow and $\sigma^\mathrm{c}_{\alpha\beta} = -P_\mathrm{h}\delta_{\alpha\beta}$ constant, where P_f exhibits a barometric pressure profile as discussed above.

3.4.2 Gravity-induced treadmilling steady state

In the case of a small but finite difference $\delta\rho \equiv \rho_\mathrm{c} - \rho_\mathrm{f} \ll \rho_\mathrm{f}$ between the mass densities of cells and the fluid, no homeostatic stationary state exists. For a tissue layer close to homeostatic state, however, a treadmilling stationary state can be found in which apoptosis is induced at the bottom of the tissue layer, balanced by cell division at the upper surface, see Fig. 3.6.

We consider a tissue contained in a box with impermeable lateral walls that are described by full slip boundary conditions and a solid bottom wall at $z = 0$, such that the problem is effectively one-dimensional. The tissue of height h is subject to a force

exerted on its upper surface by a semi-permeable membrane or piston similar to the example given in the previous section. In the long time limit, we consider the tissue as viscous and keep only the viscous part of the cell stress variations $\delta\sigma_\mathrm{c} = \sigma_\mathrm{c} + P_\mathrm{h}$ and $\tilde{\sigma}^\mathrm{c}_{\alpha\beta}$ as given by the constitutive equations (3.13) and (3.19), $\tilde{\sigma}^\mathrm{c}_{\alpha\beta} = 2\eta\tilde{v}^\mathrm{c}_{\alpha\beta}$ and $\delta\sigma_\mathrm{c} = \zeta v^\mathrm{c}_{\gamma\gamma}$.

For finite $\delta\rho$, the divergence of the total volume flux is finite in the presence of cell division and apoptosis, as discussed in section 3.2 above. Assuming that cell and fluid mass densities are constant, the incompressibility condition reads

$$\partial_\alpha v_\alpha = \left(1 - \frac{\rho_\mathrm{c}}{\rho_\mathrm{f}}\right) n_\mathrm{c}\Omega_\mathrm{c} \left(k_\mathrm{d} - k_\mathrm{a} - \frac{1}{\Omega_\mathrm{c}}\frac{\mathrm{d}}{\mathrm{d}t}\Omega_\mathrm{c}\right) . \tag{3.47}$$

Both the net cell division rate $k_\mathrm{d} - k_\mathrm{a}$ and the cell volume are proportional to the excess isotropic cell stress, *i.e.*, $k_\mathrm{d} - k_\mathrm{a} \propto \delta\sigma_\mathrm{c}$ and $\delta\Omega_\mathrm{c} \propto \delta\sigma_\mathrm{c}$ (*cf.* equation of state (3.14)). Because $\delta\sigma_\mathrm{c} \propto \delta\rho/\rho_\mathrm{f}$ as we will see below, the divergence vanishes to second order in $\delta\rho/\rho_\mathrm{f} \ll 1$. Therefore, we take $\partial_\alpha v_\alpha = 0$. Using the zero flux boundary condition at $z = 0$, we can thus express the fluid velocity as $v^\mathrm{f} = -\frac{\varphi}{1-\varphi}v^\mathrm{c}$, where we used $\mathbf{v}^\mathrm{c} = v^\mathrm{c}\mathbf{e}_z$ and $\mathbf{v}^\mathrm{f} = v^\mathrm{f}\mathbf{e}_z$ (also, $\mathbf{g} = -g\mathbf{e}_z$ in the following).

From the force balance equation of the cell phase we obtain an equation for the cell flow velocity,

$$\lambda^2\partial_z^2 v^\mathrm{c} - v^\mathrm{c} = v_0 , \tag{3.48}$$

where we introduced the characteristic velocity $v_0 = \delta\rho g\varphi(1-\varphi)/\kappa$. The characteristic length $\lambda = \sqrt{(1-\varphi)\bar{\eta}/\kappa}$ and the longitudinal viscosity $\bar{\eta} = \zeta + \frac{4}{3}\eta$ are defined as above. The general solution for Eq. (3.48) is given by

$$v^\mathrm{c} = -v_0\left(1 + Ae^{\frac{z}{\lambda}} + Be^{-\frac{z}{\lambda}}\right) , \tag{3.49}$$

where A and B have to be determined by the boundary conditions at $z = 0$ and $z = h$. We look for a steady state where the cell velocity vanishes on both surfaces, $v^\mathrm{c}(h) = v^\mathrm{c}(0) = 0$, and we find

$$v^\mathrm{c} = -v_0\left(1 - \frac{\sinh\frac{z}{\lambda} + \sinh\frac{h-z}{\lambda}}{\sinh\frac{h}{\lambda}}\right) . \tag{3.50}$$

The cell pressure $-\sigma_\mathrm{c}$ follows from the constitutive equation (3.19) in the viscous limit,

$$-\sigma_\mathrm{c} = P_\mathrm{h} - \frac{\zeta v_0}{\lambda\sinh\frac{h}{\lambda}}\left(\cosh\frac{z}{\lambda} - \cosh\frac{h-z}{\lambda}\right) . \tag{3.51}$$

For $h \gg \lambda$, this expression simplifies to

$$-\sigma_\mathrm{c} = P_\mathrm{h} + \frac{\zeta v_0}{\lambda}\left(e^{-\frac{z}{\lambda}} - e^{-\frac{h-z}{\lambda}}\right) . \tag{3.52}$$

In this case, the tissue is proliferating in a small layer of thickness λ at the upper surface and undergoing apoptosis in a layer at the bottom of the same thickness. In between,

the cells flow with a velocity $v^c \simeq -v_0$ from the top to the bottom. If $h \ll \lambda$, the cell velocity is vanishing everywhere to second order, *i.e.*, $v^{\mathrm{c}} = \mathcal{O}(\delta\rho\frac{h}{\lambda})$, and no relevant turnover takes place.

In order for the treadmilling steady state to exist, the cell stress σ^{c}_{zz} along z at $z = h \gg \lambda$ has to be balanced by a semi-permeable membrane or piston, $\sigma^{\mathrm{c}}_{zz} = -P_{\mathrm{p}}$, which exerts a pressure $P_{\mathrm{p}} = P_{\mathrm{h}} - \bar{\eta}v_0/\lambda$. The external hydrostatic pressure P_{ext} at $z = h$ enters as a boundary condition for the fluid pressure with $P_{\mathrm{f}}(h) = P_{\mathrm{ext}}$. (Note that the fluid flux across the membrane vanishes and we do not have to take the finite membrane permeability into account.) The fluid pressure can then be determined from $-\partial_z P_{\mathrm{f}} + \frac{\kappa}{1-\varphi}v^{\mathrm{c}} = \rho_{\mathrm{f}} g$, and we find

$$P_{\mathrm{f}} = P_{\mathrm{ext}} + (\rho_{\mathrm{f}} + \varphi\delta\rho)g(h-z) + \varphi\delta\rho g\lambda\frac{\cosh\frac{z}{\lambda} - \cosh\frac{h-z}{\lambda} - \cosh\frac{h}{\lambda} + 1}{\sinh\frac{h}{\lambda}}\,, \tag{3.53}$$

which in the case of $h \gg \lambda$ simplifies to

$$P_{\mathrm{f}} = P_{\mathrm{ext}} + (\rho_{\mathrm{f}} + \varphi\delta\rho)g(h-z) - \varphi\delta\rho g\lambda\left(e^{-\frac{z}{\lambda}} - e^{\frac{z-h}{\lambda}} + 1\right)\,. \tag{3.54}$$

As in the first example, the cell number density n_{c} and the cell volume Ω_{c} can in principle be determined via the equations of state (3.14). Eventually, one can check that for small $\delta\rho/\rho_{\mathrm{f}} \ll 1$ their variations are small.

3.5 Fluctuations

In the above examples, we did not consider fluctuations that may arise due to the stochasticity of cell division and apoptosis. Whereas such a mean-field might be appropriate when describing the dynamics on large scales, it does not allow to capture the diffusive behavior of single cells in a tissue which exists even at steady state; see also the discussion in the previous chapter, sections 2.5 and 2.7. Here, we investigate the role of fluctuations in the homeostatic state in the two-component description along the lines of the one-component theory developed above, notably including the effects of permeation, however.

3.5.1 Stress and velocity fluctuations

When we take the stochasticity of cell division and apoptosis into account, the cell number balance equation contains an additional noise term describing the fluctuations. To first order, fluctuations in the cell number density are described by gaussian white noise ξ^c with zero mean and local correlations in space and time. For a simple birth-and-death process, one would have $\langle\xi^c(\mathbf{r},t)\xi^c(\mathbf{r}_0,t_0)\rangle = n^c(k_{\mathrm{d}} + k_{\mathrm{a}})\,\delta(\mathbf{r}-\mathbf{r}_0)\delta(t-t_0)$, which we use here by (simplifying) analogy. Thus, we rewrite the cell number balance including noise as

$$\partial_t n_{\mathrm{c}} + \partial_\alpha(n_{\mathrm{c}}v^{\mathrm{c}}_\alpha) = n_{\mathrm{c}}(k_{\mathrm{d}} - k_{\mathrm{a}}) + \xi_{\mathrm{c}}\,. \tag{3.55}$$

The fluctuations in the cell number lead to fluctuations in the isotropic part of the cell stress according to (3.17), which close to the homeostatic state reduces to

$$\left(1+\tau\frac{\mathrm{d}}{\mathrm{d}t}\right)(\sigma_\mathrm{c}+P_\mathrm{h}) = \zeta v^\mathrm{c}_{\gamma\gamma} - \frac{\zeta}{n_\mathrm{h}}\xi_\mathrm{c}\,, \tag{3.56}$$

where $n_\mathrm{h} = n_\mathrm{c}(P_\mathrm{h})$ is the cell number density in the homeostatic state.

Fluctuations of the orientation of cell division, and stochastic cell deformations, give rise to noise in the anisotropic part of the stress,

$$\left(1+\tau_\mathrm{a}\frac{\mathrm{D}}{\mathrm{D}t}\right)\tilde{\sigma}^\mathrm{c}_{\alpha\beta} = 2\eta\tilde{v}^\mathrm{c}_{\alpha\beta} + \tilde{\xi}_{\alpha\beta}\,, \tag{3.57}$$

where $\tilde{\xi}_{\alpha\beta}$ denotes the noise source. Without giving a microscopic description of these fluctuations, we assume that they correspond to a Gaussian white noise with zero mean and delta-correlations in space and time. For an isotropic system, these correlations are characterized by a single noise strength θ such that $\langle\tilde{\xi}_{\alpha\beta}(\mathbf{r},t)\tilde{\xi}_{\gamma\delta}(\mathbf{r}_0,t_0)\rangle = \theta\left(\delta_{\alpha\gamma}\delta_{\beta\delta}+\delta_{\alpha\delta}\delta_{\beta\gamma}-\frac{2}{3}\,\delta_{\alpha\beta}\delta_{\gamma\delta}\right)\delta(\mathbf{r}-\mathbf{r}_0)\delta(t-t_0)$.

As the stochasticity of cell division and apoptosis implies fluctuations in the cell stress $\sigma^\mathrm{c}_{\alpha\beta}$, they give rise to fluctuations in the cell flow. In order to calculate the diffusion constant of single cells in the tissue, we need to solve for the correlations of the cell velocity fluctuations. The cell velocity can in turn be calculated from force balance. In the following, we assume that the mass densities of cell phase and interstitial fluid are equal and constant and neglect gravitational forces. Incompressibility then requires $\partial_\alpha v_\alpha = 0$, and assuming zero volume flux at infinity we have $v_\alpha = 0$. Thus, the fluid velocity field v^f_α can be expressed as $v^\mathrm{f}_\alpha = -v^\mathrm{c}_\alpha\varphi/(1-\varphi)$.

Following the strategy employed above for calculating the diffusion coefficient in the one-component description (*cf.* sec. 2.5), we decompose all quantities in Fourier modes in space and time according to $f(\mathbf{q},\omega) = \int\mathrm{d}t\int\mathrm{d}\mathbf{r}\,e^{-i(\mathbf{q}\mathbf{r}-\omega t)}f(\mathbf{r},t)$. We again split the cell velocity field into longitudinal and transverse components, $v^\mathrm{c}_\alpha = v^\mathrm{c}_{||}q_\alpha/q + v^\mathrm{c}_{\perp\alpha}$. Inserting Eqs. (3.56) and (3.57) into the force balance,

$$\begin{aligned} iq_\beta\sigma^\mathrm{c}_{\alpha\beta} - iq_\alpha P_\mathrm{f} &= 0\,,\\ -iq_\alpha P_\mathrm{f} + \tfrac{\kappa}{1-\varphi}v^\mathrm{c}_\alpha &= 0\,, \end{aligned}$$

we finally obtain

$$v^\mathrm{c}_{||} = \frac{1}{iq}\frac{(1-i\omega\tau_\mathrm{a})\zeta n_\mathrm{h}^{-1}\xi_\mathrm{c} - (1-\omega\tau)q_\alpha q_\beta\tilde{\xi}_{\alpha\beta}/q^2}{\left[(1-i\omega\tau_\mathrm{a})\,\zeta + (1-i\omega\tau)\,\frac{4}{3}\eta\right] + \bar{\kappa}(1-i\omega\tau)(1-i\omega\tau_\mathrm{a})}\,, \tag{3.58a}$$

$$v^\mathrm{c}_{\perp\alpha} = \frac{i}{q}\frac{q_\beta\tilde{\xi}_{\alpha\beta}/q - q_\alpha q_\gamma q_\beta\tilde{\xi}_{\gamma\beta}/q^3}{\eta+\bar{\kappa}(1-i\omega\tau_\mathrm{a})}\,, \tag{3.58b}$$

where $\bar{\kappa} = \kappa/[(1-\phi)q^2]$. Note the additional term in the denominator for finite $\bar{\kappa}$ due to the permeation of the interstitial fluid through the tissue, in comparison to the one-component tissue theory. As $\bar{\kappa}\propto q^{-2}$, friction becomes increasingly important for long wavelength modes.

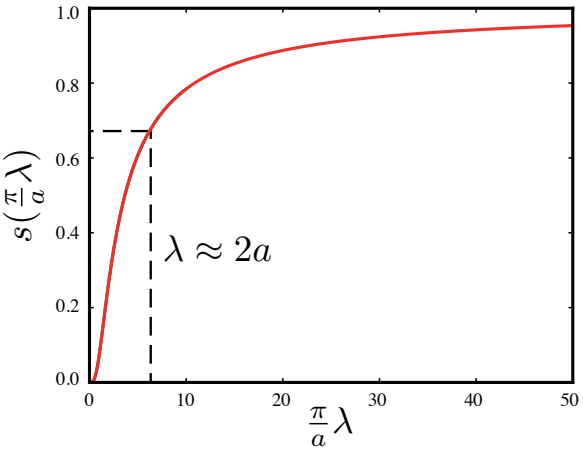

Figure 3.7. Scaling of the diffusion coefficient due to finite friction. Note that the scaling factor $s(\frac{\pi}{a}\lambda)$ is already close to one for $\lambda \gtrsim 2a$, *i.e.*, only very low permeability (high friction) of the tissue would seriously dampen cellular diffusion.

3.5.2 Diffusion in the homeostatic state

In order to determine the single cell diffusion constant at the homeostatic state, we calculate the diffusion for a tracer particle of the size of a cell that moves with the cell flow field. The respective diffusion constant in three dimensions can be written as (*cf.* sec. 2.5)

$$D = \frac{1}{3}\int_0^\infty \mathrm{d}t\, \langle v_\alpha^{\mathrm{c}}(\mathbf{r}_{\mathrm{p}}(t),t) v_\alpha^{\mathrm{c}}(\mathbf{r}_{\mathrm{p}}(0),0)\rangle \ ,$$

where $\mathbf{r}_{\mathrm{p}}(t)$ denotes the tracer particle's position at time t. Under the assumptions that particle position and velocity fluctuations decouple and that position fluctuations are Gaussian (*cf.* sec. 2.5), the diffusion coefficient is thus given by

$$D = \frac{1}{3}\int_0^\infty \mathrm{d}t \int \frac{\mathrm{d}^3 q}{(2\pi)^3}\, e^{-q^2 D t} C_{vv}^{\mathrm{c}}(q,t)\,, \tag{3.59}$$

where we introduced the velocity-velocity correlation function $C_{vv}^{\mathrm{c}}(q,t)$ as

$$\langle v_\alpha^{\mathrm{c}}(\mathbf{q},t) v_\alpha^{\mathrm{c}}(\mathbf{q}',0)\rangle = C_{vv}^{\mathrm{c}}(q,t)(2\pi)^3 \delta(\mathbf{q}+\mathbf{q}')\,. \tag{3.60}$$

In the following, we furthermore assume that diffusion is slow in comparison with the decay of the velocity-velocity correlations, *i.e.*, that $e^{-q^2 D t} \simeq 1$ for all times t at which $C_{vv}^{\mathrm{c}}(q,t)$ is finite. Note that this approximation necessarily implies the existence of a cut-off wave-length $q_{\max} = \pi/a$ related to the tracer particle's radius a. Here, a corresponds to the average radius of a cell. The expression of the diffusion constant then simplifies to

$$D = \frac{1}{6}\int_0^{q_{\max}} \frac{\mathrm{d}^3 q}{(2\pi)^3}\, \hat{C}_{vv}^{\mathrm{c}}(q,\omega)\big|_{\omega=0}\,, \tag{3.61}$$

where the Fourier transform $\hat{C}_{vv}^{\mathrm{c}}(q,\omega)$ of the cell velocity correlation function is defined according to

$$\langle v_\alpha^{\mathrm{c}}(\mathbf{q},\omega) v_\alpha^{\mathrm{c}}(\mathbf{q}',\omega')\rangle = \hat{C}_{vv}^{\mathrm{c}}(q,\omega)(2\pi)^4 \delta(\mathbf{q}+\mathbf{q}')\delta(\omega+\omega')\,. \tag{3.62}$$

The full calculation of $\hat{C}^{\mathrm{c}}_{vv}(q,\omega)$ reveals three characteristic time scales on which the velocity correlations decay; see appendix B.2 for a detailed calculation. For $\omega = 0$, the expression for the correlation function reduces to

$$\hat{C}^{\mathrm{c}}_{vv}(q,0) = \frac{2}{q^2}\left[\left(\frac{\zeta}{\bar{\eta}+\bar{\kappa}}\right)^2 \frac{k_{\mathrm{d}}}{n_{\mathrm{h}}} + \frac{2}{3}\frac{\theta}{(\bar{\eta}+\bar{\kappa})^2} + \frac{\theta}{(\eta+\bar{\kappa})^2}\right]. \tag{3.63}$$

Note that with $\bar{\eta}+\bar{\kappa} = \bar{\eta}[1+(\lambda q)^{-2}]$ we find that the characteristic length scale λ of permeation as introduced above for the piston example (see section 3.3) reappears in the diffusion problem: We see already that for $q \gg 1/\lambda$, the effect of permeation on the velocity-velocity correlations is negligible. Carrying out the integral in Eq. (3.61), the diffusion constant follows as

$$D = \frac{1}{6\pi a\bar{\eta}^2}\left[s(\tfrac{\pi}{a}\lambda)\left(\frac{\zeta^2 k_{\mathrm{d}}}{n_{\mathrm{h}}} + \frac{2}{3}\theta\right) + s(\tfrac{\pi}{a}\bar{\lambda})\left(\frac{\bar{\eta}}{\eta}\right)^2\theta\right], \tag{3.64}$$

where $\lambda = \sqrt{(1-\phi)\bar{\eta}/\kappa}$ and $\bar{\lambda} = \sqrt{(1-\phi)\eta/\kappa}$ are longitudinal and transverse permeation lengths, respectively, with $\bar{\eta} = \zeta + \frac{4}{3}\eta$ being the longitudinal viscosity. The effects of permeation are described by the function

$$s(x) = 1 + \frac{1}{2(1+x^2)} - \frac{3}{2}\frac{\arctan x}{x}, \tag{3.65}$$

which increases monotonously with x from zero to one, see Fig. 3.7 for a plot. For $\lambda, \bar{\lambda} \gg a$, however, one recovers the behavior of the one-component theory, with $s(x \gg 1) \simeq 1$. The correction due to permeation is already less than a factor of two for $\lambda, \bar{\lambda}$ in the range of the size of a cell, with $s(2\pi) \approx 0.7$.

Note that for very long relaxation times of the velocity-velocity correlations, the above expression for the diffusion coefficient might not hold true, however. In that case, the above calculation provides an upper limit for the diffusion constant. A detailed discussion of the slow diffusion approximation and the calculation for finite relaxation times can be found in the appendix, section B.2.

3.6 Discussion

In this chapter, we introduced a two-component continuum description of tissues that takes both cells plus the surrounding extracellular matrix as well as the interstitial fluid into consideration. Two main motivations let us go beyond the one-component description of tissues developed in the previous chapter: First, cell division and apoptosis cannot be consistently described without creation of matter *ex nihilo* if no material turnover between different phases is taken into account. The obvious requirement of overall mass conservation thus points towards the necessity of a multi-component description, and it is to be expected that such a description will give rise to additional mechanical conditions that may turn out to be relevant for the tissue mechanics. Second, the homeostatic

tissue pressure, first introduced by Basan and colleagues [17] and discussed above in the framework of a one-component description of tissues (section 2.3), is not unambiguously defined; its relation to the (ambient) hydrostatic pressure is at least not obvious. The distinction between a cell/ECM phase and the interstitial fluid allows to disentangle (mechanical) cell stress and hydrostatic pressure and thus allows to clarify the nature of the homeostatic pressure.

By decomposing the overall force balance for a multi-component system as separate force balances for each component, one finds that additional internal forces appear which represent momentum transfer between the individual components. In general, these internal forces follow from symmetry considerations. In a tissue described by a cell/ECM phase and a fluid component, momentum is transferred if the permeability of the tissue is finite, *i.e.*, for finite friction between the interstitial fluid and the cells or the extracellular matrix, respectively. Another contribution to the internal forces are buoyancy forces that appear if gravitation is taken into account, which breaks rotational symmetry. It turns out that a one-component description of tissues can be regarded as a friction-less limit case of the two-component theory when either gravitation is completely neglected or the mass densities of the cell/ECM phase and the interstitial fluid are equal; in this case, both components mechanically decouple as no momentum between the two is exchanged.

Finite friction or permeability implies that fluid flow relative to the cell/ECM phase gives rise to internal friction forces that have to be balanced by a gradient in hydrostatic pressure. The resulting linear relation between relative flow and fluid pressure gradient is known as Darcy's law, which describes fluid flow through porous media. Such pressure gradients can be imposed by boundary conditions or be due to locally prevailing cell division or apoptosis, *i.e.*, net material turnover. In the latter case, relative flows arise that lead to a hydrostatic pressure buildup in the tissue. As in the previous chapter, we focussed our analysis on the tissue dynamics close to the homeostatic state in the limit of long times. In this limit, finite tissue permeability has two main effects. First, the (longitudinal) tissue viscosity $\bar{\eta} = \zeta + \frac{4}{3}\eta$ and the friction coefficient κ define a characteristic length $\lambda \propto \sqrt{\bar{\eta}/\kappa}$ over which the relative flow relaxes as momentum is transferred between the cell/ECM phase and the interstitial fluid. As an example, we discussed the dynamics of a semi-permeable piston which exerts an additional force on a tissue confined in a chamber close to its homeostatic state. The cells respond to additional cell/ECM phase pressure by apoptosis or cell division, respectively, which leads to relative material flows as implied by net material turnover. If the characteristic length λ is significantly smaller than the length of the chamber, this response is confined to a region of width λ close to the moving piston; beyond this region, the hydrostatic pressure balances the additional force exerted by the piston and the tissue remains at its homeostatic state. In the limit of vanishing friction, λ diverges and one recovers the one-component behavior where the tissue response is homogeneous over the entire tissue. Second, friction between fluid and cell phase in effect slows down the diffusive motion of cells in the tissue as such motion implies relative material flows. We find that the effective diffusion constant equals the diffusion constant obtained for the one-component theory rescaled by a factor that accounts for permeation. This factor depends on the

ratio between cell radius a and the characteristic length λ, and it is significantly smaller than 1 only for $\lambda \lesssim 2a$, which does not seem to be the case in general (see below). As λ decreases with the friction coefficient as $\lambda \propto 1/\sqrt{\kappa} \propto d_\mathrm{p}$, where d_p is the typical pore size in the interstitial space, the condition $\lambda < 2a$ is most likely met in very tightly packed tissues. (Because the isotropic and the anisotropic fluctuations contribute slightly differently to the diffusion constant, another similar characteristic length $\bar{\lambda}$ appears as well, which relates the friction coefficient to the pure shear tissue viscosity η.)

Furthermore, the two-component theory allows for a coherent description of gravitational forces. For many practical purposes, the mass densities of interstitial fluid and cell/ECM phase, ρ_f and ρ_c, respectively, can be considered to be equal. In this case, gravitation gives rise to a barometric pressure gradient for the fluid pressure without exerting any additional force on the cell/ECM phase. As an anecdotal example may serve a giraffe: Although the fluid pressure at the lower part of its long neck may be significantly higher than right below the head, the cells may be just as fine all along. In principle, the homeostatic state is still well-defined. We show, however, that for a finite density difference $\rho_\mathrm{c} - \rho_\mathrm{f}$ a treadmilling steady state can be found at long times if the characteristic permeation length λ is sufficiently small and the tissue layer sufficiently thick. This example, in which the tissue is again considered to be close to its homeostatic state, gives an additional illustration of the tissue dynamics with permeation: the cell turnover response to gravitational forces is restricted to a region of width λ due to finite permeability.

What are the orders of magnitude for the characteristic lengths introduced above? A general answer to this question is rather difficult, for several reasons. Both tissue permeability and tissue viscosities are not easily measured and reported values vary over several orders of magnitude. We expect tissue permeability to depend strongly on tissue type, *i.e.*, tissue composition and architecture. Moreover, the bulk viscosity ζ in the homeostatic state, or equivalently the bulk stress relaxation time τ, have not yet been measured, see also the discussion in the previous chapter (section 2.7). When we estimate that both bulk and shear viscosity are in the range of $10^5 - 10^7\,\mathrm{Pa\,s}$ [63] and that the inverse permeability κ is in the range $10^{11} - 10^{14}\,\mathrm{Pa\,s\,m^{-2}}$ [138], we obtain orders of magnitude for the characteristic length that range from the size of a cell to centimeters, $\lambda \sim 10^{-5} - 10^{-2}\,\mathrm{m}$. Note that the reported values for the tissue permeability are consistent with the rough estimation that $\kappa \sim \eta_\mathrm{f}/d_\mathrm{p}^2$, where η_f is the viscosity of the interstitial fluid and d_p an average pore diameter in the interstitial space. Additional experiments such as the piston experiment suggested here are certainly needed to gain a quantitative understanding of the effects of permeation.

Another finding which might be experimentally relevant is that the two-component theory predicts an increased interstitial fluid pressure in the center of multicellular tumor spheroids which proliferate at the rim and undergo apoptosis in the rest of the tissue. So far, pressure measurements have been made only in vascularized solid tumors *in vivo*, for which the contribution of the pressure difference between vasculature and surrounding tissue would additionally have to be taken into account. Notwithstanding, a spatially resolved measurement of the interstitial fluid pressure in multicellular spheroids would

certainly provide a means to access the permeability of the tissue.

In this chapter, we developed the constitutive equations for the cell phase along the same lines as in the one-component description. The arguments developed in the previous chapter can consistently be transposed to the two-component theory; remarks and shortcomings that apply to the one-component description consequently carry over to the two-component theory as well, see section 2.7 of the previous chapter for a discussion. One additional "equation of state" is needed, however, to close the system of equations. In the two-component description, cell number density and cell volume are in principle two independent variables. Here, we chose the simplest possible equations of state by assuming that cell density and cell volume depend on the isotropic cell stress only. In general, cells might regulate their volume also in response to the hydrostatic pressure, although cell volume is in most cases determined by the osmotic pressure of the medium only and does not change much at all. Similarly, the cell number density could depend on the hydrostatic pressure, which we did not consider here. The equations of state could in principle also involve the history of the evolution of the system, which goes beyond the scope of this work. We assume that these effects are negligible at the level of detail with which the tissue mechanics is described in this work.

Some additional remarks are due here. We restricted our description to tissues with a minor contribution of the extracellular matrix to a combined cell/ECM phase. Our choice of constitutive equations for the cell phase which relate the isotropic stress in the cell phase to the cell number density is based on this assumption. We do not intend to describe the interstitial flows that occur in the stroma, a matrix-rich connective tissue with scattered isolated cells [174]. The general approach to use multi-component continuum descriptions remains legitimate; the constitutive equations that model the tissue mechanical properties have to be chosen appropriately, however. Similarly, our two-component description does not allow to describe active migration of cells in the extracellular matrix. To this end, the ECM would have to be described as a third, elastic phase to which the cells can transfer momentum in order to move (*i.e.*, in which they can crawl). Such a description has been proposed by Ambrosi *et al.* for a three-component mixture theory [12]. Rather microscopic descriptions on a cellular scale might be appropriate if the details of the interstitial flow do matter for the phenomenon under consideration, compare also section 1.3.

Chapter 4

Interface dynamics between two cell populations

In the previous chapters, we discussed the multicellular dynamics of tissues without distinguishing different types of cells. However, tissues often comprise more than one single type of cells. Similarly, organs often consist of different tissues that exhibit at least one common interface. In this chapter, we generalize our description of tissues to cases in which two different types of cells are present in the tissue, which can interact mechanically. Having thus established an appropriate framework, where we draw on results from the previous chapters, we discuss aspects of the dynamics of interfaces which can arise in such multi-cell type tissues.

4.1 Introduction: Cell competition & mechanics

Cells of different type often do have distinct roles in the developing and adult animal. In order for these cells to function correctly and to not interfere with each other, or to be able to coordinate certain tasks, they need to talk to each other. Communication between cells has been studied for a long time, and many signaling pathways have been described [8, 190]. However, it is conceivable that cells do not only communicate by the exchange of molecules or the recognition of certain molecular ligands but by mechanical signals such as forces exerted between them. Such mechanical interaction has first been hypothesized in the context of cell competition [168], which denotes the outgrowth of so-called "winner" cells against "loser" cells in a tissue due to a growth advantage [14, 19].

Cell competition has first been studied in the *Drosophila* wing imaginal disc, the larval precursor of the adult fly wing [131]. The authors studied the growth of clones of genetically impaired cells (*minute*-mutants) that had a growth disadvantage compared to the surrounding wild-type cells. During the growth of the wing disc, the wild-type (WT) cells eventually suppressed the *minute* cells. However, if a complete compartment was comprised of the *minute*-mutant cells, they continued to proliferate (though at a slower speed than WT cells) and eventually formed a fully grown compartment. Apparently, only the presence of both WT and *minute* cells lead to cell competition and the

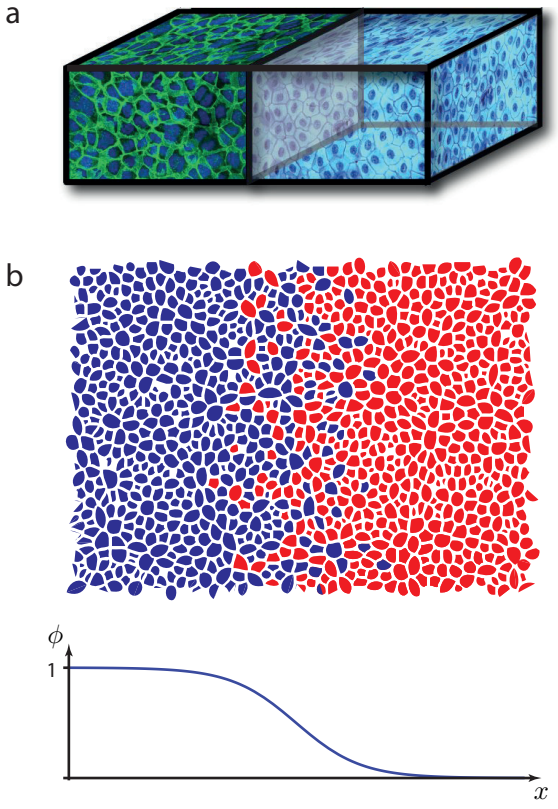

Figure 4.1. Interfaces between cells of different type. In (a), the piston experiment discussed in the previous chapters is modified such that the tissue chamber is filled with two different types of cells that are separated by a moving wall. Cells can interact mechanically by exerting forces on the wall which replaces the piston in the previous set-up. The image is taken from [17], where this *gedankenexperiment* was introduced first. In (b), the two different cell populations can freely intermingle, which gives rise to a smooth interfacial profile of the volume fraction ϕ of the blue cells.

suppression of the "loser" cells. Similarly, a so-called supercompetitor mutant was found that outcompeted the wild-type cells [132]: clones of $dMyc(+)$-mutant cells eventually suppressed WT cells in the wing imaginal disc. Since these first discoveries, cell competition has become an active and growing field of research, and considerable progress has been made. A recent study established the role of a the transmembrane protein Flower that is differently spliced for cells with "winner" and "loser" identity and thus allows cells to directly compare their fitness [159]. A cell that comes off badly in such a comparison is then eventually undergoing apoptosis. It has furthermore been shown that in some cases cells stressed by supercompetitors activate the JNK and Hid pathway [104], thus triggering cell death. However, the details are not clear yet, and it remains a matter of debate whether the reported findings are general and shared in different situations of cell competition or restricted to the specific situation in which they have been studied so far.

Although these results underline the role of cell signaling and seem to suggest a purely molecular basis of cell competition, it is not understood what leads to the adoption of the distinct "winner" and "loser" identities [19, 72]. Most importantly, the hypothesis that a mechanical interaction is at the basis of the competition between differing cells has not been ruled out. It is known that mechanical forces can activate signaling pathways; for example, it has been shown that mechano-sensitive transmembrane ion channels can be activated by mechanical stress [8]. In a seminal paper, Shraiman suggested that mechan-

ical stress due to cell division may serve as an integral-feedback mechanism in order to guarantee homogeneous growth in the imaginal wing disc [168], see also chapter 1 for a discussion. He argued that the same ideas may be relevant for cell competition, if cells respond differently to mechanical stress caused by inhomogeneous cell division. In the meantime, it has been shown that the observed spatial homogeneity of cell proliferation in the growing wing disc is probably caused by an intricate signaling mechanism and not due to mechanical stresses [166, 189], see also section 1.1 in the introduction. His argument regarding the competition of cells responding differently to stresses generated by growth itself remains an intriguing hypothesis nevertheless.

In the previous chapters, we considered the growth of a tissue against a piston that exerts an additional pressure on the cells. Instead of the tissue being enclosed by a piston, one could consider a moving wall that separates a second compartment filled with cells of a different type, see Fig. 4.1(a). Basan and colleagues introduced this *gedanken-experiment* in order to illustrate their concept of homeostatic competition between cells that have a different homeostatic pressure, along the lines of Shraiman's ideas. Here, we want to generalize these ideas to tissues with mixed populations of cells of different type, see Fig. 4.1(b) for a sketch. In principle, the rates of cell division and apoptosis may then depend not only on the mechanical stress in the tissue but on the relative concentration of cells of either type. For simplicity, we focus here mainly on purely mechanical interactions, however.

4.2 Continuum description of tissues with two cell types

We consider tissues that consist of cells of two different cell types A and B, respectively. For simplicity, we neglect the interstitial fluid and write

$$n_A\Omega_A + n_B\Omega_B = 1\,, \tag{4.1}$$

where n_A and n_B are the cell number densities of population A and B, respectively, and Ω_A and Ω_B are the respective average cell volumes. Cells of both types can undergo apoptosis, described by rates k_a^A and k_a^B, or give rise to offspring, characterized by the cell division rates k_d^A and k_d^B, respectively. Cell number balance for the two cell populations reads

$$\partial_t n_A + \partial_\alpha \left(n_A v_\alpha^A\right) = k_A n_A\,, \tag{4.2a}$$

$$\partial_t n_B + \partial_\alpha \left(n_B v_\alpha^B\right) = k_B n_B\,, \tag{4.2b}$$

where we introduced the effective proliferation rates $k_A = k_\mathrm{d}^A - k_\mathrm{a}^A$ and $k_B = k_\mathrm{d}^B - k_\mathrm{a}^B$. Each cell type is convected by a flow fieId described by the velocities v_α^A and v_α^B, respectively.

We define the volume fraction of cells of type A as $\phi = n_A\Omega_A$. We can then define an average velocity v_α and a relative flow J_α by

$$v_\alpha = \phi v_\alpha^A + (1-\phi)v_\alpha^B\,, \tag{4.3a}$$

$$J_\alpha = \phi(1-\phi)\left(v_\alpha^A - v_\alpha^B\right)\,, \tag{4.3b}$$

such that $v_\alpha^A = v_\alpha + J_\alpha/\phi$ and $v_\alpha^B = v_\alpha - J_\alpha/(1-\phi)$. Using these expressions, we can rewrite the cell number balance equations (4.2) as a balance equation for the volume fraction ϕ,

$$\partial_t\phi + v_\alpha\partial_\alpha\phi + \partial_\alpha J_\alpha = \phi(1-\phi)(k_A - k_B) + \phi(1-\phi)\left(\partial_t + v_\alpha\partial_\alpha\right)\ln\Omega_A/\Omega_B + (1-\phi)J_\alpha\partial_\alpha\ln\Omega_A + \phi J_\alpha\partial_\alpha\ln\Omega_B\,, \quad (4.4)$$

and an equation for the divergence of v_α,

$$\partial_\alpha v_\alpha = \phi k_A + (1-\phi)k_B + \phi\left(\partial_t + v_\alpha\partial_\alpha\right)\ln\Omega_A + (1-\phi)\left(\partial_t + v_\alpha\partial_\alpha\right)\ln\Omega_B + J_\alpha\partial_\alpha\ln\Omega_A/\Omega_B\,. \quad (4.5)$$

Note that in general the cell volumes are functions of the cell number densities and the pressure, *i.e.*, $\Omega_A = \Omega_A(n_A, n_B, P)$ and $\Omega_B = \Omega_B(n_A, n_B, P)$, where P is the isotropic part of the stress. Equation (4.1) then implicitly defines an equation of state $P = P(n_A, n_B)$ and eventually allows to express Ω_A and Ω_B in terms of ϕ and P. Here, we assume that the cell volumes are constant and that the tissue is incompressible. In this case, the pressure becomes a Lagrange multiplier to ensure the constraint

$$\partial_\alpha v_\alpha = \phi k_A + (1-\phi)k_B\,. \quad (4.6)$$

Please see also appendix D for a detailed discussion of incompressibility for a classical two-component fluid. For constant cell volumes, Eq. (4.4) finally simplifies to

$$\partial_t\phi + v_\alpha\partial_\alpha\phi + \partial_\alpha J_\alpha = \phi(1-\phi)(k_A - k_B)\,. \quad (4.7)$$

Changes of the volume fraction ϕ are caused by convective currents, relative flows, and an imbalance of proliferation between cells of either type.

Constitutive equations and force balance

In order to determine the dynamics of the field $\phi(\mathbf{r}, t)$, we first need to determine the average velocity v_α and the relative flow J_α. We assume that the latter is a diffusive current caused by gradients in the volume fraction ϕ, and we write

$$J_\alpha = -D\partial_\alpha\phi\,. \quad (4.8)$$

Here, D is a diffusion constant with the physical dimension [Length]^2/[Time]. In principle, $D = D(\phi)$, which we neglect for simplicity. We assume furthermore that cells of type A and type B have the same mass density $m_A/\Omega_A = m_B/\Omega_B$ and that gradients in pressure do not drive relative flows. The velocity v_α has to be determined from force balance, which neglecting inertial terms and in absence of external forces reads

$$\partial_\beta\sigma_{\alpha\beta} = 0\,. \quad (4.9)$$

The total stress, which can be split into an isotropic and a traceless part according to $\sigma_{\alpha\beta} = \sigma\delta_{\alpha\beta} + \tilde{\sigma}_{\alpha\beta}$, is given by a constitutive equation that expresses the stress in terms

of a pressure, the velocity gradient, and contributions due to gradients in ϕ. For classical two-component fluids, this constitutive relation can be derived using Onsager theory, see appendix D. Here, we use the results of chapter 2 as a justification for describing the tissue as a viscous fluid at long times. The discussion of the Ericksen stress for a two-component fluid then suggests the form of the terms arising from gradients in ϕ that have to be taken into account in the total stress. We thus assume that the traceless part of the stress is given by

$$\tilde{\sigma}_{\alpha\beta} = 2\eta\tilde{v}_{\alpha\beta} - B\left[(\partial_\alpha\phi)(\partial_\beta\phi) - \tfrac{1}{3}(\partial_\gamma\phi)(\partial_\gamma\phi)\delta_{\alpha\beta}\right] \tag{4.10}$$

in three dimensions. Here, B is a measure of interfacial tensions caused by finite volume fraction gradients, its physical dimension being [Force].

In principle, the isotropic stress σ is given by an equation of state, which can now contain additional terms proportional to $|\nabla\phi|^2$. Close to a reference cell number density n_0, one could write

$$\sigma = -P(n_A, n_B) - \bar{B}|\nabla\phi|^2\,, \tag{4.11}$$

where the first term represents the pressure that is related to a compression of cells. Note that $\bar{B} \neq B$ in general. In the following, however, we assume that the tissue is incompressible, which simplifies the analysis significantly. For an incompressible system, the pressure P plays the role of a Lagrange multiplier in order to ensure the constraint (4.6). The contribution due to a finite gradient of the volume fraction can therefore be absorbed in the definition of the isotropic part of the stress and we can consider σ as the Lagrange multiplier. The system of equations is closed by specifying the rates of proliferation k_A and k_B. In principle, they can depend on the volume fraction ϕ, the isotropic stress σ as well as on the biochemical environment of the cells. Here, we will assume that the latter dependence can be neglected because of a fixed biochemical environment.

4.3 Linear stability of a homogeneous, steady state

In order to better understand the possible dynamics of the tissue, we discuss the linear stability of possible stationary steady states of the system. One can distinguish two scenarios. First, we consider the stability of a homeostatic state of a tissue made up of a single type of cells; second, we consider a homeostatic state of a tissue with both cell populations present.

Single cell-type homeostatic state

Let us consider a tissue comprised uniquely of cells of type B. The average volume fraction at the steady state then is $\phi_0 = 0$, and the isotropic stress $\sigma = -P_B$ is chosen such that

$$k_B(\phi = 0, \sigma = -P_B) = 0\,, \tag{4.12}$$

where P_B is the homeostatic pressure of cells of type B (*cf.* sec. 2.3). How does the tissue respond to a small perturbation of ϕ by introducing cells of type A? Linearizing

Eq. (4.7) and switching to the Fourier domain for spatial coordinates, we find that

$$\partial_t \phi = -q^2 D\phi + \phi k_A\big|_{0,-P_B} \tag{4.13}$$

to first order in ϕ. Note that we implicitly allow for the spontaneous appearance of a few cells of type A. The convective terms drop out to first order. Short wave-length stability then requires $D > 0$ to prevent a local demixing of cells, which would give rise to a divergence of large-q modes. Overall stability of the homogeneous composition of the tissue requires $k_A(0, -P_B) < 0$, *i.e.*, that at the homeostatic pressure of cells of type B, apoptosis wins over cell division for cells of type A. If $k_A(0, -P_B) > 0$, however, A cells will divide more than cells of type B and continue to spread in the tissue.

Homeostatic state with two cell populations

Let us assume that there exists a homogeneous steady state with finite volume fraction ϕ^* and stress σ^* such that

$$k_A(\phi^*, \sigma^*) = k_B(\phi^*, \sigma^*) = 0\,. \tag{4.14}$$

We introduce the variations $\delta\phi = \phi - \phi^*$ and $\delta\sigma = \sigma - \sigma^*$ and express the effective cell division rates to linear order as

$$k_A = k_{A,\phi}\delta\phi + k_{A,\sigma}\delta\sigma\,, \qquad k_B = k_{B,\phi}\delta\phi + k_{B,\sigma}\delta\sigma\,, \tag{4.15}$$

where we used the respective short-hand notations $k_{A,\phi} = \partial k_A/\partial\phi$ etc. To linear order in the perturbations, the evolution equation for ϕ then becomes

$$\partial_t\delta\phi = -q^2 D\delta\phi + \phi*(1-\phi*)(k_{A,\phi} - k_{B,\phi})\delta\phi + \phi*(1-\phi*)(k_{A,\sigma} - k_{B,\sigma})\delta\sigma\,. \tag{4.16}$$

Short wave-length stability requires $D > 0$. At constant, externally imposed stress σ^*, the homeostatic state is stable if $k_{A,\phi} - k_{B,\phi} < 0$. If the proliferation rates do not depend on the volume fraction ϕ, the homeostatic state is marginally stable; in fact, ϕ^* can take all possible values as long as $k_A(\sigma^*) = k_B(\sigma^*) = 0$. In the case of a finite pressure variation $\delta\sigma$, the coexistence stationary state is stable if $k_{A,\sigma} - k_{B,\sigma} < 0$. Again, a similar argument applies: If both rates of proliferation do not depend on σ, the state is marginally stable and homeostasis is determined by ϕ only.

4.4 Non-stationary steady states: Traveling wavefront solutions

It may well be, however, that for finite ϕ, no stationary homeostatic state exists. In these cases, one cell population eventually takes over, depending on the sign of $k_A - k_B$. Here, we ask whether traveling wave solutions exist that describe the advancing front of a population of cells, say, of type A, that outcompetes a second population composed of cells of a different type B. For infinite systems, *i.e.*, very large tissues, these solutions can

be considered as non-stationary steady states. For such solutions to exist, two conditions have to be met. First, they require the existence of a stable, stationary state for a tissue composed solely of cells of type A and that the corresponding homeostatic state of a tissue that consists only of cells of type B is unstable. For simplicity, we assume here that the cell proliferation rates k_A and k_B depend on isotropic stress only, and we suppose that both cells of type A and cells of type B have well-defined homeostatic states with different homeostatic pressures $P_A > P_B$.

Second, in order for a generic traveling wavefront solution to exist, Galilean invariance must be broken. Otherwise, boundary conditions determine the dynamics instead of the latter being governed by local interaction. Mathematically speaking, the wave speed selection problem would be ill defined if the interface velocity was defined up to a constant. Therefore, we consider population dynamics on a substrate, where friction between cells and the substrate breaks Galilean invariance. The tissue is then at the homeostatic state A with $\phi = 1$ at one end and at the homeostatic B with $\phi = 0$ at the other, independent of boundary conditions on the pressure.

4.4.1 Basic equations, non-dimensionalization, traveling waves

In the following, we consider a thin tissue of height h which is confined to a solid substrate. Following the discussion in section 2.4.2 in chapter 2, we express the force balance in the plane as

$$\partial_k \varsigma_{ik} = \gamma v_i \,, \tag{4.17}$$

where latin indices stand for Cartesian coordinates (x, y) in the plane, and $\varsigma_{ik} = \int_0^h \mathrm{d}z\, \sigma_{ik}$ is the surface stress or tension tensor.[1] Cell-substrate friction is described by the friction coefficient γ, and we neglect again possible dependencies on ϕ. In the presence of gradients of ϕ, another term is allowed by symmetry, and we could add a momentum source $\propto \partial_i \phi$ to the right-hand side of the above equation. Here, we only consider passive friction as described by (4.17), however. We distinguish an isotropic and a traceless component of the tension according to $\varsigma_{ik} = \varsigma \delta_{ik} + \tilde{\varsigma}_{ik}$. For an incompressible system, ς becomes a Lagrange multiplier to ensure the constraint

$$\partial_i v_i = \phi k_A + (1 - \phi) k_B \,. \tag{4.18}$$

The constitutive equation for the traceless part then describes a viscous fluid with interfacial tension in two dimensions, and we have

$$\tilde{\varsigma}_{ik} = 2\eta' \tilde{v}_{ik} - B' \left[(\partial_i \phi)(\partial_k \phi) - \tfrac{1}{2} (\partial_l \phi)^2 \delta_{ik} \right] \,, \tag{4.19}$$

where $\eta' \sim h\eta$ (see sec. 2.4.2) and $B' \sim hB$ has the physical dimension [Force]×[Length].

[1] In this context, we use surface stress and tension interchangeably. For the isotropic part of the tension, we also say pressure or surface pressure in order to underline its close correspondence to pressure in a three-dimensional bulk tissue.

Mechanical coupling of stress and proliferation

In order to close the system of equations, we also need to specify the rates of proliferation k_A and k_B. Instead of imposing a fixed proliferation rate set by the environmental conditions, we assume that cell proliferation depends on the isotropic stress. Note that in general, cell proliferation rates could also depend on the volume fraction ϕ. Here, we want to focus on mechanical interactions between cell populations, however, and deliberately neglect this dependence. In line with the arguments put forward in the previous chapters, we therefore consider

$$k_A = \kappa_A(\varsigma + P_A)\,, \tag{4.20a}$$
$$k_B = \kappa_B(\varsigma + P_B)\,, \tag{4.20b}$$

where $\kappa_{A,B}$ are susceptibilities and P_A and P_B are the respective homeostatic (surface) pressures at which cell division and apoptosis balance. In general, $P_A \neq P_B$, which allows for a mechanical competition between the two cell populations.

In the case of an incompressible tissue, we can use the constraint (4.18) to express the isotropic part of the tension in terms of the volume fraction ϕ and the divergence of the cell flow,

$$\varsigma = \frac{\partial_i v_i - \phi\kappa_A P_A - (1-\phi)\kappa_B P_B}{\phi\kappa_A - (1-\phi)\kappa_B}\,. \tag{4.21}$$

Dynamics

Let us consider an infinite, thin incompressible tissue comprising two cell populations A and B whose respective volume fractions are homogeneous along the y-direction. Then, $\phi = \phi(x,t)$ and the problem becomes effectively one-dimensional since all derivatives along y vanish identically. We can write $\mathbf{v} = v\mathbf{e}_x$ and $\mathbf{J} = J\mathbf{e}_x$, and force balance (4.17) reduces to

$$\partial_x\varsigma + \eta'\partial_x^2 v - B\,\partial_x\phi\,\partial_x^2\phi = \gamma v\,. \tag{4.22}$$

For an incompressible tissue, we can use Eq. (4.21) for the isotropic part of the tension, and we obtain a differential equation for the average cell velocity v. For simplicity, we consider $\kappa_A = \kappa_B \equiv \kappa$ and chose $P_B = 0$. The above equation then leads to

$$\tilde{\lambda}^2\partial_x^2 v - v = \gamma^{-1}\left(P_A + B\partial_x^2\phi\right)\partial_x\phi\,, \tag{4.23}$$

where we defined the characteristic length $\tilde{\lambda} = \sqrt{(1+\eta'\kappa)/(\kappa\gamma)}$ that describes the spatial decay of perturbations due to friction. Note that although ς does no longer appear as a Lagrange multiplier in the force balance, it is determined by the constraint on $\partial_x v$. The relative flow directly follows from (4.8) as $J = -D\partial_x\phi$.

How does the volume fraction ϕ evolve in time? Using the above expressions for the cell proliferation rates with $\kappa_A = \kappa_B$ and $P_B = 0$ as well as the constitutive equation for the relative flow, equation (4.7) now reads

$$\partial_t\phi + v\partial_x\phi = D\partial_x^2\phi + \phi(1-\phi)\kappa P_A\,. \tag{4.24}$$

For the above parameter choice, $k_A - k_B = \kappa P_A$ is constant, and the evolution equation for ϕ corresponds to the well-known Fisher wave equation with an additional convective term. The Fisher wave equation was initially put forward to describe the spatial spread of a favored gene in a population of a reproducing species [62], and it has been studied to great detail since (see [134, chapter 11] for a thorough discussion and additional references). Most notably, it is known to exhibit traveling wavefront solutions, and one can expect that such solutions persist in the presence of a convective term. Different authors investigated the effect of additional convective flows on the population dynamics described by the Fisher equation with and without noise [46, 90, 149]. However, these convective flows were decoupled from the population dynamics and caused by environmental conditions in which the population were considered to spread. Here, the situation is different: The convecting velocity v depends itself on the shape of the interface described by ϕ due to the differential cell division and thus—more broadly speaking—because of the mechanical coupling between cell division and stress, where also the interfacial tension $\propto B'$ contributes to.

Non-dimensionalization

The evolution equation for ϕ introduces a characteristic time scale t_0 and a characteristic length scale l_0 according to

$$t_0 = (\kappa P_A)^{-1}\,, \qquad l_0 = \sqrt{D/(\kappa P_A)}\,. \tag{4.25}$$

We can then non-dimensionalize the above equations by defining starred, dimensionless variables $t^* = t/t_0$, $x^* = x/l_0$, and $v^* = v t_0/l_0$, and the equations for the fields $\phi(x^*, t^*)$ and $v^*(x^*, t^*)$ become

$$\partial_{t^*}\phi + v^*\partial_{x^*}\phi = \partial^2_{x^*}\phi + \phi(1-\phi)\,, \tag{4.26a}$$

$$\lambda^{*2}\partial^2_{x^*}v^* - v^* = \alpha\left(1 + \beta\partial^2_{x^*}\phi\right)\partial_{x^*}\phi\,. \tag{4.26b}$$

For notational brevity, we drop the asterisks in the following and refer always to the non-dimensionalized quantities. The dimensionless numbers $\lambda^{(*)}$, α, and β are parameters of the problem and given by

$$\lambda^2 = \frac{(1+\eta'\kappa)P_A}{\gamma D}\,, \tag{4.27a}$$

$$\alpha = \frac{P_A}{\gamma D}\,, \tag{4.27b}$$

$$\beta = \frac{B'\kappa}{D}\,. \tag{4.27c}$$

Note that $\alpha = \lambda^2/(1+\eta'\kappa) \leq \lambda^2$. Using a Green's function approach, equation (4.26b) for the velocity field is formally solved by

$$v(x,t) = -\frac{\alpha}{2\lambda}\int_{-\infty}^{+\infty} \mathrm{d}x'\, e^{-\frac{|x-x'|}{\lambda}}\left(1 + \beta\partial^2_{x'}\phi(x',t)\right)\partial_{x'}\phi(x',t)\,, \tag{4.28}$$

where we used $v(\pm\infty, t) = 0$. By plugging this expression for v into Eq. (4.26a), one obtains a highly nonlinear integro-differential equation for ϕ, which we cannot solve analytically. Before we study some simple limit cases, however, let us consider the form the equations take when we assume the solutions to describe traveling waves.

Traveling wave solutions

We look for solutions of the volume fraction $\phi(x,t)$ such that the spatial profile of the interface between the two cell populations remains constant and evolves in time according to $\phi(x,t) = \Phi(z)$, where we introduced the co-moving coordinate $z = x - ct$. Here, c is the velocity of the traveling wave with a profile described by $\Phi(x - ct)$. In line with our introductory remarks above, we assume that the tissue is in a distinct homeostatic state for $x \to \pm\infty$, and we choose here

$$\lim_{z\to-\infty} \Phi = 1\,, \qquad \lim_{z\to+\infty} \Phi = 0\,. \tag{4.29}$$

For later convenience, we define the origin by choosing $\Phi(0) = 0.5$.

The isotropic tension σ takes the respective homeostatic value at $x \to \pm\infty$, *i.e.*,

$$\lim_{z\to-\infty} \varsigma = -P_A\,, \qquad \lim_{z\to+\infty} \varsigma = -P_B\,, \tag{4.30}$$

and the average cell velocity vanishes at $\pm\infty$. For finite x, the velocity profile can analogously be written as $v(x,t) = V(z)$, and V can be found from Φ according to Eq. (4.28),

$$V(z) = -\frac{\alpha}{2\lambda} \int_{-\infty}^{+\infty} \mathrm{d}z'\, e^{-\frac{|z-z'|}{\lambda}} \left(1 + \beta\Phi''(z')\right) \Phi'(z')\,. \tag{4.31}$$

The evolution equation for ϕ, Eq. (4.26a), now reads

$$\left[-c + V(z)\right] \Phi'(z) = \Phi''(z) + \Phi\,(1 - \Phi)\ . \tag{4.32}$$

Mathematically speaking, this equation is now an eigenvalue problem for the wave speed c, *i.e.*, it is to be determined whether a solution Φ exists and what it looks like for any given c. For the original Fisher equation, *i.e.*, in the case of $V \equiv 0$, there exist solutions for all wave speeds $c \geq c_{\min} = 2$, and corresponding profiles $\Phi(z)$ can be determined via a perturbative series expansion approach. It has been shown that as long as the leading edge of an initial profile decays faster than e^{-z} for $z \to \infty$, the steady-state traveling wave eventually advances with $c = c_{\min}$.

4.4.2 Limiting cases: diffusion vs. convection

In this section, we try to give approximate solutions to the interface profiles and the wave speed of the traveling wave solutions in two different limits, namely for $\lambda \ll 1$ and $\lambda \gg 1$. These limits correspond to two different modes of interface propagation, as we will show below. Whereas the former allows to make immediate use of established quantitative methods developed for the original Fisher equation—and thus to discuss that equation along the way—, the latter rather allows for a qualitative discussion of the dynamics than for a precise calculation of the interface profile.

Diffusion-dominated regime ($\lambda \ll 1$)

Let us discuss the limit $\lambda \ll 1$ first. Since $1 + \eta'\kappa \geq 1$, this limit necessarily implies $\sqrt{P_A} \ll \sqrt{\gamma D}$, see Eq. (4.27). Note that $\alpha = \lambda^2/(1+\eta'\kappa) \lll 1$ in that case. Therefore, the convective flow due to cell division can be considered to be small. In the following, we assume that the interface width is of order $\sim 1 \gg \lambda$, since it is set by the characteristic length scale l_0; we will check this assumption later for consistency. Then, one can consider that the cell velocity along the interface at z is set by the local perturbation at z only. Formally, this is expressed by

$$\lim_{\lambda \to 0} \frac{e^{-\frac{|z-z'|}{\lambda}}}{2\lambda} = \delta(z - z')\,,$$

and the convective velocity in the co-moving frame becomes

$$V(z) \approx -\alpha \left[1 + \beta\, \Phi''(z)\right] \Phi'(z)\,. \tag{4.33}$$

As long as $\beta \sim 1$, the convective velocity is negligible against the propagation speed $c \gtrsim 2$ because $\alpha \lll 1$. The second term can become important, however, if $\beta \gg 1$. We therefore consider a convective velocity

$$V(z) \approx -\nu\, \Phi''(z)\, \Phi'(z)\,, \tag{4.34}$$

where we neglected the first term $\propto \alpha$ and introduced the coefficient $\nu = \alpha\beta$. Since $\alpha \lll 1$, we assume $\nu < 1$ (and most probably $\nu \ll 1$ as long as not $\beta \ggg 1$). In this limit, the evolution equation for ϕ leads to a modified Fisher equation of the form

$$-c\,\Phi' = \left[1 + \nu \left(\Phi'\right)^2\right] \Phi'' + \Phi\,(1 - \Phi)\ . \tag{4.35}$$

The convective term effectively adds to the diffusion in a nonlinear way. Because it scales with $(\Phi')^2$, however, it does not influence the diffusive dynamics at the leading edge. Therefore, one can expect that it does not increase the wave propagation speed c but changes the shape of the interface profile.

The solutions Φ to equation (4.35) are trajectories in the phase plane (Φ, Φ') that satisfy

$$\frac{\mathrm{d}\Phi'}{\mathrm{d}\Phi} = \frac{-c - \Phi(1-\Phi)}{\Phi'[1 + \nu\,(\Phi')^2]}\,. \tag{4.36}$$

The two singular points $(0,0)$ and $(1,0)$ correspond to the two stationary states at $z \to \pm\infty$, respectively. For a linear stability analysis around these two singular points, the additional term due to convection does not play any role, and we find the same result as for the original Fisher wave equation. The singular point $(0,0)$ is a stable node for $c \geq 2$, and a stable spiral if $c < 2$. A solution Φ to the above equation for $c < 2$ would thus imply that $\Phi < 0$ eventually, which is not consistent with the physical interpretation of Φ as a volume fraction of cells of a given type. Therefore, $c \geq 2$, and we can solve Eq. (4.35) for Φ using a perturbation series approach. Our following presentation follows closely the argument developed by Murray [134].

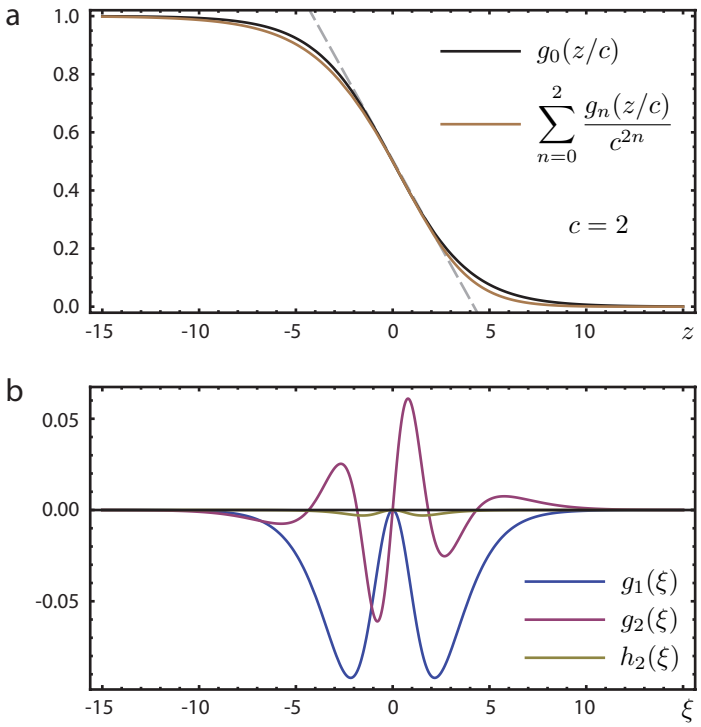

Figure 4.2. Interface profile in the limit of $\lambda \ll 1$. (a) The zeroth order solution (black line) and higher order corrections (brown line, up to second order) can be obtained by a perturbation series approch, see text for details. Curves here are shown for $c = 2$. The width of the interface is approximately given by $L \sim c/|g_0'(0)|$ as indicated by the grey dashed line. (b) The first and second order corrections, g_1 and g_2, respectively, are shown here together with the lowest order correction due to a finite convective velocity h_2, see text for details.

We introduce a change of variable in the vicinity of the front, which is located at $z = 0$, such that we can expand Φ as a Taylor series in a small parameter ϵ. We therefore define

$$\Phi(z) = g(\xi)\,, \tag{4.37}$$

where $\xi = z/c \equiv \sqrt{\epsilon} z$, *i.e.*, $\epsilon = 1/c^2$. Since $c \geq c_{\min} = 2$, we have $0 < \epsilon \leq 1/4$. In the new variables, the equation for Φ becomes

$$-g' = \epsilon \left[1 + \nu\, \epsilon\, (g')^2\right] g'' + g\,(1-g)\ , \tag{4.38}$$

with

$$g(-\infty) = 1\,, \qquad g(\infty) = 0\,,$$

and we require $g(0) = \Phi(0) = 1/2$ as before.

From Eq. (4.38) we see that the convective term is of second order in ϵ and thus does not change the wavefront profile to first order in ϵ compared to the asymptotic solution of the original Fisher equation. We can compute the full asymptotic solution by looking for solutions for Eq. (4.38) that can be written as a regular perturbation series in ϵ. We thus consider

$$g(\xi;\epsilon) = g_0(\xi) + \epsilon g_1(\xi) + \epsilon^2 g_2(\xi;\nu) + \dots\,, \tag{4.39}$$

where

$$\begin{aligned} &g_0(-\infty) = 1\,, \qquad g_0(\infty) = 0\,, \qquad g_0(0) = 1/2\,; \qquad \text{and} \\ &g_i(\pm\infty;\nu) = 0\,, \qquad g_i(0;\nu) = 0 \qquad \text{for } i = 1, 2, \dots\,. \end{aligned}$$

Inserting the above series into Eq. (4.38) and equating powers of ϵ, one obtains

$$\frac{\mathrm{d}g_0}{\mathrm{d}\xi} = -g_0\,(1-g_0) \tag{4.40}$$

to zeroth order, which is solved by

$$g_0(\xi) = \frac{1}{1+e^{\xi}}\,. \tag{4.41}$$

Note that this solution satisfies the boundary conditions and the requirement $g_0(0) = 1/2$ specified above; a plot of this function is shown in Fig. 4.2(a). From this approximate solution we can obtain an estimate for the width of the interface: Assuming that the characteristic interface width L is inversely proportional to the steepness of the interface profile at $z = 0$, see Fig. 4.2(a), we obtain $L \sim (4c) \sim 10$ for $c \approx 2$. Our initial approximation is therefore consistent with the approximative solution found above.

The terms to first and the second order in ϵ are given by

$$\mathcal{O}(\epsilon): \qquad \frac{\mathrm{d}g_1}{\mathrm{d}\xi} + g_1\,(1-2g_0) = -\frac{\mathrm{d}^2 g_0}{\mathrm{d}\xi^2}\,, \tag{4.42}$$

$$\mathcal{O}(\epsilon^2): \qquad \frac{\mathrm{d}g_2}{\mathrm{d}\xi} + g_2\,(1-2g_0) = -\frac{\mathrm{d}^2 g_1}{\mathrm{d}\xi^2} - \nu\left(\frac{\mathrm{d}g_0}{\mathrm{d}\xi}\right)^2 \frac{\mathrm{d}^2 g_0}{\mathrm{d}\xi^2} + g_1^2\,. \tag{4.43}$$

The functions $g_1(\xi)$, $g_2(\xi;\nu)$, ... can recursively be determined from the functions g_i of lower order. We find that the convective term, which acts as a nonlinear contribution to diffusion, appears at second order and higher, which implies that the deviation of the interface profile from the profile for a "classic" Fisher wavefront will be small. We give here the solutions for $g_1(\xi)$ and $g_2(\xi;\nu)$, where we write

$$g_2(\xi;\nu) = g_2(\xi) + \nu h_2(\xi)$$

in order to distinguish the contribution that arises from finite convective fluxes. One then obtains

$$g_1(\xi) = \frac{e^{\xi}}{\left(1+e^{\xi}\right)^2}\left[\xi + \ln\frac{4}{\left(1+e^{\xi}\right)^2}\right]\,, \tag{4.44a}$$

$$g_2(\xi) = \frac{e^{\xi}\left(1-e^{\xi}\right)}{2\left(1+e^{\xi}\right)^3}\left\{4\xi - \left[6 + 4\ln 2 + (\xi + 2\ln 2)^2 - 4\ln\left(1+e^{\xi}\right)\left(1 + \ln\frac{4e^{\xi}}{1+e^{\xi}}\right)\right]\right\}\,, \tag{4.44b}$$

$$h_2(\xi) = -\frac{e^{\xi}\left(1-e^{\xi}\right)^2\left(1+6e^{\xi}+e^{2\xi}\right)}{32\left(1+e^{\xi}\right)^6}\,, \tag{4.44c}$$

which we plot in Fig. 4.2(b). Already for the minimum wave speed $c_{\min} = 2$, these corrections are small. Note furthermore that the contribution due to convection, $\nu h_2(\xi)$, which is of second order in $1/c^2$, is negligible compared to the second order correction $g_a(\xi)$ for the original Fisher equation as long as $\nu \approx 1$.

Convection-dominated regime ($\lambda \gg 1$)

Let us discuss the limit $\lambda \gg 1$, while $\beta \lesssim 1$. Since $\alpha = \lambda^2/(1+\eta'\kappa)$, this limit does not necessarily imply $\alpha \gg 1$ but could also arise from $\eta'\kappa \gg 1$ while $P_A \sim \gamma D$, see also Eqs. (4.27). Does this limit allow any conclusions on the interface dynamics? The integral on the right-hand side of Eq. (4.31) which gives the convective velocity in the co-moving frame varies with z and vanishes as $z \to \pm\infty$. However, we can approximate the integral for $|z| \ll \lambda$, assuming that Φ' decays faster than $e^{|z'|/\lambda}$, *i.e.*, $\Phi' \sim 1 - e^{az'}$ for $z' \to -\infty$ and $\Phi' \sim e^{-az'}$ for $z' \to +\infty$, where $a \gg 1/\lambda$. This assumption is consistent with the limit $\lambda \gg 1$ and can be checked *a posteriori*. In this case, the interface width is of order $L = a^{-1}$, and the convective velocity is approximately constant along the interface. We can then write

$$\int_{-\infty}^{+\infty} \mathrm{d}z'\, e^{-\frac{|z-z'|}{\lambda}} \left(1+\beta\Phi''\right)\Phi' \approx \int_{-\infty}^{+\infty} \mathrm{d}z' \left(1+\beta\Phi''\right)\Phi' = \left[\Phi + \frac{\beta}{2}\left(\Phi'\right)^2\right]_{-\infty}^{+\infty} = -1 \qquad \text{for } |z| \ll \lambda\,,$$

and we find that the convective velocity V is approximately given by

$$V(z) \approx \frac{\alpha}{2\lambda} \tag{4.45}$$

as long as $|z| \ll \lambda$. To first order and close to the interface, the equation for Φ becomes the classic Fisher equation

$$-\tilde{c}\,\Phi' = \Phi'' + \Phi\,(1-\Phi)\,, \tag{4.46}$$

where $\tilde{c} = c - \frac{\alpha}{2\lambda}$. The interface profile is given to lowest order in $1/\tilde{c}^2$ by

$$\Phi_0(z) = \frac{1}{1+e^{z/\tilde{c}}}\,. \tag{4.47}$$

For an initially compact interface, the steady-state traveling wave solution is given by $\tilde{c} = 2$, and the actual wave speed thus amounts to $c = 2 + \frac{\alpha}{2\lambda}$. We find that $a = \tilde{c} \sim 1$ and indeed $a^{-1} \ll \lambda$. Convection simply adds to the propagation velocity as it is set by diffusion and differential growth along the interface. Strictly speaking, the limit $\lambda \gg 1$ does not necessarily imply that the dynamics is convection-dominated, which is the case only if $\lambda/\alpha \gg 1$. Although the interface might be sharp on length scales compared to λ, the pressure profile decreases on a characteristic length scale set by λ. Therefore, cells of type A divide in a region of width λ behind the sharp interface, and cells of type B undergo apoptosis in a corresponding region ahead of the advancing interface. This mechanism propels the interface with an approximately constant, additional velocity. This contribution can become quite important if $P_A \gtrsim \gamma D$. Note however that $\delta V(z) = V(z) - \frac{\alpha}{2\lambda}$ scales with α/λ as well. For simplicity, let us consider an infinitely sharp interface. The velocity then decays as $V(z) \sim V(0)e^{-|z|/\lambda}$, which is an upper limit on the variation with z for interfaces of finite width L. Therefore, one can expect that deviations from the predicted interface profile become important as soon as $\frac{\alpha}{\lambda}(e^{-L/\lambda} - 1) \sim 1$; in

other words, we can expect that the above approximation holds as long as $\lambda \gg \frac{\alpha}{\lambda} L \sim 10\frac{\alpha}{\lambda}$ if we assume $\tilde{c} \approx 2$.

Now consider $\lambda \gg 1$ and $\beta \gg 1$. In this case, the above approximation of the integral close to the interface breaks down: As $\beta\Phi''$ now varies strongly from $\beta\Phi'' \ll -1$ to $\beta\Phi'' \gg 1$ along the interface, the dependence of z of the exponential term can no longer be neglected. As $\Phi'' > 0$ at the leading edge of the wavefront and $\Phi'' < 0$ towards the trailing edge, the convective velocity is increased at the front and decreased at the back. One can expect that this effectively expands the interface and thus speeds up the wavefront propagation.

4.4.3 Numerical results

In order to test the validity of the approximate solutions discussed above, and to explore the dynamics in general, we solved Eqs. (4.26) numerically in the time domain. For a sharp initial profile, the dynamics eventually leads to traveling waves with a well-defined interfacial profile $\phi = \Phi(x - ct)$ and fixed wave speed c, both of which depend on the values of λ, α, and β. For details on the implementation please refer to appendix C, section C.3.

Propagation velocity

The respective wave speeds of the traveling wave solutions for different parameter values are shown in Fig. 4.3, where we distinguished between the three cases $\beta = 0$, $\beta = 100$, and $\beta = 1000$ for better readability. Note that the speed of the traveling waves with $\lambda = 1000$ is indeed well approximated by $2 + \frac{\alpha}{2\lambda}$ as indicated by the dashed blue line. For $\lambda \leq 1$, the wave speed remains constant as long as $\beta \leq 100$, as predicted above in the limit for vanishing λ. These observations of wave propagation velocities therefore seem to confirm the approximations discussed in the previous section, which we check for consistency with the observed wavefront profiles below.

It is interesting to note the effect of a (significantly strong) surface tension coefficient β on the observed wave speeds. For $\beta = 0$, the wave speed c is bounded from above by $2 + \frac{\alpha}{2\lambda}$, and c increases with λ for fixed α/λ (see upper panel). For large enough β, the reverse can be observed: For finite λ, the wave speed c actually exceeds $2 + \frac{\alpha}{2\lambda}$ and decreases with λ for fixed α/λ, see Fig. 4.3 (lower panel). This can be understood as a trade-off between damping of the convective velocity, which decreases with λ, and the averaging-out of the contribution $\beta\Phi''$ in the integral on the right-hand side of Eq. (4.31), which switches sign along the interface.

Wavefront shapes

The actual wavefront profiles $\Phi(z)$ and the corresponding average cell velocities $V(z)$ for the individual traveling wave solutions are shown in Fig. 4.4. For comparison, we plot also the solution to the original Fisher wave equation as obtained by the perturbation

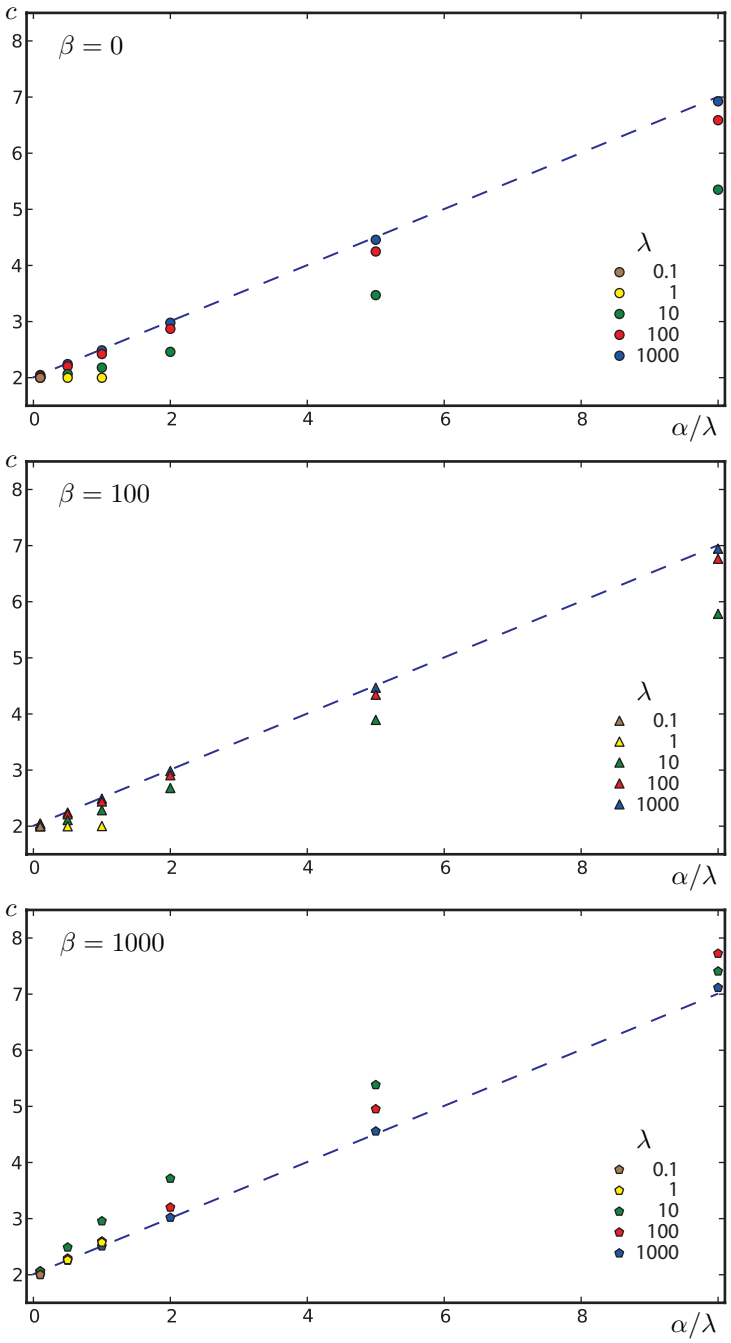

Figure 4.3. Wave speed c of traveling waves for different "propulsion strength" α/λ, cell velocity decay length λ, and surface tension β. The approximation $c = 2 + \frac{\alpha}{2\lambda}$ is plotted as a dashed blue line, see text for details.

series approach for $c = 2$ to second order,

$$\Phi_2(z) \simeq g_0(z/2) + \frac{1}{2} g_1(z/2)\,,$$

as a solid black line (*cf.* Eqs. (4.41) and (4.44a)). The respective wavefront shapes (upper panel) and corresponding velocity profiles (lower panel) are shown in three different blocks for increasing α/λ from top to bottom, and separately for increasing β from left to right.

For small "propulsion strength" $\alpha/\lambda = 0.1$, the Fisher wave profile is a good approximation for all characteristic decay lengths λ and non-dimensionalized surface tensions β, see Fig. 4.4(a-c). Even for large β, where the convective flow varies considerably along the interface for $\lambda = 1$ and $\lambda = 10$, see Fig. 4.4(f), this variation is still negligible against the minimum wave speed $c_{\min} = 2$ due to diffusion and differential proliferation.

For $\alpha/\lambda = 1$, the interface profile is still captured well by the Fisher wave profile as long as the convective velocity is approximately constant along the interface. This is perfectly true for traveling waves with $\lambda = 100$, as can be seen in panels Fig. 4.4(j-l). For $\lambda \leq 10$ and $\beta = 1000$, these variations get of the order of 1, and the interface profile starts to be distorted, see Fig. 4.4(l,i). Note also how the perturbation at the interface does not extent into the tissue far from the interface for $\lambda = 1$ (Fig. 4.4(j)), which implies that the interface is not propelled by cell division and apoptosis far from the border. Thus, the wave speed is still fixed by the diffusion and differential proliferation mechanism in the absence of convection, although the "strength" α/λ is the same for all curves shown here.

The same arguments hold for the case $\alpha/\lambda = 10$. For the parameter values chosen, only for curves with $\lambda = 1000$ does the approximation discussed in the previous section hold. Because the variation in the convective velocity across the interface roughly scales as $\delta V \sim \frac{\alpha}{\lambda}\frac{L}{\lambda}$, where L is the width of the interface, these variations can no longer be neglected for $\lambda = 10$ and lead to wavefront shape distortions already for $\beta = 0$, which become even more important for $\beta = 100$, see Fig. 4.4(m,p;n,q). For $\beta = 1000$, finally, the velocity variation becomes important for $\lambda = 100$ as well, and the corresponding wavefront shape deviates from the Fisher solution, see Fig. 4.4(r,o).

4.5 Discussion

What can we conclude from the theory developed in this chapter and the results presented above? In order to capture the growth dynamics of tissues that consist of more than one cell type, we extended our description of growing tissues developed in the previous chapters to tissues comprised of two distinct cell types. As a natural consequence of the concepts introduced before, such as the coupling between net cell division rate and isotropic stress, one finds that the two distinct cell populations can interact mechanically without having to take complicated cell signaling mechanisms explicitly into account. The resulting description of the multicellular dynamics extends earlier work insofar as smooth interfaces along which the volume fraction ϕ of cells of one type varies continuously can be considered. We derived a dynamic equation for ϕ that takes the form of a classical

Fisher wave equation with an additional convective term, see Eq. (4.7). The nonlinear growth term is proportional to the difference of the respective net cell division rates of cells of either type. Note that this difference is not necessarily a constant as is the case in the "original" Fisher equation. Relative flow between the two cell types is described by a diffusion coefficient D, which might also be a nonlinear function of the cell number densities. The convective velocity, which is the average cell velocity, is determined by force balance in the tissue. This coupling of an additional convective velocity to mechanics is truly distinct of usual Fisher wave dynamics. Initially, the Fisher wave equation was proposed to describe the expansion of an allele with selective advantage in a given species, where mechanical effects obviously do not play a role [62]. The Fisher equation was later used to describe the growth of bacterial colonies [40, 134]. Here, interactions between bacteria are lumped into a simple nonlinear proliferation rate, or a finite carrying capacity of the medium. In these descriptions, bacteria do not need to be in mechanical contact and physical forces are not considered.

On long time scales, we consider the tissue to behave as a viscous fluid, in accordance with the results obtained in the previous chapters. In the presence of finite gradients of the volume fraction ϕ, however, symmetry allows for an additional term in the off-diagonal part of the stress, which corresponds to the Ericksen stress in the case of a classical two-component fluid. In order to investigate the dynamics of interfaces between cells of different type independent of boundary conditions, we consider the tissue dynamics in a thin-film approximation, where friction between cells and the substrate breaks Galilean invariance. In this case, traveling wave solutions can exist if the homeostatic state (as defined earlier) of a "winner" cell type is stable against small perturbations and—reciprocally—the homeostatic state of a "loser" cell type unstable.

We studied the traveling wave solutions for a simple choice of the dependence of the net division rates of each cell type on the isotropic plane stress, or tension. This dependence is characterized by a difference P_A of the respective homeostatic pressures and a (common) susceptibility κ describing the response of the cell division rates on stress. Basically, one can distinguish two different regimes: If $P_A < \gamma D$, where γ is the friction coefficient between cells and the substrate, the convective velocity is negligible compared to the wave propagation due to diffusive relative flow of cells and differential cell division/apoptosis along the interface. In this case, the wave speed c is approximately given by $c \approx 2\sqrt{D\kappa P_A}$, as can be shown by making use of the solution to the original Fisher wave equation. However, vanishing D does not imply that the interface does not evolve in time: If $P_A \gg \gamma D(1 + \eta\kappa)$, where η is the tissue viscosity, the wave propagation is mainly driven by proliferation and apoptosis of cells on the respective sides of the interface. In this regime, the wave speed scales as $c \sim P_A/\sqrt{(\kappa^{-1} + \eta)\gamma}$, which is independent of D. This propagation exists also for sharp interfaces, *i.e.*, for cell populations that abut but are mechanically separated. Such interfaces are ubiquitous in development, where *e.g.* compartment boundaries have spurred some interest. Interestingly, the phenomenon of cellular competition described in the introduction to this chapter seems to be confined to individual compartments and does proceed across compartment boundaries. One possible explanation might be that the compartment boundary acts as a mechanical barrier

that could be associated to an increase in tension along the interface [113, 129].

Some technical remarks are due here. For simplicity, we neglected any additional biochemical coupling between the two cell types in our analysis. As long as a stable, stationary state with finite volume fraction ϕ^* exists towards which any volume fraction $\phi \neq \phi^*$ would eventually relax due to cell division and apoptosis for any given tension ς, the described traveling wave dynamics would similarly exist. Any interface between the homeostatic state with $\phi = \phi^*$ and the unstable homeostatic states $\phi = 0$ or $\phi = 1$ would eventually propagate. Note however that the hypothesized homeostatic state is only marginally stable if the cell division rates depend on pressure, in which case the dynamics does not obviously follow. Furthermore, we restricted our analysis to constant, positive diffusion coefficient D. For passive systems, equilibrium thermodynamics requires $D > 0$. Cells are active agents far from equilibrium, however, and $D < 0$ could be allowed in principle. Negative diffusion would correspond to active cell sorting-out, and interfaces could be considered to be sharp in that case.

Last but not least, we only considered traveling waves in a linear geometry. It is straightforward to write down the corresponding equations in the case of an axisymmetric geometry. Strictly speaking, traveling waves $\phi = \Phi(r - ct)$ as a function of the radius r with constant c do not exist, because the Laplace operator that appears in the diffusion term depends now explicitly on r. This dependence vanishes as $1/r$ for $r \to \infty$, however, and the solutions we discussed here are approximate solutions for the radial interfacial profile at long times. More importantly, due the circular geometry the interfacial tension now adds to the stress exerted on the expanding tissue. This affects the convective velocity, which follows from force balance. Whereas we can neglect this effect in the diffusion dominated regime, it can become quite important when $P_A \gtrsim \gamma D$. One finds a critical radius $R_c \approx B/(P_A L)$ for the position of an interface of width L below which the interfacial tension dominates over the expansion pressure P_A. Interestingly, this will not lead to a suppression of the expanding tissue, however. Rather, we can expect that the tissue expands slowly via diffusion with a very broad interface profile before the convection-dominated mode of propulsion eventually takes over once the critical radius is reached.

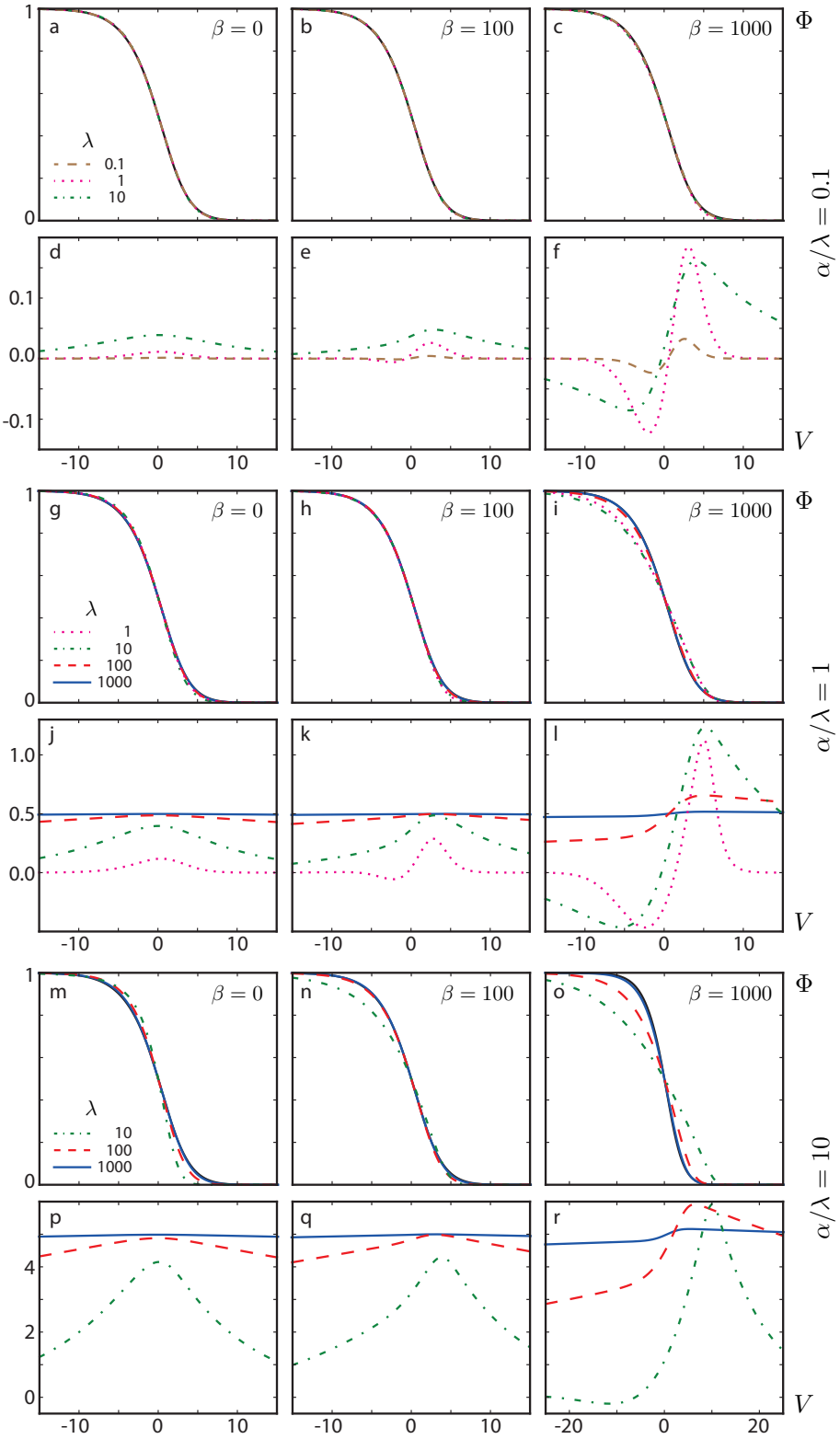

Figure 4.4. Interface profile Φ and convective cell velocity V in the co-moving frame for different "propulsion strength" α/λ, cell velocity decay length λ, and surface tension β. The solution to the original Fisher equation with $c = 2$ is plotted as a solid black line for comparison, see text for details. Both Φ and V are shown as functions of the coordinate z; note also the change of scale in the lower right panels.

Chapter 5

General conclusion and outlook

In this thesis, we studied several aspects of the physics of growing cellular tissues. The ability to grow and divide is a unique feature of living cells, and eventually allowed the evolution of ever more complex forms of life. From a physics point of view, biological tissues are out-of-equilibrium systems in constant exchange with their environment, and cell proliferation is one of the most compelling manifestations thereof.

During division and apoptosis, cells generate active forces; in the realm of continuum mechanics, these can be described as force dipoles. In a first part of this thesis (chapter 2), we discussed the effect of these active stress sources on the tissue material behavior. The stress increments due to cell division and apoptosis are anisotropic in general, where the anisotropy of the source stress is linked to the average orientation of cell division. In a perfectly isotropic system, cell divisions are random and not aligned on average. Finite anisotropic stresses orient the cell division axis on average, however, and the tissue can relax elastic stresses by cell division; a similar argument holds for the stresses associated with apoptosis events. The growing tissue therefore effectively behaves as a viscoelastic fluid with a characteristic relaxation time set by the rates of cell division and apoptosis. At long times, the tissue is able to flow in response to external forces. This stress-relaxation mechanism may be relevant for tissue formation in development, where cell generation times are short compared to the time scale of morphogenesis.

A similar mechanism of "active" stress relaxation can be found in a phenomenological theory of polar, active gels using an Onsager approach [39, 110]. Such a generic theory does not rely on specific assumptions to derive the governing equations, which follow from symmetry arguments and local entropy production. The apparent similarity lends hope that generic theories may inform biophysical descriptions of tissue mechanics even though the underlying assumption that the system is close to thermodynamic equilibrium does not hold for tissues in a straightforward way. It is therefore worthwhile to explore how far the analogy regarding the hydrodynamics of polar, active gels holds.

When considering tissues with a global polarity pattern, we furthermore found that oriented cell divisions do not only relax stress but can give rise to additional source terms in the stress that persist at long times. These active stresses, which occur when the cell division axis is aligned on average, can drive cell flow by oriented cell divisions

and may play a role in convergence-extension tissue morphogenesis. For simplicity, we assumed the global order to remain constant. However, recent work of Aigouy and coworkers found that the planar cell polarity in the *Drosophila* wing imaginal disc aligns with the shear flow of cells [7]. In order to develop a comprehensive understanding of the underlying tissue dynamics, it is therefore certainly of interest to investigate time-dependent polarity patterns and their coupling to the cell flow. Also, one can imagine that for some tissues, polarity may form spontaneously as in isotropic-to-nematic phase transitions. Here, further research might indeed be informed by the theory of liquid crystals and the aforementioned polar, active gels [39, 49, 110].

In section 2.4, we discussed zebrafish epiboly as a possible example of tissue fluidization during growth. During epiboly, blastoderm cells and cells of the enveloping layer (EVL) proliferate and spread on the underlying yolk cell. We showed that cell proliferation in conjunction with the spherical geometry gives rise to shear stresses, which in turn can orient the axis of cell division in the absence of any other directional cues. Depending on cell-substrate friction, our model furthermore suggests that the rate of cell division might be modulated along the animal-vegetal axis. The predicted orientation of cell division has indeed been observed in early stages of epipoly [44]. However, it is not clear to which degree this orientation is caused by cell polarity cues other than the mechanical cues due to shear stress [167]. A thorough experimental analysis of the tissue dynamics during epiboly seems a promising endeavor in order to disentangle different contributions. Similarly, a quantitative study of the spatial distribution of cell divisions in the EVL might give hints on the strength of mechanical coupling between the EVL and the underlying cell mass. An appropriate theoretical description of zebrafish epiboly may also require additional effects to be taken into account, as for example mass exchange in the radial direction.

Another remark concerns our choice of constitutive equation in the absence of cell division and apoptosis. In this limit, we considered the tissue to behave as an elastic solid, partly informed by experimental observations [59].[1] Our approach can be generalized in a straightforward way to include other stress relaxation mechanisms, for example those related to cell shape fluctuations [121], see also the discussion at the end of chapter 2. However, it is less clear how our account of cell division and apoptosis translates to arbitrary tissue rheologies in the absence of cell division and apoptosis, which is a question that may provide additional conceptual insight. Note also that we neglected nonlinear effects for simplicity, which may be relevant to explain a possible shear thinning [16] or strain hardening [71] response of biological tissues. Regarding the latter, a pragmatic approach may be to consider all next-higher order terms allowed by symmetry in order to investigative their respective role in the overall tissue response.

An even more interesting problem though might be the effect of active cell motility on large-scale tissue dynamics. Recent work by different groups focused on collective

[1] From a statistical physics perspective, we presented a mechanism of bulk melting of an elastic solid which does not exist for conventional solids, *i.e.* crystals. The stress relaxation mechanism related to cell division and apoptosis bears some resemblance to melting of two-dimensional crystals by unbound dislocation pairs that distort the crystal lattice [136]; however, bulk melting in three-dimensional crystals has not been observed [48].

cell migration in epithelial sheets [13, 148, 155, 175, 182]. Angelini and co-workers suggested that confluent, proliferating epithelia approach a glass-like state as the cell density increases, based on the analysis of cell velocity correlations. They found that the characteristic velocity-correlation relaxation time at the glass transition corresponds to the average cell division time [13], which corroborates our results regarding tissue fluidization. At lower cell densities, migration dominates over diffusive motion of cells, with a rheology similar to that of active particle suspensions [13, 18, 92]. Puliafito and colleagues report a similar structural transition for freely expanding epithelial cell colonies and establish a link between cell density and proliferation rate. They find that the rate of cell division is reduced for increasing cell density [155], and their observation raises the question to which extent cell proliferation remains determinant for the collective dynamics at cell densities below the glass transition mentioned above. In order to address this issue and related questions, it seems promising to explicitly account for active cell migration within the framework put forward in this thesis. Active migration necessarily implies momentum transfer between cells and the substrate, and one might attempt to model active migration as a random body force acting on the cells [155]. As we have shown in section 2.4, the interplay of cell-substrate friction and tissue viscosity defines a characteristic length scale, which might then account for the finite correlation lengths of the velocity fluctuations observed in experiments [13, 155, 175]. Certainly, more work needs to be done in order to shed light on the rich dynamical behavior that arises from the interplay of the cell migration and proliferation.

In section 2.3, we discussed the homeostatic state at which cell division and apoptosis balance on average. In a constant biochemical environment, the rates of cell division and apoptosis vary with the mechanical stress, and the homeostatic state corresponds to a well-defined homeostatic pressure. A remarkable property of tissues at the homeostatic state is that their bulk compressional modulus vanishes; in contrast with conventional materials, particle number (*i.e.* cell number) is not a conserved quantity when the homeostatic state is perturbed. The dynamics close to the homeostatic state is characterized by a second viscoelastic relaxation time, which describes the response of the net cell division rate to pressure. Recent experiments with multicellular tissue aggregates demonstrated the pressure-dependence of the cell division and apoptosis rates in the bulk of tissue spheroids, although cell proliferation at the spheroid surface seems to be regulated differently [130]. Note that this study suggests that the homeostatic pressure is negative, which does not contradict the framework put forward in this thesis. In the experiments with expanding epithelial cell colonies mentioned earlier, Puliafito and colleagues also found that cell division is reduced within the bulk of the cell colony as compared to the stronger-proliferating rim after a size threshold is reached [155]. The authors suggest that migrating cells at the margin exert a finite tension on the cell sheet, which locally promotes proliferation; in the center of the colony, cells are not under tension and unable to divide [155]. In this context, it may be worthwile to study the interplay of applied tensions, cell-substrate interactions and cell proliferation within our framework in order to explore the concept of homeostatic pressure for sheet-like tissues in two dimensions.

Our analysis of noise due to cell division and apoptosis allowed us to calculate an

effective diffusion coefficient for cells in the homeostatic state (section 2.5). When considering the height fluctuations of a tissue covered by a tensionless membrane, we found that these fluctuations can give rise to fracture of the tissue layer at a characteristic length scale set by the membrane's bending modulus. Here, we restricted our analysis to the regime of small fluctuations around the average tissue height for simplicity. It would be interesting to extend the calculation to the nonlinear regime, however, given that the cell division noise is multiplicative and scales with the tissue volume. This also manifests itself in the height-dependent diffusion coefficient of a stiff piston covering a tissue at the homeostatic state, which implies giant fluctuations related to the vanishing tissue compressibility.

In the second part of this thesis (chapter 3), we addressed the effects of the permeating extracellular fluid on tissue dynamics. To this end, we introduced a two-component description of tissues that takes both a cell phase and the interstitial fluid into consideration. Note that a second material component is necessary in order to keep track of total mass balance in the presence of cell division and apoptosis: cell division and apoptosis can then be described as an effective material turn-over between the two phases. In the two-component description, internal forces due to friction between the extracellular fluid and the cell phase appear naturally in the tissue force balance equation. The two-component descriptions allowed us to clarify the nature of the homeostatic pressure which is the isotropic part of the cell stress tensor, not to be confused with the hydrostatic pressure of the interstitial fluid. An illustrative example is the neck of a giraffe: Although the fluid pressure may exhibit a barometric profile due to gravitational forces, where fluid pressure decreases with height, cell pressure may be constant throughout the tissue and the giraffe's neck at the homeostatic state.

Moreover, the ratio between the tissue viscosity and the cell-fluid friction coefficient defines a characteristic length scale over which stresses are transferred from the cell phase to the fluid. This is illustrated by the dynamics of a moveable semi-permeable piston subject to an excess pressure that encloses a tissue at its homeostatic state, where one can distinguish different dynamical regimes depending on the value of this characteristic length. If this characteristic length is large compared to tissue size, we find that the tissue dynamics is correctly described by the one-component theory. For sufficiently high friction or low tissue viscosity, however, this length is small and the response to pressure remains confined to a small region of the tissue and the one-component description fails to account for the observed dynamics. The order of magnitude of this characteristic length in real tissues is not clear, however, see also the discussion at the end of chapter 3, and no precise predictions of the role of permeation can be made. It would be informative to design specific experiments that measure tissue permeability for different cell types, thus allowing an estimation of the effects in biologically relevant situations. Regarding the theory, the next step could consist in the consideration of biochemical regulation of growth. Although it is generally assumed that nutrient supply is governed by diffusion and fast compared to the time scale of cell division and apoptosis [153], convective flows of nutrients solved in the extracellular fluid may become relevant in certain situations. Also, it is reasonable to assume that due to increased cell pressure, the pore size in

the tissue changes and the permeability of the tissue decreases. It would be worthwile to explore whether such nonlinearities could give rise to instabilities of the cell volume fraction.

Finally, we devoted the last part of this thesis (chapter 4) to the mechanical competition between two populations of cells of different type. Extending the framework developed in chapter 2, we found the equations that govern the dynamics of a smooth interface between two such cell populations. Here, the dynamical equation for the volume fraction of one of the cell types formally corresponds to the Fisher equation with an additional convective term. Under the assumption that the respective rates of cell proliferation of either cell type are under mechanical control, this correspondence can be made more explicit. We found that if the homeostatic pressures of the two cell types differ, the more resilient cell population invades the other one, a situation that reminds of tumor growth within a healthy tissue. In the presence of cell-substrate friction, traveling wavefront solutions for the tissue interface exist, and our analysis showed that two different limit cases can be distinguished. In a first regime where diffusion dominates, relative fluxes due to diffusion allow the "malignant" cells to spread, and their resilience lets them take over locally. If the difference in the homeostatic pressures between "malignant" and "healthy" tissues is large and cell-substrate friction low, convective flows dominate the interface dynamics. In this regime, the interface between the two cell populations is propelled by excessive proliferation of the tumor and corresponding cell death in the healthy tissue. Our work thus demonstrates the importance of cell-cell interactions and fluctuations that determine the effective diffusion of cells at the tissue interface. Even in situations where surface tension effects may prevent a small mutant cell population to spread, see also the work of Basan *et al.* [17], diffusion allows to smoothen the interface and leads thus to subsequent outcompetition of the healthy tissue by the mutant cell population.

A straightforward extension of this work would be to consider geometries other than the one discussed here in order to arrive at more realistic models of tumor expansion. Another step would be to combine the dynamics of two different cell types with the theory developed in chapter 3, which additionally takes the interstitial fluid into account. Finite tissue permeability may then play the role of the cell-substrate friction and allows for the existence of traveling wave solutions in a three-dimensional geometry. Also, more detailed theoretical modeling could be informed by research on biochemical interactions between tumor and host tissue: much of cancer research has been focusing on the genetic prerequisites and regulation of cancer [190], and along with research on the tumor microenvironment such research is certainly to come. Last but not least, the problem of interacting cell populations arises in the context of tissue renewal. Here, stem cells proliferate and give rise to daughter cells that eventually differentiate. Our approach towards the mechanics of interacting cell populations should in principle allow to capture the dynamics of such self-renewing cell populations, and taking cell differentiation into account could be a promising avenue of further research.

Appendix A

Force dipoles in elastic media

A.1 Point force dipoles

For an isotropic elastic medium, the Hookian law is expressed as

$$\sigma^{\mathrm{el}}_{\alpha\beta} = C_{\alpha\beta\gamma\nu} u_{\gamma\nu} \,, \tag{A.1}$$

where $u_{\alpha\beta} = \frac{1}{2}(\partial_\alpha u_\beta + \partial_\beta u_\alpha)$ is the total elastic strain. The tensor of elastic constants is given by $C_{\alpha\beta\gamma\nu} = \chi\, \delta_{\alpha\beta}\delta_{\gamma\nu} + 2\mu\, (\delta_{\alpha\gamma}\delta_{\beta\nu} - \delta_{\alpha\beta}\delta_{\gamma\nu}/3)$, where χ and μ are bulk and shear elastic moduli, respectively. Force balance reads

$$\partial_\beta \sigma^{\mathrm{el}}_{\alpha\beta} = -f_\alpha \,, \tag{A.2}$$

where f_α is a force density that describes stress sources acting on the material. If the forces are known, the above equation allows to determine the elastic deformation u_α for given boundary conditions.

Any given force distribution can be characterized by its moments with respect to the spatial coordinate $\mathbf{r}$. The first moment is simply the sum of all forces in a given volume,

$$F_\alpha = \int \mathrm{d}V\, f_\alpha(\mathbf{r}) \,. \tag{A.3}$$

If the first moment is finite, it generally dominates the elastic deformation at long range. The second moment defines a tensor which is called a force dipole. The force dipole of a force distribution f_α is given by

$$P_{\alpha\beta} = \int \mathrm{d}V r_\alpha f_\beta(\mathbf{r}) \,. \tag{A.4}$$

Although the sum of all forces within a given volume might vanish, its force dipole may still be finite.

In the main text, we consider cell division and apoptosis events as point force dipoles. The first moment of the microscopic force distributions necessarily vanishes, because the forces are of internal origin and not possibly balanced otherwise. A point force

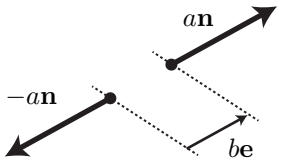

Figure A.1. The two opposed point forces form a point force dipole in the limit of $b \to 0$. Here, both forces are collinear and $\mathbf{e} = \mathbf{n}$.

dipole $d_{\alpha\beta}$ can be thought of as two point forces brought infinitely close together such that the product (force)×(distance) remains constant. Consider the force distribution $f_\alpha(\mathbf{r}) = f_{1,\alpha}(\mathbf{r}) + f_{2,\alpha}(\mathbf{r})$, where $f_{1,\alpha}(\mathbf{r}) = a\mathbf{n}_\alpha\delta(\mathbf{r} - \mathbf{r}_1)$ and $f_{2,\alpha}(\mathbf{r}) = -a\mathbf{n}_\alpha\delta(\mathbf{r} - \mathbf{r}_2)$. Here, a is a force amplitude and $\mathbf{n}$ a unit vector denoting the direction of the force. Obviously, $\int \mathrm{d}V\, f_\alpha(\mathbf{r}) = 0$. Now let $\mathbf{r}_2 = \mathbf{r}_1 - b\mathbf{e}$, where b is a length and $\mathbf{e}$ a unit vector defined by the relative position of the two point forces. A sketch of such a force dipole is shown in Fig. A.1. In the limit of $b \to 0$, we obtain

$$\begin{aligned} f_\alpha(\mathbf{r}) &= \lim_{b\to 0} an_\alpha \left[\delta(\mathbf{r} - \mathbf{r}_1) - \delta(\mathbf{r} - \mathbf{r}_1 + b\mathbf{e})\right] \\ &= -d_{\alpha\beta}\partial_\beta\delta(\mathbf{r} - \mathbf{r}_1)\,, \end{aligned} \tag{A.5}$$

where we defined the dipole moment $d_{\alpha\beta} = abn_\alpha e_\beta$. As $b \to 0$, the force amplitude $a \to \infty$ such that $ab = \text{const}$. The force density given by equation (A.5) thus describes a point force dipole at $\mathbf{r}_1$. Not suprisingly, for the second moment defined in Eq. (A.4) we find $P_{\alpha\beta} = d_{\alpha\beta}$. Note that in principle, more than two point forces can be combined in this way in order to describe more complex force distributions. Because cell division and apoptosis do not exert any net torque, we only require the $d_{\alpha\beta}$ to be symmetric. We can now introduce the force dipole density $D_{\alpha\beta} = \sum_n d^{(n)}_{\alpha\beta}\delta(\mathbf{r} - \mathbf{r}_n)$ that describes a collection of point force dipoles. Note that the force distribution described by these dipoles is given by $f_\alpha = -\partial_\beta D_{\alpha\beta}$. In the coarse-grained description, we locally average over a small volume and obtain a smooth function $D_{\alpha\beta}(\mathbf{r})$.

A.2 Green's function of force dipoles in elastic media

Let $G_{\alpha\beta}$ denote the Green's function of an elastic medium such that the deformation field $\mathbf{u}$ due to a point force $\mathbf{f}$ at $\mathbf{r}'$ is given by

$$u_\alpha(\mathbf{r}) = G_{\alpha\beta}(\mathbf{r} - \mathbf{r}')f_\beta\,. \tag{A.6}$$

The point force Greens' function can in principle be determined from Eqs. (A.1) and (A.2), which is discussed *e.g.* in [112]. For any force dipole $d_{\alpha\beta}\delta(\mathbf{r}')$, we can introduce

the force distribution $f^{\mathrm{d}}_\alpha(\mathbf{r}') = -d_{\alpha\beta}\partial_\beta\delta(\mathbf{r}')$, see the previous section. This implies

$$\begin{aligned} u_a(\mathbf{r}) &= -\int \mathrm{d}^3r'\, G_{\alpha\beta}(\mathbf{r}-\mathbf{r}')\, d_{\beta\gamma}\partial_{\gamma'}\delta(\mathbf{r}') \\ &= +\int \mathrm{d}^3r'\, \partial_{\gamma'}G_{\alpha\beta}(\mathbf{r}-\mathbf{r}')\, d_{\beta\gamma}\delta(\mathbf{r}') \\ &= -\int \mathrm{d}^3r'\, G_{\alpha\beta,\gamma}(\mathbf{r}-\mathbf{r}')\, d_{\beta\gamma}\delta(\mathbf{r}')\,, \end{aligned} \tag{A.7}$$

where $\partial_{\gamma'} = \partial/\partial x'_\gamma$ and $G_{\alpha\beta,\gamma} = (\partial/\partial x_\gamma)G_{\alpha\beta}$. Here, we have used the translational invariance of an infinite medium which is expressed by the fact that $G_{\alpha\beta}(\mathbf{r},\mathbf{r}') = G_{\alpha\beta}(\mathbf{r}-\mathbf{r}')$. Thus we have

$$u_{\alpha\beta} = \frac{1}{2}(\partial_\alpha u_\beta + \partial_\beta u_\alpha) \tag{A.8}$$

$$= -\frac{1}{2}\int \mathrm{d}^3\tilde{r}\, \{G_{\alpha\gamma,\delta\beta}(\mathbf{r}-\tilde{\mathbf{r}}) + G_{\beta\gamma,\delta\alpha}(\mathbf{r}-\tilde{\mathbf{r}})\}\, d_{\gamma\delta}\delta(\tilde{\mathbf{r}}) \tag{A.9}$$

$$\equiv \int \mathrm{d}^3\tilde{r}\, H_{\alpha\beta\gamma\delta}(\mathbf{r}-\tilde{\mathbf{r}})\, d_{\gamma\delta}\delta(\tilde{\mathbf{r}})\,, \tag{A.10}$$

where we have defined the force dipole Green's function $H_{\alpha\beta\gamma\delta}$ for the elastic strain $u_{\alpha\beta}$. When the point force Green's functions $G_{\alpha\beta}$ is known, we can now calculate $H_{\alpha\beta\gamma\delta}$ straightforward. For an isotropic, infinite elastic medium one obtains

$$\begin{aligned} A^{-1}H_{\alpha\beta\gamma\delta}(\mathbf{r}) = &-\frac{1}{r^3}\left[\delta_{\alpha\beta}\delta_{\gamma\delta} - (1-2\nu)(\delta_{\alpha\gamma}\delta_{\beta\delta}+\delta_{\alpha\delta}\delta_{\beta\gamma})\right] \\ &+\frac{3}{r^5}\left[r_\alpha r_\beta\delta_{\gamma\delta} + r_\alpha r_\gamma\delta_{\beta\delta} + r_\beta r_\gamma\delta_{\alpha\delta} + r_\gamma r_\delta\delta_{\alpha\beta}\right. \\ &\left.-(1-2\nu)(r_\alpha r_\delta\delta_{\beta\gamma} + r_\beta r_\delta\delta_{\alpha\gamma})\right] - \frac{15}{r^7}r_\alpha r_\beta r_\gamma r_\delta\,, \end{aligned} \tag{A.11}$$

with $A = (3\chi-\mu)/(24\pi\chi\mu)$ and Poisson's ratio $\nu = (3\chi-2\mu)/(6\chi-2\mu)$. See also reference [24] for a discussion of single cells acting as force dipoles in elastic media and corresponding Green's functions in more complicated geometries.

A.3 Analogy to electrostatics

There is a formal analogy between stresses in an elastic medium in the presence of force dipoles

$$\sigma_{\alpha\beta} = C_{\alpha\beta\gamma\nu}u_{\gamma\nu} - D_{\alpha\beta}\,, \tag{A.12}$$

and electrostatics in polarizable media,

$$D_\alpha = \epsilon_0 E_\alpha + P_\alpha\,. \tag{A.13}$$

Here, D_α is the dielectric displacement, ϵ_0 is the vacuum permittivity, E_α the electric field, and P_α the polarization. Note that $\partial_\alpha D_\alpha = \rho_{\mathrm{ext}}$, where ρ_{ext} is the free charge density, and $P_\alpha = \sum_n p^{(n)}_\alpha\delta(\mathbf{r}-\mathbf{r}_n)$ is a dipole density; also, $\partial_\alpha E_\alpha = (\rho_{\mathrm{ext}} - \sum_n \partial_\alpha p^{(n)}_\alpha\delta(\mathbf{r}-$

$\mathbf{r}_n))/\epsilon_0$. The analogy is then $\sigma_{\alpha\beta} \leftrightarrow D_\alpha$, $u_{\alpha\beta} \leftrightarrow E_\alpha$, $D_{\alpha\beta} \leftrightarrow -P_\alpha$, $f_\alpha^{\text{ext}} \leftrightarrow -\rho^{\text{ext}}$, and $\epsilon_0 \leftrightarrow C_{\alpha\beta\gamma\nu}$. A similar analogy between the elastic deformation around dislocation lines and the magnetic field around lines of constant current has been pointed out by [112, 147].

Appendix B

Detailed calculation of the cellular diffusion constant

In this appendix, we show the detailed calculation of the diffusion coefficient of cells both for the one-component and for the two-component theory of tissues at the homeostatic state. Whereas we use exactly the same description of the tissue material properties as put forward in the main text, and consider the same form of the noise due to cell division and apoptosis, we take here the finite decay times of the velocity-velocity correlations into account. In cases where the slow diffusion approximation which we used in the main text is not appropriate, we give the expression of the diffusion coefficient which can be used to determine its value graphically or numerically.

B.1 One-component description

In three dimensions, the diffusion constant is defined as

$$D = \lim_{t\to\infty} \frac{\langle \mathbf{r}_p^2(t)\rangle}{6t}\,, \tag{B.1}$$

where $\mathbf{r}_p$ stands for the position of a tracer particle. The position can be expressed in terms of the flow field $v_\alpha(\mathbf{r},t)$ in which the particle moves, and we find

$$\begin{aligned} D &= \frac{1}{3}\int_0^\infty \mathrm{d}t\, \langle v_\alpha(\mathbf{r}_p(t),t) v_\alpha(\mathbf{r}_p(0),0)\rangle \\ &= \frac{1}{3}\int_0^\infty \mathrm{d}t \int \frac{\mathrm{d}^3q}{(2\pi)^3}\int \frac{\mathrm{d}^3q'}{(2\pi)^3} \Big\langle e^{i[\mathbf{q}\mathbf{r}_p(t)+\mathbf{q}'\mathbf{r}_p(0)]}\, v_\alpha(\mathbf{q},t) v_\alpha(\mathbf{q}',0)\Big\rangle\,. \end{aligned} \tag{B.2}$$

Under the assumptions that particle position and velocity fluctuations decouple, the diffusion coefficient is thus given by

$$\begin{aligned} D &= \frac{1}{3}\int_0^\infty \mathrm{d}t \int \frac{\mathrm{d}^3q}{(2\pi)^3}\int \frac{\mathrm{d}^3q'}{(2\pi)^3}\left\langle e^{i[\mathbf{q}\mathbf{r}_p(t)+\mathbf{q}'\mathbf{r}_p(0)]}\right\rangle \langle v_\alpha(\mathbf{q},t)v_\alpha(\mathbf{q}',0)\rangle \\ &= \frac{1}{3}\int_0^\infty \mathrm{d}t \int \frac{\mathrm{d}^3q}{(2\pi)^3}\left\langle e^{i[\mathbf{q}\mathbf{r}_p(t)+\mathbf{q}'\mathbf{r}_p(0)]}\right\rangle C_{vv}(q,t) \\ &= \frac{1}{3}\int_0^\infty \mathrm{d}t \int \frac{\mathrm{d}^3q}{(2\pi)^3}\, e^{-q^2Dt}C_{vv}(q,t)\,, \end{aligned} \tag{B.3}$$

where we introduced the velocity-velocity correlation function $C_{vv}(q,t)$ defined by

$$\langle v_\alpha(\mathbf{q},t)v_\alpha(\mathbf{q}',0)\rangle = (2\pi)^3\delta(\mathbf{q}+\mathbf{q}')\, C_{vv}(q,t) \tag{B.4}$$

and assumed a Gaussian distribution of particle position fluctuations,

$$\begin{aligned} \left\langle e^{i\mathbf{q}[\mathbf{r}_p(t)-\mathbf{r}_p(0)]}\right\rangle &= \int \mathrm{d}^3r \frac{1}{(4\pi Dt)^{3/2}} e^{-\frac{r^2}{4Dt}} e^{i\mathbf{q}\mathbf{r}} \\ &= e^{-q^2Dt}\,. \end{aligned} \tag{B.5}$$

Equation (B.3) allows in principle to calculate the diffusion coefficient without any further approximation. Note however that D is given only in an implicit form. In the main text, we calculated the diffusion constant under the assumption that diffusion is slow compared to the relaxation of the velocity-velocity correlations, an approximation we discuss in detail below.

Velocity-velocity correlation function

In order to calculate the velocity-velocity correlations, we solve for the velocity fluctuations in the Fourier domain as driven by the stress fluctations, see Eqs. (2.63) in the main text. We then find the Fourier transform $\hat{C}_{vv}(q,\omega)$ according to

$$\langle v_\alpha(\mathbf{q},\omega)v_\alpha(\mathbf{q}',\omega')\rangle = (2\pi)^4\delta(\mathbf{q}+\mathbf{q}')\delta(\omega+\omega')\hat{C}_{vv}(q,\omega)\,, \tag{B.6}$$

and obtain

$$\hat{C}_{vv}(q,\omega) = \frac{2}{q^2}\left[\left(\frac{\zeta}{\bar{\eta}}\right)^2 \frac{k_d}{n_h}\frac{1+\omega^2\tau_a^2}{1+\omega^2\bar{\tau}^2} + \frac{2}{3}\frac{\theta}{\bar{\eta}^2}\frac{1+\omega^2\tau^2}{1+\omega^2\bar{\tau}^2} + \frac{\theta}{\eta^2}\right]. \tag{B.7}$$

Here, $\bar{\eta} = \zeta + \frac{4}{3}\eta$ is again the longitudinal viscosity and

$$\bar{\tau} = \frac{\zeta\tau_a + \frac{4}{3}\eta\tau}{\bar{\eta}} = \tau\tau_a\frac{\chi+\frac{4}{3}\mu}{\chi\tau+\frac{4}{3}\mu\tau_a}$$

as in the main text.

In the time domain, the velocity correlations decay exponentially. In the one-component theory, there is a single relaxation time, which is $\bar{\tau}$. The explicit form of the velocity-velocity correlations in the time domain can be obtained in a straightforward way from the Fourier transform

$$\int \frac{\mathrm{d}\omega}{2\pi}\, e^{-i\omega t} \frac{1+\omega^2\tau_1^2}{1+\omega^2\tau_2^2} = \left(\frac{\tau_1}{\tau_2}\right)^2 \delta(t) + \frac{\tau_2^2-\tau_1^2}{2\tau_2^3} e^{-t/\tau_2}\,. \tag{B.8}$$

Please note that the δ-correlated contribution is an "artefact" of the one-component theory, in the sense that it disappears in the two-component theory (see below).

Calculation of the diffusion constant in the slow diffusion limit

With the approximation that $e^{-q^2Dt} \simeq 1$ for all times $t \lesssim \bar{\tau}$ at which the velocity-velocity correlations are finite, Eq. (B.3) simplifies to

$$\begin{aligned} D &\simeq \frac{1}{3}\int_0^\infty \mathrm{d}t \int \frac{\mathrm{d}^3q}{(2\pi)^3}\, C_{vv}(q,t) \\ &= \frac{1}{6}\int \frac{\mathrm{d}^3q}{(2\pi)^3}\, \hat{C}_{vv}(q,\omega)|_{\omega=0} \equiv D_0\,. \end{aligned} \tag{B.9}$$

In this limit, the diffusion coefficient can be calculated directly from $\hat{C}_{vv}(q,\omega)$, and we obtain

$$\begin{aligned} D_0 &= \frac{1}{12\pi^2}\int_0^{q_{\max}} \mathrm{d}q\, \hat{C}_{vv}(q,\omega)|_{\omega=0} \\ &= \frac{1}{6\pi a}\left\{\frac{1}{\bar{\eta}^2}\left[\frac{\zeta^2 k_\mathrm{d}}{n_\mathrm{h}} + \frac{2}{3}\theta\right] + \frac{\theta}{\eta^2}\right\}, \end{aligned} \tag{B.10}$$

which is the result presented in the main text, see Eq. (2.70). Here, we chose $q_{\max} = \pi/a$ as a high wave number cut-off, where a is a cell radius.

Validity of the slow diffusion result

The approximation $e^{-q^2Dt} \simeq 1$, or $D \simeq D_0$, holds for all q and on all relevant time scales if

$$q_{\max}^2 D_0 \bar{\tau} \ll 1\,, \tag{B.11}$$

where we recall that $\bar{\tau}$ is the relaxation time of the velocity-velocity correlations. Let us get an estimate for $q_{\max}^2 D$. Using the estimations

$$k_\mathrm{d} = \mathcal{O}(\tau_\mathrm{a}^{-1})\,, \tag{B.12a}$$

$$n_\mathrm{h}^{-1} = \mathcal{O}(\pi a^3)\,, \tag{B.12b}$$

$$\theta = \mathcal{O}(\eta^2 k_\mathrm{d}/n_\mathrm{h})\,, \tag{B.12c}$$

we find

$$q_{\max}^2 D_0 \approx \frac{1}{\tau_\mathrm{a}}\left[\left(\frac{\chi\tau}{\chi\tau+\mu\tau_\mathrm{a}}\right)^2+\left(\frac{\mu\tau_\mathrm{a}}{\chi\tau+\mu\tau_\mathrm{a}}\right)^2\right]\lesssim\frac{2}{\tau_\mathrm{a}}\,. \tag{B.13}$$

In order to check the validity of assumption (B.11), we thus simply need to check whether $\bar{\tau}\ll\tau_a$.

The value of $\bar{\tau}$ depends on the ratio of the bulk elastic modulus χ to the shear elastic modulus μ. In the incompressible limit, *i.e.*, for $\chi\gg\mu$, we find $\bar{\tau}\approx\tau_a$, and it turns out that the slow diffusion approximation (B.11) is not guaranteed to hold: in this case, $q_{\max}^2 D_0\bar{\tau}=\mathcal{O}(1)$. If $\chi\approx\mu$, on the other hand, we obtain $\bar{\tau}\approx 2\tau\tau_\mathrm{a}/(\tau+\tau_\mathrm{a})$ and thus

$$q_{\max}^2 D_0\bar{\tau}\lesssim 4\frac{\tau}{\tau+\tau_\mathrm{a}}\,. \tag{B.14}$$

Thus, for the one-component description, the slow diffusion approximation does not hold in general, and the result for the diffusion coefficient needs to be checked. For a tissue where $\chi\approx\mu$ and $\tau\ll\tau_a$, however, assumption (B.11) turns out to hold and $D\simeq D_0$. Note however that in any case, the slow diffusion assumption is never grossly violated, *i.e.*, the velocity-velocity correlations never decay much more slowly than the particles diffuse away. Therefore, we would not expect corrections to be strong. For the one-component theory, which corresponds to the limit of vanishing friction in the description with permeation (see below), this argument can be made more precise.

Corrections due to finite relaxation time

Starting from expression (B.3) for the diffusion coefficient, we can carry out the integral over time without any further approximation once we have $C_{vv}(q,t)=\int\frac{\mathrm{d}\omega}{2\pi}\,e^{-i\omega t}\hat{C}_{vv}(q,\omega)$, which we find from (B.7) with the transformation (B.8). One then obtains

$$D=\frac{1}{6\pi^2}\int_0^{\pi/a}\mathrm{d}q\,\left(A+B\frac{1}{1+q^2D\bar{\tau}}\right)\,, \tag{B.15}$$

where we defined the constants

$$A=\left(\frac{\zeta}{\bar{\eta}}\right)^2\frac{k_\mathrm{d}}{n_\mathrm{h}^c}\left(\frac{\tau_a}{\bar{\tau}}\right)^2+\frac{2}{3}\frac{\theta}{\bar{\eta}^2}\left(\frac{\tau}{\bar{\tau}}\right)^2+\frac{\theta}{\eta^2}\,, \tag{B.16a}$$

$$B=\left(\frac{\zeta}{\bar{\eta}}\right)^2\frac{k_\mathrm{d}}{n_\mathrm{h}^c}\frac{\bar{\tau}^2-\tau_a^2}{\bar{\tau}^2}+\frac{2}{3}\frac{\theta}{\bar{\eta}^2}\frac{\bar{\tau}^2-\tau^2}{\bar{\tau}^2}\,. \tag{B.16b}$$

We find that for the one-component theory, the diffusion constant is thus implicitly given by

$$D=\frac{1}{6\pi a}\left(A+B\frac{\arctan\left(\frac{\pi}{a}\sqrt{D\bar{\tau}}\right)}{\frac{\pi}{a}\sqrt{D\bar{\tau}}}\right)\,. \tag{B.17}$$

For $\frac{\pi}{a}\sqrt{D\bar{\tau}} \ll 1$, we recover the result obtained in the limit of slow diffusion,

$$\begin{aligned} D &\simeq \frac{1}{6\pi a}(A+B) \\ &= \frac{1}{6\pi a}\left[\left(\frac{\zeta}{\bar{\eta}}\right)^2 \frac{k_\mathrm{d}}{n_\mathrm{h}^c} + \frac{2}{3}\frac{\theta}{\bar{\eta}^2} + \frac{\theta}{\eta^2}\right] . \end{aligned} \tag{B.18}$$

We know that $\frac{\pi}{a}\sqrt{D\bar{\tau}} = \mathcal{O}(1)$ at most. For $\frac{\pi}{a}\sqrt{D\bar{\tau}} = 3$, the arctan-term in Eq. (B.17) is of order 0.4, which is significantly different from 1. In this case, we cannot *a priori* neglect the corrections due to the finite relaxation time. Note however that for $\bar{\tau} \simeq \tau \simeq \tau_a$ these corrections are supposedly small. For $\tau \gg \tau_a$, on the contrary, the diffusion constant has to be determined graphically or numerically from Eq. (B.17) for given values of A and B.

B.2 Two-component description

In the two-component description of tissues, the expression for the cellular diffusion constant is slightly more involved, as a finite permeability may effectively slow down the diffusive motion of cells. The calculation is essentially the same as for the one-component theory; here, we simply give the expressions one ends up with in the two-component theory.

Velocity-velocity correlation function

When taking permeation into account, the velocity-velocity correlations include additional terms due to the friction between the interstitial fluid and the cell phase. From the velocity fluctuations calculated in the main text, see Eqs. (3.58), we now find

$$\begin{aligned} \hat{C}_{vv}(q,\omega) = \frac{2}{q^2}\Bigg[\left(\frac{\zeta}{\bar{\eta}+\bar{\kappa}}\right)^2 \frac{k_d}{n_h}\frac{1+\omega^2\tau_a^2}{1+\omega^2\tau_1^2+\omega^4\tau_2^4} \\ + \frac{2}{3}\frac{\theta}{(\bar{\eta}+\bar{\kappa})^2}\frac{1+\omega^2\tau^2}{1+\omega^2\tau_1^2+\omega^4\tau_2^4} + \frac{\theta}{(\eta+\bar{\kappa})^2}\frac{1}{1+\omega^2\tau_3^2}\Bigg] \end{aligned} \tag{B.19}$$

for the correlation function. We recall the abbreviations used in the main text, the q-dependent friction coefficient $\bar{\kappa} = \kappa/[(1-\phi)q^2]$ (with the physical dimension of a viscosity) and the longitudinal tissue viscosity $\bar{\eta} = \zeta + \frac{4}{3}\eta$, as well as the permeation-independent time scale

$$\bar{\tau} = \frac{\zeta\tau_a + \frac{4}{3}\eta\tau}{\bar{\eta}} = \tau\tau_a\frac{\chi + \frac{4}{3}\mu}{\chi\tau + \frac{4}{3}\mu\tau_a} \tag{B.20}$$

that already appeared in the one-component theory (see above). Furthermore, we introduced the three time scales

$$\tau_1^2 = \frac{[\bar{\eta}\bar{\tau} + \bar{\kappa}(\tau + \tau_a)]^2}{(\bar{\eta} + \bar{\kappa})^2} - 2\frac{\bar{\kappa}\tau\tau_a}{\bar{\eta} + \bar{\kappa}}\,, \tag{B.21a}$$

$$\tau_2^2 = \frac{\bar{\kappa}\tau\tau_a}{\bar{\eta} + \bar{\kappa}}\,, \tag{B.21b}$$

$$\tau_3 = \frac{\bar{\kappa}\tau_a}{\eta + \bar{\kappa}}\,, \tag{B.21c}$$

which appear in the expression of $\hat{C}_{vv}(q,\omega)$.

In the time domain, the velocity correlations decay exponentially. The respective relaxation times are not identical with the time scales defined above; they can be obtained from the Fourier transforms

$$\int \frac{\mathrm{d}\omega}{2\pi}\, e^{-i\omega t} \frac{1}{1+\omega^2\tau_3^2} = \frac{1}{2}\frac{e^{-t/\tau_3}}{\tau_3} \tag{B.22}$$

and

$$\int \frac{\mathrm{d}\omega}{2\pi}\, e^{-i\omega t} \frac{1+\omega^2\tau_0^2}{1+\omega^2\tau_1^2+\omega^4\tau_2^4} = \frac{1}{4}\left[\frac{e^{-t/\tilde{\tau}_1}}{\tilde{\tau}_1}\left(1+\frac{2\tau_0^2-\tau_1^2}{\sqrt{\tau_1^4-4\tau_2^4}}\right) + \frac{e^{-t/\tilde{\tau}_2}}{\tilde{\tau}_2}\left(1-\frac{2\tau_0^2-\tau_1^2}{\sqrt{\tau_1^4-4\tau_2^4}}\right)\right]. \tag{B.23}$$

Here, two relaxation times $\tilde{\tau}_1$ and $\tilde{\tau}_2$ appear which are given by

$$\tilde{\tau}_1 = \frac{\sqrt{2}\tau_2^2}{\sqrt{\tau_1^2+\sqrt{\tau_1^4-4\tau_2^4}}}\,, \tag{B.24a}$$

$$\tilde{\tau}_2 = \frac{\sqrt{2}\tau_2^2}{\sqrt{\tau_1^2-\sqrt{\tau_1^4-4\tau_2^4}}}\,, \tag{B.24b}$$

where $\tau_1^4 - 4\tau_2^4 \geq 0$ as can be checked with (B.21). Note that all three relaxation times τ_3, $\tilde{\tau}_1$ and $\tilde{\tau}_2$ depend on the wave number q via the q-dependent friction coefficient $\bar{\kappa}$.

Calculation of the diffusion constant in the slow diffusion limit

With the approximation that $e^{-q^2Dt} \simeq 1$ for all times t at which the velocity-velocity correlations are finite, the diffusion coefficient can be calculated directly from $\hat{C}_{vv}(q,\omega)$, see Eq. (B.9), and we obtain

$$\begin{aligned} D_0 &= \frac{1}{12\pi^2}\int_0^{q_{\max}} \mathrm{d}q\, \hat{C}_{vv}(q,\omega)|_{\omega=0} \\ &= \frac{1}{6\pi a}\left\{ s(\tfrac{\pi}{a}\lambda)\left[\left(\frac{\zeta}{\bar{\eta}}\right)^2 \frac{k_\mathrm{d}}{n_\mathrm{h}^c} + \frac{2}{3}\frac{\theta}{\bar{\eta}^2}\right] + s(\tfrac{\pi}{a}\bar{\lambda})\frac{\theta}{\eta^2}\right\}, \end{aligned} \tag{B.25}$$

which is the result presented in the main text, see Eq. (3.64). Here, $q_{\max} = \pi/a$ is the high wave number cut-off, where a is a cell radius, and we recall the definitions $\lambda^2 = (1-\phi)\bar{\eta}/\kappa$, $\bar{\lambda}^2 = (1-\phi)\eta/\kappa$ and

$$s(x) = 1 + \frac{1}{2(1+x^2)} - \frac{3}{2}\frac{\arctan x}{x}$$

as introduced in the main text, see also Fig. 3.7 for a plot of $s(x)$.

Validity of the slow diffusion result

As was the case for the one-component theory, the approximation $e^{-q^2 Dt} \simeq 1$, or $D \simeq D_0$, holds for all q and on all relevant time scales if

$$q_{\max}^2 D_0 \tau_{\max} \ll 1\,, \tag{B.26}$$

where $\tau_{\max}$ is now the longest relaxation time of the velocity-velocity correlations. Using again the estimations (B.12), we now find

$$\begin{aligned} q_{\max}^2 D_0 &\approx \frac{1}{\tau_a}\left[\left(\frac{\chi\tau}{\chi\tau+\mu\tau_a}\right)^2 + \left(\frac{\mu\tau_a}{\chi\tau+\mu\tau_a}\right)^2\right] s(\tfrac{\pi}{a}\lambda) + \frac{1}{\tau_a} s(\tfrac{\pi}{a}\bar{\lambda}) \\ &\lesssim \frac{2}{\tau_a} s(\tfrac{\pi}{a}\lambda)\,. \end{aligned} \tag{B.27}$$

In order to check the validity of assumption (B.26), we need to compare $\tau_{\max}$ to τ_a and check the role of $s(\frac{\pi}{a}\lambda)$.

The longest relaxation time in the problem is given by $\tilde{\tau}_2$. We introduce $\tau_{1'}^2 \equiv \tau_1^2 + 2\tau_2^2$ such that we can express $\tilde{\tau}_2$ as

$$\begin{aligned} \tilde{\tau}_2 &= \tau_{1'} \frac{\sqrt{2}\left(\frac{\tau_2}{\tau_{1'}}\right)^2}{\sqrt{1-2\left(\frac{\tau_2}{\tau_{1'}}\right)^2 - \sqrt{1-4\left(\frac{\tau_2}{\tau_{1'}}\right)^2}}} \\ &= \tau_{1'}\left[1 - \left(\frac{\tau_2}{\tau_{1'}}\right)^2 - \left(\frac{\tau_2}{\tau_{1'}}\right)^4 + \ldots\right], \end{aligned} \tag{B.28}$$

in order to get an estimate for $\tau_{\max} = \tilde{\tau}_2$. Because

$$\begin{aligned} \left(\frac{\tau_2}{\tau_{1'}}\right)^2 &= \frac{(\bar{\eta}+\bar{\kappa})\bar{\kappa}\tau\tau_a}{[\bar{\eta}\bar{\tau} + \bar{\kappa}(\tau+\tau_a)]^2} \\ &= \frac{\tau\tau_a[1+(\lambda q)^2]}{[(\lambda q)^2\bar{\tau} + \tau + \tau_a]^2} < 1 \end{aligned} \tag{B.29}$$

(even $\ll 1$ for many cases that can be made precise) – and as an upper bound –, we therefore consider as slowest relaxation time $\tau_{\max} = \tilde{\tau}_2 \simeq \tau_{1'}$, or directly

$$\begin{aligned}\tau_{\max} = \tau_{1'}(q_{\max}) &= \frac{\bar{\eta}\bar{\tau} + \bar{\kappa}(\tau+\tau_a)}{\bar{\eta}+\bar{\kappa}}\Big|_{q_{\max}} \\ &= \frac{(\lambda q_{\max})^2\bar{\tau} + \tau + \tau_a}{1+(\lambda q_{\max})^2}\,. \end{aligned} \tag{B.30}$$

Note once more that the dependence on q is due to the finite permeability of the tissue; here, we consider the slowest relaxation time for the cut-off wave number $q_{\max}$. The value of $\bar{\tau}$, which turns out to be the relaxation time in the limit of vanishing friction, depends on the ratio of the bulk elastic modulus χ to the shear elastic modulus μ, see the discussion for the one-component description above.

We now discuss approximation (B.26) for various strengths of friction, *i.e.*, different ratios λ/a:

a) friction dominated regime, $\lambda \ll a/\pi$:

Independent of χ/μ, the longest relaxation time is given by $\tau_{\max} = \tau + \tau_a$, and we obtain

$$q_{\max}^2 D_0 \tau_{\max} \approx 2\frac{\tau+\tau_a}{\tau_a} s(\tfrac{\pi}{a}\lambda)\,. \tag{B.31}$$

Because $s(x)$ vanishes as x^4, the slow diffusion approximation (B.26) is justified, even for $\tau \gg \tau_a$; in fact, no diffusion is taking place at all.

b) intermediate regime, $\lambda \approx a/\pi$:

In this regime, one can still argue that $\tau_{\max} \approx \tau + \tau_a$, *i.e.*, both relaxation times are present for both $\chi \gg \mu$ and $\chi \approx \mu$. Thus, we find

$$q_{\max}^2 D_0 \tau_{\max} \approx 2\frac{\tau+\tau_a}{\tau_a} s(1) \lesssim \frac{1}{5}\frac{\tau+\tau_a}{\tau_a}\,. \tag{B.32}$$

For $\tau \lesssim \tau_a$, this seems to be sufficiently smaller than one, and one may say that the approximation $D \simeq D_0$ is reasonable. For $\tau \gg \tau_a$, however, this is no longer the case, and the calculation of D needs to be refined.

c) negligible friction, $\lambda \gg a/\pi$:

In this limit, the longest relaxation time depends on χ/μ: For an incompressible tissue ($\chi \gg \mu$), the relaxation time is given by $\tau_{\max} = \tau_a$, and we find

$$q_{\max}^2 D_0 \tau_{\max} = \mathcal{O}(1) \qquad \chi \gg \mu\,; \tag{B.33}$$

for $\chi \approx \mu$, we have $\tau_{\max} \approx 2\tau\tau_a/(\tau+\tau_a)$, such that

$$q_{\max}^2 D_0 \tau_{\max} \approx \frac{4\tau}{\tau+\tau_a} \qquad \chi \gg \mu\,. \tag{B.34}$$

Thus, in the regime of negligible friction, the slow diffusion approximation does not hold in general, and the result for the diffusion coefficient needs to be checked. Note that this limit corresponds to a one-component description of the tissue dynamics.

Note that in all possible scenarios, the slow diffusion assumption is never grossly violated, *i.e.*, the velocity-velocity correlations never decay much more slowly than the particles diffuse away. This is not surprising, somehow, given that this holds true also in the one-component description and that permeation can only slow down diffusion. Again, we would not expect corrections to be strong. In the limit of vanishing friction, this argument can be made more precise. We essentially find the same result as in the one-component description.

Corrections due to the finite relaxation time in the limit of vanishing friction

Starting from expression (B.3) for the diffusion coefficient, we can carry out the integral over time without any further approximation once we have $C_{vv}(q,t)$, which we find from (B.19) with the transformations (B.22) and (B.23). Thus, we now get

$$D = \frac{1}{6\pi^2}\int_0^{\pi/a} \mathrm{d}q\, f(q)\,, \tag{B.35}$$

where $f(q) = q^2\int_0^\infty \mathrm{d}t\, e^{-q^2Dt}C_{vv}(q,t)$ is given by

$$\begin{aligned} f(q) = \frac{1}{2}\left(\frac{\zeta}{\bar\eta}\right)^2 \frac{k_\mathrm{d}}{n_\mathrm{h}^c}\frac{(\lambda q)^4}{[1+(\lambda q)^2]^2}\left[\frac{1}{1+q^2D\tilde\tau_1}\left(1+\frac{2\tau_a^2-\tau_1^2}{\sqrt{\tau_1^4-4\tau_2^4}}\right)\right.\\ \left.+\frac{1}{1+q^2D\tilde\tau_2}\left(1-\frac{2\tau_a^2-\tau_1^2}{\sqrt{\tau_1^4-4\tau_2^4}}\right)\right]\\ +\frac{1}{3}\frac{\theta}{\bar\eta^2}\frac{(\lambda q)^4}{[1+(\lambda q)^2]^2}\left[\frac{1}{1+q^2D\tilde\tau_1}\left(1+\frac{2\tau^2-\tau_1^2}{\sqrt{\tau_1^4-4\tau_2^4}}\right)+\frac{1}{1+q^2D\tilde\tau_2}\left(1-\frac{2\tau^2-\tau_1^2}{\sqrt{\tau_1^4-4\tau_2^4}}\right)\right]\\ +\frac{\theta}{\eta^2}\frac{(\bar\lambda q)^4}{[1+(\bar\lambda q)^2]^2}\frac{1}{1+q^2D\tau_3}\,. \end{aligned} \tag{B.36}$$

Different limits can be recovered from the above expression. In the limit of high friction, $f(q)$ vanishes as $(\lambda q)^4$, where $q \le q_\mathrm{max} = \pi/a$. This is in line with the result obtained for D above, Eq. (B.25), where $s(x) \propto x^4$ for $x \ll 1$.

Let us discuss the limit of vanishing friction, *i.e.*, small κ. Strictly speaking, friction cannot be neglected for any finite κ as soon as $q < 1/\lambda$. We take this into account by integrating $f(q)$ from a long wavelength, low wave number cut-off $q_c = \lambda^{-1}$ up to the short wavelength, high wave number cut-off $q_\mathrm{max} = \pi/a$, which introduces corrections of order $\frac{\pi}{a}\lambda$ due to permeation.

Thus, for $\lambda q \gg 1$, the relaxation times $\tilde\tau_1$ and τ_3 vanish, which corresponds to δ-correlated contributions to the velocity fluctuations in the time domain. Only the relaxation time $\tilde\tau_2$ remains finite, with $\tilde\tau_2 \to \bar\tau$, and we write

$$D = \frac{1}{6\pi^2}\int_{1/\lambda}^{\pi/a} \mathrm{d}q\, \left(A + B\frac{1}{1+q^2D\bar\tau}\right)\,. \tag{B.37}$$

Here, we used the definitions of A and B introduced above, Eq. (B.16); note the low wave-number cut-off $1/\lambda$ due to the finite friction that eventually dominates at long wavelengths which we did not consider in the one-component theory. We obtain the same result as in the one-component theory, see Eq. (B.17), up to a correction of order $\mathcal{O}(\frac{a}{\pi\lambda})$ due to permeation,

$$D = \frac{1}{6\pi a}\left(A + B\frac{\arctan\left(\frac{\pi}{a}\sqrt{D\bar{\tau}}\right)}{\frac{\pi}{a}\sqrt{D\bar{\tau}}}\right) + \mathcal{O}(\tfrac{a}{\pi\lambda})\,. \tag{B.38}$$

For $\frac{\pi}{a}\sqrt{D\bar{\tau}} \ll 1$, one recovers the result obtained in the limit of slow diffusion, zero friction,

$$D \simeq \frac{1}{6\pi a}\left[\left(\frac{\zeta}{\bar{\eta}}\right)^2 \frac{k_\mathrm{d}}{n_\mathrm{h}^c} + \frac{2}{3}\frac{\theta}{\bar{\eta}^2} + \frac{\theta}{\eta^2}\right]. \tag{B.39}$$

Appendix C

Numerical methods

C.1 Single-cell based model of growing tissues

Here, we provide details of the simulation scheme for dynamic tissues presented in chapter 2 and the respective parameter choices.

Dissipative particle dynamics for growing tissues

We describe the tissue by an ensemble of interacting cells, where each cell is represented by two positional variables. This allows us to capture the anisotropy of cell growth and division. In the following, we refer to these positional variables as point particles. The two particles that define a cell interact with the particles of surrounding cells via a pair potential that accounts for cell mechanics and cell-cell adhesion. The potential depends on the distance r between the interacting particles and contains a short-range repulsive and a mid-range attractive contribution. Particles farther apart than a certain cutoff length R_{pp} do not interact. The potential is given by

$$V^{CC}(r) = \begin{cases} \frac{f_0 R_{\mathrm{pp}}^5}{4r^4} + (f_0 + f_1)\, r + V_0 & r \leq R_{\mathrm{pp}}\,, \\ 0 & r > R_{\mathrm{pp}}\,. \end{cases} \tag{C.1}$$

Here, f_0 and f_1 are coefficients that describe repulsion and attraction, respectively, and $V_0 = -\left(5f_0/4 + f_1\right) R_{\mathrm{pp}}$ is chosen such that the potential vanishes continuously at $r = R_{\mathrm{pp}}$. In addition, two particles that belong to the same cell interact via a potential that describes axial cell growth. The growth potential is given by

$$V^{G}(r) = \frac{B}{r + r_0}\,, \tag{C.2}$$

where B is an expansion strength and r_0 a characteristic length. Note that particles that belong to the same cell do not interact via the cell-cell potential V^{CC}.

Cell division and apoptosis are implemented as follows. When the distance between the two particles of a cell exceeds a size threshold R_{c}, the cell divides. After the division

each of the original particles constitutes a daughter cell. For each daughter cell, a new particle is then placed randomly within a short distance r_c from the original particle. While cell division is implemented in this deterministic manner, apoptosis is included by removing cells randomly at a constant rate k_a.

Cell-cell friction is described using dissipative particle dynamics (DPD) [86, 97, 141]. We use an implementation of DPD where each particle is assigned a mass m and is subject to friction forces due to motion relative to particles of neighboring cells (friction γ_{CC}) and relative to the second particle of the same cell (friction γ_G). In addition, we introduce a friction γ_B with respect to a background medium in order to dampen movement of the center of mass of the whole system induced by cell division or apoptosis.

Furthermore, random forces are introduced to account for noise. For simplicity, we choose white noise obeying a fluctuation-dissipation relation with respect to the friction coefficients γ_{CC}, γ_G, and γ_B, so that the noise strength can be characterized by an effective temperature T_{noise}.

Standard tissue and units

The parameters of our model are specified with respect to a unit of length l_0, a unit of time t_0, and a unit of pressure p_0. We define a standard tissue which we refer to when exploring the parameter space. The parameter values of the standard tissue in the units l_0, t_0, and p_0 are given in Table C.1 of this supplementary material. These values are chosen such that important properties of the standard tissue take approximately the value of 1 in the units l_0, t_0, and p_0: For the standard tissue confined in a box of volume V_{box} with periodic boundary conditions, we obtain the cell density $\rho = \frac{\langle N \rangle}{V_{\text{box}}} \simeq l_0^{-3}$, where $\langle N \rangle$ denotes the average number of cells at the homeostatic state. Moreover, for the average cell division rate k_d of the standard tissue in the homeostatic state we have $k_d \simeq t_0^{-1}$. Finally, the homeostatic pressure p_h of the standard tissue is $p_h \simeq p_0$. Parameter values of simulations that deviate from the standard case are specified relative to the standard values denoted by an asterisk, *i.e.*, $B^* = 0.5$ denotes an expansion strength which is decreased by a factor of two with respect to the standard tissue.

Boundary conditions and measurement procedures

To measure the diffusion constant of cells in our simulations, the tissue is grown to its homeostatic state in a cubic compartment with lateral dimension $4R_{\text{pp}}$ using periodic boundary conditions in all three directions. We then track particles and determine their mean squared displacement (MSD) which shows a linear behavior in time. The diffusion constant is obtained from a linear fit to the slope of the MSD.

For a measurement of the homeostatic pressure and the tissue viscosity, the tissue is grown between two walls with fixed distance and periodic boundary conditions in the plane. We chose a bounce-back boundary condition at the walls in order to mimic a no slip boundary condition [9]. In short, the velocity of a particle is reversed the very moment it hits the wall. In the homeostatic state, the homeostatic pressure is determined from the momentum exchange between the tissue and the walls.

Parameter	Value	Unit	Description
f_0	$1.398 \cdot 10^{-1}$	$p_0 l_0^2$	repulsive cell-cell potential coefficient
f_1	$2.918 \cdot 10^{-1}$	$p_0 l_0^2$	attractive cell-cell potential coefficient
R_{pp}	1.387	l_0	range of pair potentials
B	5.616	$p_0 l_0^4$	cellular expansion pressure constant I
r_0	1.387	l_0	cellular expansion pressure constant II
R_{c}	1.11	l_0	threshold distance for cell division
r_{c}	$1.387 \cdot 10^{-5}$	l_0	distance at which new particles are placed
k_{a}	1	t_0^{-1}	rate of cell death
γ_{CC}	$4.206 \cdot 10^{-2}$	$p_0 l_0 t_0$	intracellular dissipation constant between particles of the same cell
γ_G	$2.103 \cdot 10^{-2}$	$p_0 l_0 t_0$	intercellular dissipation constant between particles of different cells, but of the same tissue
γ_B	$4.206 \cdot 10^{-5}$	$p_0 l_0 t_0$	background friction coefficient
R_{t}	1.387	l_0	range of dissipative friction forces when the cell divides
$k_{\mathrm{B}} T_{\mathrm{noise}}$	$8.096 \cdot 10^{-1}$	$p_0 l_0^3 t_0^{-1}$	noise strength in the tissue
m	$2.185 \cdot 10^{-6}$	$p_0 l_0^{-1} t_0^2$	mass of particle

Table C.1. Standard tissue parameters. This table lists all parameters of our simulation and gives their values in simulation units l_0, t_0, and p_0 for the standard tissue.

In order to determine the tissue viscosity, the top wall moves with a prescribed velocity relative to the bottom wall. In this case, the bounce-back boundary condition at the top wall is implemented in its rest frame. This creates a shear stress σ_{xz} in the tissue. Both the shear stress and the pressure are accessible by measuring the momentum exchange of particles with the wall. (In the shear simulations, we choose a box size of $5R_{\mathrm{pp}}$ and $\gamma_B = 0$.) However, since bounce-back boundary conditions do not provide perfect no slip boundary conditions, we measure and fit the velocity profile $v_x(z)$ in the tissue directly. Then the shear viscosity is given by $\eta = \sigma_{xz}/(\partial_z v_x)$.

C.2 Viscoelastic tissue growing against a piston

Here, we give the details of the numerical method used to solve for the dynamics of the piston both in the limit of an elastic tissue response and for the viscoelastic case where isotropic and anisotropic relaxation times are identical.

Elastic relaxation dynamics

In the elastic limit, the evolution of the tissue deformation $u^{\mathrm{c}}(x)$ is described by a diffusion equation, see Eq. (3.25); the boundary condition at $x = L(t)$, which depends on time, is given by Eq. (3.26). Using the characteristic length l_{el} and time t_{el} discussed in the main text,

$$l_{\mathrm{el}} = D_{\mathrm{el}}/v_{\mathrm{el}}\,, \qquad t_{\mathrm{el}} = D_{\mathrm{el}}/v_{\mathrm{el}}^2\,, \tag{C.3}$$

we non-dimensionalize the equations according to $x^* = x/l_{\mathrm{el}}$ and $t^* = t/t_{\mathrm{el}}$. With $u^* = u^{\mathrm{c}}/l_{\mathrm{el}}$ and $p^* = \delta P/\bar{\chi}$ we thus obtain

$$\partial_t u = \partial_x^2 u\,, \tag{C.4a}$$

$$\dot{u}|_L = -\left(p + \partial_x u|_L\right)\,, \tag{C.4b}$$

where we dropped the asterisks denoting non-dimensionalized quantities for convenience.

Because of the moving boundary at $L(t)$, we cannot implement these equations in a straightforward way. Therefore, we introduce the new coordinate

$$\tilde{x} = x\frac{L_0}{L(t)} \tag{C.5}$$

and the corresponding deformation field

$$\tilde{u}(\tilde{x}, t) \equiv u(\tilde{x}\tfrac{L(t)}{L_0}, t) \tag{C.6}$$

that is defined on $\tilde{x} \in [0, L_0]$ for all t. Here, $L_0 = L(0)$. In the new coordinates, equations (C.4) now become

$$\partial_t \tilde{u} = \left(\frac{L_0}{L(t)}\right)^2 \partial_{\tilde{x}}^2 \tilde{u} + \tilde{x}\frac{\dot{L}(t)}{L(t)}\partial_{\tilde{x}}\tilde{u}\,, \tag{C.7a}$$

$$\partial_t \tilde{u}|_{L_0} = -\left(p + \frac{L_0}{L(t)}\partial_{\tilde{x}} u|_{L_0}\right)\,. \tag{C.7b}$$

We discretize the quantities in space and time according to

$$u_n^i = \tilde{u}(n\Delta x, i\Delta t)\,, \qquad L^i = L(i\Delta t)\,, \tag{C.8}$$

where $n = 0, 1, \ldots, N = L_0/\Delta x$ and $i \in \mathbb{N}_0$. Additionally, we consider $\dot{L}^i = (u_N^i - u_N^{i-1})/\Delta t$ for $i \geq 1$ and set $\dot{L}^0 = -p$. According to the problem discussed in the main text, the initial conditions are specified as $u_n^0 = 0$ and $L^0 = L_0$. We then use a simple explicit Euler integration scheme to solve equations (C.7) in time. More precisely, we determine u_n^{i+1}, $n = 1, \ldots, N-1$, from the diffusion equation and u_N^{i+1} from the boundary condition at L. Note also that $u_0^i = 0$ for all times. For the plots shown in Fig 3.3 in the main text, we used $p = 0.01$ and the lattice spacing $\Delta x = 0.05$ and $\Delta t = 10^{-4}$ throughout, except for the inset for $L_0 = 100$ where $\Delta x = 0.1$.

Full viscoelastic behavior

In order to check our analytical results obtained in the viscous limit, we numerically solve the full viscoelastic equations for the cell flow field. Note that for simplicity, we assume that the isotropic and anisotropic relaxation times are equal, *i.e.*, $\tau = \tau_\mathrm{a}$, which allows us to write an evolution equation for $v^\mathrm{c}(x)$ and the corresponding time-dependent boundary condition at $x = L(t)$, see Eqs. (3.31) and (3.32) in the main text. We now non-dimensionalize all quantities using the characteristic length scale λ and the time scale τ, and we obtain

$$\partial_t v = -v + \partial_x^2 v\,, \tag{C.9a}$$

$$(1 + \partial_t)L = -\alpha^{-1}\left(p + \partial_x v|_L\right)\,. \tag{C.9b}$$

Here, $\alpha = l_\mathrm{el}/\lambda = \sqrt{t_\mathrm{el}/\tau}$ as in the main text, see also (C.3).

In order to circumvent the problem of the moving boundary, we introduce again the Lagrangian coordinate $\tilde{x} = L_0/L(t)$ and the corresponding velocity field $\tilde{v}(\tilde{x}, t) \equiv v(\tilde{x}L(t)/L_0, t)$. In the new coordinates, equations (C.9) now read

$$\partial_t \tilde{v} = -\tilde{v} + \left(\frac{L_0}{L(t)}\right)^2 \partial_{\tilde{x}}^2 \tilde{v} + \tilde{x}\frac{\dot{L}(t)}{L(t)}\partial_{\tilde{x}}\tilde{v}\,, \tag{C.10a}$$

$$\partial_t \tilde{v}|_{L_0} = -\tilde{v}|_{L_0} - \alpha^{-1}\left(p + \frac{L_0}{L(t)}\partial_{\tilde{x}}\tilde{v}|_{L_0}\right)\,. \tag{C.10b}$$

Using the same discretization scheme as above, we integrate the above equations with a simple explicit Euler method. More precisely, we solve the system of equations

$$\frac{v_n^{i+1} - v_n^i}{\Delta t} = -v_n^i + \left(\frac{L_0}{L^i}\right)^2 \frac{v_{n+1}^i + v_{n-1}^i - 2v_n^i}{\Delta x^2} + n\frac{v_N^i}{L^i}\frac{v_{n+1}^i - v_{n-1}^i}{2\Delta x}\,, \tag{C.11a}$$

$$\frac{v_N^{i+1} - v_N^i}{\Delta t} = -v_N^i - \alpha^{-1}\left(p + \frac{L_0}{L^i}\frac{v_N^i - v_{N-1}^i}{\Delta x}\right)\,, \tag{C.11b}$$

for each time step $i \geq 0$. Note that we used $\dot{L}^i = v_N^i$. The initial conditions are specified as $v_n^0 = 0$ for $n = 0, \ldots, N-1$, $v_N^0 = -p/\alpha$, and $L^0 = L_0$. The position of the piston at time $i+1$ follows as $L^{i+1} = L^i + \Delta t v_N^i$. A numerical solution of the viscoelastic dynamics is shown in Fig. C.1.

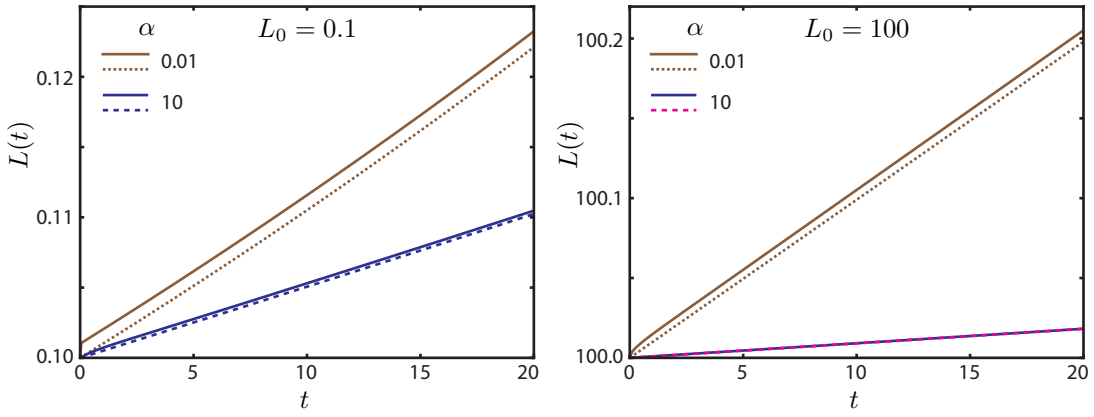

Figure C.1. Viscoelastic tissue dynamics in the limit of long times. Here, we show a comparison of the numerically solved full viscoelastic dynamics with the analytical solutions obtained in the purely viscous limit. (Left panel) Solid lines represent the numerical solution of the viscoelastic dynamics; here, we used $\Delta x = 5 \cdot 10^{-4}$ and $\Delta t = 10^{-8}$. Dashed lines show the solution to Eq. (3.38) which was obtained by using a standard ODE solver. (Right panel) Solid lines represent again the numerically obtained viscoelastic dynamics; here, $\Delta x = 0.01$ and $\Delta t = 10^{-6}$. Dashed lines show the analytical solution in the viscous limit, $L(t) = L_0 - v_0 t/(1+\alpha)$, see main text for details.

C.3 Interface propagation dynamics

In this section, we detail the numerical integration scheme used to solve the interface propagation dynamics given by Eqs. (4.26) discussed in chapter 4.

We discretize the volume fraction ϕ and the convective cell velocity v in space and time according to

$$\phi_n^i = \phi(n\Delta x, i\Delta t)\,, \qquad v_n^i = v(n\Delta x, i\Delta t)\,, \tag{C.12}$$

where $n = 0, 1, \ldots, N$, $N = L_0/\Delta x$, and $i \in \mathbb{N}_0$. At each time i, we calculate the velocity as a function of the volume fraction using the solution given in Eq. (4.28). Here, we integrate from 0 to L_0, however, assuming that the error is small due to the vanishing gradient of ϕ. More precisely, we set

$$v_n^i = -\frac{\alpha}{2\lambda}\Delta x \sum_{k=1}^{N-1} e^{-\frac{|n-k|\Delta x}{\lambda}} \left(1 + \beta \frac{\phi_{k+1}^i + \phi_{k-1}^i - 2\phi_k^i}{\Delta x^2}\right) \frac{\phi_{k+1}^i - \phi_{k-1}^i}{2\Delta x} + \text{boundary terms} \tag{C.13}$$

and calculate ϕ_n^{i+1} using a simple forward Euler method with Eq. (4.26a). For all simulations shown, we used $L_0 = 1000$, $\Delta x = 0.2$, and $\Delta t = 0.001$; the initial condition was specified as

$$\phi_n^0 = \frac{1}{1 + e^{n\Delta x - 100}}\,. \tag{C.14}$$

Appendix D

Two-component fluids

In this appendix, we discuss the equilibrium thermodynamics and close-to-equilibrum hydrodynamics of a classical two-component fluid. The particle number densities of the two components and the total momentum density obey balance equations, which are stated in the first section. Both particle number density balance equations can be restated as a conservation equation of mass and a time evolution equation for the mass fraction of one of the species. We then discuss the equilibrium thermodynamics of the fluid and the corresponding equations of state for a homogeneous system. In this framework, the incompressible limit is straightforward and is discussed in detail. In the second section, we use the formalism of irreversible thermodynamics to establish the thermodynamic fluxes and forces (in isothermal conditions), which allows us to write down the hydrodynamic equations close to equilibrium. We show that free-energy contributions of density gradients give rise to an anisotropic Ericksen stress without explicitly altering the flux-force relationships.

D.1 Equilibrium thermodynamics

Particle number balance and mass conservation

We consider a fluid that consists of two molecular species a and b with particle number densities n_a and n_b, respectively. The balance equations for these densities read

$$\partial_t n_a + \partial_\alpha (n_a v_\alpha^a) = 0\,, \tag{D.1a}$$

$$\partial_t n_b + \partial_\alpha (n_b v_\alpha^b) = 0\,, \tag{D.1b}$$

where v_α^a and v_α^b are the respective velocity fields. Note that we do not consider reactions involving the conversion of one species into the other. With the molecular masses m_a and m_b of the constituents, the total mass density of the system ρ and the center-of-mass velocity v_α are given by

$$\rho = n_a m_a + n_b m_b\,, \tag{D.2a}$$

$$v_\alpha = n_a m_a v_\alpha^a + n_b m_b v_\alpha^b\,. \tag{D.2b}$$

We denote the mass fraction of species a by ϕ,

$$\phi = \frac{n_a m_a}{n_a m_a + n_b m_b} \,. \tag{D.3}$$

Introducing the relative mass flux between the two species

$$j_\alpha = \rho\phi(1-\phi)(v_\alpha^a - v_\alpha^b) \,, \tag{D.4}$$

the balance equations (D.1) combine to

$$\partial_t \rho + \partial_\alpha(\rho v_\alpha) = 0 \,, \tag{D.5a}$$

$$\partial_t \phi + v_\alpha \partial_\alpha \phi = -\rho^{-1} \partial_\alpha j_\alpha \,. \tag{D.5b}$$

The velocities of the respective species can be written as $v_\alpha^a = v_\alpha + j_\alpha/(\rho\phi)$ and $v_\alpha^b = v_\alpha - j_\alpha/[\rho(1-\phi)]$.

Equations of state

At equilibrium, the system is described by equations of state that give the pressure as well as the chemical potential in terms of the particle densities n_a and n_b. Let us first give some definitions and introduce the relevant quantities before discussing the incompressible limit. For a homogeneous system, the total free energy can be written as

$$F(N_a, N_b, V) = V f(\tfrac{N_a}{V}, \tfrac{N_b}{V}) \,, \tag{D.6}$$

where $f(n_a, n_b)$ is a free-energy density that depends on the particle number densities. The total pressure of the fluid is given by

$$\begin{aligned} P &= -\frac{\partial F}{\partial V}\Big|_{N_a,N_b} \\ &= -f + \mu_a n_a + \mu_b n_b \,, \end{aligned} \tag{D.7}$$

where we introduced the chemical potentials

$$\mu_a = \frac{\partial f}{\partial n_a}\Big|_{n_b} \,, \quad \mu_b = \frac{\partial f}{\partial n_b}\Big|_{n_a} \,. \tag{D.8}$$

From Eq. (D.7) we obtain the Gibbs-Duhem relation, which reads

$$\mathrm{d}P = n_a \mathrm{d}\mu_a + n_b \mathrm{d}\mu_b \,. \tag{D.9}$$

The molecular volumes Ω_a and Ω_b follow as

$$\Omega_a = \frac{\partial \mu_a}{\partial P}\Big|_{N_a,N_b} \,, \quad \Omega_b = \frac{\partial \mu_b}{\partial P}\Big|_{N_a,N_b} \,. \tag{D.10}$$

The compressibility κ of the fluid is finally defined as

$$\kappa = -\frac{1}{V}\frac{V}{P}\Big|_{N_a,N_b} \,, \tag{D.11}$$

and one obtains

$$\kappa^{-1} = n_a \frac{\partial \mu_a}{\partial V}\Big|_{N_a,N_b} + n_b \frac{\partial \mu_b}{\partial V}\Big|_{N_a,N_b} .$$

In the incompressible limit, we have $\kappa^{-1} \to \infty$; however, the implications of this limit on the free energy or the particle number densities, respectively, is not obvious from the above equation.

In the following, we thus consider the free-energy density in terms of the variables ρ and ϕ, *i.e.*, we write

$$f = f(\rho, \phi) \quad \Rightarrow \quad F = V f(\tfrac{N_a m_a + N_b m_b}{V}, \tfrac{N_a m_a}{N_a m_a + N_b m_b}) . \tag{D.12}$$

From the definitions above, pressure and compressibility follow as

$$P = -f + \rho \frac{\partial f}{\partial \rho}\Big|_{\phi} \tag{D.13}$$

and

$$\kappa^{-1} = \rho^2 \frac{\partial^2 f}{\partial \rho^2}\Big|_{\phi} . \tag{D.14}$$

In the limit of $\kappa \to 0$, we thus find that the free energy is infinitely peaked at the equilibrium value of ρ. Thus, in the incompressible limit, $\rho = \rho_0(\phi)$ becomes fixed. In order to discuss the incompressible limit in more detail, we can thus define a free-energy density

$$f(\rho, \phi) = \frac{\chi}{2} \left(\frac{\rho}{\rho_0(\phi)} - 1 \right)^2 + \rho h(\phi) \tag{D.15}$$

and consider the limit $\chi \to \infty$. Before doing that, however, we first give the chemical potentials and molecular volumes in terms of the new variables ρ and ϕ.

Using the above definitions, we find that the chemical potentials μ_a and μ_b are now given by

$$\mu_a = m_a \left(\frac{\partial f}{\partial \rho}\Big|_{\phi} + \frac{1-\phi}{\rho} \frac{\partial f}{\partial \phi}\Big|_{\rho} \right) , \tag{D.16a}$$

$$\mu_b = m_b \left(\frac{\partial f}{\partial \rho}\Big|_{\phi} - \frac{\phi}{\rho} \frac{\partial f}{\partial \phi}\Big|_{\rho} \right) . \tag{D.16b}$$

It is furthermore useful to note the following expressions (that follow directly from the ones above),

$$\bar{\mu} = \frac{\mu_a}{m_a} - \frac{\mu_b}{m_b} = \frac{1}{\rho} \frac{\partial f}{\partial \phi}\Big|_{\rho} , \tag{D.17a}$$

$$n_a \mu_a + n_b \mu_b = \rho \frac{\partial f}{\partial \rho}\Big|_{\phi} , \tag{D.17b}$$

as well as

$$n_a\partial_\alpha\mu_a + n_b\partial_\alpha\mu_b = \rho\partial_\alpha\frac{\partial f}{\partial\rho}\Big|_\phi - \frac{\partial f}{\partial\phi}\Big|_\rho\partial_\alpha\phi\,, \tag{D.18a}$$

$$\mu_a\partial_\alpha n_a + \mu_b\partial_\alpha n_b = \frac{\partial f}{\partial\rho}\Big|_\phi\partial_\alpha\rho + \frac{\partial f}{\partial\phi}\Big|_\rho\partial_\alpha\phi\,. \tag{D.18b}$$

The Gibbs-Duhem relation (D.9) still holds, of course. The molecular volumes Ω_a and Ω_b are given by

$$\Omega_a = \frac{m_a}{\rho}\left[1 + (1-\phi)\left(\frac{\partial^2 f}{\partial\rho^2}\Big|_\phi\right)^{-1}\frac{\partial}{\partial\rho}\left(\frac{1}{\rho}\frac{\partial f}{\partial\phi}\Big|_\rho\right)\Big|_\phi\right], \tag{D.19a}$$

$$\Omega_b = \frac{m_b}{\rho}\left[1 - \phi\left(\frac{\partial^2 f}{\partial\rho^2}\Big|_\phi\right)^{-1}\frac{\partial}{\partial\rho}\left(\frac{1}{\rho}\frac{\partial f}{\partial\phi}\Big|_\rho\right)\Big|_\phi\right], \tag{D.19b}$$

and we have

$$n_a\Omega_a + n_b\Omega_b = 1\,. \tag{D.20}$$

Incompressible limit

In principle, the equation of state (D.13), which gives $P = P(\rho,\phi)$, allows to express ρ as a function of the pressure and the volume fraction, $\rho = \rho(P,\phi)$, and thus to switch to P and ϕ as variables. Here, we use the free-energy density (D.15) in order to give explicit expressions for the equations of state derived above, under the assumption that $\chi \gg P$. Then, the limit $\chi \to \infty$ can be carried out after having replaced ρ by $\rho(P,\phi)$.

For the free energy defined above, the pressure is given by

$$P = \frac{\chi}{2}\left[\left(\frac{\rho}{\rho_0}\right)^2 - 1\right]. \tag{D.21}$$

With $\rho = \rho_0(\phi)\,(1+\epsilon)$ we find $\epsilon = \sqrt{1+2P/\chi} - 1$, which gives

$$\rho(P,\phi) = \rho_0(\phi)\left[1 + \frac{P}{\chi} - \frac{1}{2}\left(\frac{P}{\chi}\right)^2\right] \tag{D.22}$$

to second order in P/χ. In the incompressible limit, *i.e.*, for $\chi \to \infty$, the density becomes independent of pressure and is fixed to $\rho = \rho_0(\phi)$. Using relation (D.22), we then find

$$\mu_a = \frac{m_a}{\rho_0}P\left(1 - \frac{P}{2\chi}\right)\left[1 - (1-\phi)\frac{\rho_0'}{\rho_0}\right] + m_a(1-\phi)h'\,, \tag{D.23a}$$

$$\mu_b = \frac{m_b}{\rho_0}P\left(1 - \frac{P}{2\chi}\right)\left[1 + \phi\frac{\rho_0'}{\rho_0}\right] - m_b\phi h' \tag{D.23b}$$

to linear order in P/χ. Furthermore, the molecular volumes are given by

$$\Omega_a = \frac{m_a}{\rho_0}\left(1-\frac{P}{\chi}\right)\left[1-(1-\phi)\frac{\rho_0'(\phi)}{\rho_0(\phi)}\right], \tag{D.24a}$$

$$\Omega_b = \frac{m_b}{\rho_0}\left(1-\frac{P}{\chi}\right)\left[1+\phi\frac{\rho_0'(\phi)}{\rho_0(\phi)}\right] \tag{D.24b}$$

to linear order. Note that in the incompressible limit, *i.e.*, $\chi \to \infty$, the molecular volumes become independent of pressure. As a consequence, the volume fraction $\varphi = n_a\Omega_a$ becomes a function of mass fraction $\phi = n_a m_a$ only; constant ϕ implies constant φ and vice versa. Furthermore, the chemical potentials can now be written as

$$\mu_a(P,\phi) = P\Omega_a(\phi) + \tilde{\mu}_a(\phi)\,, \quad \mu_b(P,\phi) = P\Omega_b(\phi) + \tilde{\mu}_b(\phi)\,. \tag{D.25}$$

Note that in the incompressible limit,

$$\bar{\mu} = \left(\frac{\Omega_a(\phi)}{m_a} - \frac{\Omega_b(\phi)}{m_b}\right)P + \tilde{\bar{\mu}}(\phi)\,.$$

If the mass densities of both particles are the same, $\bar{\mu}$ becomes a function of ϕ only.

In summary, the incompressibility of a two-component fluid thus implies that the total mass density ρ is fixed and depends on the mass/volume fraction of the constituents only. If the specific mass densities $m_{a,b}/\Omega_{a,b}$ of the constituents are constant and independent of pressure, the total mass density is fixed and the fluid is incompressible. For equal mass densities of the constituents, $\rho = \rho_0 = m_a/\Omega_a = m_b/\Omega_b$ independent of composition; for $\rho_a \equiv m_a/\Omega_a \neq m_b/\Omega_b \equiv \rho_b$ constant, we find $\rho = \rho_0(\phi) = \rho_a\rho_b/[(1-\phi)\rho_a + \phi\rho_b]$. Note furthermore that in the incompressible limit, the pressure is no longer determined by thermodynamics since $\partial F/\partial V$ becomes ill-defined, but has to be determined via the hydrodynamic equations, *i.e.*, force balance. The pressure then acts as a Lagrange multiplier in order to ensure the constraint $\rho = \rho_0(\phi)$.

D.2 Hydrodynamics

In this section, we derive the thermodynamic fluxes and forces close to equilibrium. We consider a free-energy density that can depend on the density gradients in order to allow for interfacial tension. The total free energy of the system, including kinetic energy, is given by

$$F = \int \mathrm{d}^3 r \left\{\frac{1}{2}\rho v_\alpha v_\alpha + f(n_a, n_b, \partial_\alpha n_a, \partial_\alpha n_b)\right\}. \tag{D.26}$$

The variation of the free energy then follows as

$$\begin{aligned}\delta F &= \int_{\delta V} \mathrm{d}^3 r \left\{\frac{1}{2}\rho v_\alpha v_\alpha + f\right\} + \int_V \mathrm{d}^3 r\, \delta\left\{\frac{1}{2}\rho v_\alpha v_\alpha + f\right\} \\ &= \int_{\delta V} \mathrm{d}^3 r \left\{\frac{1}{2}\rho v_\alpha v_\alpha + f\right\} + \int_V \mathrm{d}^3 r \left\{v_\alpha \delta(\rho v_\alpha) - \frac{1}{2}v_\alpha v_\alpha \delta\rho + \mu_a \delta n_a + \mu_b \delta n_b\right\} \\ &\quad + \int_V \mathrm{d}^3 r\, \partial_\alpha \left\{\frac{\partial f}{\partial(\partial_\alpha n_a)}\delta n_a + \frac{\partial f}{\partial(\partial_\alpha n_b)}\delta n_b\right\}, \end{aligned} \tag{D.27}$$

where the variation includes a deformation $V \to V + \delta V$ and possible changes of the free-energy density. Here, the chemical potentials are the functional derivatives of the free-energy density with respect to the particle number densities, *i.e.*,

$$\mu = \frac{\delta f}{\delta n} = \frac{\partial f}{\partial n} - \partial_\alpha \frac{\partial f}{\partial(\partial_\alpha n)} \,. \tag{D.28}$$

The partial derivatives imply that the other variables including gradients are kept constant.

Ericksen stress

Before deriving the entropy production rate, we consider a pure translation u_γ of the system in order to determine the reactive Ericksen stress. With $\int_{\delta V} \mathrm{d}^3 r = \int_{\partial V} \mathrm{d}S_\gamma u_\gamma$ and $\delta A \to -u_\gamma \partial_\gamma A$, one finds

$$\begin{aligned} \delta F = \int \mathrm{d}S_\beta u_\alpha \left\{ (f - n_a\mu_a - n_b\mu_b)\delta_{\alpha\beta} - \frac{\partial f}{\partial(\partial_\beta n_a)}\partial_\alpha n_a - \frac{\partial f}{\partial(\partial_\beta n_b)}\partial_\alpha n_b \right\} \\ + \int \mathrm{d}^3 r \, u_\gamma \left\{ n_a \partial_\gamma \mu_a + n_b \partial_\gamma \mu_b \right\} \,. \end{aligned} \tag{D.29}$$

From this expression we can read off the Erickson stress,

$$\sigma^{\mathrm{e}}_{\alpha\beta} = (f - n_a\mu_a - n_b\mu_b)\,\delta_{\alpha\beta} - \frac{\partial f}{\partial(\partial_\beta n_a)}\partial_\alpha n_a - \frac{\partial f}{\partial(\partial_\beta n_b)}\partial_\alpha n_b \,. \tag{D.30}$$

The Gibbs-Duhem relation follows as

$$\partial_\beta \sigma^{\mathrm{e}}_{\alpha\beta} = -n_a \partial_\alpha \mu_a - n_b \partial_\alpha \mu_b \,, \tag{D.31}$$

where we used that the free energy does not change due to a pure translation, or coordinate transformation, as long as f does not explicitly depend on the coordinates.

What does the Ericksen stress look like in terms of the variables ρ and ϕ and their respective gradients? For a free-energy density $f = f(\rho, \partial_\alpha\rho, \phi, \partial_\alpha\phi)$, one finds for the chemical potentials

$$\begin{aligned} \mu_a &= \frac{\partial f}{\partial n_a}\Big|_{n_b, \partial_\alpha n_a, \partial_\alpha n_b} - \partial_\alpha \frac{\partial f}{\partial(\partial_\alpha n_a)}\Big|_{n_a, n_b, \partial_\alpha n_b} \\ &= m_a \left(\frac{\delta f}{\delta \rho} + \frac{1-\phi}{\rho}\frac{\delta f}{\delta \phi} \right) \,, \end{aligned} \tag{D.32a}$$

$$\mu_b = m_b \left(\frac{\delta f}{\delta \rho} - \frac{\phi}{\rho}\frac{\delta f}{\delta \phi} \right) \,. \tag{D.32b}$$

In fact, the expressions derived in the previous section for a homogeneous system carry

over by replacing the partial derivatives with functional derivatives, *i.e.*,

$$\bar{\mu} = \frac{1}{\rho}\frac{\delta f}{\delta \phi}\,, \tag{D.33a}$$

$$n_a\mu_a + n_b\mu_b = \rho\frac{\delta f}{\delta \rho}\,, \tag{D.33b}$$

$$n_a\partial_\alpha\mu_a + n_b\partial_\alpha\mu_b = \rho\partial_\alpha\frac{\delta f}{\delta \rho} - \frac{\delta f}{\delta \rho}\partial_\alpha\phi\,, \tag{D.33c}$$

$$\mu_a\partial_\alpha n_a + \mu_b\partial_\alpha n_b = \frac{\delta f}{\delta \rho}\Big|_\phi\partial_\alpha\rho + \frac{\delta f}{\delta \phi}\Big|_\rho\partial_\alpha\phi\,. \tag{D.33d}$$

Finally, the Ericksen stress reads

$$\sigma^{\mathrm{e}}_{\alpha\beta} = \left(f - \rho\frac{\delta f}{\delta \rho}\right)\delta_{\alpha\beta} - \frac{\partial f}{\partial(\partial_\beta\rho)}\partial_\alpha\rho - \frac{\partial f}{\partial(\partial_\beta\phi)}\partial_\alpha\phi\,. \tag{D.34}$$

For an incompressible fluid with $\rho = \text{const.}$, the Ericksen stress becomes

$$\sigma^{\mathrm{e}}_{\alpha\beta} = -P\delta_{\alpha\beta} - \frac{\partial f}{\partial(\partial_\beta\phi)}\partial_\alpha\phi\,, \tag{D.35}$$

where the pressure P has to be determined from the hydrodynamic equations.

Entropy production

In order to determine the entropy production rate close to equilibrium, we calculate the total rate of change of the free energy of the system, $\dot{F} = \mathrm{d}F/\mathrm{d}t$, which we obtain from the variation of the free energy (D.27) with the replacements $\int_{\delta V}\mathrm{d}^3r \to \int \mathrm{d}S_\gamma v_\gamma$ and $\delta A \to \partial_t A$. For $f = f(\rho, \phi, \partial_\alpha\rho, \partial_\alpha\phi)$, the rate of change is thus given by

$$\begin{aligned}\dot{F} = \int \mathrm{d}S_\gamma v_\gamma \left\{\frac{1}{2}\rho v_\alpha v_\alpha + f\right\} + \int \mathrm{d}^3r \left\{v_\alpha\partial_t(\rho v_\alpha) - \frac{1}{2}v_\alpha v_\alpha\partial_t\rho + \frac{\delta f}{\delta\rho}\partial_t\rho + \frac{\delta f}{\delta\phi}\partial_t\phi\right\} \\ + \int \mathrm{d}^3r\,\partial_\alpha\left\{\frac{\partial f}{\partial(\partial_\alpha\rho)}\partial_t\rho + \frac{\partial f}{\partial(\partial_\alpha\phi)}\partial_t\phi\right\}\,.\end{aligned} \tag{D.36}$$

Using the conservation equations given in the previous section,

$$\begin{aligned}\partial_t\rho &= -\partial_\beta(\rho v_\beta)\,,\\ \partial_t\phi &= -v_\beta\partial_\beta\phi - \rho^{-1}\partial_\beta j_\beta\,,\end{aligned}$$

as well as the momentum balance equation

$$\partial_t(\rho v_\alpha) + \partial_\beta(\rho v_\alpha v_\beta) = \partial_\beta\sigma_{\alpha\beta}\,, \tag{D.37}$$

we ultimately find

$$\begin{aligned}\dot{F} = \int \mathrm{d}S_\beta v_\alpha\,\sigma_{\alpha\beta} - \int \mathrm{d}^3r\,\left\{(\sigma_{\alpha\beta} - \sigma^{\mathrm{e}}_{\alpha\beta})v_{\alpha\beta} - j_\alpha\partial_\alpha\bar{\mu}\right\} \\ - \int \mathrm{d}S_\alpha\left\{j_\alpha\bar{\mu} + \frac{\partial f}{\partial(\partial_\alpha\rho)}\rho\partial_\beta v_\beta + \frac{\partial f}{\partial(\partial_\alpha\phi)}\frac{1}{\rho}\partial_\beta j_\beta\right\}\,.\end{aligned} \tag{D.38}$$

The free energy $F = E - TS$ changes due to work, entropy production, and additional free-energy fluxes through the surface,

$$\dot{F} = \dot{W} - T \int \mathrm{d}V\, \theta + \int \mathrm{d}S_\alpha J^F_\alpha \,,$$

where θ is the rate of entropy production per unit volume. Consequently, we can identify the thermodynamic fluxes and forces that contribute to entropy production:

$$\begin{aligned} \text{flux} &\leftrightarrow \text{force} \\ \sigma^{\mathrm{d}}_{\alpha\beta} &\leftrightarrow v_{\alpha\beta}\,, \\ j_\alpha &\leftrightarrow -\partial_\alpha \bar{\mu}\,, \end{aligned}$$

where $\sigma^{\mathrm{d}}_{\alpha\beta} = \sigma_{\alpha\beta} - \sigma^{\mathrm{e}}_{\alpha\beta}$ is the dissipative stress. For an incompressible system, the total stress $\sigma_{\alpha\beta}$ is thus given by

$$\sigma_{\alpha\beta} = -P\delta_{\alpha\beta} + 2\eta\tilde{v}_{\alpha\beta} - \frac{\partial f}{\partial(\partial_\beta\phi)}\partial_\alpha\phi\,, \tag{D.39}$$

where we used the expression for the Ericksen stress derived above. For symmetry reasons, the lowest order term of gradients in ϕ is of the form $\frac{1}{2}B(\partial_\alpha\phi)^2$, and the traceless part of the stress becomes

$$\tilde{\sigma}_{\alpha\beta} = 2\eta\tilde{v}_{\alpha\beta} - B\left[(\partial_\alpha\phi)(\partial_\beta\phi) - \tfrac{1}{d}(\partial_\gamma\phi)^2\delta_{\alpha\beta}\right]\,. \tag{D.40}$$

Since P is a Lagrange multiplier, one can absorb all isotropic contributions of the Ericksen stress in P and write $\sigma_{\alpha\beta} = -P\delta_{\alpha\beta} + \tilde{\sigma}_{\alpha\beta}$. Note also that in the incompressible limit, $\bar{\mu} = \tilde{\bar{\mu}}(\phi)$ (see above), and the relative flux becomes

$$j_\alpha = -D\partial_\alpha\phi\,, \tag{D.41}$$

with $D \propto \partial\tilde{\bar{\mu}}/\partial\phi$.

Bibliography

[1] *Science Photo Library.* http://www.sciencephoto.com/image/313511/530wm/P6800244-Human_embryo_5-6_weeks_after_fertilisation-SPL.jpg [Online; accessed May 3rd, 2012].

[2] Soft tissue — Dictionary of Cancer Terms. *National Cancer Institute.* http://www.cancer.gov/dictionary?CdrID=45882 [Online; accessed Feb. 14th, 2012].

[3] Soft tissue — Wikipedia, The Free Encyclopedia. *Wikipedia*, 2011. http://en.wikipedia.org/w/index.php?title=Soft_tissue&oldid=455593038 [Online; accessed Feb. 14th, 2012].

[4] T. Aegerter-Wilmsen, C. M. Aegerter, E. Hafen, and K. Basler. Model for the regulation of size in the wing imaginal disc of drosophila. *Mech. Dev.*, 124(4):318–26, 2007.

[5] T. Aegerter-Wilmsen, A. C. Smith, A. J. Christen, C. M. Aegerter, E. Hafen, and K. Basler. Exploring the effects of mechanical feedback on epithelial topology. *Development*, 137(3):499–506, 2010.

[6] M. Affolter and K. Basler. The decapentaplegic morphogen gradient: from pattern formation to growth regulation. *Nat. Rev. Genet.*, 8(9):663–74, 2007.

[7] B. Aigouy, R. Farhadifar, D. B. Staple, A. Sagner, J.-C. Röper, F. Jülicher, and S. Eaton. Cell flow reorients the axis of planar polarity in the wing epithelium of drosophila. *Cell*, 142(5):773–86, 2010.

[8] B. Alberts *et al.*. *Essential Cell Biology.* Garland Science, New York, 3rd edition, 2009.

[9] M. P. Allen and D. J. Tildesley. *Computer simulation of liquids.* Clarendon Press, Oxford, 1989.

[10] M. Ben Amar, C. Chatelain, and P. Ciarletta. Contour instabilities in early tumor growth models. *Phys. Rev. Lett.*, 106(14):148101, 2011.

[11] M. Ben Amar and A. Goriely. Growth and instability in elastic tissues. *J. Mech. Phys. Solids*, 53(10):2284–2319, 2005.

[12] D. Ambrosi and L. Preziosi. Cell adhesion mechanisms and stress relaxation in the mechanics of tumours. *Biomech. Model. Mechanobiol.*, 8(5):397–413, 2009.

[13] T. E. Angelini, E. Hannezo, X. Trepat, M. Marquez, J. J. Fredberg, and D. A. Weitz. Glass-like dynamics of collective cell migration. *Proc. Natl. Acad. Sci. USA*, 108(12):4714–9, 2011.

[14] N. E. Baker. Cell competition. *Curr. Biol.*, 21(1):R11–5, 2011.

[15] M. Basan, J.-F. Joanny, J. Prost, and T. Risler. Undulation instability of epithelial tissues. *Phys. Rev. Lett.*, 106(15):158101, 2011.

[16] M. Basan, J. Prost, J.-F. Joanny, and J. Elgeti. Dissipative particle dynamics simulations for biological tissues: rheology and competition. *Phys. Biol.*, 8(2):026014, 2011.

[17] M. Basan, T. Risler, J.-F. Joanny, X. Sastre-Garau, and J. Prost. Homeostatic competition drives tumor growth and metastasis nucleation. *HFSP J.*, 3(4):265–72, 2009.

[18] A. Baskaran and M. C. Marchetti. Statistical mechanics and hydrodynamics of bacterial suspensions. *Proc. Natl. Acad. Sci. USA*, 106(37):15567–72, 2009.

[19] S. De Beco, M. Ziosi, and L. A. Johnston. New frontiers in cell competition. *Devel. Dyn.*, 2012.

[20] D. Bedeaux and P. Mazur. Brownian motion and fluctuating hydrodynamics. *Physica*, 76:247–258, 1974.

[21] D. A. Beysens, G. Forgacs, and J. A. Glazier. Cell sorting is analogous to phase ordering in fluids. *Proc. Natl. Acad. Sci. USA*, 97(17):9467–71, 2000.

[22] E. Bier. Drosophila, the golden bug, emerges as a tool for human genetics. *Nat. Rev. Genet.*, 6(1):9–23, 2005.

[23] J. J. Binney, N. J. Dowrick, A. J. Fisher, and M. E. J. Newman. *The Theory of Critical Phenomena*. Clarendon Press, Oxford, 1992.

[24] I. B. Bischofs, S. A. Safran, and U. S. Schwarz. Elastic interactions of active cells with soft materials. *Phys. Rev. E*, 69(2):021911, 2004.

[25] M. J. Bissell and W. C. Hines. Why don't we get more cancer? a proposed role of the microenvironment in restraining cancer progression. *Nat. Med.*, 17(3):320–9, 2011.

[26] T. Bittig, O. Wartlick, M. Gonzalez-Gaitan, and F. Jülicher. Quantification of growth asymmetries in developing epithelia. *Eur. Phys. J. E*, 30:93–99, 2009.

[27] T. Bittig, O. Wartlick, A. Kicheva, M. Gonzalez-Gaitan, and F. Jülicher. Dynamics of anisotropic tissue growth. *New J. Phys.*, 10(6):063001, 2008.

[28] G. B. Blanchard, S. Murugesu, R. J. Adams, A. Martinez-Arias, and N. Gorfinkiel. Cytoskeletal dynamics and supracellular organisation of cell shape fluctuations during dorsal closure. *Development*, 137(16):2743–52, 2010.

[29] M. Block, E. Schöll, and D. Drasdo. Classifying the expansion kinetics and critical surface dynamics of growing cell populations. *Phys. Rev. Lett.*, 99(24):248101, 2007.

[30] F. Bosveld, I. Bonnet, B. Guirao, S. Tlili, Z. Wang, A. Petitalot, R. Marchand, P.-L. Bardet, P. Marcq, F. Graner, and Y. Bellaïche. Mechanical control of morphogenesis by fat/dachsous/four-jointed planar cell polarity pathway. *Science*, 336(6082):724-727, 2012.

[31] G. W. Brodland. The differential interfacial tension hypothesis (dith): a comprehensive theory for the self-rearrangement of embryonic cells and tissues. *J. Biomech. Eng.*, 124(2):188–97, 2002.

[32] G. W. Brodland, J. Yang, and J. Sweny. Cellular interfacial and surface tensions determined from aggregate compression tests using a finite element model. *HFSP J.*, 3(4):273–81, 2009.

[33] D. M. Bryant and K. E. Mostov. From cells to organs: building polarized tissue. *Nat. Rev. Mol. Cell Biol.*, 9(11):887–901, 2008.

[34] D. T. Butcher, T. Alliston, and V. M. Weaver. A tense situation: forcing tumour progression. *Nat. Rev. Cancer*, 9:108–122, 2009.

[35] L. C. Butler, G. B. Blanchard, A. J. Kabla, N. J. Lawrence, D. P. Welchman, L. Mahadevan, R. J. Adams, and B. Sanson. Cell shape changes indicate a role for extrinsic tensile forces in drosophila germ-band extension. *Nat. Cell Biol.*, 11(7):859–64, 2009.

[36] H. M. Byrne and D. Drasdo. Individual-based and continuum models of growing cell populations: a comparison. *J. Math. Biol.*, 58(4-5):657–87, 2009.

[37] H. M. Byrne, J. R. King, D. L. S. McElwain, and L. Preziosi. A two-phase model of solid tumour growth. *Appl. Math. Lett.*, 16(4):567–574, 2003.

[38] H. M. Byrne and L. Preziosi. Modelling solid tumour growth using the theory of mixtures. *Math. Med. Biol.*, 20(4):341–66, 2003.

[39] A. C. Callan-Jones and F. Jülicher. Hydrodynamics of active permeating gels. *New J. Phys.*, 13(9):093027, 2011.

[40] M. Cates, D. Marenduzzo, I. Pagonabarraga, and J. Tailleur. Arrested phase separation in reproducing bacteria creates a generic route to pattern formation. *Proc. Natl. Acad. Sci. USA*, 107(26):11715–20, 2010.

[41] P. M. Chaikin and T. L. Lubensky. *Principles of condensed matter physics*. Cambridge University Press, Cambridge, 1995.

[42] P. Ciarletta, L. Foret, and M. Ben Amar. The radial growth phase of malignant melanoma: multi-phase modelling, numerical simulations and linear stability analysis. *J. R. Soc. Interface*, 8(56):345–368, 2011.

[43] H. Clevers. The cancer stem cell: premises, promises and challenges. *Nat. Med.*, 17(3):313–9, 2011.

[44] M. L. Concha and R. J. Adams. Oriented cell divisions and cellular morphogenesis in the zebrafish gastrula and neurula: a time-lapse analysis. *Development*, 125(6):983–94, 1998.

[45] J. Crank. *The mathematics of diffusion*. Clarendon Press, Oxford, 2nd edition, 1975.

[46] K. A. Dahmen, D. R. Nelson, and N. M. Shnerb. Life and death near a windy oasis. *J. Math. Biol.*, 41(1):1-23, 2000.

[47] H. P. G. Darcy. *Les fontaines publiques de la ville de Dijon*. Dalmont, Paris, 1856.

[48] J. G. Dash. History of the search for continuous melting. *Rev. Mod. Phys.*, 71(5):1737, 1999.

[49] P.-G. de Gennes and J. Prost. *The Physics of Liquid Crystals*. Clarendon Press, Oxford, 2nd edition, 1993.

[50] P.-G. de Gennes and C. Taupin. Microemulsions and the flexibility of oil/water interfaces. *J. Phys. Chem.*, 86(13):2294–2304, 1982.

[51] J. Dervaux and M. Ben Amar. Morphogenesis of growing soft tissues. *Phys. Rev. Lett.*, 101(6):068101, 2008.

[52] J. Dervaux, Y. Couder, M.-A. Guedeau-Boudeville, and M. Ben Amar. Shape transition in artificial tumors: from smooth buckles to singular creases. *Phys. Rev. Lett.*, 107(1):018103, 2011.

[53] A. Desai. Kinetochores. *Curr. Biol.*, 10(14):R508, 2000.

[54] D. E. Discher, P. Janmey, and Y.-L. Wang. Tissue cells feel and respond to the stiffness of their substrate. *Science*, 310(5751):1139–43, 2005.

[55] D. Drasdo. Buckling instabilities of one-layered growing tissues. *Phys. Rev. Lett.*, 84(18):4244–7, 2000.

[56] D. Drasdo, S. Höhme, and M. Block. On the role of physics in the growth and pattern formation of multi-cellular systems: What can we learn from individual-cell based models? *J. Stat. Phys.*, 128(1-2):287–345, 2007.

[57] D. Drasdo and S. Höhme. A single-cell-based model of tumor growth in vitro: monolayers and spheroids. *Phys. Biol.*, 2(3):133–47, 2005.

[58] S. Eaton and F. Jülicher. Cell flow and tissue polarity patterns. *Curr. Opin. Genet. Devel.*, 21(6):747–52, 2011.

[59] R. Farhadifar, J.-C. Röper, B. Aigouy, S. Eaton, and F. Jülicher. The influence of cell mechanics, cell-cell interactions, and proliferation on epithelial packing. *Curr. Biol.*, 17(24):2095–104, 2007.

[60] J. Fink. *Mechanotransduction in Mitotic Spindle Positioning.* PhD Thesis, Université Paris IX, 2009.

[61] J. Fink, N. Carpi, T. Betz, A. Bétard, M. Chebah, A. Azioune, M. Bornens, C. Sykes, L. Fetler, D. Cuvelier, and M. Piel. External forces control mitotic spindle positioning. *Nat. Cell Biol.*, 13(7):771–8, 2011.

[62] R. A. Fisher. The wave of advance of advantageous genes. *Ann. Hum. Genet.*, 7(4):355–369, 1937.

[63] G. Forgacs, R. A. Foty, Y. Shafrir, and M. S. Steinberg. Viscoelastic properties of living embryonic tissues: a quantitative study. *Biophys. J.*, 74(5):2227–34, 1998.

[64] R. A. Foty, G. Forgacs, C. Pfleger, and M. S. Steinberg. Liquid properties of embryonic tissues: Measurement of interfacial tensions. *Phys. Rev. Lett.*, 72(14):2298–2301, 1994.

[65] R. A. Foty, C. M. Pfleger, G. Forgacs, and M. S. Steinberg. Surface tensions of embryonic tissues predict their mutual envelopment behavior. *Development*, 122(5):1611–20, 1996.

[66] R. A. Foty and M. S. Steinberg. The differential adhesion hypothesis: a direct evaluation. *Dev. Biol.*, 278(1):255–63, 2005.

[67] S. I. Fraley, Y. Feng, R. Krishnamurthy, D.-H. Kim, A. Celedon, G. D. Longmore, and D. Wirtz. A distinctive role for focal adhesion proteins in three-dimensional cell motility. *Nat. Cell Biol.*, 12(6):598–604, 2010.

[68] C. Frantz, K. M. Stewart, and V. M. Weaver. The extracellular matrix at a glance. *J. Cell Sci.*, 123(24):4195–4200, 2010.

[69] A. Fritsch, M. Höckel, T. Kiessling, K. D. Nnetu, F. Wetzel, M. Zink, and J. A. Käs. Are biomechanical changes necessary for tumour progression? *Nat. Phy.*, 6:730–732, 2010.

[70] Y.-C. Fung. *Biomechanics. Motion, Flow, Stress, and Growth.* Springer, New York, Heidelberg, 1990.

[71] Y.-C. Fung. *Biomechanics. Mechanical Properties of Living Tissues.* Springer, New York, Heidelberg, 2nd edition, 2004.

[72] P. Gallant. Flower dooms cells to death. *Dev. Cell*, 18(6):882–3, 2010.

[73] J. Galle, M. Löffler, and D. Drasdo. Modeling the effect of deregulated proliferation and apoptosis on the growth dynamics of epithelial cell populations in vitro. *Biophys. J.*, 88(1):62–75, 2005.

[74] C. W. Gardiner. *Handbook of Stochastic Methods*. Springer, New York, Heidelberg, 3rd edition, 2004.

[75] J. Garrigues. *Statique des coques élastiques*. Lecture notes, 1999. `http://jgarrigues.perso.centrale-marseille.fr/coques.html` [Online; accessed Apr. 16th, 2012].

[76] T. C. Gasser, R. W. Ogden, and G. A. Holzapfel. Hyperelastic modelling of arterial layers with distributed collagen fibre orientations. *J. R. Soc. Interface*, 3(6):15–35, 2006.

[77] M. Geerligs, G. W. M. Peters, P. A. J. Ackermans, C. W. J. Oomens, and F. P. T. Baaijens. Linear viscoelastic behavior of subcutaneous adipose tissue. *Biorheology*, 45(6):677–88, Jan 2008.

[78] J. A. Glazier and F. Graner. Simulation of the differential adhesion driven rearrangement of biological cells. *Phys. Rev. E*, 47(3):2128–2154, 1993.

[79] N. Gorfinkiel and G. B. Blanchard. Dynamics of actomyosin contractile activity during epithelial morphogenesis. *Curr. Opin. Cell Biol.*, 23(5):531–9, 2011.

[80] N. Gorfinkiel, G. B. Blanchard, R. J. Adams, and A. Martinez-Arias. Mechanical control of global cell behaviour during dorsal closure in drosophila. *Development*, 136(11):1889–98, 2009.

[81] A. Goriely and M. Ben Amar. Differential growth and instability in elastic shells. *Phys. Rev. Lett.*, 94(19):198103, 2005.

[82] A. Goriely and M. Ben Amar. On the definition and modeling of incremental, cumulative, and continuous growth laws in morphoelasticity. *Biomech. Model. Mechanobiol.*, 6(5):289–296, 2007.

[83] A. Goriely, D. Moulton, and R. Vandiver. Elastic cavitation, tube hollowing, and differential growth in plants and biological tissues. *Europhys. Lett.*, 91:18001, 2010.

[84] A. Goriely, M. Robertson-Tessi, M. Tabor, and R. Vandiver. Elastic growth models. *Applied Optimization*, 102:1, 2008.

[85] F. Graner and J. Glazier. Simulation of biological cell sorting using a two-dimensional extended potts model. *Phys. Rev. Lett.*, 69(13):2013–2016, 1992.

[86] R. D. Groot and P. B. Warren. Dissipative particle dynamics: Bridging the gap between atomistic and mesoscopic simulation. *J. Chem. Phys.*, 107(11):4423–4435, 1997.

[87] J. Guck, S. Schinkinger, B. Lincoln, F. Wottawah, S. Ebert, M. Romeyke, D. Lenz, H. M. Erickson, R. Ananthakrishnan, D. Mitchell, J. Käs, S. Ulvick, and C. Bilby. Optical deformability as an inherent cell marker for testing malignant transformation and metastatic competence. *Biophys. J.*, 88(5):3689–98, 2005.

[88] K. Guevorkian, M.-J. Colbert, M. Durth, S. Dufour, and F. Brochard-Wyart. Aspiration of biological viscoelastic drops. *Phys. Rev. Lett.*, 104(21):218101, 2010.

[89] P. Haffter, M. Granato, M. Brand, M. C. Mullins, M. Hammerschmidt, D. A. Kane, J. Odenthal, F. J. van Eeden, Y. J. Jiang, C.-P. Heisenberg, R. N. Kelsh, M. Furutani-Seiki, E. Vogelsang, D. Beuchle, U. Schach, C. Fabian, and C. Nüsslein-Volhard. The identification of genes with unique and essential functions in the development of the zebrafish, danio rerio. *Development*, 123:1–36, 1996.

[90] O. Hallatschek and K. S. Korolev. Fisher waves in the strong noise limit. *Phys. Rev. Lett.*, 103(10):108103, 2009.

[91] F. Hamaratoglu, A. M. De Lachapelle, G. Pyrowolakis, S. Bergmann, and M. Affolter. Dpp signaling activity requires pentagone to scale with tissue size in the growing drosophila wing imaginal disc. *PLoS Biol.*, 9(10):e1001182, 2011.

[92] Y. Hatwalne, S. Ramaswamy, M. Rao, and R. A. Simha. Rheology of active-particle suspensions. *Phys. Rev. Lett.*, 92(11):118101, 2004.

[93] C. Hebner, V. M. Weaver, and J. Debnath. Modeling morphogenesis and oncogenesis in three-dimensional breast epithelial cultures. *Annu. Rev. Pathol.*, 3:313–39, 2008.

[94] W. Helfrich and R.-M. Servuss. Undulations, steric interaction and cohesion of fluid membranes. *Il Nuovo Cimento D*, 3(1):137–151, 1984.

[95] G. Helmlinger, P. A. Netti, H. C. Lichtenbeld, R. J. Melder, and R. K. Jain. Solid stress inhibits the growth of multicellular tumor spheroids. *Nat. Biotechnol.*, 15(8):778–83, 1997.

[96] S. Höhme, M. Brulport, A. Bauer, E. Bedawy, W. Schormann, M. Hermes, V. Puppe, R. Gebhardt, S. Zellmer, M. Schwarz, E. Bockamp, T. Timmel, J. G. Hengstler, and D. Drasdo. Prediction and validation of cell alignment along microvessels as order principle to restore tissue architecture in liver regeneration. *Proc. Natl. Acad. Sci. USA*, 107(23):10371–6, 2010.

[97] P. Hoogerbrugge and J. Koelman. Simulating microscopic hydrodynamic phenomena with dissipative particle dynamics. *Europhys. Lett.*, 19(3):155–160, 1992.

[98] J. Howard. *Mechanics of Motor Proteins and the Cytoskeleton*. Sinauer Associates, Sunderland, 2001.

[99] M. Hrapko, J. A. W. van Dommelen, G. W. M. Peters, and J. S. H. M. Wismans. Characterisation of the mechanical behaviour of brain tissue in compression and shear. *Biorheology*, 45(6):663–76, 2008.

[100] L. Hufnagel, A. A. Teleman, H. Rouault, S. M. Cohen, and B. I. Shraiman. On the mechanism of wing size determination in fly development. *Proc. Natl. Acad. Sci. USA*, 104(10):3835–40, 2007.

[101] M. S. Hutson, G. W. Brodland, J. Yang, and D. Viens. Cell sorting in three dimensions: topology, fluctuations, and fluidlike instabilities. *Phys. Rev. Lett.*, 101(14):148105, 2008.

[102] M Shane Hutson, J Veldhuis, Xiaoyan Ma, Holley E Lynch, P Graham Cranston, and G Wayne Brodland. Combining laser microsurgery and finite element modeling to assess cell-level epithelial mechanics. *Biophys J*, 97(12):3075–85, 2009.

[103] R. O. Hynes. The extracellular matrix: not just pretty fibrils. *Science*, 326(5957):1216–9, 2009.

[104] L. A. Johnston. Competitive interactions between cells: death, growth, and geography. *Science*, 324(5935):1679–82, 2009.

[105] G. W. Jones and S. J. Chapman. Modeling growth in biological materials. *SIAM Rev.*, 54(1):52–118, 2012.

[106] J. Käfer, T. Hayashi, A. F. M. Marée, R. W. Carthew, and F. Graner. Cell adhesion and cortex contractility determine cell patterning in the drosophila retina. *Proc. Natl. Acad. Sci. USA*, 104(47):18549–54, 2007.

[107] R. Kalluri and M. Zeisberg. Fibroblasts in cancer. *Nat. Rev. Cancer*, 6(5):392–401, 2006.

[108] C. B. Kimmel, W. W. Ballard, S. R. Kimmel, B. Ullmann, and T. F. Schilling. Stages of embryonic development of the zebrafish. *Dev. Dyn.*, 203(3):253–310, 1995.

[109] M. Krieg, Y. Arboleda-Estudillo, P.-H. Puech, J. Käfer, F. Graner, D. J. Müller, and C.-P. Heisenberg. Tensile forces govern germ-layer organization in zebrafish. *Nat. Cell Biol.*, 10(4):429–36, 2008.

[110] K. Kruse, J.-F. Joanny, F. Jülicher, J. Prost, and K. Sekimoto. Generic theory of active polar gels: a paradigm for cytoskeletal dynamics. *Eur. Phys. J. E*, 16(1):5–16, 2005.

[111] H. Kuper, H.-O. Adami, and P. Boffetta. Tobacco use, cancer causation and public health impact. *J. Intern. Med.*, 251(6):455–466, 2002.

[112] L. D. Landau and E. M. Lifshitz. *Theory of Elasticity*. Course of Theoretical Physics, vol. 7. Butterworth-Heinemann, Oxford, 3rd edition, 1986.

[113] K. P. Landsberg, R. Farhadifar, J. Ranft, D. Umetsu, T. J. Widmann, T. Bittig, A. Said, F. Jülicher, and C. Dahmann. Increased cell bond tension governs cell sorting at the drosophila anteroposterior compartment boundary. *Curr. Biol.*, 19(22):1950–5, 2009.

[114] T. Lecuit, P.-F. Lenne, and E. Munro. Force generation, transmission, and integration during cell and tissue morphogenesis. *Annu. Rev. Cell Dev. Biol.*, 27:157–84, 2011.

[115] S. E. Lepage and A. E. E. Bruce. Zebrafish epiboly: mechanics and mechanisms. *Int. J. Dev. Biol.*, 54(8-9):1213–28, 2010.

[116] K. R. Levental, H. Yu, L. Kass, J. N. Lakins, M. Egeblad, J. T. Erler, S. F. T. Fong, K. Csiszar, A. Giaccia, W. Weninger, M. Yamauchi, D. L. Gasser, and V. M. Weaver. Matrix crosslinking forces tumor progression by enhancing integrin signaling. *Cell*, 139(5):891–906, 2009.

[117] O. Lokshin and Y. Lanir. Micro and macro rheology of planar tissues. *Biomaterials*, 30(17):3118–27, 2009.

[118] T. C. Lubensky, R. Mukhopadhyay, L. Radzihovsky, and X. Xing. Symmetries and elasticity of nematic gels. *Phys. Rev. E*, 66(1):011702, 2002.

[119] W. A. Malik, S. C. Prasad, K. R. Rajagopal, and L. Preziosi. On the modeling of the viscoelastic response of embryonic tissues. *Math. Mech. Solids*, 13(1):81–91, 2007.

[120] M. L. Manning, R. A. Foty, M. S. Steinberg, and E.-M. Schoetz. Coaction of intercellular adhesion and cortical tension specifies tissue surface tension. *Proc. Natl. Acad. Sci. USA*, 107(28):12517–22, 2010.

[121] P. Marmottant, A. Mgharbel, J. Käfer, B. Audren, J.-P. Rieu, J. C. Vial, B. van der Sanden, A. F. M. Marée, F. Graner, and H. Delanoë-Ayari. The role of fluctuations and stress on the effective viscosity of cell aggregates. *Proc. Natl. Acad. Sci. USA*, 106(41):17271–17275, 2009.

[122] A. C. Martin, M. Gelbart, R. Fernandez-Gonzalez, M. Kaschube, and E. F. Wieschaus. Integration of contractile forces during tissue invagination. *J. Cell Biol.*, 188(5):735–49, 2010.

[123] A. C. Martin, M. Kaschube, and E. F. Wieschaus. Pulsed contractions of an actin-myosin network drive apical constriction. *Nature*, 457(7228):495–9, 2009.

[124] F. A. Martín, S. C. Herrera, and G. Morata. Cell competition, growth and size control in the drosophila wing imaginal disc. *Development*, 136(22):3747–56, 2009.

[125] P. C. Martin, O. Parodi, and P. S. Pershan. Unified hydrodynamic theory for crystals, liquid crystals, and normal fluids. *Phys. Rev. A*, 6(6):2401–2420, 1972.

[126] N. Minc and M. Piel. Predicting division plane position and orientation. *Trends Cell Biol.*, 22(4):193–200, 2012.

[127] J. Mombach and J. A. Glazier. Single cell motion in aggregates of embryonic cells. *Phys. Rev. Lett.*, 76(16):3032–3035, 1996.

[128] J. Mombach, J. A. Glazier, R. Raphael, and M. Zajac. Quantitative comparison between differential adhesion models and cell sorting in the presence and absence of fluctuations. *Phys. Rev. Lett.*, 75(11):2244–2247, 1995.

[129] B. Monier, A. Pélissier-Monier, A. H. Brand, and B. Sanson. An actomyosin-based barrier inhibits cell mixing at compartmental boundaries in drosophila embryos. *Nat. Cell Biol.*, 12(1):60–65, 2009.

[130] F. Montel, M. Delarue, J. Elgeti, L. Malaquin, M. Basan, T. Risler, B. Cabane, D. Vignjevic, J. Prost, G. Cappello, and J.-F. Joanny. Stress clamp experiments on multicellular tumor spheroids. *Phys. Rev. Lett.*, 107:188102, 2011.

[131] G. Morata and P. Ripoll. Minutes: Mutants of drosophila autonomously affecting cell division rate. *Dev. Biol.*, 42(2):211–221, 1975.

[132] E. Moreno and K. Basler. dmyc transforms cells into super-competitors. *Cell*, 117(1):117–29, 2004.

[133] W. Mueller-Klieser. Tumor biology and experimental therapeutics. *Crit. Rev. Oncol. Hematol.*, 36(2-3):123–39, 2000.

[134] J. D. Murray. *Mathematical Biology.* Springer, New York, Heidelberg, 2nd edition, 1993.

[135] C. M. Nelson and M. J. Bissell. Of extracellular matrix, scaffolds, and signaling: tissue architecture regulates development, homeostasis, and cancer. *Annu. Rev. Cell Dev. Biol.*, 22:287–309, 2006.

[136] D. R. Nelson and B. Halperin. Dislocation-mediated melting in two dimensions. *Phys. Rev. B*, 19(5):2457–2484, 1979.

[137] P. Nelson. *Biological Physics: Energy, Information, Life.* W. H. Freeman and Company, New York, 2003.

[138] P. A. Netti, D. A. Berk, M. A. Swartz, A. J. Grodzinsky, and R. K. Jain. Role of extracellular matrix assembly in interstitial transport in solid tumors. *Cancer Res.*, 60(9):2497–503, 2000.

[139] S. A. Newman and W. D. Comper. 'generic' physical mechanisms of morphogenesis and pattern formation. *Development*, 110(1):1–18, 1990.

[140] A. Nicoli, F. Capodanno, L. Moscato, I. Rondini, M. T. Villani, A. Tuzio, and G. B. La Sala. Analysis of pronuclear zygote configurations in 459 clinical pregnancies obtained with assisted reproductive technique procedures. *Reprod. Biol. Endocrinol.*, 8:77, 2010.

[141] P. Nikunen, M. Karttunen, and I. Vattulainen. How would you integrate the equations of motion in dissipative particle dynamics simulations?. *Comput. Phys. Commun.*, 153(3):407–423, 2003.

[142] K.-A. Norton, M. Wininger, G. Bhanot, S. Ganesan, N. Barnard, and T. Shinbrot. A 2d mechanistic model of breast ductal carcinoma in situ (dcis) morphology and progression. *J. Theor. Biol.*, 263(4):393–406, 2010.

[143] R. Nuzzo. Profile of george oster. *Proc. Natl. Acad. Sci. USA*, 103(6):1672–4, 2006.

[144] G. M. Odell, G. Oster, P. Alberch, and B. Burnside. The mechanical basis of morphogenesis: I. epithelial folding and invagination. *Dev. Biol.*, 85(2):446–462, 1981.

[145] M. J. Paszek, N. Zahir, K. R. Johnson, J. N. Lakins, G. I. Rozenberg, A. Gefen, C. A. Reinhart-King, S. S. Margulies, M. Dembo, D. Boettiger, D. A. Hammer, and V. M. Veaver. Tensional homeostasis and the malignant phenotype. *Cancer Cell*, 8(3):241–54, 2005.

[146] J. C. Pease and J. S. Tirnauer. Mitotic spindle misorientation in cancer–out of alignment and into the fire. *J. Cell Sci.*, 124(Pt 7):1007–16, 2011.

[147] P. S. Pershan and J. Prost. Dislocation and impurity effects in smectic-a liquid crystals. *J. Appl. Phys.*, 46(6):2343–2353, 1975.

[148] L. Petitjean, M. Reffay, E. Grasland-Mongrain, M. Poujade, B. Ladoux, A Buguin, and P. Silberzan. Velocity fields in a collectively migrating epithelium. *Biophys. J.*, 98(9):1790–800, 2010.

[149] S. Pigolotti, R. Benzi, M. H. Jensen, and D. R. Nelson. Population genetics in compressible flows. *Phys. Rev. Lett.*, 108(12):128102, 2012.

[150] A. D. Polyanin and V. F. Zaitsev. *Handbook of Exact Solutions for Ordinary Differential Equations*. Chapman & Hall/CRC, Boca Raton, 2nd edition, 2003.

[151] P.-A. Pouille, P. Ahmadi, A.-C. Brunet, and E. Farge. Mechanical signals trigger myosin ii redistribution and mesoderm invagination in drosophila embryos. *Sci. Signal.*, 2(66):ra16, 2009.

[152] L. Preziosi, D. Ambrosi, and C. Verdier. An elasto-visco-plastic model of cell aggregates. *J. Theor. Biol.*, 262(1):35–47, 2010.

[153] L. Preziosi, editor. *Cancer Modelling and Simulation*. Chapman & Hall/CRC, Boca Raton, 2003.

[154] L. Preziosi and A. Tosin. Multiphase modelling of tumour growth and extracellular matrix interaction: mathematical tools and applications. *J. Math. Biol.*, 58(4-5):625–56, 2009.

[155] A. Puliafito, L. Hufnagel, P. Neveu, S. Streichan, A. Sigal, D. Kuchnir Fygenson, and B. I. Shraiman. Collective and single cell behavior in epithelial contact inhibition. *Proc. Natl. Acad. Sci. USA*, 109(3):739–44, 2012.

[156] E. M. Purcell. Life at low reynolds number. *Amer. J. Phys.*, 45(1):3–11, 1977.

[157] M. Rauzi, P.-F. Lenne, and T. Lecuit. Planar polarized actomyosin contractile flows control epithelial junction remodelling. *Nature*, 468(7327):1110–4, 2010.

[158] M. Rauzi, P. Verant, T. Lecuit, and P.-F. Lenne. Nature and anisotropy of cortical forces orienting drosophila tissue morphogenesis. *Nat. Cell Biol.*, 10(12):1401–1410, 2008.

[159] C. Rhiner, J. M. López-Gay, D. Soldini, S. Casas-Tinto, F. A. Martín, L. Lombardía, and E. Moreno. Flower forms an extracellular code that reveals the fitness of a cell to its neighbors in drosophila. *Dev. Cell*, 18(6):985–98, 2010.

[160] T. Risler. Cytoskeleton and Cell Motility. [in: *Encyclopedia of Complexity and Systems Science*; R. A. Meyers, editor-in-chief; Springer, New York, Heidelberg (2009)].

[161] E. K. Rodriguez, A. Hoger, and A. D. McCulloch. Stress-dependent finite growth in soft elastic tissues. *J. Biomech.*, 27(4):455–67, 1994.

[162] T. Roose, P. A. Netti, L. L. Munn, Y. Boucher, and R. K. Jain. Solid stress generated by spheroid growth estimated using a linear poroelasticity model. *Microvasc. Res.*, 66(3):204–12, 2003.

[163] T. Rozario and D. W. DeSimone. The extracellular matrix in development and morphogenesis: a dynamic view. *Dev. Biol.*, 341(1):126–40, 2010.

[164] T. Savin, N. A. Kurpios, A. E. Shyer, P. Florescu, H. Liang, L. Mahadevan, and C. J. Tabin. On the growth and form of the gut. *Nature*, 476(7358):57–62, 2011.

[165] E.-M. Schötz, R. D. Burdine, F. Jülicher, M. S. Steinberg, C.-P. Heisenberg and R. A. Foty. Quantitative differences in tissue surface tension influence zebrafish germ layer positioning. *HFSP J.*, 2(1):42–56, 2008.

[166] G. Schwank, G. Tauriello, R. Yagi, E. Kranz, P. Koumoutsakos, and K. Basler. Antagonistic growth regulation by dpp and fat drives uniform cell proliferation. *Dev. Cell*, 20(1):123–30, 2011.

[167] M. Ségalen, C. A. Johnston, C. A. Martin, J. G. Dumortier, K. E. Prehoda, N. B. David, C. Q. Doe, and Y. Bellaïche. The fz-dsh planar cell polarity pathway induces oriented cell division via mud/numa in drosophila and zebrafish. *Dev. Cell*, 19(5):740–52, 2010.

[168] B. I. Shraiman. Mechanical feedback as a possible regulator of tissue growth. *Proc. Natl. Acad. Sci. USA*, 102(9):3318–23, 2005.

[169] H. B. Skinner. *Current diagnosis & treatment in orthopedics.* Lange Medical Books/McGraw Hill, Stamford, 2006.

[170] J. Solon, A. Kaya-Copur, J. Colombelli, and D. Brunner. Pulsed forces timed by a ratchet-like mechanism drive directed tissue movement during dorsal closure. *Cell*, 137(7):1331–42, 2009.

[171] D. B. Staple, R. Farhadifar, J.-C. Röper, B. Aigouy, S. Eaton, and F. Jülicher. Mechanics and remodelling of cell packings in epithelia. *Eur. Phys. J. E*, 33(2):117–27, 2010.

[172] M. S. Steinberg. Reconstruction of tissues by dissociated cells. *Science*, 141:401–8, 1963.

[173] S. Suresh. Biomechanics and biophysics of cancer cells. *Acta Biomater.*, 3(4):413–38, 2007.

[174] M. A. Swartz and M. E. Fleury. Interstitial flow and its effects in soft tissues. *Annu. Rev. Biomed. Eng.*, 9:229–56, 2007.

[175] D. T. Tambe, C. C. Hardin, T. E. Angelini, K. Rajendran, C. Y. Park, X. Serra-Picamal, E. H. Zhou, M. H. Zaman, J. P. Butler, D. A. Weitz, J. J. Fredberg, and X. Trepat. Collective cell guidance by cooperative intercellular forces. *Nat. Mater.*, 10(6):469–75, 2011.

[176] T. Tanaka, L. O. Hocker, and G. B. Benedek. Spectrum of light scattered from a viscoelastic gel. *J. Chem. Phys.*, 59(9):5151–5159, 1973.

[177] S. Fürthauer, M. Strempel, S. Grill, and F. Jülicher. Active chiral fluids. (*in preparation*).

[178] M. Théry and M. Bornens. Cell shape and cell division. *Curr. Opin. Cell Biol.*, 18(6):648–57, 2006.

[179] D. W. Thompson. *On Growth And Form.* University Press, Cambridge, complete revised edition, 1942.

[180] Y. Toyama, X. G. Peralta, A. R. Wells, D. P. Kiehart, and G. S. Edwards. Apoptotic force and tissue dynamics during drosophila embryogenesis. *Science*, 321(5896):1683–6, 2008.

[181] P. Tracqui. Biophysical models of tumour growth. *Rep. Prog. Phys.*, 72(5):1–31, 2009.

[182] X. Trepat, M. R. Wasserman, T. E. Angelini, E. Millet, D. A. Weitz, J. P. Butler, and J. J. Fredberg. Physical forces during collective cell migration. *Nat. Phys.*, 5(6):426–430, 2009.

[183] C. Truesdell. *A first course in rational continuum mechanics.* Academic Press, San Diego, 2nd edition, 1991.

[184] F. R. Turner and A. P. Mahowald. Scanning electron microscopy of drosophila melanogaster embryogenesis. ii. gastrulation and segmentation. *Dev. Biol.*, 57(2):403–16, 1977.

[185] R. Vandiver and A. Goriely. Morpho-elastodynamics: the long-time dynamics of elastic growth. *J. Biol. Dyn.*, 3(2):180 – 195, 2009.

[186] A. Vichas and J. A. Zallen. Translating cell polarity into tissue elongation. *Semin. Cell Dev. Biol.*, 22(8):858–64, 2011.

[187] Y. Wang and J. Nathans. Tissue/planar cell polarity in vertebrates: new insights and new questions. *Development*, 134(4):647–58, 2007.

[188] M. Warner and E. M. Terentjev. *Liquid Crystal Elastomers.* Oxford University Press, Oxford, 2003.

[189] O. Wartlick, P. Mumcu, A. Kicheva, T. Bittig, C. Seum, F. Jülicher, and M. Gonzalez-Gaitan. Dynamics of dpp signaling and proliferation control. *Science*, 331(6021):1154–9, 2011.

[190] R. A. Weinberg. *The Biology of Cancer.* Garland Science, New York, 2006.

[191] J. Whitehead, D. Vignjevic, C. Fütterer, E. Beaurepaire, S. Robine, and E. Farge. Mechanical factors activate beta-catenin-dependent oncogene expression in apc mouse colon. *HFSP J.*, 2(5):286–94, 2008.

[192] L. Wolpert. *Principles of Development.* Oxford University Press, Oxford, 2nd edition, 2005.

[193] T. Yamaue and M. Doi. The stress diffusion coupling in the swelling dynamics of cylindrical gels. *J. Chem. Phys.*, 122(8):084703–6, 2005.

[194] J. A. Zallen. Planar polarity and tissue morphogenesis. *Cell*, 129(6):1051–63, 2007.

[195] H. Zhang, C. Gally, and M. Labouesse. Tissue morphogenesis: how multiple cells cooperate to generate a tissue. *Curr. Opin. Cell Biol.*, 22(5):575–82, 2010.